THÈSE

En vue de l'obtention du

DOCTORAT DE L'UNIVERSITÉ DE TOULOUSE

Délivré par l'Université Toulouse 3 - Paul Sabatier

Présentée et soutenue par

Sharon Ann BARRETTO

Le 4 décembre 2019

Etude des interactions bidirectionnelles entre le microbiote intestinal et les récepteurs aux xénobiotiques CAR et PXR

Ecole doctorale : **BSB - Biologie, Santé, Biotechnologies**

Spécialité : **MALADIES METABOLIQUES ET CARDIOVASCULAIRES**

Unité de recherche :
TOXALIM - Laboratoire de Toxicologie Alimentaire

Thèse dirigée par
Laurence PAYRASTRE et Sandrine ELLERO-SIMATOS

Jury

M. Xavier COUMOUL, Rapporteur
Mme Lydie SPARFEL-BERLIVET, Rapporteure
M. Philippe GéRARD, Examinateur
M. Pierre GOURDY, Examinateur
Mme Laurence PAYRASTRE, Directrice de thèse
Mme Sandrine ELLERO-SIMATOS, Co-directrice de thèse

Acknowledgements

I would like to first acknowledge the Region Midi-Pyrénées and the French National Institute for Agricultural Research (INRA) -Toulouse for having assured the funding of the three years of this PhD thesis and making the results of this work possible.

My esteemed appreciation to the jury:
To **Prof. Pierre Gourrdy**, research director at the Institute of Cardiovascular and Metabolic Diseases (Toulouse), I am grateful for your enthusiasm to preside the jury of my oral defense. To **Prof. Lydie Sparfel-Berlivet** of Rennes University 1 and **Prof. Xavier Coumoul** of Paris Descartes University, my sincerest appreciation for investing your time and attention to review the thesis manuscript and for the interest to participate in the jury of my oral defense. Your feedback has been vital to the final output of this body of work. To **Dr. Philippe Gérard**, research director at the MICALIS Institute, I am honored and grateful for your presence as part of the jury and your interest in this PhD thesis.

To **Dr. Sandrine Claus** and **Dr. Emmanuelle Maguin**, I would especially like to thank both of you for having shared your precious time, attention and feedback as part of my thesis committee. Your insightful comments and encouragements have immensely facilitated the evolution and progress of this thesis.

To **Dr. Laurence Gamet-Payrastre** and **Dr. Sandrine Ellero-Simatos**, I am deeply grateful to be under the supervision of two astute and intelligent women. Thank you, Laurence, for the constant generosity of time, not only in discussing science but sharing light moments in between work. These warm memories will forever be etched in my heart and mind. Thank you, Sandrine, for mentoring me with countless learnings and refreshing me to what it means to be passionate for science and the environment. I am truly indebted to you for the rich experience gained from our exchanges, scientific and personal. Your kindness, wit and passion for work will unceasingly motivate me in my future endeavors.

To **Dr. Hervé Guillou**, I am equally appreciative and grateful that you warmly welcomed me to the team and gave me the opportunity to work and experience the field of integrative toxicology and metabolism research. Thank you for your generosity of time, knowledge and the constant cultivation of camaraderie and unity in the team.

I would like to extend my gratitude to the rest of the Integrative Toxicology and Metabolism (TIM) team, old and new, for having accompanied me through these years. Thank you, **Dr. Nicolas Loiseau** and **Dr. Laila Mselli-Lakhal** for the encouragement, insightful comments and good company. With a special mention to **Fred** for being a vital part of the many technical accomplishments in this thesis. Thank you, Fred, for your eagerness to work and speak english with me (when I started) and for being a reliable partner in the many experiments we've shared. To **Arnaud**, an equal amount of appreciation for always being responsive, available and convivial in the everyday life in the

laboratory. To **Severine**, thank you for being a dependable teammate for the logistics of my experiments, as well as for the team's. To my roomies, **Lorraine** and **Tiffany**, you have made my previous solitary life much more colorful with our daily chats, scientific or whatnot, most notably our exchanges of French and English slangs. To **Leonie**, you came late in the game, but your company has made the daily commute and everyday conversations much more interesting. Thank you, **Sarra** for your generosity, especially with health and thesis-related concerns. Thank you, **Anne**, for the encouragement and good company. To **Marion, Celine, Claire, Manon, Penny, Alain, Fabiana, Quentin, Benjamin, Marine, Alexia, Elizabeth,** thank you for the company and memories that complete this unforgettable experience of being part of TIM.

A very special gratitude goes out to all our collaborators. Without your presence and contribution, the success of this thesis would have not been realized. The MeX team: **Daniel, Elodie** and **Sandrine** for the microsome data. The EZOP team: **Elodie, Eric, Colette, Caroline, Aurélia, Géraldine** and **Mickaël** for immense support with the animal experiments; TRiX team: **Yannick, Claire** and **Anthony** for the microarray data; The MetaToul Lipidomic facility: **Justine, Aurélie** and **Anthony** for the lipidomic analyses; The GenoToul Anexplo facility: **Laurent** and **Cyrielle** for the phenotyping analyses; The GenoToul MetaToul Platform (INSA-LISBP): **Lindsay** and **Edern** and the Metabolism and Mass Spectrometry Platform (INRA-PFEM) for the metabolomics data; The MetaToul Platform (AXIOM): Laurent and Cecile for the NMR access; The NGN team: **Sandrine, Laurence** and **Hannah** and The ENTeRisk team: **Eric H., Bruno, Natalia, Eric G., Christel** and **Adèle** for collaborative experiments.

To newfound friends and acquaintances in Toxalim, I am grateful for the everyday smiles and exchanges that fill the gaps of the daily grind at the laboratory. Merci à tous! To my dearest friends: **Sara, Brian, Ghazal, Bomin, Lilia, Emeline, Ntombi, Alice, Joechelle, Seb, Claudia, Haitham, Maral, Lydia, Margaret, Boss Cheng, Boss Dan, Ma'am Sylvia, Esmée** and **Carlo**, Inspite of the distance and our busy lives, we've managed to keep in touch and stay connected. Your encouragement, support, love and care have made this experience even much more meaningful. To **Pauline**, my feisty fun french teacher and friend, you have made my life in and out of work a breeze and I could have not done it without you.

To my loving family, **Mama, Papa, Kuya** and **Marcy, Yves** and **JR,** and **Nikko.** No words can describe how much of a difference you have made in attaining this feat of mine. Thank you for the unconditional love and support. I can't wait to be back home already!

Last but not the least, to **Raph**, my north star. Your moral support, candor, open-mindedness and optimism have been indispensable in helping me thrive here in France. Thank you for being here for me and making me feel at home. Je t'aime.

Table of Contents

List of figures

List of tables

List of abbreviations

5HT	5-Hydroxytryptamine
ABCC 2/3	ATP-binding cassette transporter sub-family C member 2/3
ABCG	ATP Binding Cassette Subfamily G Member
Acc	Acetyl-CoA carboxylase
AF1/2	Activating function 1/2
AIEC	Adherent-invasive E. coli
AMP	Adenosine monophosphate
AMPK	Adenosine monophosphate-activated protein kinase
AR	Testosterone receptor
Asbt	Apical sodium-dependent bile acid transporter /IBAT
ATB	Antibiotic
ATP	Adenosine triphosphate
BAC	bacterial artificial chromosome
BBB	Blood– brain barrier
BMI	Body mass index
BSEP	Bile salt export pump
BSH	Bile salt hydrolase
C57BL/6	C57 Black 6 mice
CA	Cholic acid
cAMP	Cyclic adenosine monophosphate
CAR 1/3	Constitutive androstane receptor 1/3
CCRP	Cytoplasmic CAR Retaining Protein
CD	Celiac disease
CD36	Cluster of differeniation 36
CDCA	Chenodeoxycholic acid
CITCO	6-(4-Chlorophenyl)imidazo[2,1-b][1,3]thiazole-5-carbaldehyde O-(3,4-dichlorobenzyl)oxume
CNS	Central nervous system
CPT1a	carnitine palmitoyltransferase1a
CrD	Crohn's disease
CREB	cAMP response element-binding protein
CTE	cytosolic acyl-CoA thioesterase
CYP	Cytochrome P450
DAX1	Dosage-sensitive sex reversal, adrenal hypoplasia critical region, on chromosome X,gene 1
DBD	DNA binding domain
DCA	deoxycholic acid
DR1	Direct repeat spaced by one nucleotide
EGF	Epidermal growth factor

EGFR	Epidermal growth factor receptor
ER	Estrogen receptor
ERK	Extra-cellular signal regulated kinase
F/B	*Firmicutes/Bacteriodetes*
Fasn	Fatty acid synthase
FAT	Fatty acid translocase
FGF21	Fibroblast growth factor 21
FoxO1	Forkhead box O1
G6Pase	Glucose-6-phosphatase
GABA	gamma-Aminobutyric acid
GF	Germ-free
GI	Gastro-intestinal
GLP-1	Glucagon-like peptide-1
GM	Gut microbiota
GPR41/43	G-protein-coupled receptors 41/43
GR	Glucocorticoid receptor
GRE	Glycyl radical enzyme
GRIP	Glucocorticoid receptor interacting protein
GSTA1	Glutathione S transferase 1
HADH	3-hyoxyacyl-CoA dehydrogenase
HCC	Hepatocellular carcinoma
HDAC	Histone deacetylase
HDL	High-density lipid
HFD	High-fat diet
HMGCR	3-Hydroxy-3-Methylglutaryl-CoA Reductase
HMGCS2	3-Hydroxy-3-methylglutarate-CoA synthase 2
HNF4a	Hepatocyte nuclear factor-4a
HNF4RE	iron-responsive element
hPXR	human PXR
HSDH	Hydroxysteroid dehydrogenase
Hsp	Heat shock protein
IBD	Inflammatory bowel disease
IEC	Intestinal epithelial cells
IGF-1	Insulin-like growth factor 1
IGN	Intestinal gluconeogenesis
IPA	Indole 3-propionic acid
IRE	HNF4-responsive element
JNK 1/2	c-Jun N-terminal kinases 1/2
LBD	Ligand binding domain
LCA	lithocholic acid
LDL	Low-density lipid

LPS	Lipopolysaccharide
LSS	Lanosterol synthase
LXR	Liver x receptor
MAPK	p38 Mitogen-activated protein kinases
MDR1/3	Multidrug resistance-related protein-1/3
MEK	Mitogen activated protein kinase kinase derived from MAPK/ERK kinase
mPxr	mouse PXR
MR	Mineralocorticoid receptor
MRP	Multidrug resistant protein
NADPH	Nicotamide adenine dinucleotide phosphate
NAFL	Non-alcoholic fatty liver
NAFLD	Non-alcoholic fatty liver disease
NCoR	Nuclear receptor co-repressor
NF-Kb	Nuclear Factor Kappa B
NLRP3/6	nod-like receptorpyrin domain-containing protein 3 /6
NR	Nuclear receptors
OATP2	Organic anion transporting polypeptide-2
Ostb	Organic solute transporter beta
PBREM	Phenobarbital Response Element Module
PEPCK	Phosphoenolpyruvate carboxykinase
PGC1 α	PPARg Co activator 1α
PML	promyelocytic leukemia
PP2A	protein phosphatase A2
PPAR	Peroxisome proliferator-activated receptors
PR	Progesterone receptor
PXR	Pregnane x receptor
PYY	Peptide YY or peptide tyrosine tyrosine
QTL	Quantitative trait loci
RACK1	receptor of protein C kinase 1
RARE	Response elements of the retinoic acid
RXR	Retinoid X receptor
SAM	S-adenosyl-L-methionine
SCD1	Stearoyl-CoA desaturase-1
SCFA	Short chain fatty acid
SHIME	Simulator of the human intestinal microbial ecosystem
SHP	Small heterodimer protein
SMILE	Small heterodimer partner interacting leucine zipper protein
SMRT	Silencing mediator for retinoid and thyroid receptor
SOD	Superoxide dismutase-3
Spot14	Thyroid hormone responsive Spot14 gene
SQLE	Squalene epoxidase

SRC	Steroid receptor co-activator
SREBP-1c	Sterol regulatory element binding protein 1-c
STD	Dehydroepiandrosterone sulfotransferase
SULT2A1	Sulfotransferase 2A1
SXR	Steroid and xenobiotic receptor
TCPOBOP	1,4-*Bis*(3,5-Dichloro-2-pyridinyloxy)benzene
TGR5	Takeda G protein-coupled receptor 5
Th17	T-helper 17
TIF	Transcriptional intermediary factor
TLR 4	Toll-like receptor 4
TNFα	Tumor necrosis-α
TRb	Thyroid hormone receptor
UC	Ulcerative colitis
UGT	UDP glucuronosyltransferase
UGT1A1	UDP glucuronosyltransferase 1A1
VDR	Vitamin D receptor
VP	VP16 coactivator

INTRODUCTION

Figure 1. General structure of nuclear receptors. The nuclear receptors consist of six regions, A/B, C, D, E and F A / B is located at the tertiary N-terminus and contains the activation function (AF-1). C is composed of the DNA binding domain (DBD), while D is the minimally conserved hinge region. Regions C & D have nuclear localization signal (NLS). E is the ligand binding domain (LBD) and carries the function of AF-2 ligand-dependent transactivation Some nuclear receptors exhibit an extremely variable F domain whose function is not known.

Endocrine Receptors		Adopted Orphan Receptors		Orphan Receptors
Ligands of high affinity Hormonal lipids		*Ligands of low affinity Dietary lipids*		*unknown*
ER α and β	Estrogen	**RXR α, β and γ**	9-cis-RA	**HNF-4 α, γ**
PR	Progesterone	**PPAR α, β and γ**	Fatty acids	**SF-1**
AR	Testosterone	**LXR α and β**	Oxysterols	**LRH-1**
GR	Glucocorticoid	**FXR**	Bile acids	**DAX-1**
MR	Mineralocorticoid	**PXR**	Xenobiotics	**SHP**
		CAR	Xenobiotics	**TLX**
RAR α, β and γ	Retinoic acid			**PNR**
TR α and β	Thyroid Hormone			**NGFI-B α, β and γ**
VDR	Vitamin D			**ROR α, β and γ**
				ERR α, β and γ
				Rev-erb α, β and γ
				GCNF
				TR 2, 4
				COUP-TFα, β and γ
				NOR
				NUR
				EAR-2

Figure 2. Classification of nuclear receptors. The nuclear receptors are classified in function to their capacity to fix to ligands (Chawla *et al*., 2001)

Receptors: to estrogen (ER); to progesterone (PR); to androgens (AR); to glucocorticoids (GR); to mineralocorticoids (MR); to retinoic acid (RAR); to thyroid hormones (TR); to Vitamin D (VDR); X-retinoids (RXR); activated by peroxisome proliferators (PPAR); to oxysterols (LXR); X-farensoids (FXR); Pregnane X (PXR); constitutive androstanes (CAR); Hepatocyte Nuclear Factor 4 (HNF); Steroidogenic Factor 1(SF-1); Liver Receptor Homolog-1(LRH-1); Dosage sensitive sex reversal-Adrenal hypoplasia congenita critical region on the X chromosome, gene 1 (DAX-1); Small heterodimer Partner (SHP); tailless homolog (TLX): Photoreceptor-specific Nuclear Receptor (PNR); Nerve Growth Factor IB-like receptor (NGFI-B); related receptor to retinoid receptor (ROR); Estrogen-related receptor (ERR); Germ Cell Promoter Transcription Factor (COUP-TF); Neuron-derived orphan receptor (NOR); Neuron-derived clone (NUR);V-erbA-related (EAR-2).

Chapter 1 : Nuclear receptors CAR and PXR

1.1. Generalities on nuclear receptors

Nuclear receptors (NRs) are ligand-dependent transcription factors that belong to a superfamily of intracellular receptors comprising 49 members in humans and 48 in mice (McKenna *et al*., 2009). They regulate a variety of physiological processes by inducing the transcription of target genes. These nuclear receptors generally possess a structure composed of 6 functional domains, namely, A/B, C, D, E and F. Domain A/B is situated at the extremity of the N-terminal region and contains the activating function (AF1). Domain C is composed of the DNA binding domain (DBD), consisting of two zinc finger patterns that recognizes specific response elements. Domain D can contain nuclear localization signals and provides flexibility to the protein. Domain E, situated at the extremity of the region of the C-terminal contains the ligand binding domain (LBD) and contains the ligand-dependent activating function (AF2). Finally, the domain F is a very variable region, absent in certain NRs and exercises a regulatory function (**Figure 1**).

1.2. Classification/Nomenclature

In function to their phylogenetic similarity, NRs can be subdivided into 6 subfamilies (NR1-NR6) and further subdivided into 28 groups (A to K). Each group can then be regrouped into numerous gene paralogs (https://nursa.org/nursa/molecules/index.jsf). According to their capacity to function in monomer or in homo/heterodimer and according to the type of element of response to which they fix themselves, these NRs can also be distributed into 4 different classes I, II,, II, IV) (Evans & Mangelsdorf, 2014; Germain, *et al.*, 2006; Mangelsdorf *et al*., 1995).

In addition, NRs can equally be classified in function of their capacity for ligand binding. Thus, endocrine receptors bind to steroid hormones while adopted orphan receptors link to dietary lipid ligands and orphan receptors do not have identified ligands. Adopted orphan NRs have been discovered before the identification of their respective ligands (Alaynick, 2008) (**Figure 2**).

The family of endocrine NRs includes the glucocorticoid (GR), estrogen (ER), progesterone (PG) androgen (AR) and mineralocorticoid (MR) receptors. Their ligands are exclusively from endogenous source and under the control of the hypothalamic-pituitary axe (Wilson, 1992). Steroid hormones bind to their receptors with high affinity. Adopted orphan receptors forms a heterodimer with RXR (Retinoid X Receptor) to induce the transcription of their target genes. The members of this group include the receptors for fatty acids - the peroxisome proliferator-activated receptors (PPARs), oxysterols - the liver x receptor (LXR), bile acids – the farensoid x receptor (FXR), as well as xenobiotics – the constitutive androstane receptor (CAR) and pregnane x receptor (PXR) (Chawla, *et al.*, 2001).

1.3. Mode of action of NRs

NR ligands may have an exogenous or endogenous origin and are generally of lipophilic nature. They exert several actions on the receptor: agonist (increase in basal transcriptional activity), pure antagonist (non-modification of transcriptional activity), inverse agonist (decrease in basal transcriptional activity) and partial agonist/antagonist (partial transcriptional modification compared to pure agonist/antagonist transcriptional activity).

NRs regulate the expression of their target genes by binding to their DNA on specific response elements. Generally, these response elements are located upstream of the

promoting region of the target gene. These response elements are composed of two hexameric nucleotide sequences forming direct, indirect or inverse repetitions separated by a number of determined nucleotides. NRs bind to these response elements in the form of a monomer, homodimer or heterodimer. RXR is the principal partner for heterodimerization (Kliewer *et al*., 1992).

Gene activation by the nuclear receptors takes place in 3 stages. First is the binding of the ligand, followed by the recruitment of co-regulators and lastly, the recruitment of the transcriptional complex. The ligand binds the hydrophobic pocket (LBD) and induces a change of conformation that stabilizes the transactivation domain (AF2) (Thompson *et al.*, 1998). This stage permits the transition from the inactive form to the active form of the receptor. This ligand binding also allows the modulation of the interaction with cytoplasmic proteins such as Hsp (Heat shock protein) and further proceeding towards nuclear translocation (Hager *et al*., 2000).

Co-regulators are members of protein complexes, which are associated to NRs and modulate their activity (Rosenfeld & Glass, 2001). Co-activators are grouped in more than 100 members. For example, they can activate histone acetlytransferase, thereby favoring the decondensation of DNA to access the transcriptional machinery. In this group, there is a family of p160 proteins including steroid receptor co-activator (SRC) 1, 2 and 3 and the p300 family, where PPARγ co activator 1α (PGC1α) allows the binding of SRC1. This co-activator is specific of the nutritional status and the cellular environment, and is induced upon fasting (Mastropasqua *et al*., 2018).

The co-repressors interact with NRs that are constitutively bound to DNA or with those that are linked to antagonists or partial agonists and adopt conformations allowing the

fixation of co-repressors. The fixation of co-repressors allows the recruitment of enzymatic complexes containing histone deacetylases that prevents transcriptional activity (Bourguet *et al.*, 1995). The most known co-repressors are NCoR (nuclear receptor co-repressor) and SMRT (silencing mediator for retinoid and thyroid receptor) (Heinzel *et al.,* 1997).

1.4. Major hepatic roles

Among the 48 NRs expressed in the liver, 20 are subject to a circadian rhythm where their expression and their activity are highly modulated according to the day/night cycle and the food supply (Yang *et al*., 2006). NRs participate in the regulation of carbohydrate and lipid homeostasis. PPARα, PPARβ, PPARγ, FXR, LXRα, vitamin D receptor (VDR) and GR are the most active hepatic NR regulating energy homeostasis, while CAR and PXR are specifically involved in xenobiotic metabolism.

1.4.1. Energy metabolism

PPARs: Fatty acid sensors (NR1C1, NR1C2, NR1C3)

PPAR receptors are important regulators of energy metabolism and they are, therefore, pharmacological targets of numerous pharmaceuticals for the treatment of diabetes and obesity (López-Velázquez *et al*., 2012). PPARs are activated by saturated fatty acids, eicosanoids, and several other synthetic ligands. Each isotype of PPAR (α, β, γ) exercise a specific function to maintain lipid homeostasis. PPARα (NR1C1) is the most abundant isotype in a healthy liver. During fasting, PPARα senses increased levels of free fatty acids released from adipocytes, and in response, controls the expression of hundreds of genes involved in fatty acid uptake, transport, and catabolism in hepatocytes (Montagner, Polizzi, et al., 2016). Fibroblast growth factor 21 (FGF21) is a hepatokine, a liver-derived

hormone produced by hepatocytes. FGF21 controls a broad range of endocrine responses involved in the regulation of energy metabolism, growth, fertility and longevity (Kliewer & Mangelsdorf, 2019). The laboratory has provided recent evidence that hepatocyte FGF21 expression is strongly induced in response to fasting (Montagner, Polizzi, et al., 2016; Régnier *et al*., 2018) and in response to glucose overload (Iroz *et al*., 2017), two contrasted metabolic signals. In both cases, *FGF21* expression is under the specific control of the PPARα. Thus, mice with a hepatocyte-specific deletion of *Pparα* show impaired fatty acid catabolism leading to hepatic steatosis and defective ketonemia in response to fasting (Montagner *et al*., 2016; Régnier *et al*., 2018). Ketogenesis is a metabolic pathway occurring in the liver that produces ketone bodies from adipose fatty acids. Ketone bodies are used as an alternative energy source by peripheral tissues to survive episodes of starvation. Thus, ketogenesis is a crucial metabolic adaptation to prolonged periods of nutrient insufficiency (Puchalska & Crawford, 2017). Altogether, data from the laboratory show that PPARa is a pioneering transcription factor required for the control of FGF21 and is critical for ketogenesis.

LXR (NR1H3) : Sterol sensor

LXRα is abundantly expressed in tissues associated to lipid metabolism such as the liver, adipose tissues, kidneys, and the intestine while *LXRβ* is expressed ubiquitously. LXR is activated by oxysterols (Quinet *et al*., 2004). It is a key factor in cholesterol metabolism: in response to elevated levels of cholesterol, LXR promotes its transport, its catabolism and its elimination (Chawla *et al*., 2001). The activation of LXR at the hepatic level induces the expression of transporters of cholesterol ATP binding cassette subfamily G member 5 (*ABCG5*) and *ABCG8* to augment the secretion of cholesterol in the form of bile (Peet *et al.*,

1998). The expression of *CYP7A1*, the limiting enzyme of biliary synthesis and the elimination of cholesterol, is also regulated by LXR. Lastly, LXRα also regulates the expression of genes implicates in lipogenesis such as sterol regulatory element binding protein 1-c (*SREBP-1c*), stearoyl-CoA desaturase-1 (*SCD1*) and fatty acid synthase (*FAS*N) (Repa *et al*., 2000).

FXR (NR1H4) : Bile acid sensor

FXR is highly expressed at the entero-hepatic system including the liver and intestine where it acts as a sensor of bile acids, thereby protecting the organism against elevated level of bile acids. The endogenous ligands of this receptor are for example, cholic and chenodeoxycholic acids. Activation of hepatic FXR induces the expression of the bile salt export pump *(BSEP*) allowing the efflux of bile acids through bile and leads to the repression of the cholesterol 7α-hydroxylase (*CYP7A1*) gene which regulates the pathway through which cholesterol is converted into bile acids (Sinal *et al.*, 2000).

1.4.2. Detoxification

CAR-PXR (NR1I3-NR1I2)

The constitutive androstane receptor (CAR), and the pregnane X receptor (PXR) are members of the adopted orphan nuclear receptor subfamily. Based on their structural features, CAR and PXR have been placed in nuclear receptor group 1, subgroup I; which also contains VDR. CAR and PXR are relatively promiscuous nuclear receptors that are activated by numerous xenobiotics, drugs, bile acids, and hormones.

Therefore, they may be considered adopted orphans that recognize a number of endobiotic and xenobiotic chemicals. In turn, they act as master regulators of the phase I, phase II, and phase III enzymes and transporters critical for detoxification and elimination of steroids, bile acids, and xenobiotics following heterodimerization with RXRα. These two NRs will be further described in sections 1.5 and 1.6.

AhR(ARNT)

The aryl hydrocarbon receptor (AhR) is not *per se* a nuclear receptor, but a transcription factor structurally distinct from the nuclear receptor superfamily. It belongs to the Per-Arnt-Sim family of transcription factors and possesses helix-loop-helix interaction domains. AhR is present in the mammary glands, the liver, the central nervous system, the cardiovascular system and the uterus of all vertebrates (Guéguen *et al.*, 2006). In the absence of the ligand, AhR is sequestered into the cytoplasm in a complex of chaperone molecules. Upon ligand binding, it translocates into the nucleus and associates with its partner AhR-nuclear translocator (Arnt). The target genes of AhR are principally phase I and II xenobiotic metabolizing enzymes such as CYP1A1, CYP1A2, CYP1B1, UGT1A1 and MDR1 (Nebert et al., 2000). It was demonstrated that the pharmacologic activation of AhR is able to induce the expression of CAR and its target genes in the liver in rodent and human hepatocytes (Patel *et al*., 2007).

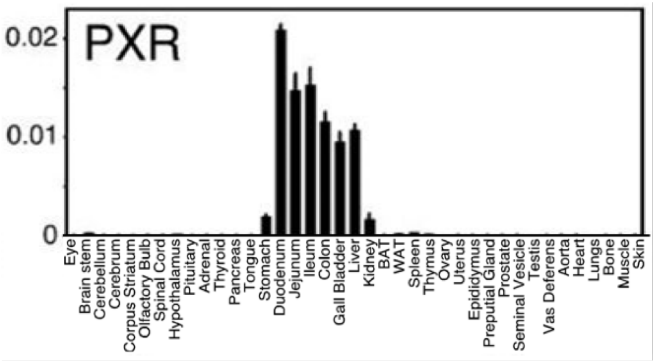

Figure 3. Expression of Pregnane X Receptor in specific tissue systems of C57Bl/6 mice. PXR is highly expressed in the gastroenteric system, liver and kidneys of C57Bl/6 mice which implies the existence of common transcriptional mechanisms to regulate their expression (Bookout *et al.*, 2006).

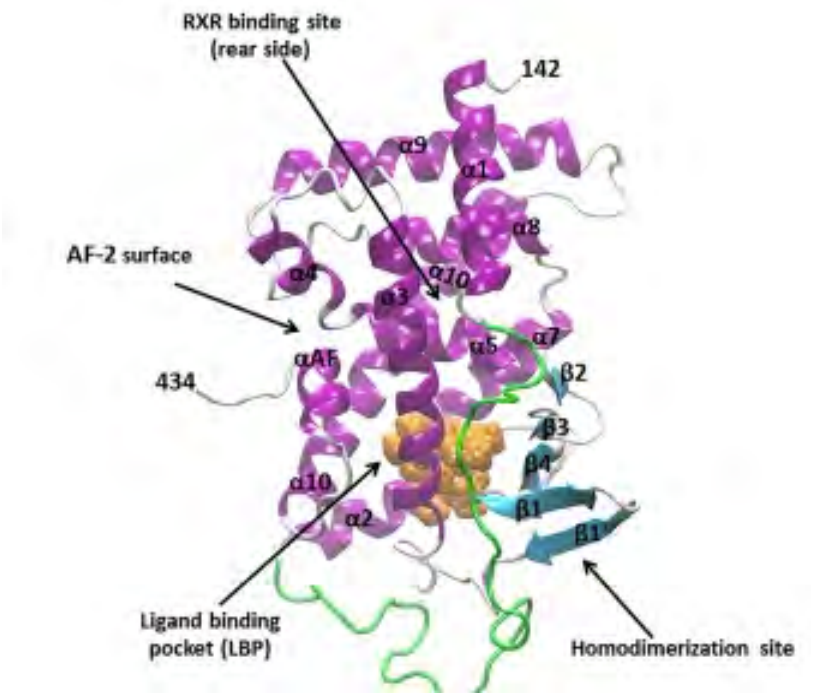

Figure 4. **3D image of the human Pregnane X Receptor.** LBD in complex with colupulone bound to the ligand binding pocket (LBP), highlighting different regions of interest. The α-helices are shown in magenta and β-strands are in cyan. PXR heterodimerizes with RXR through the interface formed at α5, α9 and α10 helices. The AF2-surface, formed with αAF (known as activation function-2 helix), that facilitates the interaction with transcriptional coactivators and corepressors, is also labeled. The flexible loop region between α1 and α3 helices is highlighted in green color (Chandran & Vishveshwara, 2016).

1.5. Pregnane X receptor (PXR)

1.5.1. General Characteristics

The pregnane X receptor (PXR; NR1I2), identified in 1998, has been established as a xenosensor and master regulator of xenobiotic responses (Gao & Xie, 2010; Ma *et al*., 2008). It is also known as steroid and xenobiotic receptor (SXR), as it was identified by different research teams independently in mouse and in human (Willson & Kliewer, 2002). PXR is expressed predominantly in the liver, specifically in the hepatocytes and Kupffer cells (Haughton *et al*., 2006; Wright, 2006) and in the intestine (**Figure 3**), which are important organs involved in the absorption, distribution, metabolism and elimination of potentially harmful xenobiotics and endobiotics (Gao & Xie, 2010; Ihunnah *et al*., 2011; Ma *et al*., 2008). It is also expressed in the lungs, bone marrow and the brain (Lamba *et al*., 2004). PXR has the capacity to recognize a large spectrum of ligands due to its wide and flexible binding pocket (Timsit & Negishi, 2007). It is activated by exogenous chemicals and endogenous metabolites and controls the transcription of xenobiotic metabolizing enzymes (XMEs) when activated by its ligand (Bookout *et al*., 2006; Honkakoski, Sueyoshi, & Negishi, 2003; Ma *et al*., 2008a). Moreover, its role in energy metabolism is now increasingly recognized.

1.5.1.1. Structure

Similar to other NRs, PXR is composed of an N-terminal nuclear receptors (AF1), a DNA binding domain (DBD), a ligand binding domain (LBD) binding domain, and a C-terminal activation domain (AF2) (**Figures 1 and 4**). PXR is activated by a wide variety of ligands of various structures due to several hallmark features: (1) a small number of polar residues spaced through a smooth, hydrophobic large ligand-binding domain (LBD), (2) a

Compounds	Category	Species	References
Ketoconazole			
Dexamethasone	Anti-inflammatory agent	Human, Rabbit, Rat	Ihunnah *et al.,* 2011; Ma *et al*., 2008; Jones *et al*., 2000
Acetaminophen			
Rifampicin	Antibiotic	Human, Rabbit	Ihunnah *et al.,* 2011; Ma *et al*., 2008; Jones *et al*., 2000, Hernandez *et al*, 2009
Rifaximin		Human	Ihunnah et al., 2011
Clotrimazole	Antibiotic	Human, Rabbit, Rat	Ihunnah *et al.,* 2011; Jones *et al*., 2000
Metyrapone	Anti-hypercortisolism drug	Human	Ihunnah *et al.,* 2011
Ritonavir	Antibiotic	Human	Ma *et al*., 2008
Paclitaxel	Chemotherapeutic		
Taxol	Chemotherapeutic		
Pregnolone-16a-carbonitrile (PCN)	Anti-glucocorticoid drug	Mice, Rat	Ihunnah *et al.,* 2011; Ma *et al*., 2008; Hernandez *et al*, 2009
Progesterone	Steroid		
Ethinylestradiol	Steroid		
Cyclophosphamide	Antineoplastic drug	Human	Ma *et al*., 2008
Cyproterone acetate	Antineoplastic drug	Human	Ma *et al*., 2008
Taxol	Antineoplastic drug	Human	Ma *et al*., 2008
Tamoxifen	Antineoplastic drug	Human	Ma *et al*., 2008
RU486	Antineoplastic drug	Human, Rabbit, Rat	Ma *et al*., 2008; Jones *et al.,* 2000
Troglitazone	Anti-diabetic drug	Human	Ma *et al*., 2008
Lovastatin	Anti-hypertensive drug	Human	Lehmann *et al.,* 1998 ; Ihunnah *et al.,* 2011
Nifedipine	Anti-hypertensive drug	Human	Ma *et al*., 2008
Spironolactone	Anti-hypertensive drug	Human, Rabbit, Rat	Ma et al., 2008; Jones *et al*., 2000
Glutethimide	Sedative	Human	Ma *et al*.,2008
Phenobarbital.	Sedative	Human, Rabbit, Rat	Ma *et al*., 2008; Jones *et al.,* 2000
Piper methysticum (chloraseptic)	Chloraseptic (Herbal medicine)	Human	Ihunnah *et al.*, 2011
Schisandra chinensis	Anti-perspiration (Herbal medicine)	Human	Ihunnah *et al.*, 2011
Agauria salicifolia	Arrhythmia (Herbal medicine)	Human	Ihunnah *et al.*, 2011
St. John's Wort	Herbal medicine	Human	Ma *et al*.,2008
Gugulipid®	Herbal medicine	Human	Ma *et al*.,2008
Kava kava		Human	Ma *et al*.,2008
nutritional compounds flavonoids	Herbal medicine		
Vitamin E	Dietary Supplement	Human	Ma *et al*., 2008
Vitamin K_2	Dietary Supplement	Human	Ma *et al*., 2008
Organochlorine pesticides	Pesticides (Environmental pollutant)	Human	Ma *et al*., 2008
1,1,1-trichloro-2,2-bis(*p*-chlorophenyl)ethane (DDT)	Pesticide	Human	Ihunnah *et al*., 2011
di-n-butyl phthalate (DBP)	Plasticizer		Ihunnah *et al*., 2011
Chlordane	Pesticide	Human	Ihunnah *et al*., 2011
Dieldrin	Pesticide	Human	Ihunnah *et al*., 2011
Endosulfan	Pesticide	Human	Ihunnah *et al*., 2011
Bisphenol analogs (BPA)	Plasticizer		
Polychlorinated biphenyls (PCBs)	Environmental pollutant		
Dethylhexyl phthalates (DHEP)	Plasticizer		
Organochlorides	Environmental pollutant		
Trans-nonachlor	Pesticide	Rabbit, Rat	Jones *et al.,* 2000
Chlordane	Pesticide		
Polybrominated diphenyl ether	Flame retardant	Human	Ma *et al*., 2008
Bile acid precursors	Endobiotic	Human	Ma *et al*., 2008
Estrogens	Endobiotic	Human	Ma *et al*., 2008
Progestogen	Endobiotic	Human	Ma *et al*., 2008

Table 1. List of PXR ligands

flexible loop which may be responsible for PXR's ability to bind ligands of different sizes, and (3) its ability to use only a portion of its pocket to bind and in turn, be activated by ligands, allowing for PXR to serve as a more promiscuous receptor unlike other nuclear receptors (Hernandez, Mota, & Baldwin, 2009).

1.5.1.2. Ligands

PXR ligands are structurally diverse and include prescription drugs, herbal medicines, dietary supplements, environmental pollutants, and endobiotics (**Table 1**). Therefore, it may be considered as an adopted orphan that recognizes a number of endobiotic and xenobiotic chemicals (Garcia *et al*., 2018; Hernandez *et al.*, 2009). Among these ligands, the catatoxic steroid pregnenolone 16α-carbonitrile (PCN), was first known to induce the transcription of *CYP3A*, which metabolizes most prescription drugs (Kliewer, 2015). PCN robustly induces *CYP3A* in rodent but not human hepatocytes. Conversely, rifampicin induces *CYP3A* in human but not rodent hepatocytes. These species-specific differences are due to 76% similarity on the ligand-binding domains of mPXR vs hPXR, which is much lower than the identity between orthologs of other nuclear receptors. This divergence provided the first hint that mouse and human PXR may have distinct pharmacologic activation profiles. Thus, PCN is considered a rodent-specific PXR ligand (Ma *et al.*, 2008a) while Rifampicin is the prototypical pharmaceutical ligand used in human studies. PXR activation regulates a large network of genes involved in the metabolism and transport of xenobiotics.

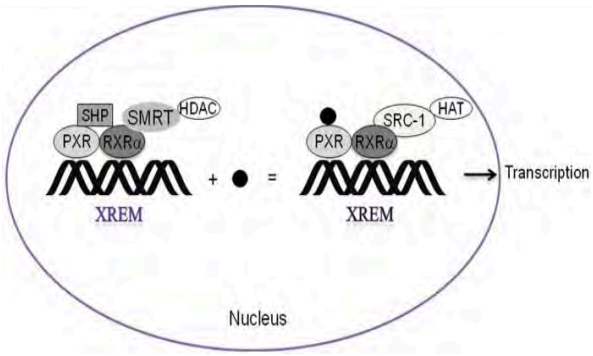

Figure 5. Activation of PXR. Ligand (●) activation of PXR triggers the release of co-repressors and histone deacetylases, and the subsequent interaction of PXR with co-activators and histone acetylases, leading to transcription of target genes(Hernandez *et al*., 2009).

1.5.2. Activation

As illustrated in **Figure 5**, the classical mechanism of activation of PXR involves the binding of a ligand specific to its LBD, modification of the conformation of the receptor and the transition from an inactive state to an active state. When bound to and activated by a ligand, PXR translocates from the cytoplasm to the nucleus of the cells and forms a heterodimer with the RXR that binds to PXR response elements, located in the 5′-flanking regions of PXR target genes, thereby activating the transcription of target genes. PXR is also capable of recruiting a host of coactivators which includes members of the p160 family of coactivators such as SRC-1, transcriptional intermediary factor (TIF)/glucocorticoid receptor interacting protein (GRIP) (SRC-2), and PGC-1α (Ihunnah *et al*., 2011).

1.5.3. Target genes

PXR primarily induces the transcription of the cytochromes P450 CYP3A family such as *CYP3A4* and *3A7*, but the prototypical target gene of PXR in humans is *CYP3A4* (Goodwin *et al*., 1999). *CYP3A4 i*s the most abundant of the P450s expressed in the liver, and participates in the metabolism of more than 50% of marketed drugs, and some endogenous substrates such as steroids and bile acid (Ma *et al*., 2008; Tolson & Wang, 2010). PXR shares a vast amount of target genes with the nuclear receptor CAR among them *CYP2B6, CYP2C8* and *2C9* (Hernandez et al., 2009), glutathione S transferase (GSTA1), sulfotransferase (*SULT2A1)*, UDP glucuronosyltransferase (*UGT1A1)*. PXR activation also upregulates transporter genes such as the *MDR1* gene that encodes the P-glycoprotein, organic anion transporting polypeptide-2 (*OATP2*) and multidrug resistance-related protein-3 (*MRP3*). Due to the role of PXR in regulation of metabolic enzymes and transporters, PXR activation therefore extensively affects the fate of xenobiotics (Ma *et al*., 2008). A summary of the

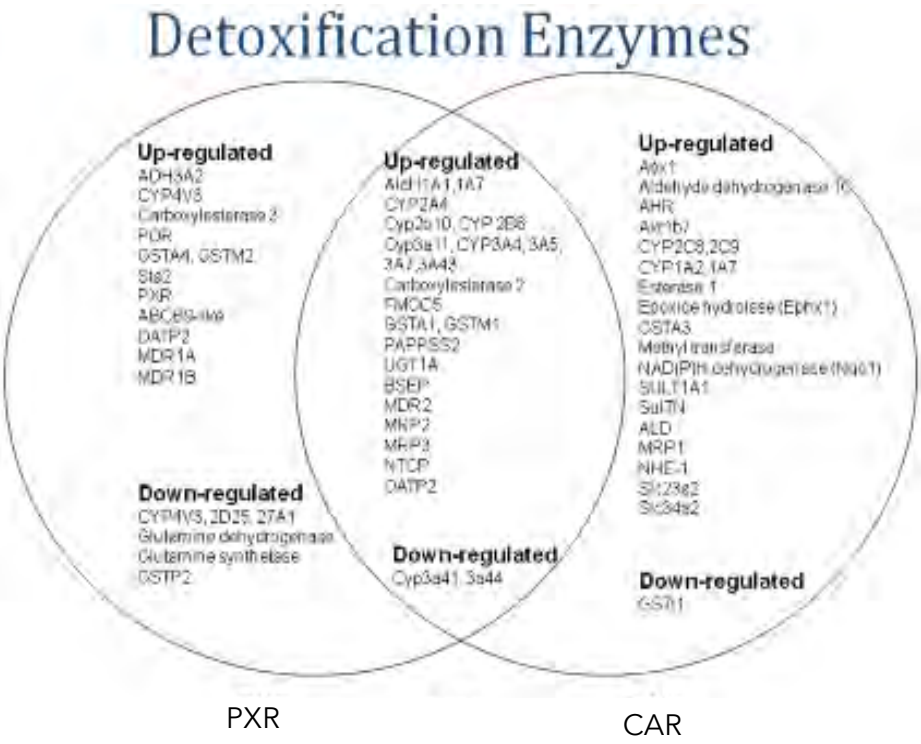

Figure 6. PXR target genes. A summary of both human and mouse PXR encoded target genes for detoxification enzymes (Hernandez *et al*., 2009).

regulated genes in human and mouse is listed in **Figure 6.**

1.5.4. Experimental models

High-throughput *in vitro* PXR activation and binding assays have been used to identify PXR ligands. Primary cultures of human hepatocytes have also been frequently utilized to study PXR activation and PXR target gene regulation, and for prediction of drug-drug interactions. However, there are limitations of extrapolating from *in vitro* findings to the clinical situation *in vivo* and several animal models complement to evaluate the functions of PXR in a whole animal system (Ma *et al.*, 2008b).

The *Pxr*-null mouse model was generated by disrupting the mouse *Pxr* gene by homologous recombination and did not display any overt phenotypic abnormalities, suggesting that PXR is not essential for mouse development or physiological homeostasis. The first described *Pxr*-null mice were confirmed to be fertile and viable with PXR expression absent in both the liver and intestine (Xie *et al*., 2000). Thus, the *Pxr*-null mouse was validated as a reliable model to identify PXR-dependent signaling pathways. Recently, liver- and intestine-specific *Pxr*-deletion models have been published that allowed to unravel organ-autonomous functions of *Pxr* (Gwag *et al.*, 2019; Meng *et al.*, 2019).

PXR-humanized mouse models provided a solution to the problem of species differences in ligand specificity. So far, three different humanized mouse models have been created that aimed to delete the mPxr and replace it with the hPXR either at the whole organism level or in a liver-specific way: the Alb-hPXR mice (produced by use of a cDNA), BAC-hPXR (generated with a bacterial artificial chromosome (BAC)), and the P-hPXR (the human PXR protein was fused to a viral VP16 coactivator). **The Alb-hPXR mice** was bred into a PXR-null background, and the resulting PXR-null/SXR-transgenic mice lacked mouse PXR

gene but had human SXR transgene (Xie *et al.*, 2000). In the hPXR mouse model, *PXR* was selectively expressed in the liver and intestine, the same tissue expression pattern as *CYP3A*. Both models were developed in the *Pxr*-null mouse background and responded to the human-specific PXR ligand rifampicin but not the rodent-specific *Pxr* ligand PCN. The notable differences between first 2 models is driven by heterologous promoter that yields liver-specific expression, while the BAC transgene, containing the complete PXR gene, is under control of the native human PXR promoter. This distinction is quite important since PXR is also expressed in the gut where it can influence the metabolism and transport of drugs. (Ma *et al.,* 2008). **VP-hPXR** (the human PXR protein was fused to a viral VP16 coactivator). VP-hPXR was expressed in the liver and throughout the intestinal tract, including the duodenum, jejunum, ileum, cecum, and colon. In contrast, the expression of hPXR was undetectable in the stomach and kidney. The tissue distribution of transgene expression was similar to that of endogenous mouse PXR (mPXR), although the relative expression of the transgene was higher in the cecum and colon (Gong *et al*., 2006).

1.5.5. Physiological functions

1.5.5.1. Drug-drug interaction

The identification of PXR revealed a molecular mechanism for many drug-drug interactions. When two or more drugs are combined, and one is a PXR ligand, and others are the substrates of PXR target gene encoded enzymes or transporters, drug-drug interactions can occur consequently leading to decreased therapeutic efficacy. This is for example illustrated by decreased Rifampicin efficacy to cyclosporin in patients simultaneously taking either oral contraceptives, midazolam for dental extractions, anti-HIV protease inhibitors, and St. John's Wort (a herbal medicine used for mental disorders and

simultaneously taking either oral contraceptives, midazolam for dental extractions, anti-HIV protease inhibitors, and St. John's Wort (a herbal medicine used for mental disorders and nerve pain) to cyclosporine (Zhang, Xie, & Krasowski, 2008).

1.5.5.2. Lipid Metabolism

Lipogenesis. Transgenic mice expressing a constitutively activated PXR showed hepatomegaly and marked hepatic steatosis, and treatment of mice with a PXR agonist elicited a similar effect. PXR-induced lipogenesis was independent of the activation of *SREBP-1c* and was associated with the induction of fatty acid translocase (*FAT/CD36),* peroxisome proliferator-activated receptor γ2 (PPARγ2), and *Scd1* (Gao & Xie, 2010; Zhou *et al*., 2008) and long-chain free fatty acid elongase (Ma *et al*., 2008).

Lipid oxidation. In mice, activation of PXR by its agonist PCN can inhibit lipid oxidation by down-regulating the mRNA expression of carnitine palmitoyltransferase1α (*CPT1α)* and mitochondrial 3-hydroxy-3-methylglutarate-CoA synthase 2 (*HMGCS2*), two key enzymes involved in β-oxidation and ketogenesis, in a PXR-dependent manner (Gao & Xie, 2010).

1.5.5.3. Glucose Metabolism

Hepatic gluconeogenesis. The regulation of the gluconeogenic pathway by PXR was initially suggested by the suppression of phosphoenolpyruvate carboxykinase (*PEPCK)* and glucose-6-phosphatase (*G6Pase)* in VP-hPXR transgenic mice (Zhou *et al*., 2006). Treatment of wild-type mice with the PXR agonist PCN also suppressed cyclic adenosine monophosphate (cAMP)-dependent induction of G6Pase in a PXR-dependent manner (Kodama *et al.*, 2004) where PXR can form a complex with phosphorylated cAMP response

element-binding protein (CREB) in a ligand-dependent manner to prevent CREB binding to the cAMP (Gao & Xie, 2010).

PXR can also physically bind to Forkhead box O1 (FoxO1) and suppress its transcriptional activity by preventing its binding to the insulin response sequence in the gluconeogenic enzyme gene promoters (Kodama et al., 2004). PXR and CAR may also inhibit hepatocyte nuclear factor-4α (HNF4α) activity by competing for the DR1 (direct repeat spaced by one nucleotide) binding motif in the gluconeogenic enzyme gene promoters (Miao *et al*., 2006).

1.5.5.4. Bilirubin Detoxification

Bilirubin, the breakdown product of heme proteins, conjugates with UGT converting the neurotoxic unconjugated bilirubin to nontoxic bilirubin glucuronide. Xie *et al.* (2003) reported that activation of PXR prevented experimental hyperbilirubinemia in mice. PXR activates the transcription of *UGT1A1* and several other genes critically involved in bilirubin detoxification, such as *OATP2* and *MRP2*. *OATP2* mediates bilirubin uptake from blood into liver, whereas multidrug resistant protein (*MRP2)* facilitates the excretion of conjugated bilirubin to bile canaliculus. Ihunnah *et al*. (2011) therefore reports that PXR ligands may represent potential therapeutic agents in treating hyperbilirubinemia.

1.5.5.5. Bile Acid Regulation and Detoxification

Bile acids, synthesized in the liver via the primary pathway for cholesterol elimination, are end products of cholesterol catabolism. They are produced in the liver from cholesterol *via* multiple enzyme-dependent steps with the rate-limiting step being 7-hydroxylation of cholesterol by *CYP7A1*. Upon cholesterol entry in the intestine, bile acids

promote its absorption of and that of fat-soluble vitamins. However, when cholesterol synthesis becomes dysregulated, excess bile acids become cytotoxic and can lead to pathological cholestasis. Therefore, bile acid levels need to be tightly regulated to protect the human body from their toxic effects (Ihunnah *et al.,* 2011). Studies have established that PXR regulates several detoxification enzymes and transporters important to bile acid metabolism including *Cyp2b10 and Cyp3a11*, *Sult2a1*, dehydroepiandrosterone sulfotransferase (*STD*), *Mrp 2,3,4*, and *Oatp2* (Hernandez et al., 2009). In humans, positive regulation of *SULT2A1* gene expression by FXR and PXR may play a central role in regulating bile acid sulfation in conjunction with the constitutive androstane receptor (CAR) (Garcia *et al*., 2018). Staudinger et al. (2001) have also reported that ligand activated PXR reduced the expression of *Cyp7a1* without affecting *Shp* expression in mice. However, hPXR can regulate SHP expression directly in HepG2 cancer cells . (Frank *et al*., 2005). PXR has also been reported as an FXR target gene (Garcia *et al*., 2018; Jung *et al*., 2006). Finally, treatment of mice with PCN is known to alleviate the lithocholic acid-induced hepatotoxicity (Staudinger *et al*., 2001; Xie *et al*., 2003). Altogether, these results suggested the link between PXR and FXR in protecting the human body from bile acid toxicity.

1.5.5.6. Inflammation

Numerous studies have suggested a negative correlation between infectious disease/inflammation and drug metabolism capacity that would involve PXR. Teng & Piquette-Miller (2005) showed that IL6-treated wild type mice decreased PXR protein levels, and its target genes' expression of *Mrp2, Bsep,* and *Cyp3a11*. A (2002) revealed that lipopolysaccharide (LPS) challenge induced the acute phase response in mouse liver and caused a significant decrease in the mRNA expression of *Pxr* and its

target genes. In rifampicin-treated patients, immunosuppression is expected. Zhou *et al*. (2006) further elucidated *in vitro* and *in vivo* that the attenuation of nuclear factor κ B (NF-κb) proteins may be due to PXR activation by rifampicin. NF-κb proteins are important in facilitating immune response and inflammation suggesting that basal PXR activity is integral to proper mucosal health (Terc *et al*., 2014).

1.5.5.7. Regulation of intestinal mucosal homeostasis and intestinal permeability

A rapidly increasing amount of studies have also demonstrated that PXR may play a role in regulating intestinal mucosal homeostasis. PXR has been implicated to regulate similar cellular processes in intestinal epithelial cells (IECs) and hepatocytes, initiating the transcription of genes related to metabolism and detoxification, as well as the regulation of additional processes in non-IEC systems; the regulation of cell migration, cell survival, apoptosis, and autophagy. PXR's interaction with signaling cascades like p38 mitogen-activated protein kinases (MAPKs), c-Jun N-terminal kinases (JNKs1/2) and 5' adenosine monophosphate-activated protein kinases (AMPKs), has basically linked it to key functions of IECs that contribute to intestinal mucosal barrier function (Ranhotra *et al*., 2016). Other studies using animal models of intestinal bowel disease have reported that the selective activation of PXR attenuates colonic inflammation and tissue damage (Dou *et al*., 2013; Ma *et al*., 2007; Shah *et al*., 2007; Terc *et al*., 2014), while others have shown that PXR activity attenuates inflammation-induced barrier dysfunction and accelerates mucosal healing after a bout of colitis (Terc *et al*., 2014; Venkatesh *et al*., 2014).

Intestinal microbial metabolites are conjectured to affect mucosal integrity through mechanisms that have yet to be fully understood. Venkatesh *et al*. (2014) showed that

microbial-specific indoles regulated intestinal barrier function through PXR. Indole 3-propionic acid (IPA), a PXR ligand *in vivo*, downregulated enterocyte tumor necrosis-α (TNF-α) while it upregulated junctional protein-coding mRNAs. Furthermore, PXR-deficient mice showed a distinctly "leaky" gut physiology coupled with upregulation of the toll-like receptor (TLR) signaling pathway demonstrating the direct chemical communication between the intestinal symbionts and PXR, thereby regulating mucosal integrity through a pathway that involves luminal sensing and signaling by TLR4.

1.6. Constitutive androstane receptor (CAR)

1.6.1. General Characteristics

The Constitutive Androstane Receptor (CAR) or (NR1i3) has been cloned for the first time in 1994 and named MB67 by the Baes team (Baes et al., 1994). They demonstrated that it is essentially expressed in the liver and its LBD has been fused with the DNA binding domain by the thyroid hormone receptor (TRβ) and with a plasmid containing the response elements to TRβ. The authors have also shown that, even in the absence of an exogenous ligand, this construction was still able to activate a reporter gene under the control of the response elements of TRβ. Therefore, CAR was shown to be active in a constitutive manner and is capable of heterodimerization with RXR.

Between 1997 and 1998, the characterization in the murine form of the receptor showed the capacity to form a heterodimer with RXR and binds to the response elements of the retinoic acid (RARE) even in the absence of an exogenous ligand (Choi *et al.*, 1997). The authors named this receptor “Constitutive Androgen Receptor”. It is identified in two isoforms: CAR1 and CAR3 which differ by their LBD. CAR3 is truncated to one part of the

Compound	Species	Reference
Perfluorocarboxylic acid, PFCA (detergent)	Mouse	Abe et al., 2017; Cheng & Klaassen, 2008
Perfluorooctanoic acid, PFOA (detergent)	Mouse	Kawamoto *et al*., 2000; Oshida *et al*., 2015
Perfluorooctanesulfonic acid, PFOS (detergent)	Rat	Elcombe et al., 2012
Alachlor (pesticide)	Mouse	Baldwin & Roling, 2009
Arsenite (chemical)	Mouse	Baldwin and Roling, 2009
Azoic colorants (paint)	Mouse Rat	Pakharukova *et al.*, 2007
Bisphenol A (chemical)	Mouse	Baldwin and Roling, 2009
Butylate (pesticide)	Mouse	Baldwin and Roling, 2009
Chlorpropham (pesticide)	Mouse	Baldwin and Roling, 2009
Chlorpyriphos (pesticide)	Mouse	Baldwin and Roling, 2009
Cypermythrin (pesticide)	Mouse	Baldwin and Roling, 2009
Cyproconazole (pesticide)	Mouse	Peffer *et al.*, 2007
Di-n-butylphthalate, DBP (plastifiant)	Rat	Wyde *et al.*, 2005
Dichlorodiphenyldicholorethylene, DDE (pesticide)	Mouse	Wyde *et al.*, 2003
Di-isonyl phthalate, DiBP (plastifiant)	Human	Laurenzana *et al.*, 2016
O, p-DDT,1, 1, 1-Trichloro-2-(2-chlorophenyl)-2-(4-chlorophenyl)ethane (pesticide)	Mouse Rat	Sueyoshi *et al.*, 1999; Wyde *et al.*, 2003
DEHP (plastifiant)	Human Mouse	Baldwin and Roling, 2009; DeKeyser *et al.*, 2009
Dieldrine (pesticide)	Mouse	Wei *et al.*, 2002
Endosulfan (pesticide)	Human Mouse	Baldwin and Roling, 2009; Savary et al., 2014
Fernitrothion (pesticide)	Mouse	Baldwin and Roling, 2009
Polycyclic aromatic hydrocarbons	Mouse	Zhang *et al.*, 2015
Imazalil (pesticide)	Mouse	Baldwin and Roling, 2009
Kepone (pesticide)	Mouse	Baldwin and Roling, 2009
MEHP (plastifiant)	Mouse	Baldwin and Roling, 2009
Metolachlor (pesticide)	Mouse	Baldwin and Roling, 2009
Methoxychlor (pesticide) and metabolites	Human Mouse Rat	Baldwin and Roling, 2009; (Blizard *et al.*, 2001); Savary et al., 2014
Monosodium methane arsenate	Mouse	Baldwin and Roling, 2009
Nonylphenol (plastifiant)	Human	Hernandez *et al*., 2007)
Parathion (pesticide)	Mouse	Hernandez *et al.*, 2007
Polchlorobiphenyls, PCB (derived chemicals)	Mouse	Sueyoshi *et al.*, 1999
Propachlor (pesticide)	Mouse	Baldwin and Roling, 2009
2, 3, 7, 8-Tetrachlorodibenzo-p-dioxin (TCDD)	Mouse	Prokopec *et al.*, 2015
SSS-Tributylphoshorotithioate (pesticide)	Mouse	Baldwin and Roling, 2009
Valproic acid	Human	Cerveny et al., 2007
Acetaminophene	Mouse	Zhang *et al.*, 2002; Zhang *et al.*, 2004
Antifungal triazoles	Mouse	Goetz *et al.*, 2006; Peffer *et al.*, 2007
Artemisinine	Human Mouse	Burk *et al.*, 2005; Swales & Negishi, 2004
Benzodiazepines	Human	Li *et al.*, 2008
Clotrimoxazole	Human	Moore *et al.*, 2000
Cocaine	Human	Malaplate-Armand *et al.*, 2005
Dexamethasone	Human	Pascussi *et al.*, 2000; Qatanani, Wei, & Moore, 2004
Ketoconazole	Human	Duret *et al.*, 2006
Meclizine	Human Mouse	Huang *et al.*, 2004
Metamizole	Human	Saussele et al., 2007
Methotrexate	Mouse	Chen *et al.*, 2006; Shibayama *et al.*, 2006
Orphenadrine	Rat	Murray *et al.*, 2003
Phenobarbital	Mouse Rat	Currie *et al.*, 2014; Li *et al.*, 2017
Phenytoin	Human	Jackson *et al.*, 2004; Wang *et al.* et al., 2004
Statines	Human	Howe *et al.*, 2011

Table 2. Activators of CAR

region C-terminal and cannot bind to the DNA nor can it form a heterodimer with RXR. The murine form of CAR1 possesses an independent ligand-binding trans-activator.

The tissue distribution of CAR is the same in both human and mice. It is strongly expressed in the liver and intestine (Wei *et al.*, 2002; Xu *et al.*, 2005). Lower mRNA levels are found in the heart, muscles, kidneys, lungs and the brain. At the hepatic level CAR is highly expressed around the centrilobular vein.

1.6.1.1. Structure

In the human liver, 2 isoforms have been identified: CAR1 and CAR3 (Auerbach *et al.*, 2005) that possess respectively 4 or 5 more amines in their LBD. This insertion could modify the structure of the ligand binding pocket and, thus, accommodates different ligands for CAR. CAR possesses a typical structure of nuclear receptors, although the studies show a particularity to this receptor: its ligand pocket is smaller than others, 500 Ä, compared to 1200 Ä for PXR and 990 Ä for VDR, which limits the number of potential ligands (Suino *et al.*, 2004).

1.6.1.2. Ligands

In 1998, Forman's research paved way to the identification of two endogenous ligands, androstanol and androstenol acting like inverse agonists. The LBD possesses a conformation even in the absence of a ligand, however in the presence of an inverse agonist, this conformation is lost. This receptor is the first example of a transcription factor regulated negatively by an endogenous ligand (Forman *et al.*, 1998). Listed in **Table 2** are ligands of CAR. CITCO is the prototypical pharmaceutical ligand of CAR for *CYP2B6*

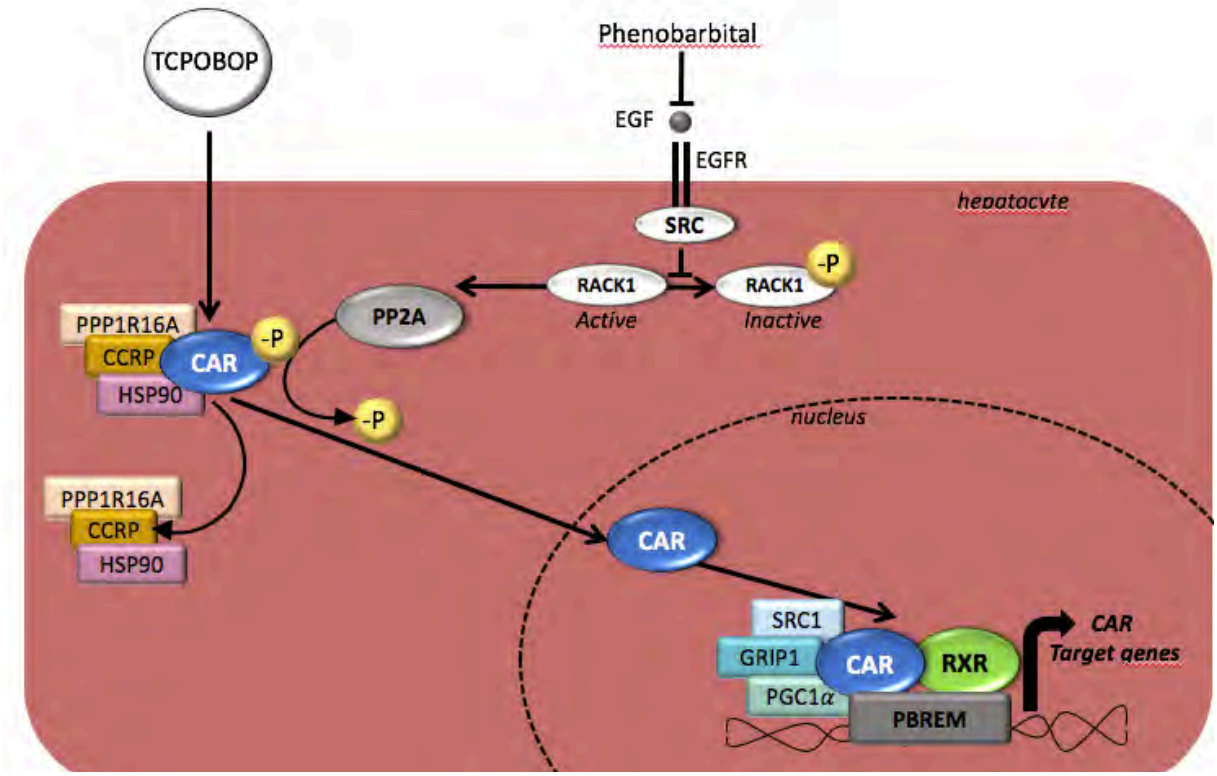

Figure 7. Direct activation (TCPOBOP) and indirect activation (Phenobarbital) of the constitutive androstane receptor (CAR). The fixation of TCPOBOP in the ligand binding pocket of CAR allows the recruitment of phosphatase protein 2A (PP2A) and the dephosphorylation of CAR ant the liberation of its cytosolic retention complex (PPP1R16A, CCRP, HSP90). CAR translocates in the nucleus, forms a heterodimer with RXR and recruits different co-activators (SRC-1, GRIP-1,PGC-1α). Phenobarbital prevents the fixation of EGF (Epidermal Growth Factor) on its receptor EGFR, SRC kinase cannot anymore phosphorylate protein kinase RACK1, RACK1 activates PP2A, which results in the dephosphorylation of CAR.

CCRP: cytoplasmic CAR retention protein, EGF: Epidermal Growth Factor, EGFR: Epidermal Growth Factor Receptor, GRIP-1, Glutamate Receptor Interacting Protein 1, HSP90: heat shock protein 90, PBREM: phenobarbital (PB)-responsive enhancer module, PGC-1: PPARγ coactivator-1, PP2A: protein phosphatase2 (isoformα), PPP1R16A: protein phosphatase 1 regulatory subunit 16A , RACK1: Receptor for Activated C Kinase 1, RXR: retinoid X receptor, SRC: steroid receptor coactivator: ,SRC-1: steroid receptor coactivator-1, TCPOBOP: 1,4-Bis[2-(3,5-dichloropyridyloxy)]benzene.

expression in humans, while TCPOBOP is the prototypical pharmaceutical ligand for *Cyp2b10* expression in murine models.

1.6.2. Mechanisms of activation

CAR possesses certain particularities which differentiates it from the other NRs. One of this particularity is the localization in the cytoplasm in an active conformation forming a complex of different chaperone proteins: cytoplasmic CAR retaining protein (CCRP), HSP90, and the membrane subunit of protein phosphatase 1β (Kobayashi *et al.*, 2003; Sueyoshi *et al*., 2008; Yoshinari *et al.*, 2003). In addition, it has the capacity to be active in an indirect or direct manner (**Figure 7**). Once active, it migrates to the nucleus. After its heterodimerization with its partner, RXR, CAR can link to its response elements of type DR4 or DR5 (Direct repetitive separate sequence 4 to 5 nucleotides) named PBREM (phenobarbital response element module). These PBREMs are situated on the promoters of the target genes of CAR, like *CYP2B6*, the human prototypical target gene or *Cyp2b10*, the murine prototypical target gene in murine form (Mäkinen *et al.*, 2002).

1.6.2.1. Direct Activation

The fixation of a synthetic agonist ligand such as TCPOBOP (murine form) or CITCO (human form) in the ligand binding pocket induces CAR nuclear translocation (Tzameli *et al.*, 2000). This transformation solicits the recruitment of the protein phosphatase A2 (PP2A) in charge of the dephosphorylation at the threonine level 38 (human form) or 48 (murine form) of CAR (Mutoh *et al*., 2009) and of its liberation of the cytosolic complex (Tatsuya Sueyoshi *et al*., 2008; Yoshinari *et al*., 2003). Freed from its complex, CAR migrates to the nucleus after heterodimerization with RXR and recruits different co-activators allowing its

interaction with the transcriptional machinery. GRIP-1) PGC-1α and SRC-1 are the co-activators allowing initiation of the transcription of the target genes of CAR (Min *et al*., 2002; Wright *et al.*, *2007*). The co-repressors prevent the fixation of these co-activators. Thus, the small heterodimer partner interacting leucine zipper protein (SMILE) can enter in competition with other co-activators for the recruitment of histones, deacetylases (Xie, *et al*., 2009). CAR can also interact with other co-repressors such as NCoR, SMRT, small heterodimer protein (SHP) and dosage-sensitive sex reversal, adrenal hypoplasia critical region, on chromosome X, gene 1 (DAX1) modulating its transcriptional activity (Bae *et al*., 2004; Laurenzana *et al*., 2012.; Lempiäinen *et al*., 2005).

1.6.2.2. Indirect Activation

CAR can also be activated by endogenous or exogenous molecules via the stimulation of the translocation without direct binding to the ligand binding pocket. Such is the case of phenobarbital which induces the transcriptional activity of CAR through the induction of its nuclear translocation. The cytoplasmic retention of CAR is due to the phosphorylation initiated by the kinase C protein *(*Mutoh *et al.*, 2009). The phenobarbital enters in competition with the epidermal growth factor (EGF) compared to the fixation by its receptor EGFR. Thus, it prevents the activity of kinase Src, inducing the dephosphorylation of the receptor of protein C kinase 1 (RACK1). RACK1 activates PP2A which results into the dephosphorylation of CAR by PP2A and its nuclear translocation (Mutoh *et al.*, 2009). A new signaling path controlling the activity of CAR has been identified by the team of Negishi. It interacts to the signalization cascade of mitogen activated protein kinase kinase/extra-cellular signal regulated kinase (MEK/ERK). Immunoprecipitation experiments showed an interaction between CAR and ERK1/2 in Hugh-7 cells. This interaction prevents the

Type	Mice	Human
Phase I	*Cyp1a1, Cyp1a2,Cyp2a4, Cyp2b10, Cyp2c29, Cyp2c37, Cyp2c55, Cyp3a11, Nqo1, Aldh1a1, Aldh1a7, Akr1b7, Ces6*	*CYP1A1,CYP1A2, CYP2B6, CYP2C8, CYP2C9, CYP2C19, CYP3A4, CYP3A5*
Phase II	*Ugt1a1, Ugt1a9, Ugt2b34, Ugt2b35, Ugt2b36, Sult1e1, Sult2a1, Sult2a2, Sult3a1, Sult5a1, Gsta1, Gsta4, Gstm1, Gstm1, Gstm2, Gstm3, Gstm4, Gstp, Gst1*	*UGT1A1, SULT2A1*
Transporters	*Mrp2, Mrp3, Mrp4, Oatp1a4*	*MDR1*

Table 3. Target genes of CAR in the different phases of detoxification.

dephosphorylation of CAR and thus explains the nuclear translocation. The activation of p38 mitogen-activated protein kinase by anisomycin increases the expression of CAR target genes, *CYP2B6 c*ertifying its activities in HepG2 cells (Saito *et al.*, 2013) Thus, the growth hormones and cytokines have an equal impact on the expression of CAR target genes.

In cases of energetic depletion, the protein kinase activated by adenosine monophosphate (AMP), AMPK is activated, thus the AMP/ATP ratio increases. This enzyme then proceeds to initiate catabolic pathways after the generation of ATP (Hardie & Ashford, 2014). *In vivo,* the activator of AMPK induces the nuclear translocation of CAR but fails to induce the expression of its target genes (Shindo *et al.*, 2007). Other studies also show that metformin, an activator drug of AMPK can remove the induction of CAR target genes by modulating the phosphorylation of CAR. Yang *et al*. (2014) have shown that metformin phosphorylates CAR through AMPK and ERK1/2 and prevents its translocation. Although the precise role of AMPK in the activation of CAR remains controversial, research shows the importance of the physiological status for the control of CAR activation.

1.6.3. Target genes

Table 3 presents target genes of CAR involved in the different phases of detoxification. CYP2B6 is the prototypical target gene in humans, while Cyp2b10 in mice.

1.6.4. Sexual dimorphism

The link of CAR to sex hormones is strong and numerous elements in the literature report an important sexual dimorphism that relates to CAR activity. A number of studies have already shown that CAR is more expressed and more active in females than in males. Thus, female mice treated with TCPOBOP present a higher induction of CAR target genes

compared to males (Ledda-Columbano *et al.*, 2003; Lu *et al.*, 2013). The same observation has been made in humans after treatment with phenobarbital (Weghorst & Klaunig, 1989). Basal CAR expression is also higher in females compared to males (Petrick & Klaassen, 2007). Basal CAR activity is also higher in females: the constitutive expression of *Cyp2b* mRNA in the liver of mice in the prepubertal stage was demonstrated to be sex-independent and the expression of *Cyp2b9* was diminished markedly only in males during the maturation stage, resulting in a sexually dimorphic expression in adult mice (Jarukamjorn, Sakuma, & Nemoto, 2002). Functional studies confirmed these results using Zoxazolamine, a myorelaxant, a known substrate for CAR-target CYPs. Upon treatment, an increase in the time of paralysis signifies an inhibition of CYPs, while a decrease signifies an increase of CYP activity. Female mice deficient in CAR ($Car^{-/-}$) are more resistant than males presenting a shorter paralysis time. In addition, none of the female $Car^{-/-}$ mice died after treatment while in male $Car^{-/-}$ mice, 5 out of 6 did not recover from the paralysis (Hernandez *et al.*, 2009). These phenotypes could be explained by the inhibition of CAR activity in males by metabolites from testosterone like androstanol, which is identified as inverse agonists of CAR. It could also be explained by the effect of CAR activation by estrogens reported in certain studies (Kawamoto *et al.*, 2000). This difference could be explained by a more significant CAR activity by the nuclear receptor HNF4α in females (Kamiyama *et al.*, 2007). This nuclear receptor is involved in the dimorphic regulation of the basal expression of CYPs (Holloway *et al.*, 2008). Numerous data on human and mice suggest that HNF4α regulates the expression of CAR (Wiwi *et al.*, 2004; Wortham *et al.*, 2007).

Reciprocally, CAR seems to play an important role in the status of androgens in the liver (Hernandez *et al*., 2009). Testosterone is metabolized through several steps of hydroxylation. The activity of hydroxylase 6α is more significant in females than hydroxylase 15α in males. The ratio of 6α/15α hydroxylase reveals the state of androgen levels and is considered a biomarker of androgen perturbations (Wilson *et al.*, 1999). A study further showed that the metabolism of testosterone and in particular the ratio of 6α/15α hydroxylase is decreased in CAR deficient females. This ratio, decreased in *Car*$^{-/-}$ females, demonstrates the masculinization of these mice (Hernandez *et al*., 2009).

1.6.5. Physiological functions

The generation of CAR-deficient mice by the team of D.D. Moore (Wei *et al*., 2000) demonstrated the major role of CAR in the detoxification of xenobiotics. CAR deletion altered the sensitivity of mice to toxins, rendering *Car*$^{-/-}$ mice incapable of inducing key enzymes for detoxification. CAR also plays a major role in the metabolism of different endogenous substances wherein its accumulation to the cells may lead to toxicity.

1.6.5.1. Xenobiotic detoxification

CAR coordinates the expression of numerous hepatic genes involved in xenobiotic catabolism. It induces the biotransformation of phase I and II genes, as well as transporters (**Table 3**). The hepatoprotective action of CAR against xenobiotics does not only consists of the induction of the expression of detoxifying genes, but also the conduction of the repression of expression of certain genes. Thus, CAR prevents, for example the induction of *CYP4A*, a major enzyme for lipid peroxidation by inducing of the superoxide dismutase-3 (SOD) thereby limiting oxidative stress (Swales & Negishi, 2004).

1.6.5.2. Detoxification of endogenous compounds

Through the regulation of these xenobiotic metabolic enzymes, CAR is equally involved in the metabolism of a certain number of endogenous substances such as steroids, thyroid hormones, bile acids and bilirubin.

Steroid hormones were the first identified ligands of CAR causing the dissociation of CAR from the co-activator SRC1 (Forman *et al.*, 1998). Similarly, the progesterone and testosterone also inhibits the activity of CAR (Swales & Negishi, 2004). Levels of steroid hormone are regulated due to a dynamic balance between their synthesis and their activation. The storage capacity of steroid hormones is limited; therefore, a coordination of their synthesis and their biotransformation is essential for the regulation of normal physiological functions. A number of CYPs (CYP11, CYP17, CYP19, CYP21) are specifically responsible for hormone synthesis, their catabolism, as well as their inactivation (Ruckpaul *et al.*,1985). The liver is the major site of the catabolism of steroid hormones and CAR plays a fundamental role in this catabolism through the regulation of the expression of CYPs and sulfotransferases. The activation of CAR and its target genes by TCPOBOP induces the catabolism of estrogens and favors their excretion (Yamamoto *et al.*, 2006).

Thyroid hormones. The level of thyroid hormone is also controlled by the balance between synthesis, metabolism, and secretion. CAR is equally implicated in the catabolism of thyroid hormones. This catabolism implies the conjugation of sulfate or glucuronide groups (Visser et al., 1998). These reactions are catabolized by two enzymes of phase II, UGT1A1 and SULT1A1 which are both CAR-regulated (Hernandez *et al*., 2009).

Bilirubin and heme. Bilirubin is a product of degradation from heme, one of the most toxic compounds of an organism. Its accumulation is associated with jaundice and in cases

of prolonged accumulation this leads to neurotoxicity. The glucuronidation by the enzyme UGT1A1 is the major pathway of detoxification of this compound, which then is secreted in bile by the active transporter MRP2. CAR is involved in the clearance of bilirubin by the induction of enzymes UGT1A1, GSTa1 (Sugatani et al., 2001) and transporters OATP and MRP2 (Guo *et al.*, 2002). On mouse primary hepatocytes, bilirubin like phenobarbital is capable of inducing nuclear translocation of CAR.

1.6.5.3. Regulation of hepatic energy metabolism

The role of CAR in the regulation of energy metabolism has been recently attributed to this receptor on the basis of clinical studies which have been then confirmed by animal studies.

Glucose Metabolism. The role of CAR on carbohydrate homeostasis had been first suggested after different clinical studies in diabetic patients treated with phenobarbital presented an improvement in their sensitivity to insulin as well as the decrease of their glycemia (Lahtela et al., 1985; Sotaniemi *et al.*, 1983). Diabetic mice also presented an improvement in their glucose tolerance after treatment with TCPOBOP (Dong *et al.*, 2009). The improvement of glucose tolerance is principally allowed by the suppression of the production of hepatic glucose by neoglucogenesis. The activation of CAR leads to the repression of limiting enzymes of neoglucogenesis: *PEPCK* and *G6Pase*. Various models propose the repression of these genes by CAR. In the first model, CAR competes with the *FoxO1* and *HNF4α* for the fixation of their response elements IRE (iron-responsive element) and HNF4RE (HNF4-responsive element), respectively, on the promoter of *PEPCK* and *G6Pase* (Kodama *et al.,* 2004). In the second model, CAR binds to

SRC2/GRIP1 and *PGC1α* which are the two co-activators of HNF4α, thus, decreasing the gene expression of neoglucogenesis (Miao *et al.*, 2006). The third model proposes the nuclear translocation of CAR leading to the physical interaction of CAR with *PGC1α*. This interaction will allow the recruitment of ligase E3 culline allowing in turn to address nuclear bodies PML (promyelocytic leukemia) macromolecular nuclei sequestering and liberating the transcription factors and co-activators in the nucleus. In this structure, *PGC1α* is ubiquitinated after being degraded by the proteasome. With the decreased availability of *PGC1α*, the gene expression of neoglucogenesis is repressed (Gao *et al.*, 2015) **(Figure 8**). Finally, the last model proposes that CAR through its regulation of *SULT2b1* on the deacetylation of *HNF4α* prevents its nuclear translocation and its action on the genes for neoglucogenesis (Shi *et al.*, 2014). The CAR-dependent repression of neoglucogenesis is confirmed in primary cultures of human hepatocytes (Lynch *et al.*, 2014).

The fact that xenobiotic receptors induce the repression of neoglucogenesis can explain the involvement of this pathway in the synthesis of the co factor NADPH (Nicotamide adenine dinucleotide phosphate), which is essential for the activities of cytochromes P450. In consequence, the hepatic pathway of phosphate pentoses allows the conversion of glucose-6-phosphate in ribose-5-phosphate after NADPH generation. The increase in the production of glucose-6-phosphate by the repression of G6Pase is a way to generate NADPH. Therefore, the repression of neoglucogenesis by CAR allows the sufficient storage of NADPH for detoxification.

Lipid metabolism. CAR acts on the β-oxidation pathway of fatty acids in interfering with the major regulator of this pathway, which is PPARα. CAR competes with PPARα in the

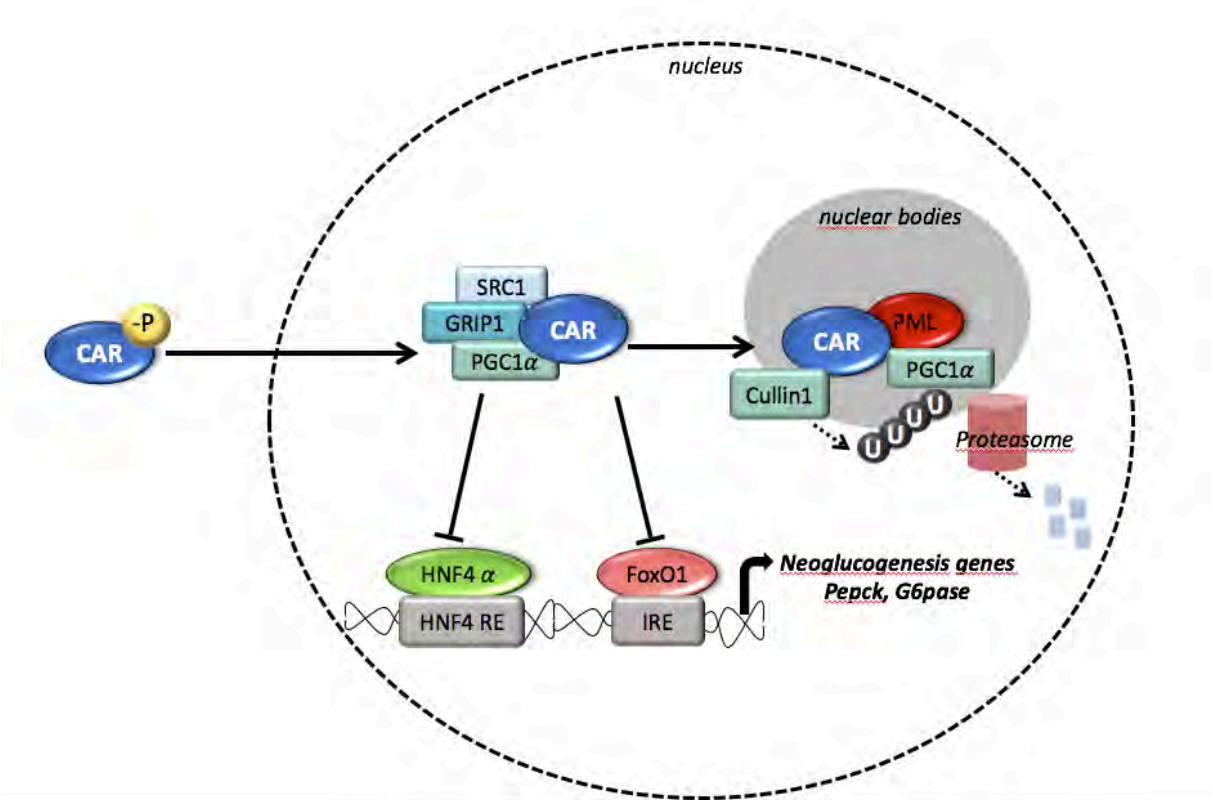

Figure 8. Repression of neoglucogenesis genes expressed by CAR. The different proposed models: (i) CAR enters in competition for the same elements as HNF4α (HNF RE) and FoxO1 (1RE) situated on the promoter of the genes of neoglucogenesis, (ii) CAR enters in competition with HNF4α for the recruitment of the same co-activators (SRC1 and GRIP1), thus decreasing its transactivating activity on neoglucogenic genes, (iii) CAR binds to PGC1α to be ubiquitylated and degraded by the proteasome (Gao *et al*., 2015; Yan *et al.*, 2015).

FoxO1: Foxhead box protein O1, GRIP1: Glutamat Receptor Interacting Protein 1, HNF4α: Hepatocyte nuclear factor 4 alphaf, IRE: insulin responsive elements, PGC1α: PPARγ coactivator-1-alpha, PML: promyelocytic leukemia, SRC1: steroid receptor coactivator-1

binding of response elements on the promoter of the 3-hyoxyacyl-CoA dehydrogenase (HADH) gene, a key enzyme of the peroxisomal β-oxidation (Kassam *et al.*, 2000). In addition, the activation of CAR by phenobarbital in wild-type mice leads to the repression of PPARα and its target genes such as *Cyp4a14, Cpt1α* and cytosolic acyl-CoA thioesterase (CTE). This effect is not observed in CAR-deficient ($Car^{-/-}$) mice (Maglich *et al.*, 2004; Ueda *et al*., *2002*) (**Figure 9B**).

Numerous studies have also shown the involvement of CAR in *de novo* lipogenesis, however the results obtained are contradictory. In obese mice (type ob/ob) subjected to a high fat diet, the activation of CAR by prolonged exposition to TCPOBOP allows the decrease of hepatic steatosis by the inhibition of *de novo* lipogenesis via the repression of the following genes: *Scd1, Fas, Acc* (Acetyl-CoA carboxylase) and *SREBP-1c* (Dong *et al.,* 2009b; Gao *et al*., 2009). An alternative hypothesis is that CAR interacts on *de novo* lipogenesis genes by the intermediary nuclear receptor LXR which is one of the regulator genes of hepatic lipogenesis. It accomplishes this by contributing to the inactivation of oxysterols, the endogenous ligands of LXR, through the regulation of the expression of sulfotransferase *Sult2B1b*. The inactivation of oxysterols allows the decreased activation of LXR and reduction of the LXR-SREBP pathway (Chen *et al.*, 2007). In agreement with this, *Sult2B1b*-deficient mice treated with TCPOBOP do not present anymore this repression of *de novo* lipogenesis genes (**Figure 9A**).

However, the effect of CAR on the regulation of *de novo* lipogenesis gene expression stays controversial as one study shows the inverse activation of CAR in human primary hepatocyte cultures inducing the expression of *de novo* lipogenesis genes, such as Fatty acid synthase (*Fasn)* and *Scd1* (Breuker *et al*., 2010).

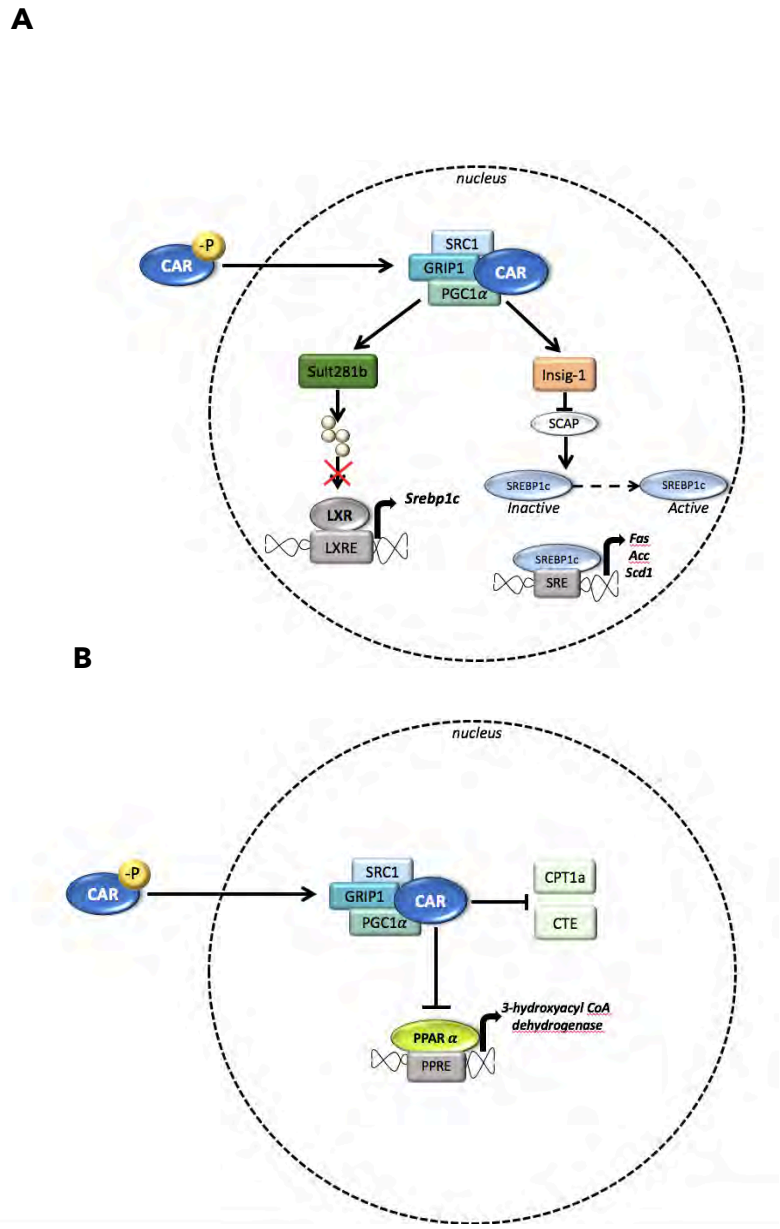

Figure 9. Involvement of CAR in the regulation of lipid metabolism: (A) *de novo* lipogenesis. Sult2B1b is a CAR target gene that allows the inactivation of oxysterols, endogenous ligands of LXR. The transactivating activity of LXR on these target genes are thus decreased. Car induces the expression of Insig-1 which links to SCAP and prevents its proteolytic action and the maturation of Srebp1c. **(B) β-oxidation.** CAR enters in competition with PPARα in binding to response elements, by the promoter 3-hydroxyacyl-CoA dehydrogenase, the key gene for β-oxidation, the activation of CAR leads to the repression of gene expression of CPT1a, CTE (Yan *et al.*, 2015; Gao *et al.*, 2015).

CPT1a: Carnitine Palmitol transferase 1a, CTE: constitutive transport element, Fas: Fatty acid synthase, GRIP-1: Glutamate Receptor Interacting Protein 1, Insig-1: Insulin induced gene 1, LXR: Liver X receptor, LXREs: LXR response elements, PGC-1α: PPARγ coactivator-1, SREBP1c: Sterol regulatory element-binding transcription factor 1, Sult2B1b: Hydroxysteroid sulfotransferase 2B1b.

1.6.5.4. Cholesterol Metabolism and Bile Acids

The same research team also showed that *Spot14,* a CAR target gene is an important modulator for hepatic lipogenesis. However, these results were not demonstrated in another team using CITCO (Lynch *et al*., 2014). On the contrary, this effect is found *in vivo* in mice fed with a standard diet and treated with TCPOBOP inducing the increase of *de novo* lipogenesis, as well as ketogenesis with a repression of the mitochondrial β-oxidation (Rezen *et al*., 2009). These contradictory results could be explained by a different role of the nuclear receptor CAR in function of the physiopathology found within organisms. The lipoprotein profile is modified after CAR activation in mice, as shown in an experimental study where the activation of CAR via TCPOBOP leads to decreased plasma concentrations of total cholesterol, high-density lipid (HDL) and low-density lipid (LDL)-cholesterol. It seemed that these effects were partly due to the repression of the gene transcription of lipoprotein A-I at the hepatic level by CAR (Masson *et al.*, 2008). The same team also showed that when mice are fed with a high-fat diet, CAR activation reduces hepatic cholesterol load by stimulating the expression of synthesis enzymes of bile acids and thus their fecal excretion in the bile form (Sberna *et al.,* 2011). In a similar manner, *Car*$^{-/-}$ mice showed an increase of HDL-cholesterol in the condition of cholestasis.

Hepatic transcriptomic analysis show that the activation of CAR induces expression of genes in cholesterogenesis such that 3-Hydroxy-3-Methylglutaryl-CoA Reductase (HMGCR), squalene epoxidase (SQLE), and lanosterol synthase (LSS). However, this effect is not associated to the ratio increase of lathosterol/cholesterol indicating that the change in gene expression is not associated with the increase of the biosynthesis of cholesterol (Rezen *et al*., 2009).

The activation of CAR also prevents the formation of gallstones by decreasing the gene expression of *Abcg5* and *Abcg8* and increasing the expression of *Cyp7a1,* favoring the conversion of cholesterol in bile acids. In the intestine, CAR favors bile reabsorption in inducing the expression of transporters *Asbt* (apical sodium-dependent bile acid transporter) and *Ostβ (*organic solute transporter *β).* This allows the decrease of cholesterol load of bile acids and to limit the formation of gallstones (Cheng *et al*., 2017).

The hepatoprotective role of CAR against bile acids have been largely described in the induction of their metabolization by the stimulation of SULT(2A1 and 2A9) and their excretion by the increase of bile acid transporters (MRP2/ABCC2; MRP3/ABCC3) in hepatocytes (Cherrington *et al*., 2002; Kast *et al*., 2002; Staudinger *et al.,* 2003). In agreement with these observations, CAR agonist drugs are used for the treatment of cholestasis (Stedman *et al*., 2005).

`

1.6.5.5. Bone Mass Regulation

Given the extensive crosstalk with many nuclear receptors including VDR (Moreau *et al.,* 2007), ER (Min *et al*., 2002), GR (Pascussi *et al.*, 2000) and PPARs, (Guo *et al.*, 2007) it was hypothesized that CAR may play a role in regulation of bone metabolism. Cho *et al.*, 2014 demonstrated that *in vivo* deletion of CAR resulted in higher bone mass in male mice, resulting from the reduced metabolism of testosterone, the major gonadal androgen in males. Furthermore, this was directly corelated to the suppression of *Cyp2b9* and *Cyp2b10* in $CAR^{-/-}$ mice, key enzymes for testosterone metabolism. There was no difference in bone mass in female $CAR^{-/-}$ mice compared to WT females. However, the exact mechanism for these sex-specific bone phenotypes is still unknown and remains to be further studied.

1.6.5.5. Inflammation

Given the similarities between PXR and CAR and the emerging evidence of the strong intestinal role of PXR, it can be hypothesized that CAR also plays a role in IECs, as well as a sensor for microbial metabolites (Cheng *et al.*, 2010; Garg *et al*., 2016; Shah *et al.*, 2007; Venkatesh *et al.*, 2014). Though, CAR's role on the intestinal mucosa has yet to be explored, its expression on the intestinal epithelium has already been confirmed (Burk *et al.*, 2005; Martin *et al*., 2008; Rezen *et al.*, 2009). Having similar function as PXR, sharing a number of ligands and target genes in xenobiotic metabolism, Hudson *et al*. (2017) tested the hypothesis that CAR would also function as a protective entity in the intestinal mucosa. Quite recently, their study has identified a novel role for CAR in regulation of intestinal mucosal healing demonstrating that CAR transcript expression was significantly reduced in mild to moderately inflamed colonic mucosa from patients with either ulcerative colitis (UC) or Crohn's disease (CrD) and was reproduced *in vivo* in colitic mice. Furthermore, their *in vitro* and *in vivo* approaches provided functional evidence that CAR can regulate intestinal epithelial wound healing and mucosal repair following inflammation-associated tissue damage. This is accomplished by CAR's activation enhancing IEC migration through p38 MAPK activation. On the other hand, CAR expression was also demonstrated in tumor-associated macrophages in the airways implicating that its activation may regulate inflammation (Fukumasu *et al*., 2015).

Chapter 2 : Gut Microbiota and its impact to the host

2.1. Introduction

The microbiome consists of the ecological community of commensal, symbiotic, and pathogenic microorganisms that share our body (Lederberg & McCray, 2001). The human body is estimated to be composed of 3×10^{13} eukaryotic cells and is colonized by 3.9×10^{13} microorganisms, with a ratio of prokaryotic to eukaryotic cells of at least 1:1 up to 10:1 (Sender *et al*., 2016). In addition, the gene content of the microbiome is estimated to have 2–20 million microbial genes, exceeding the ~20,000 human genes by at least a factor of 100 (Knight *et al*., 2017; Rastelli, Knauf & Cani, 2018). The host's microbiota is well tolerated by our immune system due to the coevolution of these microorganisms over time (Thomas *et al*., 2017). The human microbiota comprises all the microorganisms that reside on the skin and in all other tissues and organs including the gastrointestinal tracts. The largest concentrations of microbes occupy the gut, skin, and oral cavity. Among the host's various sites of microbial communities, the gut microbiota is the most stable, dense, diversified, and individually specific (Turroni *et al*., 2018), with the vast majority of commensal bacteria residing in the colon (Sender *et al*., 2016).

2.2. General characteristics of human gut microbiota

The human symbiont gut microbiota is a diverse and complex community composed of more than 100 trillion cells and 5 million non-redundant genes (Li *et al*., 2014), thus, making the human gut microbiota probably the most densely populated bacterial ecosystem described (Turroni *et al*., 2018). The microbiome includes bacteria, fungi, and archaea. As established by the Human Project Consortium in 2012, the community in stool

was one of the most diverse microbial communities in terms of number of different organisms present, exhibiting tremendous variability. To date, thousands of different bacterial species have been detected. The physicochemical conditions in the gut influence the composition of the intestinal microbiota and the microbial density increases along the gastro-intestinal (GI) tract with10^1–10^4 microbial cells in the stomach and duodenum, 10^4 to 10^8 cells in the jejunum and ileum, to 10^{10} to 10^{12} cells per gram in the colon and feces. The great majority belongs to only 6 of the hundreds of bacterial phyla populating our planet: *Firmicutes* and *Bacteroidetes*, which together represent approximately 90% of the community, and *Actinobacteria, Proteobacteria, Fusobacteria and Verrucomicrobia,* as subdominant phyla (Turroni *et al*., 2018). The methanogens, *Methanobrevibacter and Methanosphaera* are the most dominant archaeal groups. The two common fungal phyla in the gut include *Ascomycota* (which includes the genera Candida and Saccharomyces) and *Basidiomycota* (Thomas *et al*., 2017).

2.3. Factors affecting the gut microbiome

2.3.1. Age

Humans initially develop their microbiota at birth, with bacterial exposure through the vaginal birth canal or *via* maternal skin contact by transferring at least some portion of the maternal microbiome to the baby (Costello *et al*., 2009). Infants delivered vaginally tend to harbor microbiota that are typically encountered in the female reproductive tract, such as *Lactobacillus*. In contrast, cesarean delivery is typically associated with *Staphylococcus spp*. and other bacteria that are associated with the mother's skin and hospital environment. In general, the infant microbiome is often dominated by the genera *Bifidobacterium, Bacteroidetes*, and members of clostridial taxa (Thomas *et al*., 2017). Infancy is a period of

Rapid colonization by microbial consortia that shifts in response to events such as illness or changes in diet (i.e. introduction to solid food, **Figure 10A** and **B**). Opportunistic microbes then modify this initial microbiota during infancy in an ecological succession to ultimately form a predominantly anaerobic microbial community (*clostridia, bifidobacteria, bacteroides*) in the gut luminal habitat within the first few days after birth. After which, this microbiota is subsequently modulated by environmental, genetic, and epigenetic factors that ultimately form the unique microbial landscape within an individual (Costello *et al*., 2009). These microbial populations converge toward an adult community by three years of age (Thomas *et al.,* 2017). Gut communities start with low phylogenetic and species richness, which increases with the rate of encounters with new bacteria, the increasing size of the gut or the proliferation of ecological niches that consequently promote diversity.

The composition of the microbiome changes as humans age. Aging is accompanied by the onset of various clinical changes, including a basal proinflammatory state ("inflamm-aging") that directly interfaces with the microbiota of older adults and enhances their susceptibility to age-related diseases. Studies in older adults demonstrate that the gut microbiota correlates with diet, basal level of inflammation and location of residence (e.g., community dwelling, long-term care settings). The most drastic change associated with the aging gut is the change in the relative proportion of organisms, such as the domination of *Firmicutes* in the young vs. *Bacteroidetes* in the elderly.

2.3.2. Diet

Diet is also a critical factor in shaping the composition of the gut microbiota. Vegans, vegetarians, and omnivores have distinct microbiomes. Total counts of *Bacteroides* spp.,

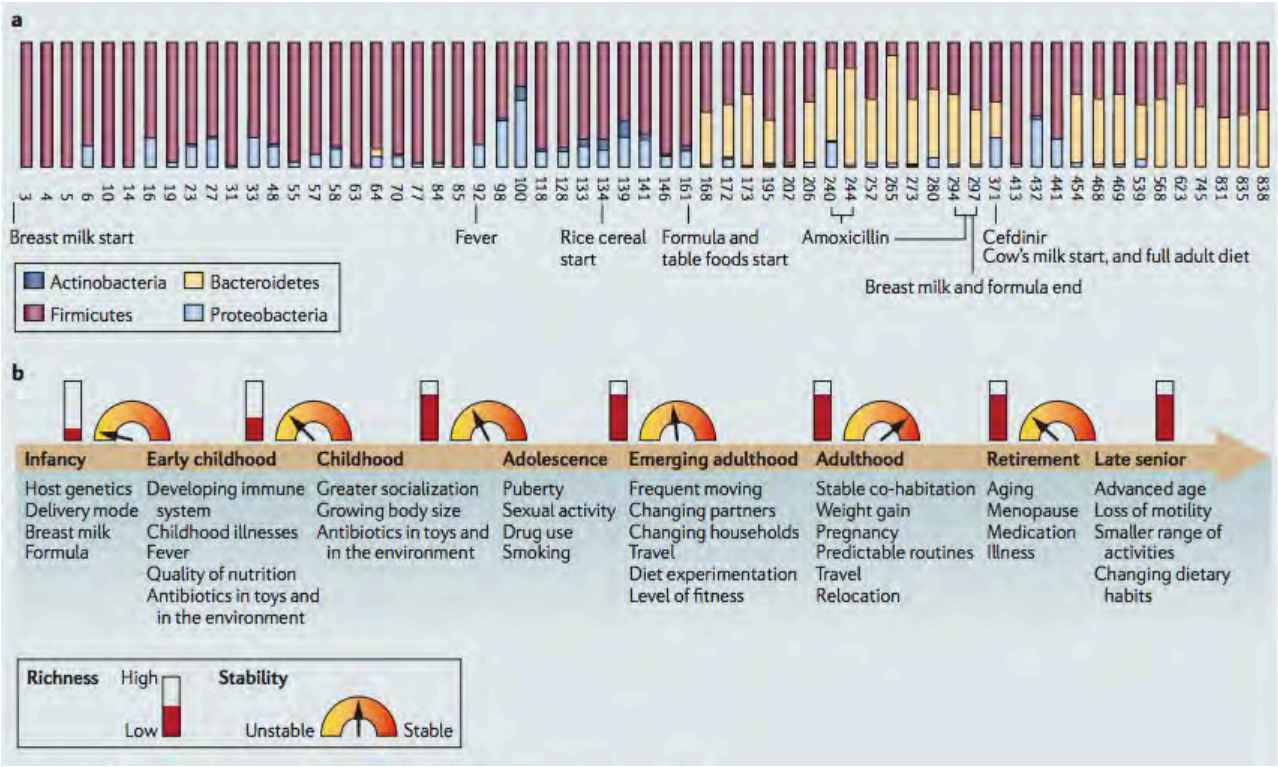

Figure 10. Assembly and stability of the gut microbiota and environmental factors affecting the gut microbiota during life. A) The succession of bacterial consortia (in terms of the four dominant phyla) over time (days after birth) in a developing infant gut microbiome from birth to around 2.5 years of age, according to 16S ribosomal RNA sequencing). B) Various factors that influence the microbiome throughout the lifetime of a typical Westernized human (Spor, Koren, & Ley, 2011).

Bifidobacterium spp., *Escherichia coli*, and *Enterobacteriaceae* spp. were significantly lower in vegan samples than in controls. In contrast, total counts of *Klebsiella* spp., *Enterobacter* spp., *Enterobacteriaceae, Enterococcus* spp., *Lactobacillus* spp., *Citrobacter* spp., and *Clostridium* spp. were similar in people with different diets. Subjects on a vegetarian diet ranked between vegans and omnivores. However, the total microbial count did not differ between the dietary groups (Zimmer *et al*., 2012). Moreover, the microbiome of a person can be rapidly modified simply by changing dietary patterns. David *et al*., (2014) have demonstrated that short-term consumption (5 days) of diets of purely animal or plant products can alter the microbial community composition. An animal-based diet increased the abundance of bile-tolerant microorganisms, including *Alistipes, Bilophila*, and *Bacteroides* and decreased the levels of *Firmicutes* that metabolize dietary plant polysaccharides (*Roseburia spp, Eubacterium rectale*, and *Ruminococcus bromii*) (Thomas *et al*., 2017). Spor, Koren, & Ley (2011) further highlight that *Erysipelotrichaceae*, from bacterial phylum *Firmicutes*, is dependent on changes in the amount of dietary fat; Butyrate-producing *Roseburia* spp. depends on the amount of certain carbohydrates; and *Bacteroides* spp. differ in their ability to use specific substrates such as inulin. He further reiterates that these differences can predict the outcomes of competitive interactions between the species and actually drive the niche space according to their substrate preference, thus, altering the relative abundances of the taxa that are present.

Microbiota can also metabolize estrogen-like compounds from the diet to biologically active forms, and these estrogen-like compounds may promote the proliferation and growth of certain types of bacteria (Frankenfeld *et al.*, 2014). Soy isoflavones, such as genistein and glycitin, can alter the structure and the composition of

the fecal bacterial community in post-menopausal women by increasing the concentration of the beneficial gram-positive *Bifidobacterium*, while suppressing *Clostridiaceae* (Frankenfeld *et al.*, 2014; Nakatsu *et al.*, 2014); equol, produced by bacteria upon activation of soy phytoestrogens may LDL lipoprotein levels, (Usui *et al.*, 2013) ; and supplementation of chalconoid isoliquiritigenin, a low-affinity ER ligand found in licorice root, alter gut microbiotaactivity although the exact mechanism remains unclear (Madak-Erdogan *et al.*, 2016).

2.3.3. Host genetics

Host genetics is also hypothesized to influence gut microbiota composition. Various studies have been done to measure this heritability. In human studies between identical and fraternal twins, using metagenomics and 16S ribosomal RNA gene sequence data from clone libraries and from deep pyrosequencing, significant differences were not detected in fecal microbiomes and did not detect any heritable components (Turnbaugh *et al.*, 2009). Thus, if host genotype does exert an effect on the composition of the microbiota, they are likely to be small and detecting them in a healthy population will require a large number of subjects (Spor *et al.*, 2011).

In addition, using an approach called 'quantitative trait loci' (QTL), a large scale mouse study of 645 mice has revealed that host genetic control was found to affect the tips of the bacterial tree (genus and species levels rather than higher-order taxa), particularly for the *Bacteroidetes* and *Firmicutes* (Benson *et al.*, 2010). A QTL associated with specific bacterial abundances was found to contain genes with important roles in mucosal immunity (Presley *et al.*, 2010).

2.3.4. Sexual dimorphism

It is also hypothesized that the gut microbiota could be sexually dimorphic**.** Several human cohorts have indeed demonstrated gender differences in the composition of the gut microbiota (Haro *et al*., 2016; Santos-Marcos *et al*., 2019). Recent research suggests that women harbor a higher ratio of *Firmicutes/Bacteriodetes* (F/B) in comparison to men (Dominianni *et al*., 2015; Li *et al*., 2008; Mueller *et al.,* 2006) and a higher relative abundance of *Lachnospira* and *Roseburia* was found in pre-menopausal vs. post-menopausal women who had similar levels to men (Santos-Marcos *et al*., 2018), suggesting that in humans, estrogenic status influences gut microbiota composition. Estrogens have been shown to directly influence the composition of the gut microbiota with both 17β-estrogen supplementation and ovariectomy significantly affecting the microbiota taxa (Kaliannan *et al*., 2018).

The F/B ratio is heavily influenced by the body mass index (BMI) (Kasai *et al*., 2015) and overall adiposity represents an additional mechanism by which sex might influence the gut microbiota (Haro *et al.*, 2016). Min *et al*. (2019) present a high-resolution association between microbiome, android and gynoid fat ratio using the precise measurement of fat distribution. The sex-induced difference in regional adiposity could potentially lead to the difference in the species of functioning microbiome that are in turn modulating fat distribution. With a BMI greater than 33, a significantly lower F/B ratio has been seen in men compared to women, while the opposite holds true in those with a BMI less than 33 as well as in postmenopausal women (Haro *et al.*, 2016). Adjusting for BMI, higher proportions of *Firmicutes* have been found in women compared to men.

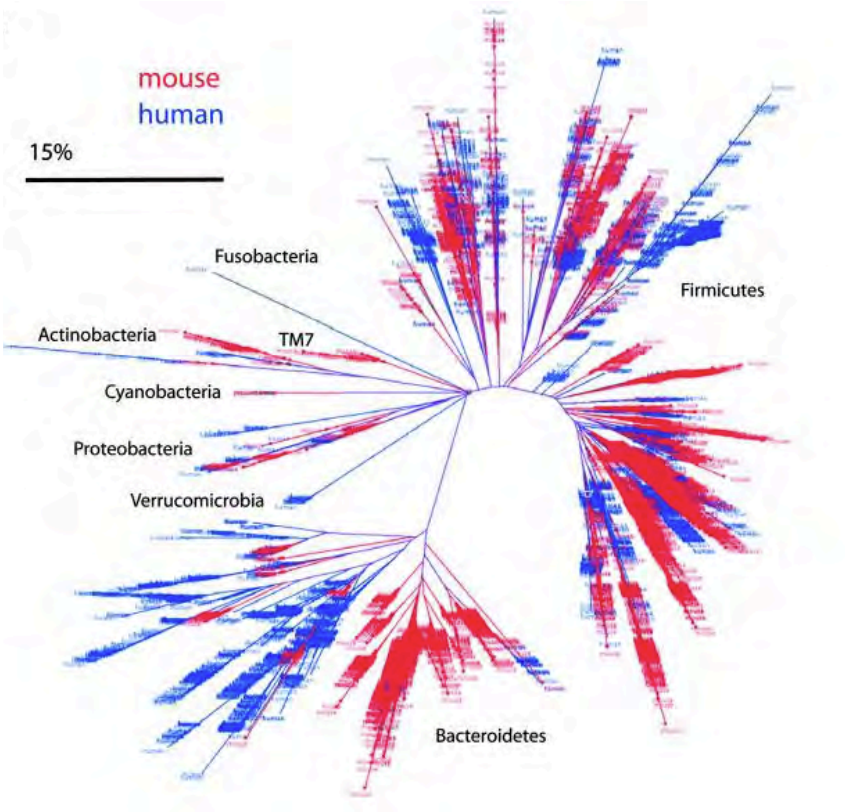

Figure 11. A comparison of the bacterial diversity from 16S rRNA analysis of mouse caeca and human colons. The bar represents 15% sequence divergence. Bacterial genera in human microbiomes (11,831 colon-associated 16S rRNA sequences) and mice microbiomes (5,088 caecum-associated 16S rRNA sequences) where only 15% of the mouse microbiome genera have been found to be represented in humans. (modified from Ley *et al*., 2005).

Furthermore, higher numbers of *Proteobacteria, Veillonella,* and *Blautia* have been reported in women (Haro *et al.,* 2016; Li *et al.*, 2008; Schnorr *et al*., 2014).

2.4. Animal & human models in gut microbiota research

2.4.1. Mice

The laboratory mouse has been instrumental for establishing roles for the gut microbiota in many aspects of mammalian physiology: obesity and malnutrition (Smith *et al.*, 2013; Turnbaugh *et al*., 2006), hepatic function (Dapito et al., 2012; Henao-Mejia et al., 2012), intestinal response to injury and repair (Rakoff-Nahoum *et al.*, 2004; Swanson *et al.*, 2011), and innate and adaptive immune function (Hooper, Littman, & Macpherson, 2012; Littman & Pamer, 2011). Ninety-nine percent of mouse genes are shared with humans at the host genetic level and differ by 14% in genome size (2.5 gigabases and 2.9 gigabases respectively) (Waterston *et al*., 2002). In addition, mouse microbial genes share key similarities with the human gut microbiome at the phylum through family levels (**Figure 11**), making them a powerful model system for evaluating host–microbiota interactions applicable to human biology (Spor et al., 2011). In most studies with disease models, germ-free systems or dietary interventions, inbred strains that originate from either the *Mus musculus domesticus* or *M. musculus musculus* and show considerable genetic and phenotypic similarity (Beck *et al.*, 2000; Hugenholtz & de Vos, 2018) are utilized. An important confounder has shown to be the housing of mice. In some cases, complete phenotypes disappeared after a mouse house was renovated or renewed (Dingemanse et al., 2015). The housing effect seems even to be larger than the effect of the genetic background (Friswell *et al*., 2010; Verbeke *et al*., 2015; Xiao et al., 2015). In addition, what the effect the birth mother has on microbiota composition is at the moment under debate

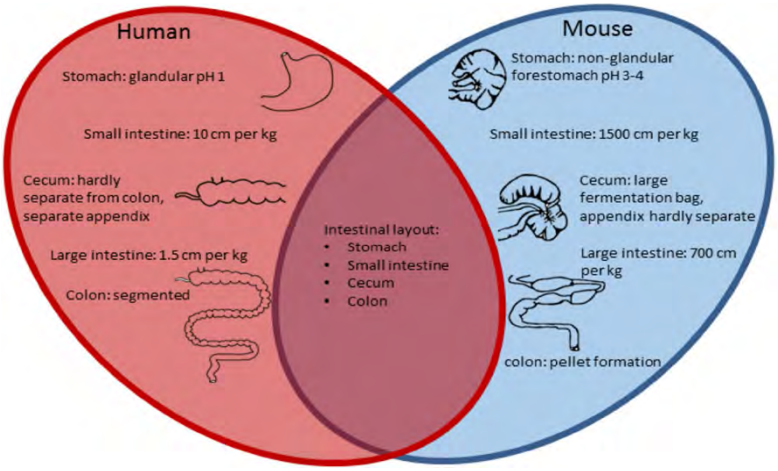

Figure 12. Comparison of the intestinal tract features of human and mouse. The main similarities and differences are listed in a venn diagram (Hugenholtz and de Vos, 2018).

since in some studies, the genotype (mouse strain) of the mouse had a more pronounced effect on the microbiota development than the genotype of the birth (Friswell *et al*., 2010; Kovacs *et al*., 2011).

2.4.1.1. Comparison of mouse and human intestinal physiology

Mice and humans vastly differ in overall body size, intestinal physiology and diet. The main difference is the size of the intestinal tract in relation to the total size of the species (**Figure 12**). relative to body weight, the large intestine is a much larger organ in mice than in man. Both humans and mice have a ceca appendix, although it is not a pronounced separate section in humans as it is in mice (Scholtens *et al.*, 2012). The human colon is segmented, with pouches called haustra, while the mouse colon has a smooth serosal appearance. In addition, the outer mucosa layer of the small intestine differs the most between human and mouse. The overall appearance of the mouse mucosal surface is smooth, while the human mucosal contains circular folds, known as *plicae circularis*, to increase the surface area (Treuting *et al.*, 2011). This specificity in the human small intestine provides a niche for mucus-associated bacteria, which is not present in mice and could, therefore contribute an important difference, influencing microbial composition. Similarly, the architecture of the villi varies through the small intestine with distinct differences in mouse and human. Other factors such as the overall intestinal transit time, mucus growth rate, final mucus layer, mucus penetrability, structural Muc proteins, intestinal pH values, oxygen tension levels, a different glycan profile in the mucus, and the presence of a non-glandular forestomach in mice affect the differences in intestinal microbiota. Furthermore, differences in body size, eating behavior, feeding patterns and biorhythms between mouse and human yield different metabolic turnover rates. And lastly, coprophagy, the murine

behavior by which feces is re-ingested, is known to affect the intestinal microbiota (Hugenholtz & de Vos, 2018).

2.4.1.2. Comparison of mouse and human microbiota

Similar phyla dominate the distal guts of mice and humans: *Firmicutes* (usually 60–80% of 16S ribosomal RNA gene sequences) (Ley *et al.,* 2005), *Bacteroidetes* (usually 20–40% of 16S rRNA gene sequences) (Ley et al., 2005) and *Actinobacteria*. In addition, these same bacterial phyla are found to inhabit the gastrointestinal tracts of many other mammals as well (Ley *et al.*, 2008). However, when comparing the bacterial genera in human microbiomes (11,831 colon-associated 16S rRNA sequences) and mice microbiomes (5,088 caecum-associated 16S rRNA sequences), only 15% of the mouse microbiome genera have been found to be represented in humans (**Figure 11**) (Ley *et al*., 2005).

However, recently when the mouse microbial genes were compared with that found in human, only 4% were found to share 95% identity and a coverage of 90%. Remarkably, almost 80% of the annotated functions were common between the two datasets, indicating significant functional overlap (Hugenholtz & de Vos, 2018). Around 80 microbial gut genera were reportedly shared between mouse and man, and this number was recently confirmed in a comparison of murine and human 16S rDNA datasets (Nguyen *et al.*, 2015).However, there are considerable variations in the genera that were observed in the mouse data sets and, for instance, *Faecalibacterium, Succinivibrio and Dialister* were not found in some laboratory mice, due to the use of different mouse strains and providers and differences in analysis (Hildebrand *et al.*, 2013; Krych *et al.*, 2013). Another extensive mouse microbiome catalog confirmed that the human and mouse intestinal microbiota show considerable

similarity at the genus level but reveal large quantitative differences (**Figure 13**) (Xiao *et al*., 2015).

2.4.1.3. Germ-free models

Gnotobiotics is the science of well-controlled microbial environments within and for biological specimens encompassing the generation and maintenance of both germ-free (GF) and defined microbial community animals (Ward & Trexler, 1958). GF life is a biological condition characterized by the complete absence of living microorganisms (Geurts *et al*., 2011; Ley *et al*., 2005). Gnotobiotic techniques have been essentially used to interrogate host–microbiota dialogue mechanisms in mice (Yi & Li, 2012). Rederivation of any combination of genetic mutant mice is possible via embryo transfer into GF pseudo pregnant mice or aseptic harvesting of a gestational uterine package and transfer of the fetuses to a GF foster female. Colonization of GF mice with one or two bacteria has been useful both to understand the features of microbes needed to colonize the intestinal ecosystem and to dissect how specific microbes contribute to immune system development and disease (Kostic *et al.*, 2013). However, generating and maintaining these mice requires specialized facilities, and the cost, labor, and skills required to maintain them can make these models inaccessible to many researchers. GF mice must be monitored regularly for contamination using a combination of culturing microscopy, serology, gross morphology, and sequencing-based detection techniques (Fontaine *et al.*, 2015; Nicklas, Keubler, & Bleich, 2015).

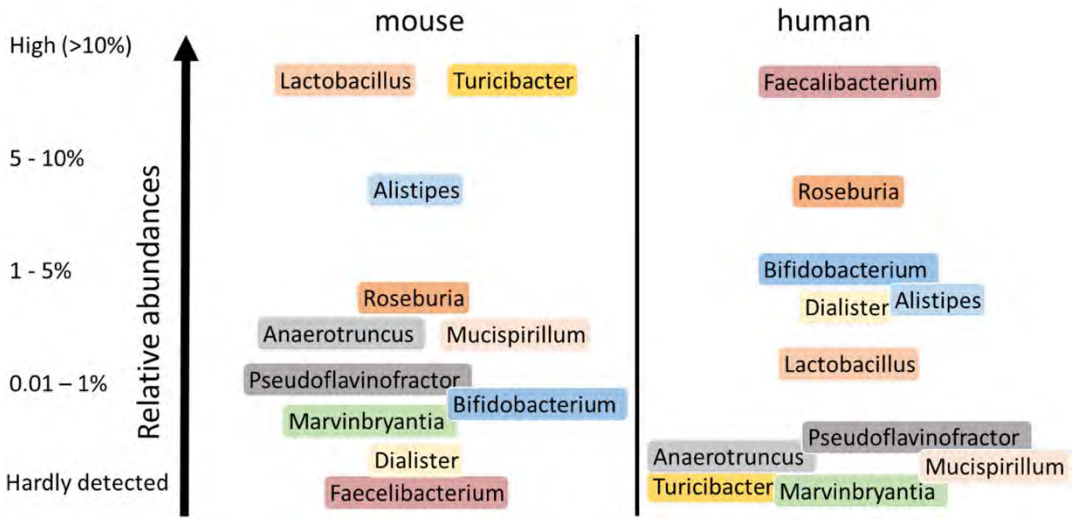

Figure 13. Major different human and murine intestinal genera. Only genera are shown that showed consistent differences in relative abundance between humans and mice (Hugenholtz and de Vos, 2018).

2.4.1.4. Depletion of microbiota by antibiotics

Treatment with broad-spectrum antibiotics is an alternate method commonly used to deplete the gut microbiota of mice, and can be readily applied to any genotype or condition of mouse. Compared to the GF model, antibiotics can deplete bacterial populations in mice which were normally colonized since birth. Unlike GF mice where many aspects of development and early immune education are broadly impaired, the antibiotic model in adult mice specifically allows for study of the role of bacteria in maintaining cell functionality and signaling pathways after development (Deshmukh *et al.*, 2014; Gonzalez-Perez *et al*., 2016; Lamousé-Smith, Tzeng, & Starnbach, 2011; Li *et al.*, 2017).

Antibiotics can selectively deplete different populations of the microbiota through varying mechanisms of action. For example, metronidazole and clindamycin both target anaerobes, while vancomycin is only effective against gram-positive bacteria, and polymyxin B specifically targets gram-negative bacteria (Atarashi *et al.*, 2008; Schubert, Sinani, & Schloss, 2015). Individual antibiotics can be used to make composition changes in the gut microbiota in order to identify classes of bacteria relevant to different phenotypes (Schubert, Sinani, & Schloss, 2015; Zackular *et al.*, 2016). In contrast, a cocktail of different classes of antibiotics can be used to broadly deplete the gut microbiota. Researchers have used various regimens, which differ in antibiotic combination, dose, and length of treatment (**Table 4**). All of these combinations broadly target gram-positive, gram-negative, and anaerobic bacteria. Often, antibiotics are diluted in drinking water and mice are allowed to drink *ad libitum* throughout the course of treatment.

Antibiotic-treated mice are not completely cleared of bacteria, but significant reductions in bacterial load are associated with shifts in cell populations, signaling

Method	Antibiotics	Concentration	Duration	References
Drinking water (*ad libitum*)	Vancomycin + metronidazole	0.5–1.0 g/L each	10 weeks	Atarashi *et al.*, 2008
	Ciprofloxacin + metronidazole	1 g/L each	2 weeks	Josefsdottir *et al.*, 2017
	Vancomycin + ampicillin + polymixin	0.1–1.0 g/L each	4 weeks	Kim *et al.*, 2017
	Vancomycin + neomycin + metronidazole	0.5–1.0 g/L each	7 days	Brandl *et al.*, 2008; Kinnebrew *et al.*, 2010
			2 weeks	Josefsdottir *et al.*, 2017
	Streptomycin + colistin + ampicillin	1–5 g/L each	6 weeks	Sawa *et al.*, 2011
	Ampicillin + neomycin + streptomycin + vancomycin	0.5–1.0 g/L each	4–5 weeks	Khosravi *et al.*, 2014
	Cefoxitin + gentamicin + metronidazole + vancomycin	1 g/L	10 days	Ganal *et al.*, 2012
	Gentamicin + ciprofloxacin + streptomycin + bacitracin	0.15–2 g/L each	4 weeks	Yan *et al.*, 2016
	Vancomycin + neomycin + kanamycin + metronidazole	0.5–1.0 g/L each	3 weeks	Gury-BenAri *et al.*, 2016
	Vancomycin + ampicillin + kanamycin + metronidazole	0.5–1.0 g/L each		Levy *et al.*, 2015
	Vancomycin + neomycin + ampicillin + metronidazole	0.35–1.0 g/L each	7 days	Ochoa-Repáraz *et al.*, 2009
			2 weeks	Hägerbrand *et al.*, 2015; Hashiguchi *et al.*, 2015; Knoop *et al.*, 2015; Brown *et al.*, 2017; Emal *et al.*, 2017; Josefsdottir *et al.*, 2017; Steed *et al.*, 2017; Burrello *et al.*, 2018; Thackray *et al.*, 2018
			3 or more weeks	Rakoff-Nahoum *et al.*, 2004; Ivanov *et al.*, 2008; Vaishnava *et al.*, 2008; Ichinohe *et al.*, 2011; Ismail *et al.*, 2011; Yoshiya *et al.*, 2011; Naik *et al.*, 2012; Corbitt *et al.*, 2013; Diehl *et al.*, 2013; Balmer *et al.*, 2014; Mortha *et al.*, 2014; Oh *et al.*, 2014; Johansson *et al.*, 2015; Wu *et al.*, 2015; Zhang *et al.*, 2015; Park *et al.*, 2016; Yan *et al.*, 2016; Cervantes-Barragan *et al.*, 2017; Ge *et al.*, 2017; Li *et al.*, 2017; Durand *et al.*, 2018

			3 4-day treatments with 3 day rests	Adami *et al.*, 2018
	Ampicillin + Neomycin + Métronidazole + Vancomycin	7mg/L each except Vancomycin 3.5mg/L	49 days	Lasserre, 2013 (In-house experiments, ToxAlim)
	Ampicillin + Neomycin + Métronidazole + Vancomycin	1.0g/L each except Vancomycin 0.5g/L	28 days	Lasserre, 2013 (In-house experiments, ToxAlim)
Gavage	Vancomycin + neomycin + ampicillin + metronidazole + gentamicin	200 µl of 0.5–1.0 g/L each by daily gavage	3 day	Kelly *et al.*, 2015
			10 days	Hill *et a*l., 2010
	Bacitracin + neomycin + streptomycin	200 mg/kg body weight	3 days	Sayin *et al.*, 2013; Wichmann *et al.*, 2013; Fernández-Santoscoy *et al.*, 2015
	Neomycin + bacitracin	20 mg each in 200 µl by daily gavage	7 days	Grasa *et al.*, 2015
Combination	Ampicillin by drinking water; vancomycin + neomycin + metronidazole by gavage	1.0g/L in water 10 ml/kg of 5–10 g/L by gavage every 12 h	10–21 days	Reikvam *et al.*, 2011; Hintze *et al.*, 2014
	Vancomycin + neomycin + ampicillin + metronidazole	10 mg each by daily gavage 0.5–1.0 g/L each in water	5 days gavage followed by 7–10 days drinking water	Kuss *et* al., 2011
	Kanamycin + gentamicin + colistin + metronidazole + vancomycin	200 µl of 0.35–4 mg/ml by daily gavage, and mixed 2:100 into drinking water	7 days gavage followed by administration in water	Bashir *et al.*, 2004; Stefka *et al.*, 2014
	Metronidazole + colistin + streptomycin by gavage, vancomycin by drinking water	0.3–2 mg each by daily gavage, and 0.25 mg/ml in water	2 weeks	Zákostelská *et al.*, 2016
	Oral streptomycin + ampicillin in drinking water	20 mg/mouse orally and 1 g/L in drinking water	1–2 weeks	Kim *et al.*, 2018
	Streptomycin by gavage, followed by vancomycin + neomycin + ampicillin + metronidazole by drinking water	100 mg/mouse for single gavage and 0.5–1.0 g/L in drinking water	single gavage followed by >7 days drinking water	Kernbauer *et a*l., 2014

Table 4. Broad spectrum antibiotics treatment regimen (modified from Kennedy, King, & Baldridge, 2018)

pathways, and organ morphology, offering a model system similar to that of germ-free mice (Kennedy, King, & Baldridge, 2018).

2.4.2. Other animal models

The tiny **Hawaiian bobtail squid (*Euprymna scolopes*)** selectively acquires the bacteria *V. fischeri* from its environment to create one of the best-understood models of bacterial–animal symbiosis. *E. scolopes* does not harbor *V. fischeri* within its gut, and this symbiosis does not contain a consortium of microbes. Instead, the squid forms a naturally occurring one-on-one relationship with *V. fischeri* within a ventrally located cavity called the light organ. The development of this light organ only occurs with a specific association with *V. fischeri*, as squid raised without *V. fischeri* remain uncolonized by other bacteria, and the light organ fails to mature (McFall-Ngai & Ruby, 1991). This model offers several experimental advantages, as it is a naturally occurring one-on-one relationship where each participant can be grown independently. The use of microbial genetics with *V. fischeri* has provided surprising and powerful insights into the molecular and even photoluminescent dialogue that mediates a productive relationship between microbes and their hosts (Kostic *et al.*, 2013).

The **fruit fly (*Drosophila melanogaster*)** has contributed greatly to the understanding of basic cellular and developmental biology over the past decades. The *Drosophila* model is a powerful model to explore innate immunity and microbial pathogenesis, more particularly, toll-like receptor (TLR) functioning (Dionne & Schneider, 2008; O'Callaghan & Vergunst, 2010). The *Drosophila* model provides substantial genetic tools with a relatively simple microbiota to create an experimentally tractable system to discover the molecular mechanisms of host–commensal interactions (Kostic *et al*., 2013).

The **zebrafish (*Danio rerio*),** having a diverse microbiota but still among the simplest vertebrate models, is considered a powerful model system for studying the complexities of host–microbiota interactions. Due to the high degree of homology between zebrafish and mammals not only in the adaptive immune system, but also in the digestive system. To date, most GF zebrafish studies have centered on the early post-embryonic period and therefore focused on the impact of the microbiota on the innate immune system, as the adaptive immune system has yet to fully develop at that time. Inflammatory bowel disease, which involves the dysfunctional mucosal immune responses to commensal bacteria, can also be modeled in zebrafish using a chemical called oxazolone, which induces intestinal inflammation (Brugman *et al*., 2009).

2.4.3. SHIME®

SHIME is an acronym for the Simulator of the Human Intestinal Microbial Ecosystem and it is a multi-compartment dynamic simulator of the human gut developed in 1993 (Molly *et al*., 1993). Since 2010, the name has been jointly registered by ProDigest and Ghent University. Built as a modular setup, the SHIME is highly flexible and it can be technically modified to target digestive conditions of interest. The development of multi-compartment simulators of (parts of) the human gut originated from the awareness that fecal microbiota significantly differs from the in vivo colon microbiota in terms of community composition and metabolic activity (**Figure 14**) (Van de Wiele *et al*., 2015).

2.5. Roles of the gut microbiota

The estimated 10^{13} microbes with its immense catalog of genes allow these microbes to easily adapt to their environment and energy sources available. Gut microbes

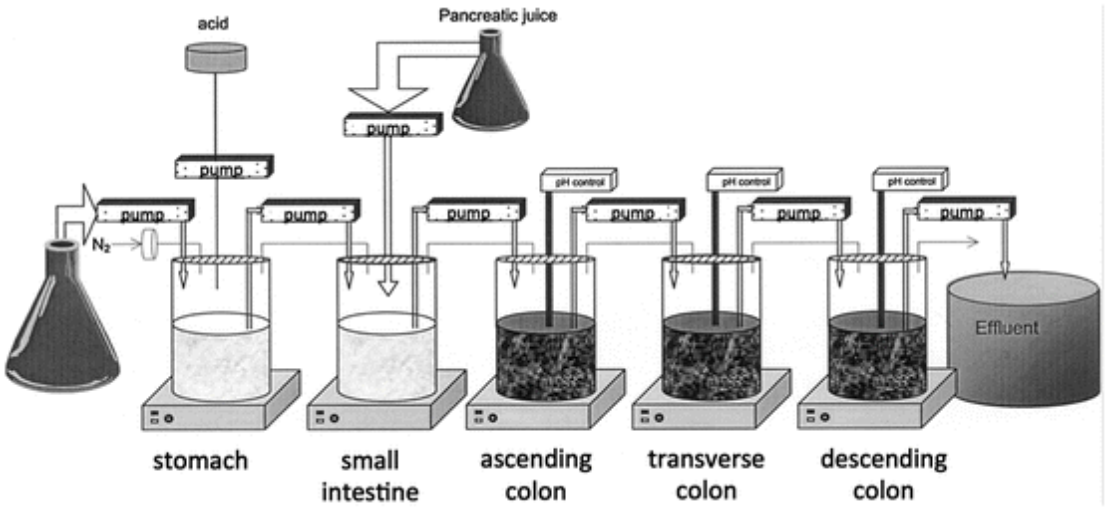

Figure 14. Schematic representation of the SHIME®(Van de Wiele *et al*., 2015).

metabolize an extensive list of dietary compounds to extract nutrients and energy, varying substantially among individuals. This may be due to variability of presence and abundance of gut microbial enzymes, and their corresponding bioactivities and metabolites. This qualifies the gut microbiota to be a massive "organ" able to perform complex biological processes (metabolic, nutritional, physiological) and immune system modulation (Rastelli *et al.*, 2018).

2.5.1. Roles of the gut microbiota in metabolic and nutritional processes

The gut lumen is rich in both host and microbial proteases, and research are increasingly associating human disease to differential microbial proteolytic activity. For example, celiac disease (CD), a common autoimmune disorder characterized by an inflammatory response to dietary gluten found in wheat-based foods, gut microbiota is implicated via alterations in gluten proteolysis. This proline-rich protein evades complete digestion by host proteases, resulting in the generation of high-molecular weight, immunogenic peptides (Caminero *et al*., 2015). Gut microbes can also metabolize amino acids obtained from dietary protein, including L-phenylalanine, L-tyrosine, and L-tryptophan into a range of bioactive products. Gut microbiota can specifically metabolize L-tryptophan into the antioxidant IPA, the neurotransmitter tryptamine, and indole, the latter of which can undergo hydroxylation and sulfation by hepatic enzymes to generate the uremic toxin indoxyl sulfate (Devlin *et al*., 2016; Wikoff *et al*., 2009; Williams *et al*., 2014)

Gut microbiota is also associated in the metabolism of lipids and lipid-derived compounds (Cho & Caudill, 2017; Fennema, Phillips, & Shephard, 2016). For example, gut microbial reduction (bacteria *Eubacterium coprostanoligenes*) of cholesterol generates coprostanol, which cannot be reabsorbed and is excreted. This transformation

Dietary Substrate	GM product	GM metabolic pathway/enzyme	Role in human physiology and pathophysiology
Fermentation end-products			
Polysaccharides	Acetate	Fermentation	Metabolism: anti-lipolytic activity, appetite reduction
Polysaccharides	Propionate	Fermentation	Metabolism: appetite regulation, glucose homeostasis, regulation of intestinal transit; immune modulation
Polysaccharides	Butyrate	Fermentation	Metabolism: energy source, IEC turnover, appetite regulation, inhibition of gut motility, regulation of insulin release; immune modulation; regulation of microglial function; serotonin production; amelioration of stress response, anxiety and depression
Polysaccharides	Lactate	Fermentation	Lipolysis inhibition; IEC turnover; immune homeostasis
Protein	Isobutyrate	Fermentation	Insulin resistance
Protein	2-methylbutyrate	Fermentation	Insulin resistance
Protein	Isovalerate	Fermentation	Insulin resistance
Polysaccharides	Sphingolipids	Fermentation	Metabolic regulation; anti-inflammatory activity
Polysaccharides	Glycerophospholipids	Fermentation	Strengthening of the intestinal barrier
Bioactive GM metabolites			
Isoflavones (daidzein)	Equol	Glycoside cleavage and reduction	Anti-cancer activity (breast, prostate)
Lignans	Enterolignans	/	Anti-cancer activity (breast, prostate)
Ellagitannins	Urolithins	/	Anti-cancer activity; anti-inflammatory properties
Glucosinolates	Isothiocyanates	Myrosinases	Increased production of host cytoprotective proteins
/	GABA	/	Regulation of intestinal motility and visceral pain perception
/	Noradrenalin	/	Increased energy expenditure
/	Dopamine	/	Regulation of psychomotricity
Tryptophan	Nicotinic acid	Tryptophan metabolism	Regulation of immune homeostasis
Tryptophan	Tryptamine	Tryptophan decarboxylation	Serotonin release (regulation of visceral sensitivity, intestinal immunity and inhibition of depressive-like behaviors)
Tryptophan	Indole-3-acetaldehyde	Tryptophanases	Regulation of immune homeostasis
Tryptophan	Indole propionic acid	Tryptophanases	Regulation of immune homeostasis; improved intestinal barrier function
Tryptophan	Indole	Tryptophanases	Regulation of immune homeostasis
/	Ethylphenyl sulfate	/	Exacerbation of autistic behavior
Phosphatidylcholine, choline, carnitine	TMA	TMA lyases	Accumulation of cholesterol deposition with increased risk of major adverse cardiac effects, obesity, metabolic syndrome
Aromatic amino acids	Indoxyl sulfate	Aromatic amino acids metabolism	Poor cardiovascular outcomes
Aromatic amino acids	p-cresol sulfate	Aromatic amino acids metabolism	Poor cardiovascular outcomes
Branched-chain amino acids	Branched-chain SCFAs	/	Insulin resistance, diabetes, inflammation
/	Polyamines	/	Intestinal epithelial cell turnover; immune modulation
/	Spermine	/	Immune modulation
Omega-6-fatty acids	Conjugated linoleic acid	/	Activation of cyclooxigenases and lipoxygenases; increase of insulin sensitivity; anti-inflammatory properties
/	Menaquinone	/	Blood coagulation; bone metabolism; insulin sensitivity
/	Folate	/	Cell division
/	Cobalamin	/	Metabolic co-factor whose deficiency increases the risk of cardiovascular diseases
/	Riboflavin	/	Flavin adenin dinucleotide and flavin mononucleotide precursor
GM-host co-metabolites			
Conjugated primary bile acids	Deconjugated bile acids	Bile salt hydrolases	Prevention of active host bile acid uptake
Deconjugated bile acids	Secondary bile acids	7-Dehydroxylation	Modulation of glucose homeostasis; increase of energy expenditure
Glucuronidated drugs – xenobiotics – hormones – bile acids	Aglycone	Beta-glucuronidases	Favoring of enterohepatic recirculation; increase of drugs and xenobiotics toxicity

[a] *When available, for each gut microbiome-derived bioactive compound, the substrate, the metabolic activity involved, and the specific role in human biology are reported. In red are the metabolites with a link to disease.*

Table 5. Principal Gut Microbiome Bioactive Compounds with a Major Role in Human Physiology and Pathophysiology[a] (modified from Turroni *et al.*, 2018) ·

consequently removes cholesterol from circulation, making up to 50% of the steroids in human feces (Macdonald *et al*., 1983) and GF mice colonized with microbes from high and low cholesterol-reducing patients produce distinct amounts of coprostanol (Gérard et al., 2004).

Gut microbiota is involved in the digestion of indigestible dietary polysaccharides including resistant starch and dietary fibers thereby leading to the production of important nutrients, such as short chain fatty acids (SCFAs) (Macfarlane & Macfarlane, 2012), vitamins (vitamin K, vitamin B2 & B12, folic acid)((O'Hara & Shanahan, 2006) and certain amino acids (O'Mahony *et al*, 2015; Rothhammer *et al*., 2016) that humans are unable to synthesize themselves (**Table 5**). The plant polysaccharides in our diet are rich in xylan-, pectin-, and arabinose-containing carbohydrate structures. The human genome lacks most of the enzymes required for degrading these glycans. Nevertheless, the distal gut microbiome provides us with this capacity to process these polysaccharides. The human gut microbiome is enriched for genes involved in glucose, galactose, fructose, arabinose, mannose, and xylose, starch and sucrose metabolism. Our microbiome also has significantly enriched metabolism of glycans, amino acids, and xenobiotics; methanogenesis; and 2-methyl-d-erythritol 4-phosphate pathway-mediated biosynthesis of vitamins isoprenoids (Gill et al., 2006).

Gut microbiota also metabolizes poorly absorbed, polyphenolic compounds from plant-derived foods such as soy isoflavones (Atkinson, Frankenfeld, & Lampe, 2005), lignans from flaxseed and sesame seeds, flavonoids like the catechins and gallate esters found in tea, and ellagic acid (García-Villalba *et al.*, 2013) from nuts and berries (Clavel *et al.*, 2006).

2.5.2. Metabolism of xenobiotics

Gut microbes also modify the chemical structures of numerous ingested foreign compounds (xenobiotics), including, environmental pollutants, and pharmaceuticals thereby producing an exhaustive list of different metabolites (Turroni *et al.*, 2018). Gut microbial xenobiotic metabolism alters bioactivity, bioavailability, and toxicity, and interfere with the fates of ingested molecules. Clinical studies have revealed tremendous interindividual variability in these microbial transformations equivocal consequences to the host. Gut microbiota metabolites and gut microbiota-derived bioactive molecules represent the functional connection between the gut microbiota and the physiology of the human holobiont.

2.5.2.1 Common metabolizing enzymes

Both the host and gut microbiota use hydrolytic chemistry to break down large ingested compounds into smaller products that may be further metabolized. Hydrolase enzymes catalyze the addition of a water molecule to a substrate, followed by bond cleavage. The most abundant and relevant hydrolases in the gastrointestinal tract are proteases, glycosidases, and sulfatases, with the microbiota contributing a broader range of activities than host enzymes. Host and gut microbes possess Lyase activities modify polysaccharides that contain a glycosidic bond β- to a carboxylic acid (e.g. alginate, pectin, chondroitin and heparan). As in the host, gut microbes can also reduce a wide range of functional groups, including alkenes and α, β-unsaturated carboxylic acid derivatives, nitro-, *N*-oxide, azo-, and sulfoxide group. Reduction typically decreases the polarity of compounds and can alter charge, hybridization, and electrophilicity, which can affect the lifetimes and activities of metabolites in the body. The gut microbiota has transferase

activities and transfers methyl and acyl groups to or from xenobiotic scaffolds. Key classes of gut microbial radical enzymes include radical S-adenosyl-L-methionine (SAM) enzymes, cobalamin (B_{12})-dependent enzymes, and glycyl radical enzymes (GREs) (Koppel *et al*., 2017).

2.5.2.2. Metabolism of pharmaceuticals

The human gut microbiota can directly or indirectly transform a wide spectrum of drugs and host targets into metabolites with altered pharmacological properties. Anti-inflammatory drugs and gastrointestinal agents rely on microbial metabolism for converting inactive precursors (prodrugs) to pharmaceutically active compounds (Deloménie *et al*., 2001; Lavrijsen *et al.*, 1995; Peppercorn & Goldman, 1972). In cancer chemotherapy, patient response can dramatically differ between individuals, in terms of efficacy and severity of side effects due to gut microbiota composition. It was shown that *E. coli* or *Listeria welshimeri* either increased or decreased the efficacy of half of a panel of 30 anticancer drugs towards cancer cell lines. In addition to modulating the host immune system, gut microbes can directly alter the structures of cancer therapies molecules and their metabolites, affecting their interactions with host cells (Lehouritis *et al*., 2015). In addition to affecting drugs that act locally, gut microbial metabolism can also influence the efficacy of therapeutics that target distant organ systems such as the central nervous system (CNS) (Lehouritis *et al*., 2015). Extensive metabolism (Goldin *et al.*, 1973) within the gut by both host and microbial enzymes affect the concentration of drug reaching the brain. (Bergmark *et al*., 1972). Differences in these activities may contribute to the substantial variation observed in patient response to L-dopa for Parkinson's disease. (Nutt & Holford, 1996).

2.5.2.3. Metabolism of contaminants

A recent review from literature indicates that gut microbes have an extensive capacity to metabolize environmental chemicals and are involved in the metabolism of >30 environmental contaminants generally classified in five core enzymatic families (azoreductases, nitroreductases, β-glucuronidases, sulfatases and β-lyases). Moreover, there is clear evidence that bacteria-dependent metabolism of pollutants modulates the toxicity for the host (Claus, Guillou, & Ellero-Simatos, 2016). Specific examples include metabolization of azo compounds (textile dyes, food colorings, and pharmaceuticals), some of the first industrially important synthetic chemicals (Rafii, Franklin, & Cerniglia, 1990). Gut microbes also metabolize melamine, an industrial chemical used in the production of various plastics. Melamine added to infant formula in China caused kidney stones in 300,000 children and led to at least six deaths (Ingelfinger, 2008). Subsequent studies in mice revealed that gut microbes from the *Klebsiella* species are associated with the production of cyanuric acid in (Wang *et al.*, 2014; Zheng *et al.*, 2013). In addition to organic pollutants, human gut microbes modify the structures and alter the toxicities of various heavy metals, including bismuth, arsenic, and mercury. Mercury bioaccumulates in living organisms, posing a threat to human health, and gut microbial metabolism may affect mercury toxicity and lifetime in the body. Pesticide molecules like glyphosate, the active component of the herbicide Roundup (Montsanto, St Louis, MO, USA), has been shown to perturb the growth of beneficial bacteria *Enterococcus faecalis* in cattle and horse (Krüger *et al.*, 2013), *Enterococcus faecium, Bacillus badius, Bifidobacterium adolescentis* and *Lactobacillus sp*. in poultry (Shehata *et al.*, 2013).

The microbiome may also interact with components of our diets that are added in the process of food manufacturing (e.g. artificial sweeteners, emulsifiers, and preservatives). For example, gut microbes convert the artificial sweetener cyclamate into cyclohexylamine via hydrolytic cleavage of its sulfamate linkage. The mutagenic potential of heterocyclic amines, poorly absorbed molecules produced during charring of meat and fish, can be altered by gut microbial metabolism. These results appear to implicate the gut microbiota in the known link between charred meat and cancer (Cross *et al.*, 2010). A variety of other environmental chemicals presented in **Table 6** shows the metabolism by the gut microbiota and conversely the effect on the composition of the gastrointestinal tract. The exposure to these environmental chemicals has been linked to various health disorders, including obesity, type 2 diabetes, cancer and dysregulation of the immune and reproductive systems highlighting that gastrointestinal microbiota critically contributes to a variety of host metabolic and immune functions (Claus *et al.*, 2016).

2.5.3. Role of gut microbiota in host Immunity

The immune system plays a central role in shaping the composition of the microbiota as well as its proximity to host tissues. It maintains a well-orchestrated "inside-out" control over microbiota localization and community composition by minimizing direct contact between intestinal bacteria and the epithelial cell surface, and, by confining and limiting the exposure from pathogenic bacteria to intestinal sites and the systemic immune compartment (Hooper, Littman & Macpherson, 2012).

The commensal gut microbiota, thus, has important effects on the normal development of immunity. Germ-free mice models have been paramount in revealing the profound effect of microbial colonization on the formation of lymphoid tissues and

Human exposure to pollutants and their interaction with the GI microbiota

Chemical	*Source*	*Human exposure*	*Metabolism by microbiota*	*Effect on microbiota*
PAHs	Air and food pollutants resulting from incomplete combustion of fossil fuel, tobacco	Mean total intake of 3.12 mg per day (97% through food, 1.6% air, 0.2% water, 0.4% soil)	*In vitro*: hydroxylation; *in vivo*: deconjugation of liver metabolites, involved in the formation of CH_3S-metabolites	
Nitro-PAHs	Air and food pollutants, derivatives of PAHs	Diesel exhaust identified as main source of exposure. 2NF: range from 0 to 92 ng/m^3	Reduction to amine metabolites	
Nitrotoluenes	Intermediates in the manufacture of dyes, chemicals, explosives	Mainly occupational. 2-nitrotoluene: 0.35–0.7 mg/m^3 through air; 420 mg per day through skin	Reduction to amine metabolite and hydolysis of glucuronide conjugates	
Pesticides	Pollutants in air and food	Chlorpyrifos: mainly through diet 0.01 to 0.14 µg/kg bw per day; DDT: through diet 0.29 µg/kg bw per day	Dechlorination of organochlorides. Deconjugation of propachlor *in vivo*	Perinatal exposure to chlorpyrifos (1 mg/kg bw per day) induced dysbiosis at adulthood (rat)
PCBs	Industrial chemicals now prohibited but persistent in water sediments and soils	Mainly through diet DL-PCBs: 0.29 pg TEQ WHO_{98}/kg bw per day; NDL-PCBs: 2.71 ng/kg bw per day	Bacterial C–S-lyase plays an important role in formation of methyl sulfone ($MeSO_2$)-metabolites *in vivo*	Mixture of PCBs (150 µM/kg for 2 days) decreased the abundance of many bacteria (mainly Proteobacteria)
Metals	Ubiquitous environmental contaminants	Mainly through diet: arsenic 0.78 µg/kg bw per day; lead 0.2 µg/kg bw per day; cadmium 0.16 µg/kg bw per day	Involved in demethylation of mercury, methylation of arsenic and bismuth	Cadmium (20–50 mg/kg bw/d for 45 days); lead (100 or 500 mg/l) or arsenic (10 p.p.m. for 4 weeks) induced dysbiosis (mouse)
Azo dyes	Food colourants	Mainly through diet	Azoreduction of the azo bound to produce aromatic amines	
Melamine	Widely used in plastics, illegal food contaminant	TDI: 0.2 mg/kg bw (EU)	Metabolised to cyanuric acid	
Artificial sweeteners	Food additives	ADI (FDA, US): Aspartame: 50 mg/kg bw; saccharin: 15 mg/kg bw	Cyclamate metabolised to cyclohexamine	Aspartame (5–7 mg/kg/d), sucralose and saccharin (5 mg/kg per day) induce dysbiosis in animals with potential deleterious metabolic effect for the host (mouse and human)
Other POPs (e.g., PCDFs)	Pollutants formed during industrial processes	Mainly through diet: PCDD/Fs 0.176 pg TEQ WHO_{98}/kg bw per day		2,3,7,8 TCDF (24 µg/kg) induced dysbiosis and affected the faecal metabolic profiles (mouse)

Abbreviations: ADI, acceptable daily intake; DL-PCBs, dioxin-like PCBs; EU, European Union; FDA, Food and Drug Administration; NDL-PCBs, Non-dioxin-like PCBs; PCBs, polychlorobiphenyls; PAHs, polycyclic aromatic hydrocarbons; POPs, persistent organic pollutants; TEQ, toxic equivalency; TDI, tolerable daily intake.

Table 6. Human exposure to pollutants and their interaction with the gastrointestinal microbiota (Claus, Guillou and Ellero-Simatos, 2016).

subsequent immune system development. This furthered current knowledge that the microbiota influences the immune system from "outside-in". Recent studies have greatly expanded this understanding and have revealed some of the cellular and molecular mediators of these interactions. In addition, gut microbiota has been shown to enhance the anti-inflammatory branches of the adaptive immune system. However, recent studies in animal models have shown that commensal microbiota may contribute to systemic autoimmune and allergic diseases at sites distal to the intestinal mucosa , although mechanisms are still unclear (Wu et al., 2010).Gut bacteria can also trigger inflammatory responses in immunodeficient hosts. Surprisingly, gut microbiota can protect against autoimmune disease like Type1 diabetes (Schmidt *et al*., 1999; Verdaguer *et al*., 1997). Altogether, interactions with a faulty innate immune system can result in dysbiosis of the gut microbiota with downstream metabolic consequences for the host.

2.5.4. Role of gut microbiota in other host processes

The microbiota of the intestine is also involved in promoting bone formation as well as resorption leading to skeletal growth. Microbiota induces the hormone insulin-like growth factor 1 (IGF-1), promoting bone growth and remodeling (Yan *et al.*, 2016). When the microbiota ferment fiber, SCFAs are produced leading to induction of IGF-1 that promotes bone growth.

Lastly, the gut microbiota has been increasingly recognized as an integral component of our CNS, with a significant capacity to modulate our behavior via neural, endocrine and immune pathways (Duszka & Wahli, 2018; Rastelli *et al.*, 2018). Multiple potential mechanisms have been proposed. Exogenously administered potential probiotic bacteria or infectious agents can alter the composition of the gut microbiota and can

compete for dietary ingredients as growth substrates, bioconvert sugars into fermentation products with inhibitory properties, produce growth substrates for other bacteria, produce bacteriocins, compete for binding sites on the enteric wall, improve gut barrier function, reduce inflammation (thereby altering intestinal properties for colonization and persistence), and stimulate innate and adaptive immune responses (O'Toole & Claesson, 2010). Gut bacteria also modulate various host metabolic reactions, resulting in the production of metabolites such as, bile acids, choline and short-chain fatty acids (Dalile *et al.*, 2019; Nicholson *et al.*, 2012) such as n-butyrate, acetate and propionate, which are known to have neuroactive properties (Barrett *et al.*, 2012; Lyte, 2011) and tryptophan to serotonin (Ruddick *et al.*,, 2006). In addition, bacteria have the capacity to generate many neurotransmitters and neuromodulators by the following: Lactobacillus spp. and Bifidobacterium spp. produce gamma-Aminobutyric acid (GABA); Escherichia spp., Bacillus spp. and Saccharomyces spp. produce noradrenalin; Candida spp., Streptococcus spp., Escherichia spp. and Enterococcus spp. produce serotonin; Bacillus spp. produce dopamine; and Lactobacillus spp. produce acetylcholine (Barrett *et al.*, 2012; Lyte, 2011; Matur & Eraslan, 2012). To date, research predominate on behavioral disorders (anxiety, depression, and cognitive dysfunction) but evidence on the involvement of gut microbiota with CNS conditions like pain, autism, multiple sclerosis and obesity is growing (Cryan & Dinan, 2012).

2.5.5. Gut microbiota dysbiosis' association with chronic diseases

In the recent years, an immensely growing number of publications have associated the gut microbiota to other diseases (e.g. liver diseases, digestive diseases, cancer, neurodegenerative disorders), yet its exact role on the onset of these diseases remain to be

explored. Current knowledge establishes the disease state as a result from the progression of a pre-existing dysbiosis, or an unbalanced compositional and functional layout of the gut microbiota (Turroni *et al*., 2018). Although a direct causality is not completely proven, numerous studies have consistently associated the link between gut microbiota composition, its metabolic activity (e.g., metabolite production), and its host metabolism. In other words, the activity of the gut bacteria may influence not only our health but also the risk of developing diseases (Rastelli, Kanuf, & Cani, 2018).

Overweight, obesity, type 2 diabetes and related metabolic disorders have reached epidemic proportions and are considered one of the most serious global health issues in our society. Obesity results from an imbalance of food intake, basal metabolism, digestive tract microbial composition and energy expenditure (Turnbaugh *et al*., 2006). According to Turnbaugh *et al.* (2006) the gut microbiome should be considered as a set of genetic factors that together with host genotype and lifestyle contribute to the pathophysiology of obesity. It is observed that the intestinal bacteria in obese humans and mice differ from those in lean individuals. Obese mice microbiota was found to be rich in *Firmicutes* compared to the lean mice microbiota, which was abundant in *Bacteroidetes* (Turnbaugh *et al*., 2006). Strikingly, colonization of germ-free mice with microbiota from obese mice was sufficient to cause a significant increase in total body fat, as compared to colonization with microbiota from lean mice (Turnbaugh *et al.,* 2006). The obese microbiome has an increased capacity to harvest

energy from the diet, thereby increasing weight gain in the host (Turnbaugh *et al.*, 2006; Kallus *et al.*, 2012). Colonization of adult germ-free mice with a gut microbial community harvested from conventionally raised mice increased body fat within 10–14 days, despite an associated decrease in food consumption. This change involves several linked mechanisms: microbial fermentation of dietary polysaccharides that cannot be digested by the host; subsequent intestinal absorption of monosaccharides and short-chain fatty acids; their conversion to more complex lipids in the liver; and microbial regulation of host genes that promote deposition of the lipids in adipocytes (Bäckhed et al., 2004).

Non-alcoholic fatty liver disease (NAFLD) is a spectrum of liver damage ranging from simple steatosis (or non-alcoholic fatty liver, NAFL) to non-alcoholic steatohepatitis (NASH) with the development of fibrosis, cirrhosis and hepatocellular carcinoma (HCC) (Burt, Lackner, & Tiniakos, 2015; Gerbes *et al.*, 2018; Stickel & Hellerbrand, 2010). The pathogenesis of NAFLD involves environmental, genetic and metabolic factors, such as limited physical activity and a dysbalanced diet (Day, 2010) leading to changes in the intestinal microbiota (Le Roy *et al.*, 2013). Multiple studies found that germ-free C57BL/6 mice gained less weight than conventional mice when given a sugar-rich and lipid-rich diet despite similar amounts of food consumption indicating the critical role of microbes in the pathology of obesity and NAFLD. Interestingly, total body fat and liver triglyceride content increased following microbial colonization of germ-free (Bäckhed *et al.*, 2004; Bäckhed *et al.*, 2007). Mice lacking the nod-like receptorpyrin domain-containing protein 3 (NLRP3) and NLRP6 inflammasomes have increased susceptibility to NASH, due to changes in the gut microbiota. Co-housing inflammasome-deficient mice with wild-type mice increased the susceptibility of wild-type mice to NASH, so fatty liver risk might be affected by the

surrounding faecal microbiota (Henao-Mejia *et al.,* 2012). Moreover, epididymal fat weight, hepatic steatosis, multifocal necrosis and infiltration of liver by inflammatory cells were significantly increased in germ-free mice colonized with faeces from patients with NASH and then fed a high-fat diet (HFD) (Burt *et al.*, 2015).

Inflammatory bowel disease (IBD), including Crohn's disease and ulcerative colitis, is characterized by chronic immune-mediated intestinal inflammation that is driven by both genetic predisposition and environmental factors such as diet, antibiotic use and socioeconomic development (Manichanh *et al.*, 2012). IBDs are characterized by aberrant innate and adaptive immune responses to commensal luminal bacteria (Ciorba *et al.,* 2010) and associated with compositional and metabolic changes in the intestinal microbiota (dysbiosis) (Ni *et al.*, 2017). In IBD, the key role of the gut microbiota and its interplay with a compromised gastrointestinal barrier has been extensively reviewed. However, definitive cause-effect mechanisms have been challenging to prove outside of specific animal models. Evidence from these experimental models suggest that although gut bacteria often drive immune activation, chronic inflammation in turn shapes the gut microbiota and contributes to dysbiosis (Ni *et al*., 2017).

Ulcerative colitis (UC) is thought to be caused by some strains of *E. coli* (Campieri & Gionchetti, 2001), associated with *Enterobacteriaceae,* particularly certain strains of adherent-invasive *E. coli* (AIEC) (Darfeuille-Michaud *et al.*,1998) and *Fusobacterium nucleatum* with a link to the development of colon cancer (Zeller *et al.*, 2014). Pathogenic *E. coli* have been implicated in Crohn's disease, (Darfeuille-Michaud, 2002).

2.6. Gut microbiota and host dialogue

2.6.1. The gut-liver axis

Gut microbiota interacts with the host in multiple different ways, with numerous links between the gut and other organs, such as brain (Sampson & Mazmanian, 2015), kidney (Whiteside *et al*., 2015),and liver (Schnabl & Brenner, 2014). The term 'gut-liver axis' was first described in 1978, when Volta *et al*., (1987) showed the production of immunoglobulin A antibodies to dietary antigens in patients with liver cirrhosis, indicating interactions between gut and liver. The liver is a unique organ that has two sources of blood supply flowing into the liver, from the hepatic artery and portal vein. About 70%–75% of the liver blood supply comes from the portal vein, which drains blood from mesenteric veins of the intestinal tract (Abdel-Misih & Bloomston, 2010). Small molecules such as monosaccharides and amino acids are then absorbed by specialized transporters on enterocytes and reach the liver through the portal vein, where many are taken up by hepatocytes and metabolized. If the gut barrier is disrupted, the liver is the first organ in the body that encounters the microbial metabolites, toxins and microorganisms from the intestine. Thus, the liver serves as a large collection base for compounds and substances originating from the intestine (Chu *et al*., 2019).

2.6.2. Bile acids

Bile acid synthesis begins in the liver and can be accomplished via two different pathways (**Figure 15**). The classical (or neutral) pathway produces at least 75% of bile acid production under normal conditions and is initiated by 7a-hydroxylation of cholesterol catalyzed by *CYP7A1* (Thomas *et al*., 2008)the rate-limiting enzyme that determines the amount of bile acids produced. The alternative (or acidic) pathway is initiated by sterol-27-

hydroxylase (*CYP27A1*) (Russell, 2003). The 27-hydroxycholesterol formed is further hydroxylated by oxysterol 7a-hydroxylase (*CYP7B1*). The primary bile acids produced are different between human and rodent (Falany *et al.*, 1997; Falany *et al.*, 1994; Sayin *et al.*, 2013). Conjugated bile acids are then actively transported into bile via the BSEP. Approximately 95% of biliary secreted bile acids are then reabsorbed from the intestine, predominantly as conjugated bile acids in the distal ileum by the ASBT (also known as IBAT), and recirculated via the portal vein to the liver, from which they are secreted again. This process is called enterohepatic circulation and occurs in humans about six times per day.

Certain studies have shown that in the absence of bacteria (as in GF or ATB-treated mice or rats), the bile acid pool consists of mainly primary conjugated bile acids (Kellogg, Knight, & Wostmann, 1970; Kellogg & Wostmann, 1969; Sayin *et al.*, 2013; Selwyn *et al.*, 2016). However, the primary bile acid synthesis has been shown to be regulated by microbiota, through several enzymes or reaction steps in the liver (Wahlström *et al.*, 2016). The complex process of 7-dehydroxylation comprises a number of reactions carried out by bacteria with bile acid-inducible (bai) genes (Doerner *et al*. 1997; Ridlon, Kang, & Hylemon, 2006). Bacteria with capability to produce secondary bile acids have been identified in *Clostridium* (clusters XIVa and XI) and in *Eubacterium*, both genera belonging to the *Firmicutes* phylum (Kitahara *et al.*, 2000, 2001; Ridlon *et al.*, 2014; Ridlon, Kang, & Hylemon, 2006). Synthesis of taurine as well as bile acid acyl-CoA-synthetase, which is the first of two enzymes required for bile acid conjugation, is also under microbial regulation (Sayin *et al*., 2013). ASBT is under microbial regulation, providing additional functional evidence that the gut microbiota may not only regulate bile acid synthesis but also bile acid uptake, both

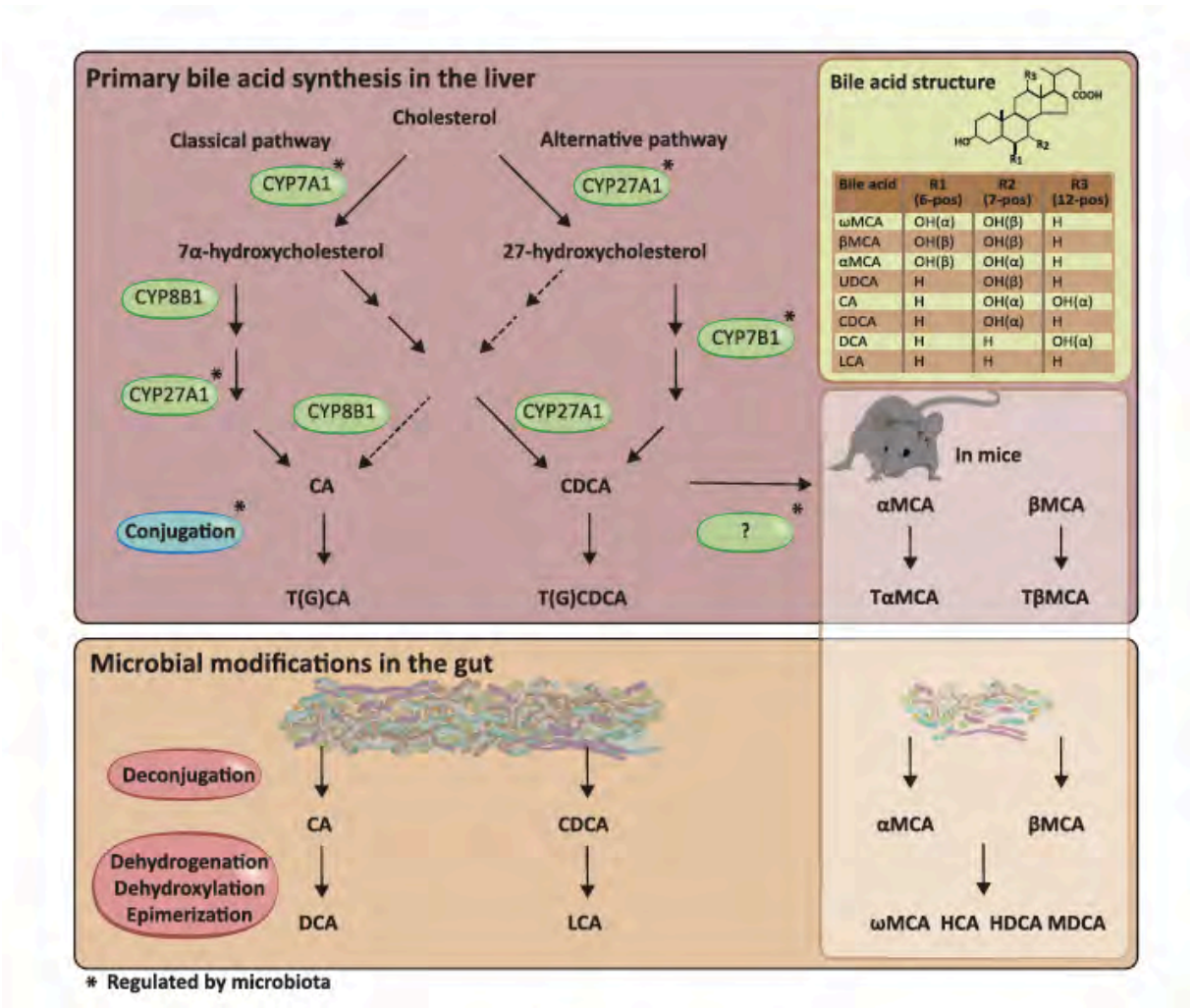

Figure 15. Bile Acid Synthesis and Metabolism. Schematic representation of synthetic pathways of primary bile acids in hepatocytes (pink) and secondary bile acids in the intestine (orange). Inset top right: table summarizing sites of hydroxylation on steroid nucleus of most common bile acid species. Inset bottom right: murine bile acid species that differ from humans. Asterisks indicate enzymes or reaction steps regulated by microbiota. G, glycine-conjugated species; T, taurine-conjugated species. (Wahlström *et al*., 2016).

contributing to the larger bile acid pool in GF mice (Sayin *et al*., 2013). Moreover, Gut Microbiota is in charge of bile acid deconjugation (i.e., removal of the glycine or taurine conjugate) that prevents active reuptake from the small intestine via the ASBT. Bile acid deconjugation is carried out by bacteria with bile salt hydrolase (BSH) activity. Metagenomic analyses demonstrated that functional BSH is present in all major bacterial divisions and archaeal species in the human gut including members of *Lactobacilli, Bifidobacteria, Clostridium and Bacteroides* (Archer, Chong, & Maddox, 1982; Jones *et al.*, 2000; Ridlon *et al*., 2006). Deconjugated primary bile acids that escape uptake through ASBT enter the colon, where they are further metabolized through 7-dehydroxylationinto secondary bile acids (**Figure 15**); lithocholic acid (LCA) from chenodeoxycholic acid (CDCA) and deoxycholic acid (DCA) from cholic acid (CA) (Macdonald *et al.*, 1983; Ridlon & Bajaj, 2015). Another major microbial biotransformation of bile acids is the generation of oxo- (or keto-) bile acids by oxidation of hydroxyl groups at ring position 3, 7, or 12 that are catalyzed by bacteria with hydroxysteroid dehydrogenases (HSDHs), which are present in *Actinobacteria*, *Proteobacteria*, *Firmicutes,* and *Bacteroidetes* (Fukiya *et al.*, 2009; Kisiela, Skarka, Ebert, & Maser, 2012; Macdonald *et al.*, 1983; Sutherland & Macdonald, 1982).

Microbial metabolism of bile acids leads to increased diversity and in general a more hydrophobic bile acid pool, which facilitates fecal elimination of bile acids, in total about 5%. A minor part of deconjugated secondary bile acids is also absorbed from the gut through passive diffusion and gets enriched in the enterohepatic circulation and may then act as signaling molecules in the host.

These bioconversions of bile acid by microbiota activity modulate the signaling properties of bile acids via FXR and the G protein-coupled bile acid receptor-1 (Takeda G

protein-coupled receptor 5 [TGR5]), which regulates bile acid metabolism and glucose and insulin sensitivity. Thus, the gut microbiota plays a critical role in bile acid metabolism and signaling to regulate metabolic homeostasis in health and disease. For example Pathak *et al*., (2018) shown that FXR activation of intestinal FXR shaped the gut microbiota to induce *Acetatifactor* and *Bacteroides* to convert CDCA to LCA, which activates TGR5 to stimulate glucagon-like peptide-1 (GLP-1) secretion, ultimately improving liver function and insulin and glucose tolerance.

2.6.3. Short-chain fatty acids

SCFAs are organic fatty acids that are end-products of gut microbiota fermentation of non-digestible dietary fibers, proteins and glycoproteins (Rastelli *et al.*, 2018) (**Table 5**) Acetate, propionate, and butyrate compose 95% of SCFAs. SCFA concentration varies along the gut, showing a higher value in the proximal colon (70– 140 mM), which progressively declines toward the distal colon (20– 40 mM) (den Besten *et al.*, 2013). SCFAs are involved in all the main physiological functionalities of the human host, such as metabolic regulation, immune function, and the activity of the CNS. At the molecular level, they act primarily through the activation of the "metabolite sensing" G-protein-coupled receptors (namely GPR41 and GPR43) (Sun *et al*., 2019), which are expressed by several cell types throughout the body (including colonocytes but also immune cells, endocrine cells, and adipocytes).

Another mechanism of action for SCFAs involves the inhibition of histone deacetylases (HDACs) which are important in several aspects of our metabolic homeostasis. SCFAs also play an important role as signaling molecules, controlling the expression and secretion of the major appetite and glucose regulatory peptides, peptide YY (PYY), and the

incretin hormone GLP-1 (Martin *et al.*, 2019). Absorbed SCFAs are then released into the bloodstream and reach the liver through the portal vein. From there, they can diffuse systemically to the peripheral venous system. As a preferred energy source for colonocytes, butyrate is mostly consumed locally, while propionate is metabolized in the liver.

Propionate and butyrate occur at low concentration in the periphery. Conversely, acetate abounds in the peripheral circulation. Able to cross the blood− brain barrier (BBB), it can be considered the most "systemic" of the SCFAs. However, despite their low peripheral concentration, propionate and butyrate still retain the potential to control distant organs by activating hormonal and nervous systems. Acetate and propionate are the most potent activators of GPCRs. Moreover, butyrate and propionate have been reported, in rats, to activate intestinal gluconeogenesis (IGN) by (i) butyrate triggering IGN gene expression by increasing the cAMP concentration in colonocytes, and (ii) propionate activating IGN by regulating gene expression through a gut− brain neural circuit involving GPCR41 and itself can be converted into glucose by IGN. This IGN mechanism ultimately regulates body weight, modulating the host glucose control by increased insulin sensitivity and glucose tolerance. Finally, butyrate also represents an important energy source for the host, providing its total daily energy requirement while maintaining anaerobiosis in the gut lumen (De Vadder *et al.*, 2014).

SCFAs are also potent immune regulators. The mammalian immune system, especially the adaptive immunity, has evolved in parallel to gut microbiota acquisition, probably in response to the need to maintain control over the millions of microbial cells inhabiting our gut (Belkaid & Harrison, 2017). On the other hand, the microbiota has become an active and essential component of the host immune system, being strategic for

training the immune system during infancy as well as for its functional tuning for the rest of our lives (Martin *et al.*,, 2010; Torow & Hornef, 2017). First, the SCFA action is of primary importance in fortifying the innate immunity of the intestinal mucosa by reinforcing the IEC barrier, increasing mucus production by goblet cells, and strengthening the tight junctions (TJs). Moreover, by supporting the production of the inflammasome-related cytokine interleukin (IL)-18 by IECs (Spiljar, Merkler, & Trajkovski, 2017), as demonstrated in mouse models, SCFAs may contribute to the maintenance of epithelial integrity. Finally, by signaling to GPCRs, SCFAs have been reported in mice to control the activation process of the inflammasome (Kabat, Pott, & Maloy, 2016; Spiljar *et al.*, 2017).

2.6.4. Other GM-derived small molecules

Endogenous vitamins. Bacterial metabolites or structural components, can diffuse throughout the body, affecting organs either directly or by hormonal and neuronal signaling. To fulfill their metabolic needs, some gut microorganisms can produce menaquinone, folate (Pompei et al., 2007), cobalamin and riboflavin, which, from the host perspective, act as vitamins K2, B9, B12, and B2 (Bacher,*et al*., 2000; Rowland *et al*., 2018). These vitamins are known to be involved in several biological functions, from blood coagulation to bone metabolism and insulin sensitivity (Vernocchi, Del Chierico, & Putignani, 2016).

Neurotransmitters. Several neurotransmitters, including serotonin, catecholamines (adrenaline, noradrenalin, and dopamine), GABA), amino acids, and indolic compounds, are controlled by the gut microbiota. In addition, some intestinal bacteria have been reported to be sources of 5-hydroxytryptamine (5HT) and nitric oxide (Rastelli, Knauf, & Cani, 2018; Turroni *et al.*, 2018).

Tryptophan metabolites. The gut microbiota can produce a range of tryptophan metabolites with an important role in modulating the host immune and metabolic homeostasis (Agus *et al.,* 2018). In particular, tryptophan is metabolized by intestinal microbes to several AhR agonists, such as indole, indolic acid, IPA, indole-3-acetaldehyde, tryptamine, nicotinic acid, skatole, and tryptamine (Gao *et al.*, 2018; Roager & Licht, 2018).

Lactate. Another noteworthy GM-produced metabolite is lactate. Principally produced by the milk-fermenting GM ecosystem of breast-fed infants, bacterial lactate can exert important metabolic and regulatory effects being an energy source and acting as an immune modulator, HDAC inhibitor, and signaling molecule (Engevik & Versalovic, 2017).

Very long chained fatty acids. Intestinal microbes are potentially capable of producing a range of fatty acids with longer chain lengths than SCFAs, with different impacts on the host health. For instance, gut microbiota-produced long-chain fatty acid that can modulate lymphocyte T-helper 17 (*Th17*) gene expression, forcing the balance between homeostatic and potentially pathogenic Th17 cells toward the latter, as shown in murine T cell cultures. In contrast, some gut microbes can conjugate ω -6 fatty acids to produce conjugated linoleic acid, which has been reported to have anti-inflammatory properties and increase insulin sensitivity, reducing adiposity, atherosclerosis, and carcinogenesis. These effects are likely related to its action on PPARα and γ, cyclooxygenases, and lipoxygenases (Abdul Rahim *et al.*,, 2019; Engevik & Versalovic, 2017).

EXPERIMENTAL RESULTS

General Objectives

The liver is a unique organ in the human body that has two sources of blood supply, from the hepatic artery and from the portal vein. The hepatic portal vein transports nutrients and xenobiotics present in food from the gastrointestinal tract to the liver and ensures that these are processed in the liver before they reach the rest of the organism. This enables the liver with a broad range of functions that can be divided into detoxification of xenobiotics, intermediary metabolism (including a central role in carbohydrate, lipid and nitrogen metabolism), secretion of bile, synthesis of various serum proteins, degradation of hormones, and immunological activity. If the gut barrier is disrupted, the liver is the first organ in the body that encounters the microbial metabolites, toxins and microorganisms from the intestine. The liver therefore stands at the crossroad between the portal blood flow coming from the intestine and the rest of the organism. In the liver, transcription factors from the nuclear receptor superfamily can sense fluctuating levels of nutrients and xenobiotics and promptly adapt hepatic metabolism by modulating the transcription of genes. Among these, 2 nuclear receptors, the pregnane X receptor (PXR) and the constitutive androstane receptor (CAR) are commonly described as xenobiotic sensors in the liver. They are known to regulate the expression of phase 1 xenobiotic metabolizing enzymes (XMEs) from the cytochrome p450 family (CYPs), thereby facilitating the elimination of xenobiotics. A growing number of studies have also demonstrated that CAR and PXR play a role in energy homeostasis through the regulation of glucose and lipid metabolism. Recently, several new natural ligands, kynurenine and planar indoles resulting from the microbial metabolism of dietary tryptophan for AhR, a ligand-activated transcription factor from the helix-loop-helix Per-Arnt-Sim family and also

a xenobiotic sensor, have been discovered. Microbial ligand-driven activation of AhR is thought to limit intestinal inflammation and intestinal permeability and may be dysfunctional in inflammatory bowel disease (IBD) and in metabolic diseases (Lamas *et al*., 2016). Indole derivatives, such as indole-3-propionic acid (IPA) from gut microbial conversion of tryptophan has also been implicated to activate PXR and to decrease intestinal permeability in the small intestine in a PXR-dependent way (Venkatesh *et al*., 2014). Furthermore, a study by Montagner *et al*. (2016) has demonstrated that gut microbiota influences the circadian activity of CAR & PXR in the liver. Lastly, *Cyp3a11* mRNA expression in the liver of germ-free mice is significantly reduced compared to control mice (Claus *et al*., 2011). These studies have raised the awareness that factors involved in xenobiotic metabolism could be intimate partners with the gut microbiota.

In this PhD work, we aimed to further study the interactions between the xenobiotic sensors CAR and PXR and addressed the following objectives:

1. To investigate the hepatic responses dependent on PXR in vivo in mouse using a pharmaceutical approach and transcriptomic analysis;
2. To investigate the role of PXR in the ileum and compare it to previously obtained liver data using microarray analysis;
3. To understand the impact of the gut microbiota on the PXR-dependent hepatic functions and whether PXR may in turn influence the gut microbiota. Thus, we aimed at establishing the importance of the bi-directional interaction of PXR and the gut microbiota using animal models, molecular biology, transcriptomic and metabolomic approaches, and microbiota sequencing;

4. To investigate the bi-directional interaction between CAR and the gut microbiota through similar approaches.

Furthermore, the question of a potential sexual dimorphism in the interactions between CAR/PXR and the gut microbiota was present throughout this work and particularly in our 3rd and 4th objectives.

Chapter 3.1

Gene Expression Profiling Reveals that PXR Activation Inhibits Hepatic PPARα Activity and Decreases FGF21 Secretion in Male C57Bl6/J Mice

Context: In this first experimental chapter, we used a pharmacological approach to investigate the hepatic responses dependent on PXR in vivo in mouse. Through unbiased transcriptome analysis we provided a novel set of experimental data highlighting PXR's roles in both xenobiotic and metabolic homeostasis. We also first report the role of PXR in the control of the liver-derived hormone FGF21. This body of work was published in the "International Journal of Molecular Sciences".

International Journal of
Molecular Sciences

MDPI

Article

Gene Expression Profiling Reveals that PXR Activation Inhibits Hepatic PPARα Activity and Decreases FGF21 Secretion in Male C57Bl6/J Mice

Sharon Ann Barretto †, Frédéric Lasserre †, Anne Fougerat, Lorraine Smith, Tiffany Fougeray, Céline Lukowicz, Arnaud Polizzi, Sarra Smati, Marion Régnier, Claire Naylies, Colette Bétoulières, Yannick Lippi, Hervé Guillou, Nicolas Loiseau, Laurence Gamet-Payrastre, Laila Mselli-Lakhal and Sandrine Ellero-Simatos *

Institut National de la Recherche Agronomique (INRA), UMR1331 Toxalim, F31-027 Toulouse CEDEX 3, France

* Correspondence: sandrine.ellero-simatos@inra.fr

† These authors contributed equally to this work.

Received: 21 June 2019; Accepted: 31 July 2019; Published: 1 August 2019

Abstract: The pregnane X receptor (PXR) is the main nuclear receptor regulating the expression of xenobiotic-metabolizing enzymes and is highly expressed in the liver and intestine. Recent studies have highlighted its additional role in lipid homeostasis, however, the mechanisms of these regulations are not fully elucidated. We investigated the transcriptomic signature of PXR activation in the liver of adult wild-type vs. *Pxr*$^{-/-}$ C57Bl6/J male mice treated with the rodent specific ligand pregnenolone 16α-carbonitrile (PCN). PXR activation increased liver triglyceride accumulation and significantly regulated the expression of 1215 genes, mostly xenobiotic-metabolizing enzymes. Among the down-regulated genes, we identified a strong peroxisome proliferator-activated receptor α (PPARα) signature. Comparison of this signature with a list of fasting-induced PPARα target genes confirmed that PXR activation decreased the expression of more than 25 PPARα target genes, among which was the hepatokine fibroblast growth factor 21 (*Fgf21*). PXR activation abolished plasmatic levels of FGF21. We provide a comprehensive signature of PXR activation in the liver and identify new PXR target genes that might be involved in the steatogenic effect of PXR. Moreover, we show that PXR activation down-regulates hepatic PPARα activity and FGF21 circulation, which could participate in the pleiotropic role of PXR in energy homeostasis.

Keywords: nuclear receptors; hepatokines; transcriptomics

1. Introduction

Pregnane X receptor (PXR, systematic name NR1I2) is a member of the nuclear receptor superfamily and is highly expressed in the liver and intestine of mammals [1]. PXR was characterized as a xenosensor that regulates the expression of xenobiotic-metabolizing enzymes and transporters, thereby facilitating the elimination of xenobiotics and endogenous toxic chemicals such as bile acids [2]. Upon ligand-binding, PXR translocates to the nucleus, heterodimerizes with retinoid X receptor (RXR, NR2B1) and binds to PXR direct repeat 4 (DR-4) response elements (PXRE) that are usually located upstream of target genes. Because of an unusually large and flexible binding pocket, PXR can be activated by a variety of structurally diverse chemicals, including pharmaceutical drugs, dietary supplements, herbal medicines, environmental pollutants, and endogenous molecules [3]. In line with the role of PXR as a master regulator of xenobiotic metabolism, its first described target gene was cytochrome P450 (CYP) 3A4 in humans [4], which represents 10% of all clinically relevant drug-metabolizing CYPs in the human liver and up to 75%–85% in the intestine [5] and is responsible for the metabolization of 60% of marketed drugs [6].

Besides its original function as part of the detoxification machinery, recent studies have also unveiled functions for PXR in intermediary metabolism. There is an increasing amount of clinical evidence showing that PXR agonists cause hyperglycemia in humans [7] and pre-clinical work suggesting that PXR regulates hepatic glucose metabolism, however, there is still no solid understanding of the consequences, or of the mechanisms involved. Activated PXR has been shown to repress expression of the gluconeogenic genes glucose-6-phosphatase (*G6Pase*) and phosphoenolpyruvate carboxykinase (*PCK1*) [8], and of genes involved in glucose uptake such as *GLUT2* and of glucokinase (*GCK*) [9]. Although there is limited data on the relationship between PXR and fatty liver in humans in vivo, many studies have demonstrated that PXR activation also causes hepatic lipid accumulation in human cell models, and in vitro and in vivo mouse models [7,10]. This pro-steatotic effect is thought to result from both the activation of lipogenesis and inhibition of β-oxidation [7]. However, the mechanisms by which PXR activation induces perturbations of lipid metabolism are not fully elucidated. Recently, it was shown that the activation of intestinal PXR signaling induced dyslipidemia and intestinal cholesterol accumulation [11], while activation of hepatic PXR signaling was sufficient to promote hypercholesterolemia and hepatic lipid accumulation [12].

Here, we aimed to gain insights into the potential metabolic dysregulations induced upon PXR activation and performed a transcriptomic comparison of the hepatic gene profiles of wild type (WT) vs. *Pxr*$^{-/-}$ male mice treated with the rodent specific PXR ligand pregnenolone 16α-carbonitrile (PCN). As expected, we observed that PCN treatment-induced hepatic steatosis. We unraveled several previously unknown PXR target genes involved in liver lipid accumulation and discovered a very robust peroxisome proliferator-activated receptor α (PPARα) signature amongst the PXR down-regulated target genes. The PXR-induced decrease in PPARα activity included the regulation of the hepatokine FGF21, a liver-derived hormone with major endocrine roles [13]. This cross-talk between PXR and PPARα in the regulation of FGF21 may contribute to endocrine disruption by xenobiotics acting as ligands for PXR.

2. Results

2.1. Effect of PXR Activation on Physiological Parameters and Liver Lipids

We investigated the effect of PXR activation by its pharmacological ligand PCN in WT and *Pxr*$^{-/-}$ male mice. PCN treatment did not affect body weight but increased relative liver mass in a PXR-dependent way (Figure 1a). In the liver, PXR activation significantly increased cholesterol esters and triglyceride levels but did not significantly impact free cholesterol (Figure 1a). In the plasma, PXR activation increased alanine transaminase (ALT) and decreased total cholesterol levels but did not impact free fatty acids, triglycerides (Figure 1a), HDL, LDL, or glucose levels (Figure S1).

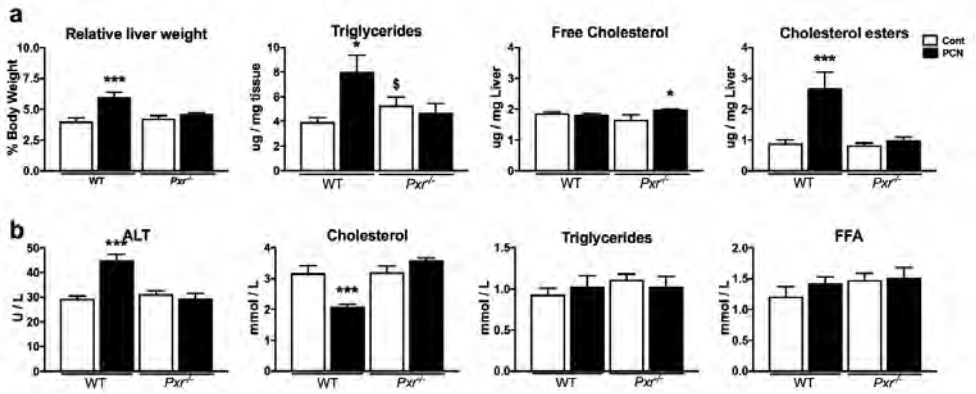

Figure 1. Effect of pregnenolone 16α-carbonitrile (PCN) treatment on liver parameters (**a**) and plasma biochemistry (**b**). Data are shown as mean ± SEM of n = 5–6 per group. * $p \leq 0.05$, ** $p \leq 0.01$, *** $p \leq 0.005$ for PCN effect using 2-way ANOVA and Tukey's post-tests. $ $p \leq 0.05$ for genotype effect. ALT: Alanine amino-transferase; FFA: Free fatty acids.

Figure 1. Effect of pregnenolone 16α-carbonitrile (PCN) treatment on liver parameters (**a**) and plasma biochemistry (**b**). Data are shown as mean ± SEM of n = 5–6 per group. * $p \leq 0.05$, ** $p \leq 0.01$, *** $p \leq 0.005$ for PCN effect using 2-way ANOVA and Tukey's post-tests. $ $p \leq 0.05$ for genotype effect. ALT: Alanine amino-transferase; FFA: Free fatty acids.

Int. J. Mol. Sci. **2019**, *20*, 3767 3 of 13

2.2. Effects of PXR Activation on the Hepatic Transcriptome

2.2. Effects of PXR Activation on the Hepatic Transcriptome

Using microarrays, we obtained global transcriptional profiles. Principal component analysis (PCA) first illustrated that PCN treatment significantly impacted the hepatic transcriptome (Figure 2a). The discrimination of WT PCN vs. WT Cont seems stronger than that of the *Pxr*$^{-/-}$ PCN vs. *Pxr*$^{-/-}$ Cont, confirming, as expected, a significant PXR-dependent transcriptional effect of PCN. We next used linear models and considered genes to be significantly regulated with a fold-change >1.5 and a false discovery rate (FDR) <0.05. Heatmap clustering confirmed the PCA results (Figure S2). It indeed revealed five gene clusters with the largest cluster (1602 probes) comprised of genes up-regulated by PCN in WT mice only (cluster 5). Another cluster (cluster 2) showed 407 probes down-regulated upon PCN treatment in WT mice only. Cluster 4 contained 498 probes that showed genes differentially regulated in WT vs. *Pxr*$^{-/-}$ mice, independently of PCN. Finally, cluster 3 (605 probes) illustrated a PCN effect in both WT and *Pxr*$^{-/-}$ mice.

Using microarrays, we obtained global transcriptional profiles. Principal component analysis (PCA) first illustrated that PCN treatment significantly impacted the hepatic transcriptome (Figure 2a). The discrimination of WT PCN vs. WT Cont seems stronger than that of the *Pxr*$^{-/-}$ PCN vs. *Pxr*$^{-/-}$ Cont, confirming, as expected, a significant PXR-dependent transcriptional effect of PCN. We next used linear models and considered genes to be significantly regulated with a fold-change >1.5 and a false discovery rate (FDR) <0.05. Heatmap clustering confirmed the PCA results (Figure S2). It indeed revealed five gene clusters with the largest cluster (1602 probes) comprised of genes up-regulated by PCN in WT mice only (cluster 5). Another cluster (cluster 2) showed 407 probes down-regulated upon PCN treatment in WT mice only. Cluster 4 contained 498 probes that showed genes differentially regulated in WT vs. *Pxr*$^{-/-}$ mice, independently of PCN. Finally, cluster 3 (605 probes) illustrated a PCN effect in both WT and *Pxr*$^{-/-}$ mice.

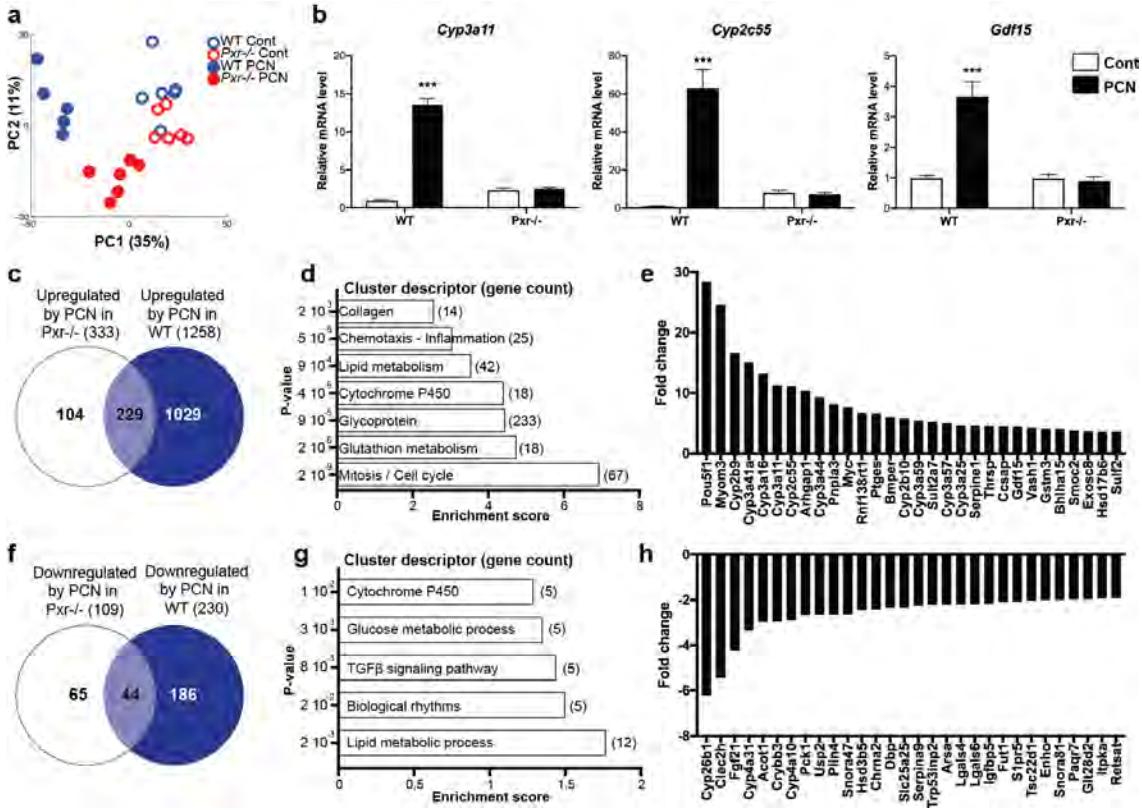

Figure 2. Impact of pregnane X receptor (PXR) activation on the hepatic transcriptome. (**a**) Principal component analysis (PCA) score plots of the whole transcriptomic dataset. (**b**) qPCR confirmation on selected genes. * $p \leq 0.05$, ** $p \leq 0.01$, *** $p \leq 0.005$ for PCN effect using 2-way ANOVA and Tukey's post-tests. (**c**,**f**) Venn diagram representing the numbers of genes affected by PCN treatment. (**d**,**g**) Gene enrichment analyses of the PXR target genes. (**e**,**h**) The 30 genes with the highest fold changes upon PCN treatment.

Figure 2. Impact of pregnane X receptor (PXR) activation on the hepatic transcriptome. (**a**) Principal component analysis (PCA) score plots of the whole transcriptomic dataset. (**b**) qPCR confirmation on selected genes. * $p \leq 0.05$, ** $p \leq 0.01$, *** $p \leq 0.005$ for PCN effect using 2-way ANOVA and Tukey's post-tests. (**c**,**f**) Venn diagram representing the numbers of genes affected by PCN treatment. (**d**,**g**) Gene enrichment analyses of the PXR target genes. (**e**,**h**) The 30 genes with the highest fold changes upon PCN treatment.

We next sought to decipher the biological functions affected by PXR activation. PCN treatment significantly up-regulated the expression of 1258 genes in WT animals, and of 333 genes in *Pxr*$^{-/-}$ mice (Figure 2c). Using the 1029 prototypical PXR target genes (those that were up-regulated only in WT animals), we conducted a pathway enrichment analysis, which revealed seven functional clusters significantly enriched (Figure 2d and Table S1) with genes involved in cell cycle, cell division and mitosis, glutathione metabolism, cytochromes P450, lipid metabolism, chemotaxis, and positive regulation of inflammatory response. Figure 2e confirms these results by illustrating the fold-changes of the top 30 most up-regulated genes. These results first confirmed the well-described influence

We next sought to decipher the biological functions affected by PXR activation. PCN treatment significantly up-regulated the expression of 1258 genes in WT animals, and of 333 genes in *Pxr*$^{-/-}$ mice (Figure 2c). Using the 1029 prototypical PXR target genes (those that were up-regulated only in WT animals), we conducted a pathway enrichment analysis, which revealed seven functional clusters significantly enriched (Figure 2d and Table S1) with genes involved in cell cycle, cell division and mitosis, glutathione metabolism, cytochromes P450, lipid metabolism, chemotaxis, and positive regulation of inflammatory response. Figure 2e confirms these results by illustrating the fold-changes of the top 30 most up-regulated genes. These results first confirmed the well-described influence

of PXR activation on hepatic xenobiotic-metabolizing enzymes, mainly those from the Cyp3 family. Table S2 provides a full description of the impact of PCN treatment on all xenobiotic-metabolizing enzymes. Induction of two of the most well-described PXR targets, *Cyp2c55* and *Cyp3a11* were further confirmed using RT-qPCR (Figure 2b). Interestingly, the "lipid metabolism" pathway was also highly significantly enriched upon PXR activation and, among the 30 genes with the highest fold-change, the patatin-like phospholipase domain containing 3 (*Pnpla3*), the thyroid hormone-responsive spot 14 (*Thrsp* or *Spot14*), and the growth/differentiation factor 15 (*Gdf15*) belonged to this pathway. Induction of *Gdf15* was also confirmed by RT-qPCR (Figure 2b). Finally, the regulation of genes involved in de novo lipogenesis was also confirmed by qPCR and showed a significant increase of the SREBP-1 lipogenic pathway in *Pxr*$^{-/-}$ mice compared to WT mice (Figure S3).

We next investigated the effect of PCN on gene down-regulation. PCN treatment significantly decreased the expression of 186 genes in a PXR-dependent manner (Figure 2f). GO analyses revealed that these genes were involved in lipid metabolic process, biological rhythms, transforming growth factor-β (TGFβ) signaling pathway, glucose metabolism, and cytochromes P450 (Figure 2g). The 30 genes with the highest fold-changes are illustrated in Figure 2h. Interestingly, among these 30 genes, five (namely *Fgf21*, *Cyp4a10*, *Cyp4a31*, *Acot1,* and *Plin4*) are well-described target genes of PPARα, a key hepatic transcriptional regulator involved in lipid homeostasis.

2.3. Comparison of PXR and PPARα-Dependent Transcriptome

This prompted us to investigate the intersection between PXR and PPARα activation to test the hypothesis that PXR activation influenced PPARα activity. We took advantage of our previously published microarray dataset [14], in which C57Bl6/J male mice carrying an hepatocyte-specific deletion of *Pparα* (*Pparα*$^{hep-/-}$) were fasted for 24 h to induce PPARα activity and compared to their wild-type littermates (*Pparα*$^{hep+/+}$). We have indeed previously shown that, during fasting, PPARα senses increased levels of free fatty acids released from adipocytes, and in response, controls the expression of hundreds of genes involved in fatty acid uptake, transport, and catabolism in hepatocytes [14,15]. Figure 3a indeed illustrates that a large number of the fasting-induced hepatic genes are PPARα sensitive, with 538 genes significantly up-regulated in a PPARα-dependent manner. Also, 461 genes were significantly down-regulated in a PPARα-dependent manner upon fasting (Figure 3d). We compared these genes with those regulated upon PXR activation. We found 27 genes that were both up-regulated upon PPARα activation and down-regulated upon PXR activation (Figure 3b). These genes are illustrated in Figure 3c and include, among others, *Pparα* itself, *Cyp4a14*, *Cyp4a10*, *Cyp4a31,* and *Fgf21*. There were also 46 genes that were regulated in the opposite direction, i.e., that were down-regulated upon PPARα activation and up-regulated upon PXR activation (Figure 3e,f).

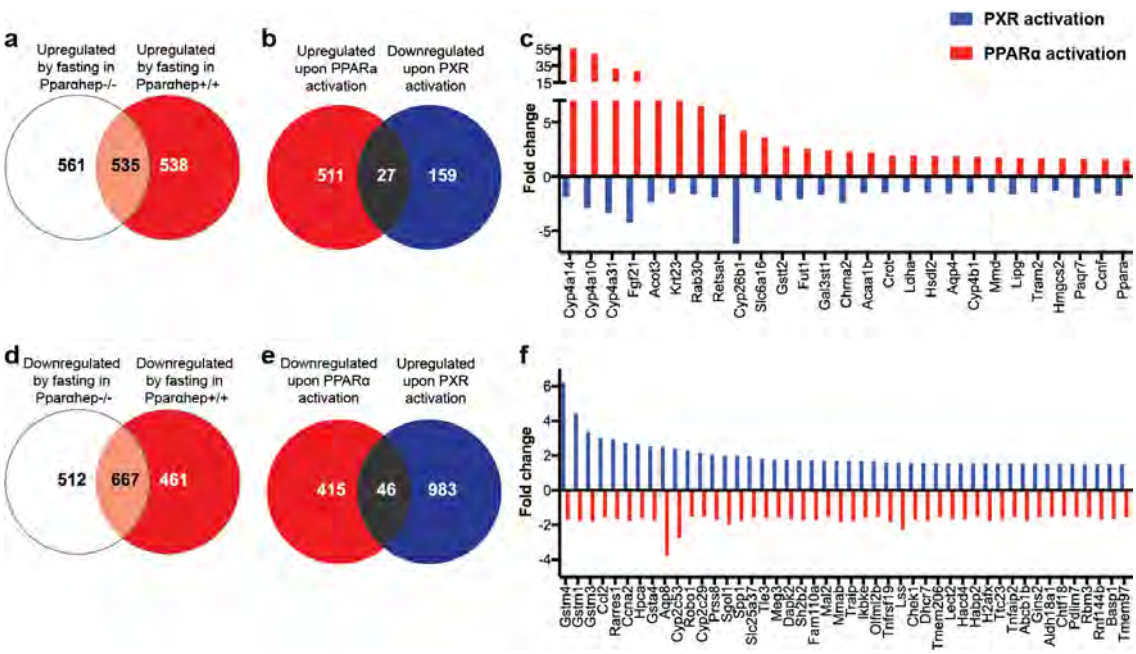

Figure 3. Comparison between PXR and peroxisome proliferator-activated receptor α (PPARα) target genes. (**a**,**d**) Venn diagrams representing the number of genes up-(**a**) or down-(**d**) regulated upon fasting in $Ppar\alpha^{hep+/+}$ vs. $Ppar\alpha^{hep-/-}$ mice. (**b**,**e**) Venn diagrams representing the number of genes regulated upon PPARα (red) or PXR (blue) activation. (**c**,**f**) Fold-changes for the genes that are shared in the previous Venn diagrams.

2.4. Regulation of FGF21

Using RT-qPCR analyses, we confirmed that PXR activation down-regulated *Pparα* and its target genes expression (Figure 4a), among which was *Fgf21*. FGF21 is a recently described hepatokine with systemic metabolic effects [16]. We measured plasmatic FGF21 and confirmed that circulating FGF21 was decreased upon PCN treatment, since its levels were not detectable anymore in WT-treated mice (Figure 4b). Surprisingly, PXR deletion also influenced FGF21 level since *Pxr*$^{-/-}$ mice also showed no detectable levels of circulating FGF21. These differences were not due to different fasting states since glycemia was not significantly different between the four groups (Figure S1).

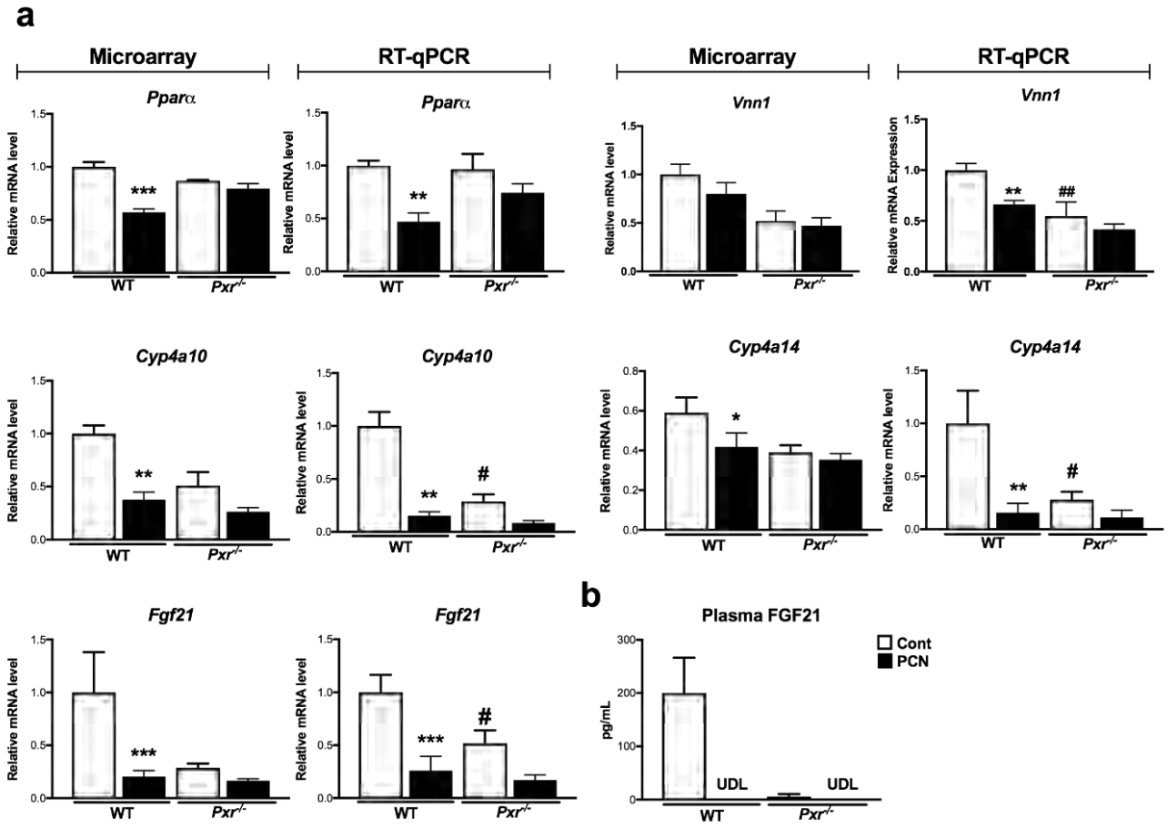

Figure 4. Impact of PXR activation on hepatic PPARα activity. Gene expression in the liver (**a**) derived from the microarray and from complementary qPCR experiments. (**b**) Plasma levels of FGF21. Data are mean ± SEM of $n = 5–6$ per group. * $p \leq 0.05$, ** $p \leq 0.01$, *** $p \leq 0.005$ for PCN effect, # $p \leq 0.05$, ## $p \leq 0.01$ for genotype effect using 2-way ANOVA and Tukey's post-tests. UDL: Under the detection limit.

3. Discussion

The liver is one of the major organs involved in energy production. Hepatic lipid metabolism plays a crucial role during fasting and/or prolonged exercise. Upon lowering of blood glucose, the liver increases glucose production by augmenting gluconeogenesis and glycogenolysis to maintain blood glucose levels, increases fatty acid oxidation and ketogenesis to provide extra-hepatic tissues with ketone bodies, and decreases lipogenesis to attenuate triglyceride storage. These processes are under tight transcriptional control and, in response to hormones such as glucagon and glucocorticoids, many transcription factors cooperate to regulate various genes involved in metabolic pathways aimed at restoring homeostasis [17]. Among those, hepatic PPARα has been well described as crucial for this adaptation. However, recent data have highlighted that other nuclear receptors, such as the aryl H receptor (AhR), the constitutive androstane receptor (CAR), and PXR, which were historically described as xenobiotic sensors, can also interact with the hormone-responsive transcription factors to regulate the liver metabolic processes [18].

Here, we investigated the transcriptomic effects of a pharmacological activation of PXR. The expression of PXR was not described as highly circadian, however, its activity, as measured by the expression of its prototypical target gene *Cyp3a11*, has been shown to be influenced by the time of the day, and is highest as zeitgeber time (ZT) 6 [19]. Therefore, we decided to investigate the effects of PXR activation at ZT6, a time at which mice were in a physiological semi-fasted state.

Several studies have already investigated the hepatic signature of PXR activation in vivo [20–22] or in vitro [23]. However, most of these studies focused on the effect of PXR activation on xenobiotic-metabolizing enzymes. Here, we confirm that the regulation of xenobiotic metabolism is one of PXR's most potent functions in the hepatocytes (Figure 2; Table S3). However, our gene enrichment analyses also revealed that lipid metabolism was among the top-dysregulated pathways

also revealed that lipid metabolism was among the top-dysregulated pathways upon PXR activation, considering both the up-regulated, as well as the down-regulated genes.

First, PXR activation induced a very significant decrease in plasma cholesterol levels and a significant increase in liver triglycerides and cholesterol esters (Figure 1). The pro-steatotic effects of acute PXR activation have been shown in many studies. However, its role in the regulation of cholesterol homeostasis is more controversial. The anti-HIV drug Efavirenz has been recently shown to induce steatosis and hypercholesterolemia, an effect that was absent in a model of hepatic deletion of PXR [12]. These perturbations were mediated through increased fatty acid transport and cholesterol synthesis, via the PXR-dependent regulation of *Cd36* and *Sqle*. In our data, we confirmed that PXR activation significantly affected *Cd36* and other transporters involved in cholesterol transport, but did not observe any regulation of genes involved in cholesterol biosynthesis, such as *Cyp7a1*, *Sqle,* and *Hmgcr* (Figure S4). This resulted in decreased circulating cholesterol.

Among the up-regulated genes in the liver, we observed that PXR activation increased the expression of several genes that correlate with lipogenesis, such as the patatin-like phospholipase domain containing 3 (*Pnpla3*) and the thyroid hormone-responsive spot 14 (*Thrsp* or *Spot14*). *Spot14* was first identified as a thyroid-responsive gene and is known to transduce hormone- and nutrient-related signals to genes involved in lipogenesis [24]. Regulation of *SPOT14* by PXR was previously described in human hepatocytes [25] and led to increased fatty acid synthase (FASN) expression and triglyceride accumulation. The PNPLA3 protein has lipase activity towards triglycerides in hepatocytes and a loss-of-function polymorphism of this gene has been shown to be strongly associated with nonalcoholic fatty liver disease [26]. However, to our knowledge, the regulation of *Pnpla3* expression by PXR has not been previously described. Among the lipid-metabolic-related genes, we also observed that the expression of the growth/differentiation factor 15 (*Gdf15*), also known as *MIC-1*, was increased by a factor of four upon PCN treatment, in a PXR-dependent way. GDF15 is a distant member of the transforming growth factor-ß (TGF-ß) superfamily that is considered a crucial hormone in regulating lipid and carbohydrate metabolism. In animal models, overexpression of GDF15 leads to a lean phenotype and improvements of metabolic parameters by increasing the expression of key thermogenic and lipolytic genes in brown and white adipose tissue [27]. Hepatic and circulating GDF15 levels were also increased in animals with blunted ß-oxidation ($Cpt2^{hep-/-}$ mice) to maintain systemic energy homeostasis upon fasting [28]. Whether the observed increase in *Gdf15* mRNA upon PCN treatment results from direct regulation of *Gdf15* by PXR or represents a secondary adaptation to decreased ß-oxidation remains to be determined. In both cases, regulation of GDF15 levels upon PXR activation might be of physiological relevance since GDF15 has been implicated in a wide variety of biological functions including control of food intake and body weight [29].

Among the genes that were down-regulated upon PXR activation, we observed a very consistent PPARα-like signature, with the decreased expression of many *Cyp4* genes, which are highly sensitive PPARα target genes [14,15]. These results coincide with previous findings in which PCN decreased the hepatic expression of *Pparα*, *Cyp4a10,* and *Cyp4a14* [21]. Neonatal exposure to a single dose of PCN also persistently down-regulated *Cyp4a* expression and decreased PPARα binding to the *Cyp4a* gene loci in adult mice [20]. By comparing the list of genes down-regulated upon PXR activation to a list of genes up-regulated upon PPARα activation, we here extend these previous findings and demonstrate that the inhibition of PPARα activity by PXR affects more than the expression of *Cyp4* genes. For example, the PXR–PPARα interaction probably inhibited the expression of the acetyl-Coenzyme A acyltransferase 1B (*Acaa1b*), of the acyl-coA thioesterase 3 (*Acot3*), of *Krt23* and *Rab30*, of the rate-limiting enzyme in ketogenesis 3-hydroxy-3-methylglutaryl-CoenzymeA synthase 2 (*Hmgcs2*) and of the hepatokine *Fgf21*, all of which are well-described PPARα targets [14]. Using a similar approach in human primary hepatocytes treated with the hPXR ligand rifampicine and the hPPARα ligand WY14643, Kandel et al. had previously shown that more than 14 genes were responsive to both WY14643 (up-regulated) and to rifampicine (down-regulated), among which ACAA2, CYP4A11, and HMGCS2 [23], therefore suggesting the human relevance of our results.

FGF21 is predominantly produced in the liver [30] and exerts pleiotropic effects on the body to maintain overall metabolic homeostasis. FGF21 metabolic benefits range from reducing body weight to alleviating hyperglycemia, insulin resistance, and improvement of lipid profiles [16]. In animal models of obesity, as well as in obese patients, FGF21 has been shown to induce body weight loss and to increase insulin sensitivity and lipid homeostasis [30]. The effects of FGF21 on fertility, growth, and longevity are also well documented [31,32]. Finally, FGF21 seems to be involved in food preferences. For example, FGF21 production in response to carbohydrate intake significantly decreases sugar preferences [33].

Although PXR is mainly expressed in the liver and in the intestine, and not in adipose tissue [34], deletion of *Pxr* appears to influence insulin sensitivity in white adipose tissue and in the muscle [35], serum leptin, and adiponectin levels [36] and PXR activation regulates gene expression in both white and brown adipose tissues [37]. This suggests systemic effects of *Pxr* deletion and activation for which mechanisms have not been described yet. White and brown adipose tissues are among the most described target tissues of FGF21 [16]. Whether FGF21 could be an effector of the systemic effects of PXR remains an open question. Here, we demonstrate that both PXR-activation and PXR deletion decrease the hepatic *Fgf21* mRNA levels and completely abolished the circulating FGF21 levels. This apparent contradictory effect was not limited to the regulation of FGF21 but was also observed in other PPARα target genes (Figure 4). Therefore, it seems that both PXR activation and silencing result in the inhibition of PPARα activity, probably through distinct mechanisms that would need additional investigations. However, it is worth noticing that the same apparent contradictory effect was observed for the regulation of de novo lipogenesis. In human HepG2 cells, PXR activation by rifampicin promoted steatosis via induction of SREBP-1 pathway (mainly SREBP-1a), whereas PXR silencing enhanced AKR1B10 expression, which subsequently stabilized the acetyl-CoA carboxylase, thereby promoting de novo lipogenesis [10]. However, these mechanisms are probably species-specific as, in our data, we did not observe this increase in AKR1B10 expression, whereas the SREBP-1 pathway was increased by PXR ablation and not by PCN treatment (Figure S3). Overall, this demonstrated that complex species-specific mechanisms occur in the regulation of lipogenic pathways by PXR activation and ablation, and our results suggest that this might also be true for the regulation of ß-oxidation and PPARα activity.

Perspectives and limitations of our study include the use of male mice only, while PXR activation has been shown to impact both xenobiotic-metabolizing enzymes and glucose and lipid metabolism in a sexually-dimorphic way [38,39]. Therefore, it would be interesting to decipher whether the signature of PXR activation described in our study is also valid in female mice. Second, our study focused on short-term changes. An important remaining question is to determine the effect of multiple weak PXR agonists such as those present in our environment on the observed regulations, especially on FGF21 secretion. Indeed, PXR's main target gene *CYP3A4* is known to be involved in the metabolism of more than 60% of the currently marketed drugs [6] and several hundreds of environmental, occupational, and natural products are demonstrated PXR agonists in both mice and humans [3]. Therefore, regulation of hepatic lipid accumulation by acute or chronic PXR activation might be an important mechanism of xenobiotic-induced steatosis. Finally, the fact that we did not generate the PXR and PPARα dependent transcriptomes in a parallel fashion might have underestimated the number of genes affected by the cross-talk between the two receptors. Therefore, it would be interesting to investigate the effect of PXR activation upon prolonged fasting such as the one used to trigger PPARα. It could also be interesting to decipher whether the pro-steatotic effect of PCN depends on PPARα by treating PPARα knock-out mice with PCN.

Altogether, our results present an additional resource of transcriptome analyses that confirm and extend previous findings on the genes involved in the pro-steatotic effects of PXR. As previously observed in various models [7], we confirm that the observed pro-steatotic effect of PXR activation probably results from both induction of lipogenesis and repression of β-oxidation, and further highlight that this repression is certainly mediated, at least in part, through inhibition of PPARα. We also provide

new hypotheses regarding the yet poorly explored pleiotropic effects of PXR that could result from the regulation of recently discovered hepatokines, such as GDF15 and/or FGF21. More studies are needed to confirm the physiological relevance of these regulations. Our findings might have clinical and public health relevance given the wide range of drugs and environmental xenobiotics that have been described as PXR ligands and potential endocrine disruptors.

4. Materials and Methods

4.1. Animals

In vivo studies were performed in a conventional laboratory animal room following the European Union guidelines for laboratory animal use and care. The current project was approved by an independent ethics committee (CEEA-86 Toxcométhique) under the authorization number 2018062810452910. The animals were treated humanely with due consideration to the alleviation of distress and discomfort. All mice were housed at 21–23 °C on a 12 h light (ZT0–ZT12) 12 h dark (ZT12–ZT24) cycle and allowed free access to the diet (Teklad Global 18% Protein Rodent Diet) and tap water. ZT stands for Zeitgeber time; ZT0 is defined as the time when the lights are turned on. Twelve six-week-old wild-type (WT) C57BL/6J male mice were purchased from Charles River and 12 *Pxr*$^{-/-}$ animals (backcrossed on the C57Bl/6J background) were engineered in Pr. Meyer's laboratory [40] and were bred for 10 y in our animal facility. Mice were acclimatized for two weeks, then randomly allocated to the different experimental groups: Wild-type control (WT CONT, $n = 6$), wild-type PCN-treated (WT PCN, $n = 6$), *Pxr*$^{-/-}$ control (*Pxr*$^{-/-}$ CONT, $n = 6$), *Pxr*$^{-/-}$ PCN-treated (*Pxr*$^{-/-}$ PCN, $n = 6$). PCN-treated mice received a daily intraperitoneal injection of PCN (100 mg/kg) in corn oil for 4 days while control mice received corn oil only. Mice were killed at ZT6, 6 h after the last PCN injection.

4.2. Blood and Tissue Samples

Bodyweight was monitored at the beginning and at the end of the experimental period. Prior to sacrifice, the submandibular vein was lanced, and blood was collected into lithium heparin-coated tubes (BD Microtainer, Franklin Lake, NJ, USA). Plasma was prepared by centrifugation (1500 g, 10 min, 4 °C) and stored at −80 °C. At sacrifice, the liver was removed and snap-frozen in liquid nitrogen and stored at −80 °C until used for RNA extraction.

4.3. Gene Expression

Total RNA was extracted with TRIzol reagent (Invitrogen, Carlsbad, CA, USA). Gene expression profiles were obtained at the GeT-TRiX facility (GénoToul, Génopole Toulouse Midi-Pyrénées, France) using Sureprint G3 Mouse GE v2 microarrays (8 × 60 K; design 074,809; Agilent Technologies, Santa Clara, CA, USA) following the manufacturer's instructions Microarray data and experimental details are available in NCBI's Gene Expression Omnibus [41] and are accessible through GEO Series accession numbers GSE123804. For real-time quantitative polymerase chain reaction (qPCR), 2 µg RNA samples were reverse-transcribed using the High-Capacity cDNA Reverse Transcription Kit (Applied Biosystems, Foster City, CA, USA). Table S3 presents the SYBR Green assay primers. Amplifications were performed using an ABI Prism 7300 Real-Time PCR System (Applied Biosystems, Foster City, CA, USA). qPCR data were normalized to TATA-box-binding protein mRNA levels and analyzed with LinRegPCR.v2015.3.

4.4. Plasma Analysis

Alanine transaminase (ALT), total cholesterol, triglycerides and free fatty acids (FFA) were determined using a Pentra 400 biochemical analyzer (Anexplo facility, Toulouse, France). Plasma FGF21 was assayed using the rat/mouse FGF21 ELISA kit (EMD Millipore, Billerica, MA, USA) following the manufacturer's instructions.

4.5. Liver Neutral Lipid Analysis

Tissue samples were homogenized in methanol/5 mM EGTA (2:1, *v/v*); then, lipids (corresponding to an equivalent of 2 mg tissue) were extracted according to the Bligh and Dyer method [42] with chloroform/methanol/water (2.5:2.5:2.1, *v/v/v*), in the presence of the following internal standards: glyceryl trinonadecanoate, stigmasterol, and cholesteryl heptadecanoate (Sigma, Saint-Louis, MO, USA). Triglycerides, free cholesterol, and cholesterol esters were analyzed with gas–liquid chromatography on a Focus Thermo Electron system equipped with a Zebron-1 Phenomenex fused- silica capillary column (5 m, 0.25 mm i.d., 0.25 mm film thickness). The oven temperature was programmed to increase from 200 to 350 °C at 5 °C/min, and the carrier gas was hydrogen (0.5 bar). Injector and detector temperatures were 315 °C and 345 °C respectively.

4.6. Statistical Analysis

Microarray data were processed using R (http://www.r-project.org, accessed at 22 September 2017) and Bioconductor packages (www.bioconductor.org, accessed at 22 September 2017, v 3.0). Raw data (median signal intensity) were filtered, log2 transformed, corrected for batch effects (microarray washing bath), and normalized using CrossNorm method [43]. Normalized data were first analyzed using Matlab (v2014.8). The principal component analysis was performed using an in-house function. The linear model was fitted using the limma lmFit function [44]. Pair-wise comparisons between biological conditions were applied using specific contrasts. A correction for multiple testing was applied using the Benjamini–Hochberg procedure for false discovery rate (FDR). Probes with FDR ≤ 0.05 and |fold-change| > 1.5 were considered to be differentially expressed between conditions. Gene-annotation enrichment analysis and functional annotation clustering were evaluated using DAVID [45]. For non-microarray data, differential effects were analyzed by analysis of variance followed by Tukey's post-hoc tests. A p-value < 0.05 was considered significant.

Supplementary Materials: Supplementary materials can be found at http://www.mdpi.com/1422-0067/20/15/3767/s1.

Author Contributions: Conceptualization, H.G. and S.E.-S.; methodology, S.A.B., F.L., L.S., C.N., C.B., S.S., C.L., and T.F.; software, Y.L.; formal analysis, S.A.B., Y.L., and S.E.-S.; investigation, S.A.B., F.L., M.R., and A.P.; writing—original draft preparation, S.A.B. and S.E.-S.; writing—review and editing, A.F., C.L., H.G., and S.E.-S.; supervision, H.G., L.G.-P., L.M.-L., N.L., and S.E.-S.; project administration, H.G., L.G.-P., L.M.-L., N.L., and S.E.-S.; funding acquisition, H.G., L.G.-P., L.M.-L., N.L., and S.E.-S.

Funding: S.A.B. is supported by a Ph.D. grant from Région Occitanie and INRA AlimH department. This work was supported by grants from Agence Nationale de la Recherche (ANR), Fond Européen de Développement Régional (FEDER), and Région Occitanie. SES is supported by a Joint Programming Initiative (JPI) grant Fatmal.

Acknowledgments: We thank all members of the EZOP staff for their careful help with this project. We thank the staff from the Genotoul: Anexplo, Get-TriX, and Metatoul-Lipidomic facilities. *Pxr*$^{-/-}$ mice are a generous gift from Pr Steven Kliewer (University of Texas Southwestern Medical School, Dallas, TX, USA). Colony founders were kindly provided by Pr Urs A Meyer (Biozentrum, University of Basel, Basel, Switzerland).

Conflicts of Interest: The authors declare no conflict of interest.

Abbreviations

ACAA	acetyl-Coenzyme A acyltransferase
Acot	acyl-coA thioeserase
AhR	aryl H receptor
CAR	constitutive androstane receptor
Cpt	carnitine palmitoyltransferase
CYP	cytochrome P450
DR4	direct repeat 4
FASN	fatty acid synthase
FDR	false discovery rate
FGF21	fibroblast growth factor 21
G6Pase	glucose-6-phosphatase
GDF15	growth/differentiation factor 15
GCK	glucokinase
GO	gene ontology
GLUT2	glucose transporter 2
HMGCS	3-hydroxy-3-methylglutaryl-CoenzymeA synthase
hPPARα	Human PPARα
hPXR	human PXR
Krt23	keratin 23
PXR	pregnane X receptor
PXRE	pregnane X receptor response elements
PCA	principal component analysis
PCN	pregnenolone 16α-carbonitrile
PEPCK	phosphoenopyruvate carboxykinase
PNPLA3	patatin-like phospholipase domain containing 3
PPARα	peroxisome proliferator-activated receptor α
Rab30	ras-related protein rab-30
RT-qPCR	quantitative reverse transcription PCR
RXR	retinoid X receptor
SPOT14	thyroid hormone-responsive spot 14
TGFβ	transforming growth factor-ß
Thrsp	thyroid hormone-responsive spot 14
WT	wild-type
ZT	Zeitgeber time

References

1. Bookout, A.L.; Jeong, Y.; Downes, M.; Yu, R.T.; Evans, R.M.; Mangelsdorf, D.J. Anatomical profiling of nuclear receptor expression reveals a hierarchical transcriptional network. *Cell* **2006**, *126*, 789–799. [CrossRef] [PubMed]
2. Kliewer, S.A.; Moore, J.T.; Wade, L.; Staudinger, J.L.; Watson, M.A.; Jones, S.A.; McKee, D.D.; Oliver, B.B.; Willson, T.M.; Zetterström, R.H.; et al. An orphan nuclear receptor activated by pregnanes defines a novel steroid signaling pathway. *Cell* **1998**, *92*, 73–82. [CrossRef]
3. Hernandez, J.P.; Mota, L.C.; Baldwin, W.S. Activation of CAR and PXR by Dietary, Environmental and Occupational Chemicals Alters Drug Metabolism, Intermediary Metabolism, and Cell Proliferation. *Curr. Pharm. Pers. Med.* **2009**, *7*, 81–105. [CrossRef] [PubMed]
4. Guengerich, F.P. Cytochrome P-450 3A4: Regulation and role in drug metabolism. *Annu. Rev. Pharm. Toxicol.* **1999**, *39*, 1–17. [CrossRef] [PubMed]
5. Drozdzik, M.; Busch, D.; Lapczuk, J.; Müller, J.; Ostrowski, M.; Kurzawski, M.; Oswald, S. Protein Abundance of Clinically Relevant Drug-Metabolizing Enzymes in the Human Liver and Intestine: A Comparative Analysis in Paired Tissue Specimens. *Clin. Pharmacol. Ther.* **2018**, *104*, 515–524. [CrossRef] [PubMed]

6. Yu, J.; Petrie, I.D.; Levy, R.H.; Ragueneau-Majlessi, I. Mechanisms and Clinical Significance of Pharmacokinetic-based Drug-drug Interactions with Drugs Approved by the U.S. Food and Drug Administration in 2017. *Drug Metab. Dispos.* **2019**, *47*, 135–144. [CrossRef]
7. Hakkola, J.; Rysä, J.; Hukkanen, J. Regulation of hepatic energy metabolism by the nuclear receptor PXR. *Biochim. Biophys. Acta* **2016**, *1859*, 1072–1082. [CrossRef]
8. Kodama, S.; Koike, C.; Negishi, M.; Yamamoto, Y. Nuclear receptors CAR and PXR cross talk with FOXO1 to regulate genes that encode drug-metabolizing and gluconeogenic enzymes. *Mol. Cell. Biol.* **2004**, *24*, 7931–7940. [CrossRef]
9. Rysä, J.; Buler, M.; Savolainen, M.J.; Ruskoaho, H.; Hakkola, J.; Hukkanen, J. Pregnane X receptor agonists impair postprandial glucose tolerance. *Clin. Pharmacol. Ther.* **2013**, *93*, 556–563. [CrossRef]
10. Bitter, A.; Rümmele, P.; Klein, K.; Kandel, B.A.; Rieger, J.K.; Nüssler, A.K.; Zanger, U.M.; Trauner, M.; Schwab, M.; Burk, O. Pregnane X receptor activation and silencing promote steatosis of human hepatic cells by distinct lipogenic mechanisms. *Arch. Toxicol.* **2015**, *89*, 2089–2103. [CrossRef]
11. Meng, Z.; Gwag, T.; Sui, Y.; Park, S.-H.; Zhou, X.; Zhou, C. The atypical antipsychotic quetiapine induces hyperlipidemia by activating intestinal PXR signaling. *JCI Insight* **2019**, *4*, 1. [CrossRef]
12. Gwag, T.; Meng, Z.; Sui, Y.; Helsley, R.N.; Park, S.-H.; Wang, S.; Greenberg, R.N.; Zhou, C. Non-nucleoside reverse transcriptase inhibitor efavirenz activates PXR to induce hypercholesterolemia and hepatic steatosis. *J. Hepatol.* **2019**, *70*, 930–940. [CrossRef]
13. Kliewer, S.A.; Mangelsdorf, D.J. A Dozen Years of Discovery: Insights into the Physiology and Pharmacology of FGF21. *Cell Metab.* **2019**, *29*, 246–253. [CrossRef] [PubMed]
14. Régnier, M.; Polizzi, A.; Lippi, Y.; Fouché, E.; Michel, G.; Lukowicz, C.; Smati, S.; Marrot, A.; Lasserre, F.; Naylies, C.; et al. Insights into the role of hepatocyte PPARα activity in response to fasting. *Mol. Cell. Endocrinol.* **2017**, *471*, 75–88. [CrossRef]
15. Montagner, A.; Polizzi, A.; Fouché, E.; Ducheix, S.; Lippi, Y.; Lasserre, F.; Barquissau, V.; Régnier, M.; Lukowicz, C.; Benhamed, F.; et al. Liver PPARα is crucial for whole-body fatty acid homeostasis and is protective against NAFLD. *Gut* **2016**, *65*, 1202–1214. [CrossRef] [PubMed]
16. BonDurant, L.D.; Potthoff, M.J. Fibroblast Growth Factor 21: A Versatile Regulator of Metabolic Homeostasis. *Annu. Rev. Nutr.* **2018**, *38*, 173–196. [CrossRef] [PubMed]
17. Goldstein, I.; Hager, G.L. Transcriptional and Chromatin Regulation during Fasting–The Genomic Era. *Trends Endocrinol. Metab.* **2015**, *26*, 699–710. [CrossRef]
18. Konno, Y.; Negishi, M.; Kodama, S. The roles of nuclear receptors CAR and PXR in hepatic energy metabolism. *Drug Metab. Pharmacokinet.* **2008**, *23*, 8–13. [CrossRef] [PubMed]
19. Montagner, A.; Korecka, A.; Polizzi, A.; Lippi, Y.; Blum, Y.; Canlet, C.; Tremblay-Franco, M.; Gautier-Stein, A.; Burcelin, R.; Yen, Y.-C.; et al. Hepatic circadian clock oscillators and nuclear receptors integrate microbiome-derived signals. *Sci. Rep.* **2016**, *6*, 20127. [CrossRef]
20. Li, C.Y.; Cheng, S.L.; Bammler, T.K.; Cui, J.Y. Editor's Highlight: Neonatal Activation of the Xenobiotic-Sensors PXR and CAR Results in Acute and Persistent Down-regulation of PPARα-Signaling in Mouse Liver. *Toxicol. Sci.* **2016**, *153*, 282–302. [CrossRef]
21. Cui, J.Y.; Klaassen, C.D. RNA-Seq reveals common and unique PXR- and CAR-target gene signatures in the mouse liver transcriptome. *Biochim. Biophys. Acta* **2016**, *1859*, 1198–1217. [CrossRef]
22. Nagahori, H.; Nakamura, K.; Sumida, K.; Ito, S.; Ohtsuki, S. Combining Genomics To Identify the Pathways of Post-Transcriptional Nongenotoxic Signaling and Energy Homeostasis in Livers of Rats Treated with the Pregnane X Receptor Agonist, Pregnenolone Carbonitrile. *J. Proteome Res.* **2017**, *16*, 3634–3645. [CrossRef]
23. Kandel, B.A.; Thomas, M.; Winter, S.; Damm, G.; Seehofer, D.; Burk, O.; Schwab, M.; Zanger, U.M. Genomewide comparison of the inducible transcriptomes of nuclear receptors CAR, PXR and PPARα in primary human hepatocytes. *Biochim. Biophys. Acta* **2016**, *1859*, 1218–1227. [CrossRef]
24. LaFave, L.T.; Augustin, L.B.; Mariash, C.N. S14: Insights from knockout mice. *Endocrinology* **2006**, *147*, 4044–4047. [CrossRef]
25. Moreau, A.; Téruel, C.; Beylot, M.; Albalea, V.; Tamasi, V.; Umbdenstock, T.; Parmentier, Y.; Sa-Cunha, A.; Suc, B.; Fabre, J.-M.; et al. A novel pregnane X receptor and S14-mediated lipogenic pathway in human hepatocyte. *Hepatology* **2009**, *49*, 2068–2079. [CrossRef]
26. Dai, G.; Liu, P.; Li, X.; Zhou, X.; He, S. Association between PNPLA3 rs738409 polymorphism and nonalcoholic fatty liver disease (NAFLD) susceptibility and severity: A meta-analysis. *Medicine* **2019**, *98*, e14324. [CrossRef]

27. Chrysovergis, K.; Wang, X.; Kosak, J.; Lee, S.-H.; Kim, J.S.; Foley, J.F.; Travlos, G.; Singh, S.; Baek, S.J.; Eling, T.E. NAG-1/GDF-15 prevents obesity by increasing thermogenesis, lipolysis and oxidative metabolism. *Int. J. Obes. (Lond)* **2014**, *38*, 1555–1564. [CrossRef]
28. Lee, J.; Choi, J.; Scafidi, S.; Wolfgang, M.J. Hepatic Fatty Acid Oxidation Restrains Systemic Catabolism during Starvation. *Cell Rep.* **2016**, *16*, 201–212. [CrossRef]
29. Mullican, S.E.; Lin-Schmidt, X.; Chin, C.-N.; Chavez, J.A.; Furman, J.L.; Armstrong, A.A.; Beck, S.C.; South, V.J.; Dinh, T.Q.; Cash-Mason, T.D.; et al. GFRAL is the receptor for GDF15 and the ligand promotes weight loss in mice and nonhuman primates. *Nat. Med.* **2017**, *23*, 1150–1157. [CrossRef]
30. Markan, K.R.; Naber, M.C.; Ameka, M.K.; Anderegg, M.D.; Mangelsdorf, D.J.; Kliewer, S.A.; Mohammadi, M.; Potthoff, M.J. Circulating FGF21 is liver derived and enhances glucose uptake during refeeding and overfeeding. *Diabetes* **2014**, *63*, 4057–4063. [CrossRef]
31. Zhang, Y.; Xie, Y.; Berglund, E.D.; Coate, K.C.; He, T.T.; Katafuchi, T.; Xiao, G.; Potthoff, M.J.; Wei, W.; Wan, Y.; et al. The starvation hormone, fibroblast growth factor-21, extends lifespan in mice. *Elife* **2012**, *1*, e00065. [CrossRef]
32. Owen, B.M.; Bookout, A.L.; Ding, X.; Lin, V.Y.; Atkin, S.D.; Gautron, L.; Kliewer, S.A.; Mangelsdorf, D.J. FGF21 contributes to neuroendocrine control of female reproduction. *Nat. Med.* **2013**, *19*, 1153–1156. [CrossRef]
33. Iroz, A.; Montagner, A.; Benhamed, F.; Levavasseur, F.; Polizzi, A.; Anthony, E.; Régnier, M.; Fouché, E.; Lukowicz, C.; Cauzac, M.; et al. A Specific ChREBP and PPARα Cross-Talk Is Required for the Glucose-Mediated FGF21 Response. *Cell Rep.* **2017**, *21*, 403–416. [CrossRef]
34. Ellero-Simatos, S.; Chakhtoura, G.; Barreau, C.; Langouët, S.; Benelli, C.; Penicaud, L.; Beaune, P.; de Waziers, I. Xenobiotic-metabolizing cytochromes p450 in human white adipose tissue: Expression and induction. *Drug Metab. Dispos.* **2010**, *38*, 679–686. [CrossRef]
35. He, J.; Gao, J.; Xu, M.; Ren, S.; Stefanovic-Racic, M.; O'Doherty, R.M.; Xie, W. PXR ablation alleviates diet-induced and genetic obesity and insulin resistance in mice. *Diabetes* **2013**, *62*, 1876–1887. [CrossRef]
36. Spruiell, K.; Jones, D.Z.; Cullen, J.M.; Awumey, E.M.; Gonzalez, F.J.; Gyamfi, M.A. Role of human pregnane X receptor in high fat diet-induced obesity in pre-menopausal female mice. *Biochem. Pharm.* **2014**, *89*, 399–412. [CrossRef]
37. Ma, Y.; Liu, D. Activation of pregnane X receptor by pregnenolone 16 α-carbonitrile prevents high-fat diet-induced obesity in AKR/J mice. *PLoS ONE* **2012**, *7*, e38734. [CrossRef]
38. Lu, Y.-F.; Jin, T.; Xu, Y.; Zhang, D.; Wu, Q.; Zhang, Y.-K.J.; Liu, J. Sex differences in the circadian variation of cytochrome p450 genes and corresponding nuclear receptors in mouse liver. *Chronobiol. Int.* **2013**, *30*, 1135–1143. [CrossRef]
39. Spruiell, K.; Gyamfi, A.A.; Yeyeodu, S.T.; Richardson, R.M.; Gonzalez, F.J.; Gyamfi, M.A. Pregnane X Receptor-Humanized Mice Recapitulate Gender Differences in Ethanol Metabolism but Not Hepatotoxicity. *J. Pharm. Exp.* **2015**, *354*, 459–470. [CrossRef]
40. Staudinger, J.L.; Goodwin, B.; Jones, S.A.; Hawkins-Brown, D.; MacKenzie, K.I.; LaTour, A.; Liu, Y.; Klaassen, C.D.; Brown, K.K.; Reinhard, J.; et al. The nuclear receptor PXR is a lithocholic acid sensor that protects against liver toxicity. *Proc. Natl. Acad. Sci. USA* **2001**, *98*, 3369–3374. [CrossRef]
41. Edgar, R.; Domrachev, M.; Lash, A.E. Gene Expression Omnibus: NCBI gene expression and hybridization array data repository. *Nucleic Acids Res.* **2002**, *30*, 207–210. [CrossRef]
42. Bligh, E.G.; Dyer, W.J. A RAPID METHOD OF TOTAL LIPID EXTRACTION AND PURIFICATION. *Can. J. Biochem. Physiol.* **2011**, *37*, 911–917. [CrossRef]
43. Cheng, L.; Lo, L.-Y.; Tang, N.L.S.; Wang, D.; Leung, K.-S. CrossNorm: A novel normalization strategy for microarray data in cancers. *Sci. Rep.* **2016**, *6*, 18898. [CrossRef]
44. Smyth, G.K. Linear models and empirical bayes methods for assessing differential expression in microarray experiments. *Stat. Appl. Genet. Mol. Biol.* **2004**, *3*. [CrossRef]
45. Huang, D.W.; Sherman, B.T.; Lempicki, R.A. Bioinformatics enrichment tools: Paths toward the comprehensive functional analysis of large gene lists. *Nucleic Acids Res.* **2009**, *37*, 1–13. [CrossRef]

Chapter 3.2

Gene expression profiling reveals intestine and liver specific PXR target genes in C57Bl6/J male mice

Context: The role of PXR in the liver has been studied by many different groups. By contrast, little is known about the significance of PXR activity in the intestine. In this second experimental chapter, we analyzed the role of PXR in the ileum through microarray analysis. Our data was compared to those obtained in the liver in order to highlight intestine specific functions that may depend on PXR. This body of work is subject to a publication in preparation.

Gene expression profiling reveals intestine and liver specific PXR target genes in C57Bl6/J male mice

Sharon Ann Barretto*,[1], Frederic Lasserre*,[1] *et al*.

[1]Institut National de la Recherche Agronomique (INRA), UMR1331 ToxAlim, Toulouse, France

* These authors contributed equally to this work.

Correspondence to sandrine.ellero-simatos@inra.fr ; +33 582 06 63 49

ORCID numbers: SES 0000-0002-9282-1804

Acknowledgments

We thank all members of the EZOP staff for their careful help with this project. We thank the staff from the Genotoul: Anexplo, Get-TriX and Metatoul-Lipidomic facilities. *Pxr*$^{-/-}$ mice are a generous gift Pr Steven Kliewer (University of Texas Southwestern Medical School, Dallas, TX, USA). Colony founders were kindly provided by Pr Urs A Meyer (Biozentrum, University of Basel, Basel, Switzerland).

Fundings

S.A.B. is supported by a PhD grant from Région Occitanie and INRA AlimH department. This work was supported by grants from Agence Nationale de la Recherche (ANR), Fond Européen de Développement Régional (FEDER) and Région Occitanie. SES is supported by a Joint Programming Initiative (JPI) grant Fatmal.

Keywords: Transcriptomics - nuclear receptor - cytochromes P450 - FGF21

Abbreviations: CYP-cytochrome P450, PCA-principal component analysis, PCN-pregnenolone 16α-carbonitrile, PXR-pregnane X receptor, RT-qPCR-real-time quantitative polymerase chain reaction, RXR-retinoid X receptor, TLR-toll-like receptor, WT-wild-type, XMEs-xenobiotic metabolizing enzymes, ZT-zeitgeber time

ABSTRACT

The pregnane X receptor (PXR) is the main nuclear receptor regulating the expression of xenobiotic metabolizing enzymes and is highly expressed in the liver and intestine. Recent studies have highlighted its additional role in energy homeostasis, intestinal barrier function and innate immunity. However, its intestinal role remains poorly described.

We performed a transcriptomic comparison of the PXR-regulated genes in the liver and intestine (ileum and colon) using microarrays in adult wild-type (WT) vs *Pxr*$^{-/-}$ C57Bl6/J male mice treated with the rodent specific PXR ligand pregnenolone 16α-carbonitrile (PCN) (100 mg/kg i.p. once daily for 4 days).

In the liver, PXR activation significantly regulated the expression of 1215 genes, while in the ileum and colon the number of significant PXR-targets were much lower (119 and 0). Thirty-four prototypical PXR target genes were shared among the liver and ileum, mostly xenobiotic metabolizing enzymes. In the liver and the ileum, up-regulated genes were also involved in immune processes, such as the bacteria-recognizing toll-like receptors 1, 2, 4, 5 and 6. We

provide a comprehensive description of the transcriptomic signature of PXR activation in the intestine.

INTRODUCTION

Pregnane X receptor (PXR, systematic name NR1I2) is a member of the nuclear receptor superfamily and is highly expressed in the liver and intestine of mammals (Bookout et al. 2006). These 2 organs are the two major determinants of oral drug bioavailability and of food contaminant toxicity. In both organs, activity of xenobiotic-metabolizing enzymes (XMEs) and transporters are the major players. PXR was characterized as a xenosensor that regulates the expression of XMEs and transporters, thereby facilitating elimination of xenobiotics and endogenous toxic chemicals such as bile acids (Kliewer *et al.,* 1998). Upon ligand-binding, PXR translocates to the nucleus, heterodimerizes with retinoid X receptor (RXR, NR2B1) and binds to PXR direct repeat 4 (DR-4) response elements (PXRE) that are usually located upstream of target genes. Because of an unusually large and flexible binding pocket, PXR can be activated by a variety of structurally diverse chemicals including pharmaceutical drugs, dietary supplements, herbal medicines, environmental pollutants and endogenous molecules (Hernandez *et al.,* 2009). In line with the role of PXR as a master regulator of xenobiotic metabolism, its first described target gene was cytochrome P450 (CYP) 3A4 in humans (Guengerich 1999), which represents 10% of all clinically relevant drug-metabolizing CYPs in the human liver and up to 75-85% in the intestine (Drozdzik *et al.,* 2018) and is responsible for the metabolization of 60% of marketed drugs (Yu et al. 2018).

Besides its original function as part of the detoxification machinery, recent studies have also unveiled functions for PXR in intermediary metabolism. There are increasing clinical evidence that PXR agonists cause hyperglycaemia in humans (Hakkola *et al.*, 2016) and experimental evidence indicating that PXR regulates hepatic glucose metabolism but there is still no solid understanding of the consequences or of the mechanisms involved. Activated PXR has been shown to repress expression of the gluconeogenic genes glucose-6-phosphatase (G6Pase) and phosphoenopyruvate carboxykinase (PEPCK) (Kodama et al. 2004), and of genes involved in glucose uptake such as GLUT2 and of glucokinase (GCK) (Rysä *et al.,* 2013). Although there are limited data on the relationship between PXR and fatty liver in humans *in vivo,* many studies have demonstrated that PXR activation also causes hepatic lipid accumulation in human cell models and *in vitro* and *in vivo* mouse models (Bitter *et al.*, 2015; Hakkola *et al.*, 2016): the main mechanisms involved are the induction of lipogenesis and inhibition of β-oxidation. Moreover, previous work suggests an intestine-specific impact of PXR-ligands that could impact cholesterol homeostasis (Sui *et al.,* 2015).

Finally PXR has also been shown to play a role in inflammatory processes across many tissues, with PXR activation being mostly anti-inflammatory through inhibition of NFkB (Garg *et al*., 2016). In the intestine, PXR activation by gut microbiota-produced indoles protects against inflammation-induced gut barrier defects and histologic damages by inhibiting downstream toll-like receptor 4 (TLR-4)-activated kinase activation (Venkatesh *et al.*, 2014). Indeed, PXR agonists such as rifampicin have been proposed as therapies for inflammatory bowel disease (Cheng *et al.*, 2012).

Despite an established role at the cross-road of xenobiotic detoxification, energy metabolism and control of inflammatory processes, and a growing awareness of the

importance of the intestinal role of PXR, the transcriptomic signature of PXR activation in the intestine remains poorly investigated. One study used PXR agonists in rats (Hartley *et al.*,2004) but this study did not control for off-target effects of the ligands since no Pxr-null rodent models were used. Here, we performed a comparison of the hepatic and intestinal gene profiles after pharmacological activation of PXR in WT *vs. Pxr-/-* mice.

MATERIALS AND METHODS

Animals

In vivo studies were performed in accordance with European guidelines for the use and care of laboratory animals, and were approved by an independent Ethics Committee. All mice were housed at 21-23°C on a 12-hour light (ZT0-ZT12) 12-hour dark (ZT12-ZT24) cycle and allowed free access to the diet (Teklad Global 18% Protein Rodent Diet) and tap water. ZT stands for Zeitgeber time; ZT0 is defined as the time when the lights are turned on. *Study 1:* Sixteen male and 8 female six-week old C57BL/6J mice were purchased from Charles River, kept for two weeks of acclimatization and killed at ZT6 (males, n=8) or ZT18 (males, n=8 and females, n=8). *Study 2:* Twelve six-week old wild-type (WT) C57BL/6J male mice were purchased from Charles River and 12 *Pxr*$^{-/-}$ animals (backcrossed on the C57Bl/6J background) were engineered in Pr. Meyer's laboratory (Staudinger et al. 2001) and are bred for 10y in our animal facility. Mice were acclimatized for two weeks, then randomly allocated to the different experimental groups: wild-type control (WT CONT, n=6), wild-type PCN-treated (WT PCN, n=6), *Pxr*$^{-/-}$ control (*Pxr*$^{-/-}$ CONT, n=6), *Pxr*$^{-/-}$ PCN-treated (*Pxr*$^{-/-}$ PCN, n=6). PCN-treated mice received a daily intraperitoneal injection of PCN (100 mg/kg, Bertin

Technologies, Saint-Quentin-en-Yvelines, France) in corn oil for 4 days while control mice received corn oil only. Mice were killed at ZT6, 6 hours after the last PCN injection, in the fed state.

For the oral gavage experiment, the same protocol was used using both male and female C57Bl6/J mice. Mice were acclimatized for two weeks, then randomly allocated to the different experimental groups: wild-type control (WT CONT, n=6), wild-type PCN-treated (WT PCN, n=6), *Pxr*$^{-/-}$ control (*Pxr*$^{-/-}$ CONT, n=6), *Pxr*$^{-/-}$ PCN-treated (*Pxr*$^{-/-}$ PCN, n=6). PCN-treated mice received a daily oral gavage of PCN (100 mg/kg) in corn oil for 4 days while control mice received corn oil only. Mice were killed at ZT6, 6 hours after the last PCN injection, in the fed state.

Tissue samples

Body weight was monitored at the beginning and at the end of experimental period. At sacrifice, the liver, the three parts of the small intestine (duodenum, jejunum, ileum), and the colon were removed and snap-frozen in liquid nitrogen and stored at -80°C until used for RNA extraction.

Gene expression

Total RNA was extracted with TRIzol reagent (Invitrogen). Gene expression profiles were obtained at the GeT-TRiX facility (GénoToul, Génopole Toulouse Midi-Pyrénées, France) using Sureprint G3 Mouse GE v2 microarrays (8x60K; design 074,809; Agilent technologies) following the manufacturer's instructions Microarray data and experimental details are available in NCBI's Gene Expression Omnibus (Edgar et al. 2002) and are

accessible through GEO Series accession numbers GSE123804. For real-time quantitative polymerase chain reaction (qPCR), 2 µg RNA samples were reverse-transcribed using the High-Capacity cDNA Reverse Transcription Kit (Applied Biosystems). Amplifications were performed using an ABI Prism 7300 Real-Time PCR System (Applied Biosystems). qPCR data were normalised to TATA-box-binding protein mRNA levels, and analyzed with LinRegPCR.v2015.3.

Statistical analysis

Microarray data were processed independently for each organ using R (http://www.r-project.org) and Bioconductor packages (www.bioconductor.org, v 3.0, Gentleman, Carey et al. 2004). Raw data (median signal intensity) were filtered, log2 transformed, corrected for batch effects (microarray washing bath) and normalized using CrossNorm method (Cheng et al. 2016) for liver dataset and using quantile method (Bolstad et al. 2003) for ileum and colon datasets. Normalized data were first analysed using Matlab (v2014.8). Principal component analysis was performed using an in-house function. Two-way ANOVA was used to investigate the effect of PCN treatment, the effect of Pxr deletion and the interaction between the 2 factors. Then a model was fitted using the limma lmFit function (Smyth 2004). Pair-wise comparisons between biological conditions were applied using specific contrasts. A correction for multiple testing was applied using Benjamini-Hochberg procedure for False Discovery Rate (FDR). Probes with FDR ≤ 0.05 and |fold-change| > 1.2 were considered to be differentially expressed between conditions. Gene-annotation enrichment analysis and functional annotation clustering were evaluated using DAVID

(Huang et al. 2009). For non- microarray data, differential effects were analyzed by analysis of variance followed by Tukey's post-hoc tests. A p-value <0.05 was considered significant.

RESULTS

Circadian rhythm and sex have minor impact on Pxr and its target gene expression in the liver and in the intestine.

Because *Pxr* activity has been shown to be influenced by both circadian rhythm and sex (Montagner *et al.*, 2016), we first investigated the expression of *Pxr* ant its 2 most-described target genes, *Cyp3a11* and *Cyp2c55*, in the liver and the different portions of the intestine (duodenum, jejunum, ileum and colon) at different time points in male and female WT mice (**Figure 1**). *Bmal1* and *Rev-erbα*, 2 genes of the circadian clock served as positive controls. *Pxr* was expressed to the same levels in the liver and ileum, and to a lower extend in the colon, *Cyp3a11* expression was mostly hepatic, while *Cyp2c55* was highly expressed in the colon. We observed no significant circadian difference in *Pxr*, *Cyp3a11* or *Cyp2c55* expression. We next assessed the effect of sex and found no significant difference in the expression of these 3 genes between males and females. In light of these results, we decided to continue our study in male mice at ZT6.

Effects of Pxr activation on the hepatic and intestinal transcriptomes

Using microarrays, we obtained global transcriptional profiles in the liver, and in one representative section of the small (ileum) and of the large intestine (colon). Principal component analysis (PCA) first illustrated that PCN-treatment significantly impacted the hepatic transcriptome (**Figure 2A**). The discrimination of WT PCN vs WT Cont seems stronger

than that of the *Pxr*$^{-/-}$ PCN *vs.* *Pxr*$^{-/-}$ Cont, suggesting a significant PXR-dependent transcriptional effect of PCN in this organ. In the ileum, the PCN-treated groups also clustered separately from their respective controls, but to a similar extent in the WT and the *Pxr*$^{-/-}$ animals (**Figure 2B**). In the colon, the clustering of PCN-treated *vs.* control groups was not seen (**Figure 2C**). Two-way ANOVA models were then fitted to further investigate the effect of PCN treatment, the effect of *Pxr* deletion and the interaction between these factors. We observed a large transcriptional response to PCN in the liver (3351 genes, blue circle in **Figure 2D**), a less pronounced one in the ileum (1710 genes, **Figure 2E**) and a very weak one in the colon (107 genes, **Figure 2F**). The effect of *Pxr* deletion on the transcriptome followed the same pattern with 3363 genes affected by the genotype independently of PCN in the liver (green circle, **Figure 2D**), 489 genes in the ileum (**Figure 2E**) and only 117 in the colon (**Figure 2F**).

Deciphering prototypical Pxr-target genes

We next sought to decipher the biological functions affected by PXR activation. We used linear models and considered genes to be significantly regulated with a fold-change > 1.2 and a FDR < 0.05. In the liver, PCN treatment significantly up-regulated the expression of 1258 genes in WT animals, and of 333 genes in *Pxr*$^{-/-}$ mice (**Figure 3A**). Using the 1029 "prototypical" PXR target genes (those that were up-regulated only in WT animals), we conducted a pathway enrichment analysis, which revealed 7 functional clusters significantly enriched (**Figure 3B and Supplementary Table 1**) with genes involved in cell cycle, cell division and mitosis, glutathione metabolism, cytochromes P450, lipid metabolism, chemotaxis and positive regulation of inflammatory response. **Figures 3C & D** confirm these

results by illustrating the overall enrichment of XMEs in the PCN-affected genes in WT (**Figure 3C**) but not in *Pxr*$^{-/-}$ animals (Figure 3D).

In the ileum, PCN treatment significantly up-regulated the expression of 359 genes in WT animals, and of 816 genes in *Pxr*$^{-/-}$ mice (**Figure 3E**). Pathway enrichment analysis of the 179 ileal prototypical PXR targets highlighted 5 significantly enriched clusters (**Figure 3F and Supplementary Table 2**) with genes involved in xenobiotic metabolism, inflammation and innate immunity and glycosyl transfer. Figure 3G illustrates the enrichment of the PCN-affected genes in XMEs in WT animals, however, with lower fold-changes and higher p-values compared to what was observed in the liver.

In the colon, no gene was significantly regulated considering a FDR < 0.05.

We next investigated the shared target genes of PXR in the 2 organs and we found 46 common PXR targets (**Figure 3I**). As expected, these common target genes were mainly involved in xenobiotic metabolism, among which 12 genes encoding for phase I XME; 7 genes encoding for phase II XMEs and 2 encoding for phase III XMEs (**Figure 3J**). Overall, these shared target-genes were regulated to a higher extend in the liver than in the ileum (**Figure 3K**). The comprehensive effect of PCN treatment on hepatic and ileal XMEs is provided in **Supplementary Table 3**.

Among the shared PXR-targets, we also observed Toll-Like Receptor 1 (*Tlr1*), which was induced to a similar extent in the liver and the ileum (**Figure 3J**). Because TLRs are important receptors in the regulation of innate immunity, this prompted us to further investigate the impact of *Pxr* activation on *Tlrs* expression (**Supplementary Figure 1**). PCN-induced the expression of *Tlr1* and *Tlr5* in the liver and the ileum in a PXR-dependent way, and of *Tlr2, 4* and *6* in the liver only.

Liver- and ileal-specific PXR prototypical target genes are illustrated in **Supplementary Figure 2**.

PXR-dependent transrepression in the liver and the intestine

We investigated the effect of PCN on gene down-regulation (**Figure 4, Supplementary Table 4**). In the ileum, PCN treatment down-regulated the expression of 27 genes in WT mice among which 19 were PXR dependent (**Figure 4D-E**). Enrichment analyses did not highlight any specific pathway related to this set of genes.

Comparison of ip vs. oral activation of PXR

Given the much lower number of genes affected by PCN treatment in the ileum and colon vs. the liver, we wondered if this was due to the mode of administration of the ligand (intraperitoneal) that could have favored liver over intestinal exposure. We repeated the protocol of PXR activation in both male and female C57Bl6/J WT vs. *Pxr*$^{-/-}$ mice using oral gavage. Surprisingly, we observed that both in the ileum and the liver, the fold-changes of induction of PXR target genes were lower using oral gavage compared to intraperitoneal route (**Figure 5**).

DISCUSSION

We aimed to compare the effect of PXR activation in the liver and in intestine. We first observed that the number of genes affected by PCN treatment independently of the genotype was much higher in the liver (3351 genes) > ileum (1710) > colon (107). We hypothesized that this might be explained by the intraperitoneal administration that favored liver over intestinal exposure. To increase intestinal PXR activation, we tested another protocol of PCN administration via oral gavage. Using qPCR, we observed that the induction of PXR target genes was not higher, and even much lower, when mice received PCN orally than with ip PCN treatment. Moreover, in the ip protocol, Cyp3a11 mRNA levels were increased by a factor of 24 in the ileum vs. a factor of 10 in the liver. Therefore, the ip administration protocol induced Cyp3a11 mRNA transcription in the ileum to a similar extent than in the liver, therefore supporting a satisfactory activation of PXR in the intestine with this protocol.

Another hypothesis explaining the much lower number of genes activated upon PXR activation in the intestine vs. the liver could also be that PXR is less activated by PCN in the intestine. Supporting this idea, we found 479 genes with a significant PCN*genotype interaction in the liver upon 3351 genes significantly impacted by PCN, which represents 14.3%, while in the ileum, the proportion of PXR-dependent genes (83) compared to the total number of PCN responsive genes (1710) represents only 4.8%. Similarly, the number of genes impacted by *Pxr* deletion reaches 3363 in the liver, for only 489 in the ileum and 117 in the colon, despite a relatively similar expression of *Pxr* itself in the 3 organs. These results suggest a lower basal, as well as ligand-activated, transcriptional activity of PXR in the intestine compared to the liver. They are in agreement with a previous rat study with two PXR

agonists given orally in which the number and factors of induction of XME genes were much higher in the liver than in the intestine (Hartley *et al.,* 2004).

We confirm the strong Pxr-dependent induction of *Cyp3a11* mRNA with similar fold-changes in the liver and ileum. This might be of toxicological relevance since a broad assessment of >300 drugs in humans indicated that for 30% of the compounds, the fraction escaping intestinal metabolism was less than 0.8 (Varma *et al.*,2010). Moreover, CYP3A4, the human homolog of *Cyp3a11*, was recently demonstrated as the major XME in the human intestine, representing up to 85% of all CYPs (Drozdzik *et al.,* 2018). The same authors showed that the quantity of CYPs in the human colon was very low, an organ in which we also observe a low transcriptional activity of PXR. Therefore, our data confirm that PXR plays a key role in regulating the expression of the most toxicologically relevant XMEs in the small intestine.

PXR-activation also enhanced the transcription of many genes involved in the regulation of innate immunity, among which some members of the TLR family. TLRs are pattern recognition receptors that recognize molecules shared by pathogens, by the resident microbiota or endogenous molecules derived by tissue damage. We observed a PXR-dependent up-regulation of *Tlr2* and its heterodimer partners, *Tlr1* and *Tlr6*, as well as *Tlr4* and *5* in the liver and ileum. These are all the main bacteria-recognizing TLRs, notably interacting with the gut microbiota. PXR activation by PCN has recently been shown to modulate the gut microbiota composition (Dempsey *et al.,* 2018). Gut microbiota might have also been perturbated in our study, which could explain the observed changes in TLR expression. However, *Tlr5* expression is not modulated by presence of the gut microbiota (Brandão *et al.,* 2015), therefore, there might also be a direct transcriptional effect of PXR on

Tlr genes. Activation of TLRs regulates the release of pro- and anti-inflammatory cytokines, and, in mice, deletion of *Tlr2*, *4* and *5* or of the TLR signaling adapter *MyD88* contributes to exacerbated disease in models of inflammatory bowel disease (Rakoff-Nahoum et al. 2004; Chassaing et al. 2014), while hepatocyte deletion of *Tlrs* or *MyD88* regulates glucose and lipid metabolism (Duparc *et al.*, 2016; Etienne-Mesmin *et al*., 2016).

Perspectives and limitations of our study include first the use of only one ligand (PCN) for PXR activation. Although we have several arguments in favor of a significant activation of PXR in the intestine using this protocol, the number of PXR responsive genes in the intestine was much lower than in the liver. Furthermore, we observe more genes induced in *Pxr*$^{-/-}$ mice compared to WT mice in the intestine (**Figures 3E and 4D**). This could be due to the hepatic first pass effect that is stronger in WT than in *Pxr*$^{-/-}$ mice. But this could also suggest that PXR might not be the main factor mediating PCN response in the intestine. It was previously shown that different PXR ligands could induce weakly over-lapping gene signatures (Hartley *et al.,* 2004). Therefore, it might be interesting to test several other PXR agonists such as dexamethasone. The antipsychotic drug quetiapine was also recently described as a gut activator of PXR (Meng *et al.,* 2019) and might be an interesting ligand to provide a more comprehensive view of the intestinal PXR signature. Second, littermates were not used, which did not allow extensive analysis of the impact of *Pxr* deletion, especially in the ileum and colon for which differences in gut microbiota composition impact gene expression. However, our results mainly focus on the effect of PCN treatment within genotypes. Third, we used only male mice, but PXR activation has a sexually dimorphic impact on both XMEs and glucose and lipid metabolism (Lu *et al.,* 2013; Spruiell *et al.,* 2015). Therefore, it would be interesting to decipher whether the signature of PXR activation described in our study is also valid in

female mice. Finally, our study focused on short-term changes. An important remaining question is to determine the effect of multiple weak PXR agonists such as those present in our environment on the observed regulations.

In conclusion, we present a comprehensive gene signature of PXR activation in the liver and in ileum. In both tissues, PXR activation mainly impacted the expression of XMEs and of genes involved in innate immunity such as the TLRs. More studies are necessary to study the physiological relevance of these regulations.

Conflict of Interest:

The authors declare that they have no conflict of interest.

REFERENCES

Bitter A, Rümmele P, Klein K, et al (2015) Pregnane X receptor activation and silencing promote steatosis of human hepatic cells by distinct lipogenic mechanisms. Arch Toxicol 89:2089–2103. doi: 10.1007/s00204-014-1348-x

Bolstad BM, Irizarry RA, Astrand M, Speed TP (2003) A comparison of normalization methods for high density oligonucleotide array data based on variance and bias. Bioinformatics 19:185–193.

Bookout AL, Jeong Y, Downes M, et al (2006) Anatomical profiling of nuclear receptor expression reveals a hierarchical transcriptional network. Cell 126:789–799. doi: 10.1016/j.cell.2006.06.049

Brandão I, Hörmann N, Jäckel S, Reinhardt C (2015) TLR5 expression in the small intestine depends on the adaptors MyD88 and TRIF, but is independent of the enteric microbiota. Gut Microbes 6:202–206. doi: 10.1080/19490976.2015.1034417

Chassaing B, Ley RE, Gewirtz AT (2014) Intestinal epithelial cell toll-like receptor 5 regulates the intestinal microbiota to prevent low-grade inflammation and metabolic syndrome in mice. Gastroenterology 147:1363–77.e17. doi: 10.1053/j.gastro.2014.08.033

Cheng J, Shah YM, Gonzalez FJ (2012) Pregnane X receptor as a target for treatment of inflammatory bowel disorders. Trends Pharmacol Sci 33:323–330. doi: 10.1016/j.tips.2012.03.003

Cheng L, Lo L-Y, Tang NLS, et al (2016) CrossNorm: a novel normalization strategy for microarray data in cancers. Sci Rep 6:18898. doi: 10.1038/srep18898

Dempsey JL, Wang D, Siginir G, et al (2018) Pharmacological Activation of PXR and CAR Down-regulates Distinct Bile Acid-metabolizing Intestinal Bacteria and Alters Bile Acid Homeostasis. Toxicol Sci. doi: 10.1093/toxsci/kfy271

Drozdzik M, Busch D, Lapczuk J, et al (2018) Protein Abundance of Clinically Relevant Drug-Metabolizing Enzymes in the Human Liver and Intestine: A Comparative Analysis in Paired Tissue Specimens. Clinical Pharmacology & Therapeutics 104:515–524. doi: 10.1002/cpt.967

Duparc T, Plovier H, Marrachelli VG, et al (2016) Hepatocyte MyD88 affects bile acids, gut microbiota and metabolome contributing to regulate glucose and lipid metabolism. Gut. doi: 10.1136/gutjnl-2015-310904

Edgar R, Domrachev M, Lash AE (2002) Gene Expression Omnibus: NCBI gene expression and hybridization array data repository. Nucleic Acids Res 30:207–210.

Etienne-Mesmin L, Vijay-Kumar M, Gewirtz AT, Chassaing B (2016) Hepatocyte Toll-Like Receptor 5 Promotes Bacterial Clearance and Protects Mice Against High-Fat Diet-Induced Liver Disease. Cell Mol Gastroenterol Hepatol 2:584–604. doi: 10.1016/j.jcmgh.2016.04.007

Garg A, Zhao A, Erickson SL, et al (2016) Pregnane X Receptor Activation Attenuates Inflammation-Associated Intestinal Epithelial Barrier Dysfunction by Inhibiting Cytokine-Induced Myosin Light-Chain Kinase Expression and c-Jun N-Terminal Kinase 1/2 Activation. J Pharmacol Exp Ther 359:91–101. doi: 10.1124/jpet.116.234096

Guengerich FP (1999) Cytochrome P-450 3A4: regulation and role in drug metabolism. Annu Rev Pharmacol Toxicol 39:1–17. doi: 10.1146/annurev.pharmtox.39.1.1

Hakkola J, Rysä J, Hukkanen J (2016) Regulation of hepatic energy metabolism by the nuclear receptor PXR. Biochim Biophys Acta. doi: 10.1016/j.bbagrm.2016.03.012

Hartley DP, Dai X, He YD, et al (2004) Activators of the rat pregnane X receptor differentially modulate hepatic and intestinal gene expression.

Hernandez JP, Mota LC, Baldwin WS (2009) Activation of CAR and PXR by Dietary, Environmental and Occupational Chemicals Alters Drug Metabolism, Intermediary Metabolism, and Cell Proliferation. Curr Pharmacogenomics Person Med 7:81–105. doi: 10.2174/187569209788654005

Huang DW, Sherman BT, Lempicki RA (2009) Bioinformatics enrichment tools: paths toward the comprehensive functional analysis of large gene lists. Nucleic Acids Res 37:1–13. doi: 10.1093/nar/gkn923

Kliewer SA, Moore JT, Wade L, et al (1998) An orphan nuclear receptor activated by

pregnanes defines a novel steroid signaling pathway. Cell 92:73–82.

Kodama S, Koike C, Negishi M, Yamamoto Y (2004) Nuclear receptors CAR and PXR cross talk with FOXO1 to regulate genes that encode drug-metabolizing and gluconeogenic enzymes. Mol Cell Biol 24:7931–7940. doi: 10.1128/MCB.24.18.7931-7940.2004

Lu Y-F, Jin T, Xu Y, et al (2013) Sex differences in the circadian variation of cytochrome p450 genes and corresponding nuclear receptors in mouse liver. Chronobiol Int 30:1135–1143. doi: 10.3109/07420528.2013.805762

Meng Z, Gwag T, Sui Y, et al (2019) The atypical antipsychotic quetiapine induces hyperlipidemia by activating intestinal PXR signaling. JCI Insight 4:1. doi: 10.1172/jci.insight.125657

Montagner A, Korecka A, Polizzi A, et al (2016) Hepatic circadian clock oscillators and nuclear receptors integrate microbiome-derived signals. Sci Rep 6:20127. doi: 10.1038/srep20127

Rakoff-Nahoum S, Paglino J, Eslami-Varzaneh F, et al (2004) Recognition of commensal microflora by toll-like receptors is required for intestinal homeostasis. Cell 118:229–241. doi: 10.1016/j.cell.2004.07.002

Rysä J, Buler M, Savolainen MJ, et al (2013) Pregnane X receptor agonists impair postprandial glucose tolerance. Clinical Pharmacology & Therapeutics 93:556–563. doi: 10.1038/clpt.2013.48

Smyth GK (2004) Linear models and empirical bayes methods for assessing differential expression in microarray experiments. Stat Appl Genet Mol Biol 3:Article3–25. doi: 10.2202/1544-6115.1027

Spruiell K, Gyamfi AA, Yeyeodu ST, et al (2015) Pregnane X Receptor-Humanized Mice Recapitulate Gender Differences in Ethanol Metabolism but Not Hepatotoxicity. J Pharmacol Exp Ther 354:459–470. doi: 10.1124/jpet.115.224295

Staudinger JL, Goodwin B, Jones SA, et al (2001) The nuclear receptor PXR is a lithocholic acid sensor that protects against liver toxicity. Proc Natl Acad Sci USA 98:3369–3374. doi: 10.1073/pnas.051551698

Sui Y, Helsley RN, Park S-H, et al (2015) Intestinal pregnane X receptor links xenobiotic exposure and hypercholesterolemia. Mol Endocrinol 29:765–776. doi: 10.1210/me.2014-1355

Varma MVS, Obach RS, Rotter C, et al (2010) Physicochemical space for optimum oral bioavailability: contribution of human intestinal absorption and first-pass elimination. J Med Chem 53:1098–1108. doi: 10.1021/jm901371v

Venkatesh M, Mukherjee S, Wang H, et al (2014) Symbiotic bacterial metabolites regulate gastrointestinal barrier function via the xenobiotic sensor PXR and Toll-like receptor 4.

Immunity 41:296–310. doi: 10.1016/j.immuni.2014.06.014

Yu J, Petrie ID, Levy RH, Ragueneau-Majlessi I (2018) Mechanisms and Clinical Significance of Pharmacokinetic-based Drug-drug Interactions with Drugs Approved by the U.S. Food and Drug Administration in 2017. Drug Metab Dispos dmd.118.084905. doi: 10.1124/dmd.118.084905

FIGURE LEGENDS

Figure 1: Effect of circadian rhythm on clock genes and sex on the expression of Pxr and its target genes. RT-qPCR in male mice at ZT6 and ZT18 (A) or in males vs females at ZT18 (B). C57Bl6/J wild-type male mice were killed at ZT6 or ZT18. RT-qPCR was conducted in the liver and the different parts of the intestine. Results are presented as mean+/- SEM for n=6 per group. P-values were derived from 2-way ANOVA analyses. Letters refer to significant differences in gene expression compared to the liver (L), duodenum (D), jejunum (J), ileum (I) and colon (C) at p>0.05 using Tukey's post-tests.

Figure 2: Impact of PCN treatment and Pxr deletion on the liver and intestinal transcriptomes. (A-C) PCA score plots of the whole transcriptomic datasets in the liver (A), the ileum (B) and the colon (C). (D-F) Venn diagram representing the number of genes affected by PCN treatment independently of the genotype (blue circles), by the genotype independently of PCN (green circles) and affected under the interaction between PCN and genotype (red circles) in the liver (D), ileum (E) and colon (F). Genes were considered significant at p<0.001 using 2-way ANOVA. N=4-6 per group.

Figure 3: PXR-dependent up-regulated genes. (A) Venn diagram of genes significantly up-regulated by PCN in the liver (FC>1.2 & FDR<0.05). (B) Gene enrichment analysis of the 1029 hepatic prototypical target genes of PXR. (C) Volcano plot of differences in gene expression between WT PCN and WT Cont. Colors indicate phase I XMEs (red), phase II XMEs (green) and phase III XMEs (blue). (D) Volcano plot of differences in gene expression between *Pxr*$^{-/-}$ PCN and *Pxr*$^{-/-}$ Cont in the liver. Color code is identical to (C). (E) Venn diagram of genes significantly up-regulated by PCN in the ileum (FC>1.2 & FDR<0.05). (F) Gene enrichment analysis of the 179 ileal prototypical target genes of PXR. (G) Volcano plot of differences in gene expression between WT PCN and WT Cont in the ileum. Color code is identical to (C). (H) Volcano plot of differences in gene expression between *Pxr*$^{-/-}$ PCN and *Pxr*$^{-/-}$ Cont in the ileum. Color code is identical to (C). (I) Venn diagram of genes significantly up-regulated by PCN in WT mice only in the liver *vs*. the ileum. (J) The 35 genes with the highest fold-change in WT PCN *vs*. WT mice that are prototypical targets of PXR in the liver and ileum. (K) Log2 fold-changes in WT PCN *vs*. WT Cont for the 46 PXR-targets shared between the liver and ileum.

Figure 4: Shared and tissue-specific PXR-dependent down-regulated genes in the liver and ileum. (A) Venn diagram of genes significantly down-regulated by PCN in the liver (FC<-1.2 & FDR<0.05) (B) Gene enrichment analysis of the 186 hepatic genes down-regulated by PCN in a PXR-dependent way (C) The 40 genes with the highest fold change in WT PCN vs

WT mice. (D) Venn diagram of genes significantly ileal down-regulated by PCN (FC<-1.2 & FDR<0.05). (E) The 19 ileal genes with the highest fold change in WT PCN *vs.* WT mice.

Figure 5: Impact of PXR activation on hepatic and intestinal PXR activity by intraperitoneal injection and oral gavage. Gene expression of *Cyp3a11* and *Cyp2c55* from qPCR experiments in the (A) liver of male mice by intraperitoneal injection; (B) male and (C) female mice by oral gavage. Gene expression of *Cyp3a11* and *Cyp2c55* from qPCR experiments in the (D) ileum of male mice by intraperitoneal injection; (E) male and (F) female mice by oral gavage. Data are mean±SEM of n=6-7 per group. *p≤0.05, **p≤0.01, ***p≤0.005 for PCN effect, #p≤0.05 ##p≤0.01, ###p≤0.005for genotype effect using 2-way ANOVA and Tukey's post-tests.

SUPPLEMENTARY FIGURE LEGENDS

Supplementary Figure 1: Effect PXR activation on the expression of *Tlrs* in the (A) liver and (B) ileum.

Supplementary Figure 2: Effect PXR activation on the expression of prototypical genes in the liver and ileum. Forty genes with the highest fold change in the (A) liver and the (B) ileum.

SUPPLEMENTARY TABLE LEGENDS

Supplementary Table 1: Effect PXR activation on the expression of *Tlrs* in the (A) liver and (B) ileum.

Supplementary Table 2: Gene enrichment analyses of upregulated genes in the liver.

Supplementary Table 3: The comprehensive effect of PCN treatment on hepatic and ileal XMEs.

Supplementary Table 4: Gene enrichment analyses of downregulated genes upon Pxr activation in the liver.

Figure 1: Effect of circadian rhythm on clock genes and sex on the expression of *Pxr* and its target genes.

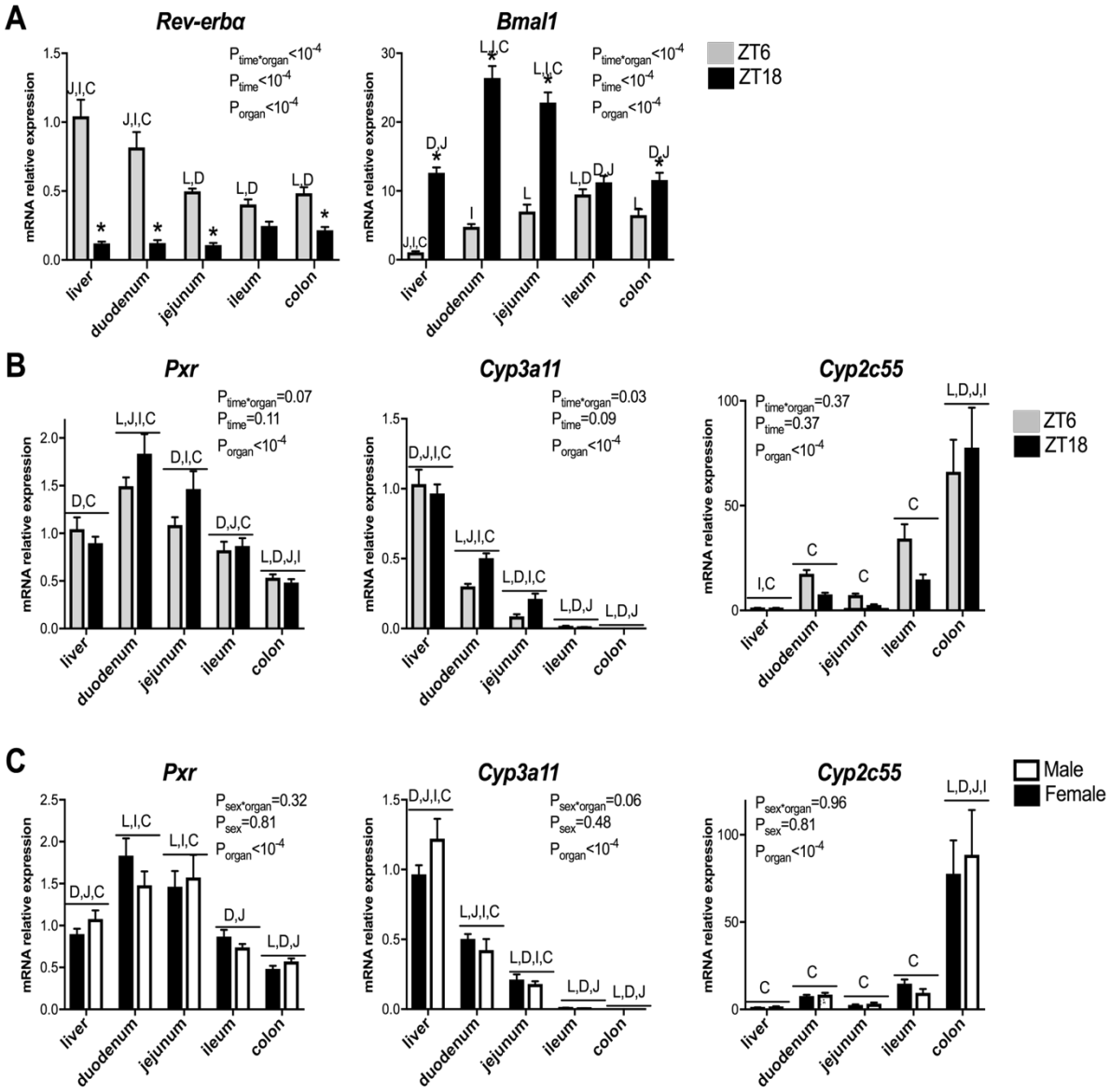

Figure 2: Impact of PCN treatment and *Pxr* deletion on the liver and intestinal transcriptomes.

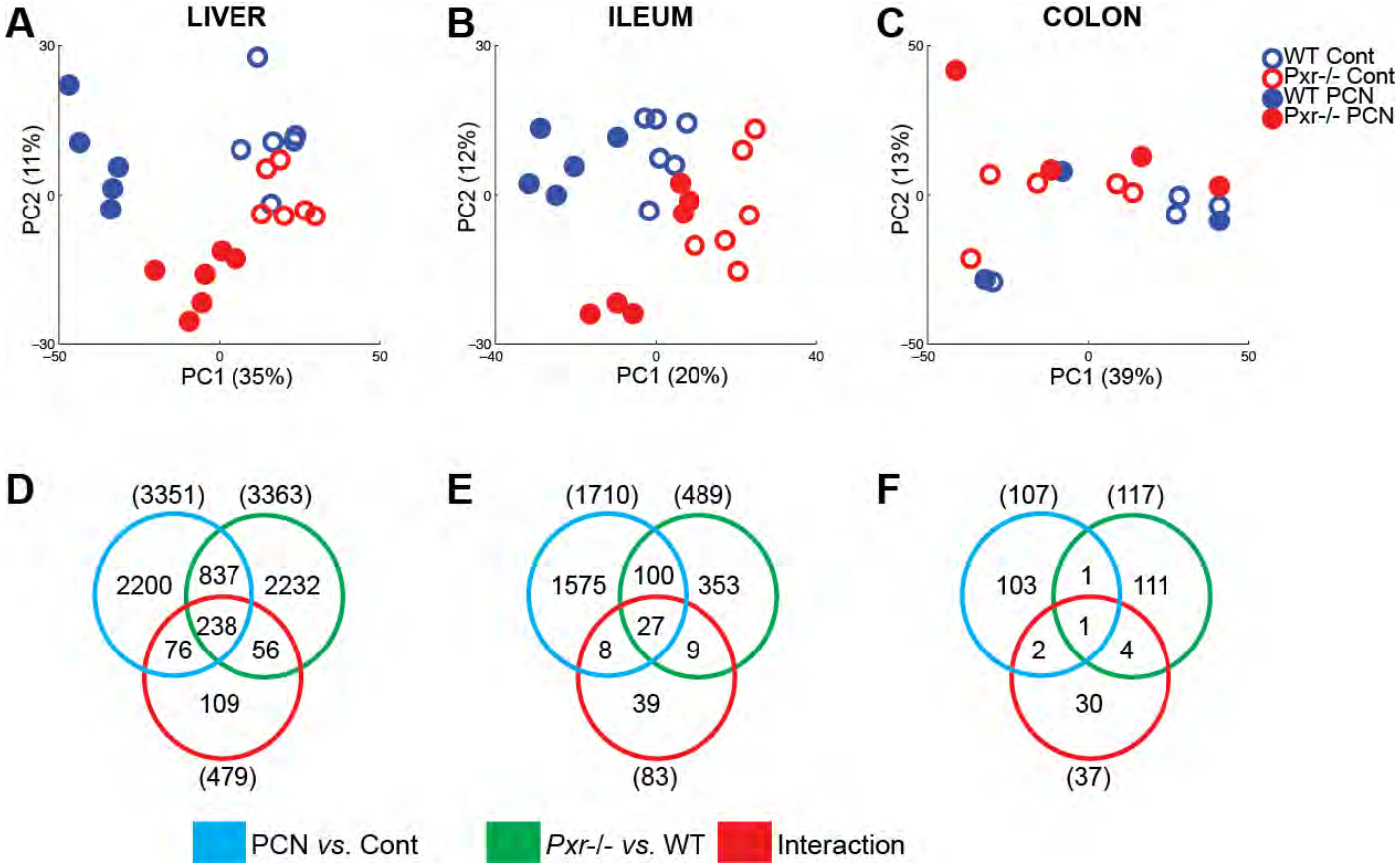

Figure 3: PXR-dependent up-regulated genes.

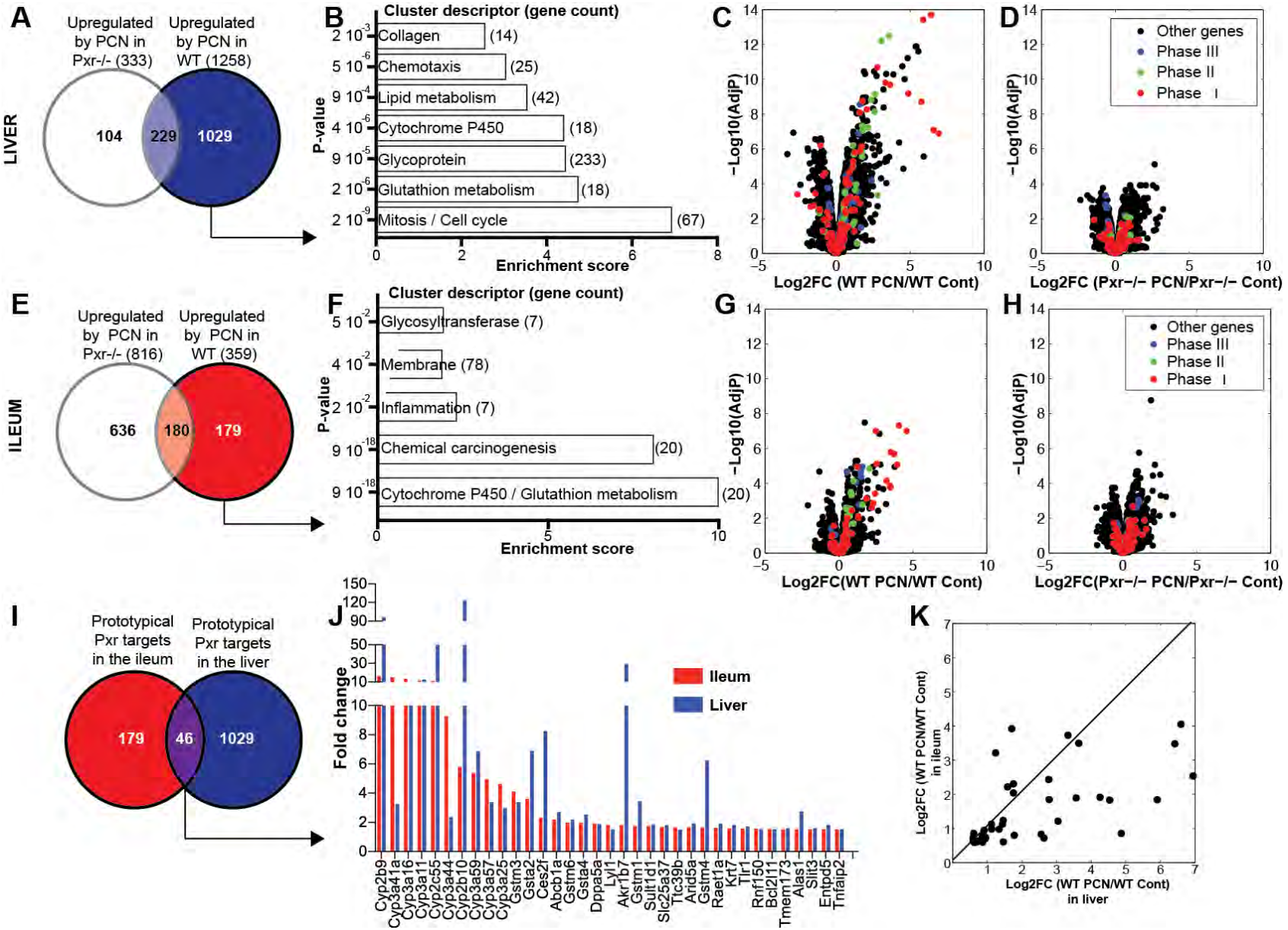

Figure 4: Shared and tissue-specific PXR-dependent down-regulated genes in the liver and ileum.

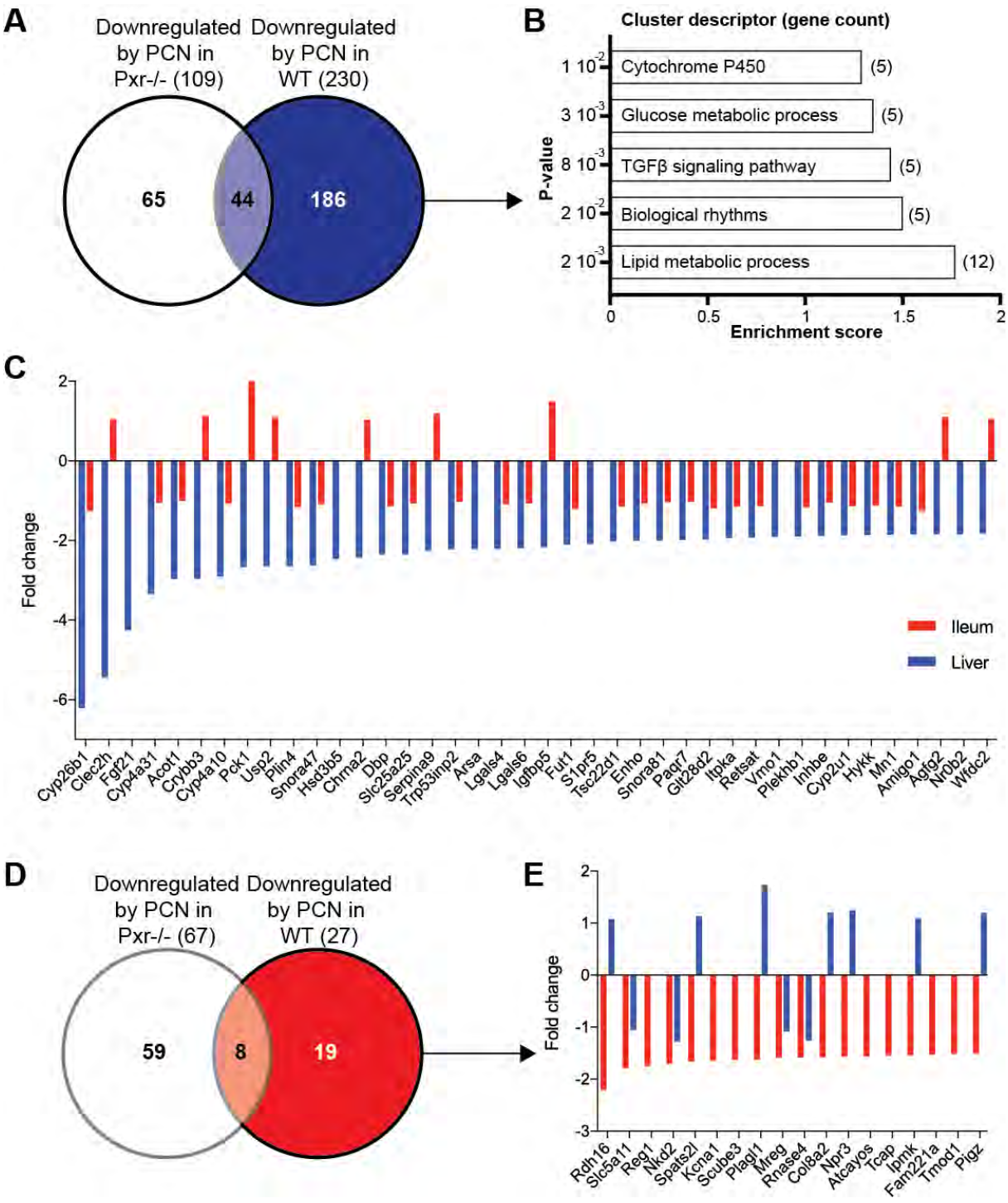

Figure 5: Impact of PXR activation on hepatic and intestinal PXR activity by intraperitoneal injection and oral gavage.

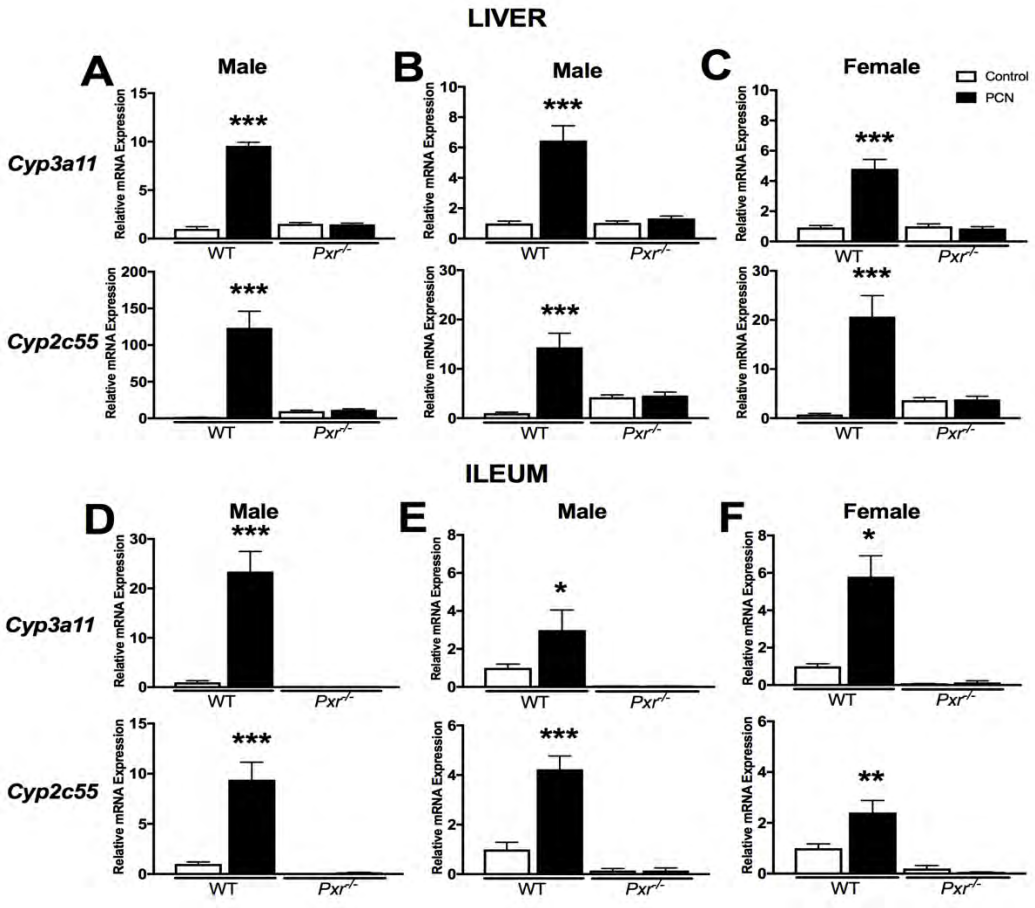

SUPPLEMENTARY FIGURES

Supplementary Figure 1: Effect PXR activation on the expression of Tlrs in the (A) liver and (B) ileum.

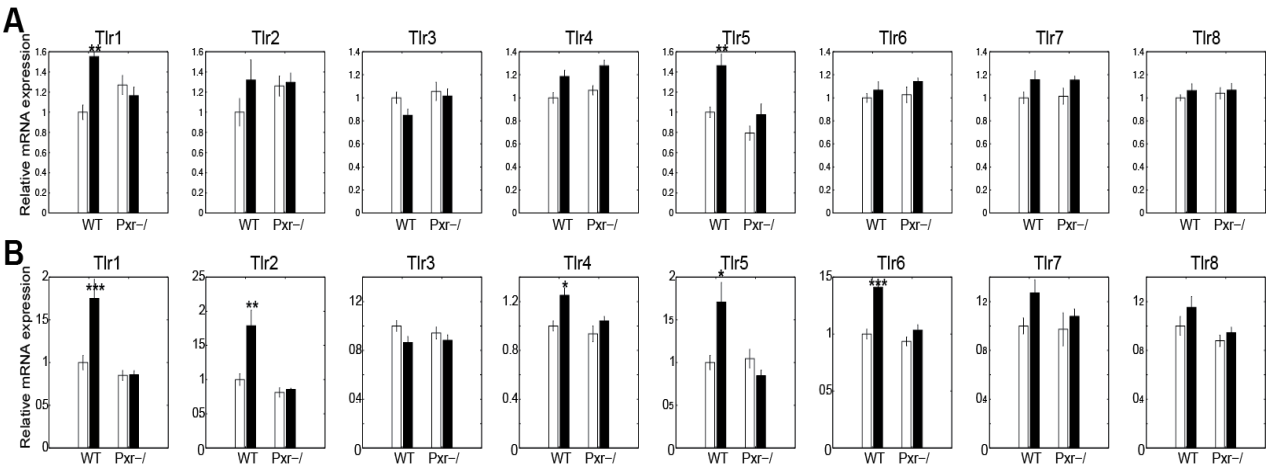

Supplementary Figure 2: Effect PXR activation on the expression of prototypical genes in the liver and ileum.

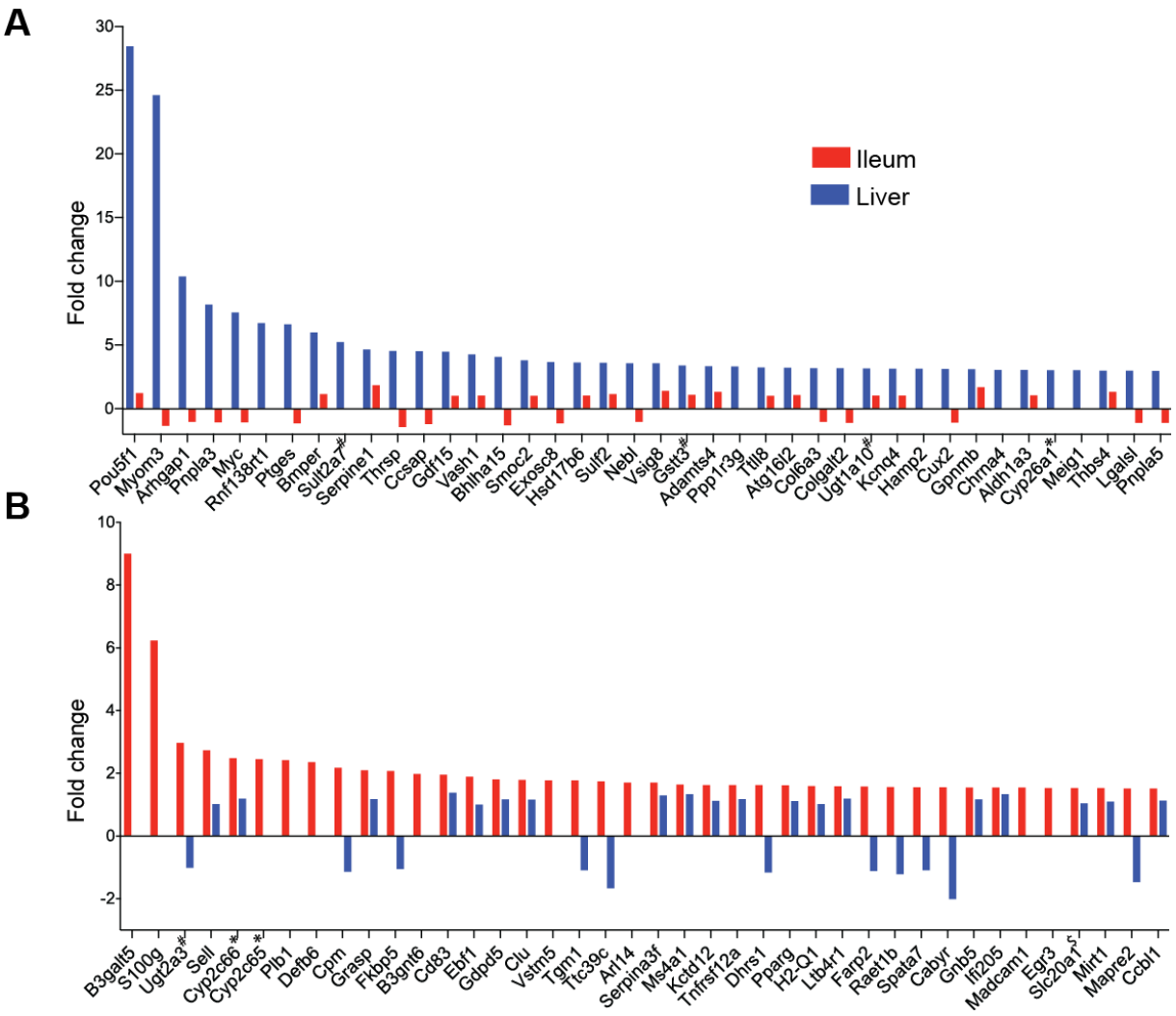

SUPPLEMENTARY TABLES

Supplementary Table 1: Effect PXR activation on the expression of *Tlrs* in the (A) liver and (B) ileum.

Cluster number	Enrichment score	Adjusted P-value	Ontology		Gene count	Genes
1	6.94	1.50E-09	mitosis	Up_keywords	41	BUB1B, mitotic checkpoint serine/threonine kinase(Bub1b);CTF18, chromosome transmission fidelity factor 18(Chtf18);E2F transcription factor 7(E2f7);Fanconi anemia, complementation group I(Fanci);H2A histone family, member X(H2afx);H2A histone family, member Y3(H2afy3);H2B histone family, member M(H2bfm);MAD1 mitotic arrest deficient 1-like 1(Mad1l1);MAD2 mitotic arrest deficient-like 1(Mad2l1);MAD2 mitotic arrest deficient-like 2(Mad2l2);MIS18 binding protein 1(Mis18bp1);N-terminal Xaa-Pro-Lys N-methyltransferase 1(Ntmt1);NSL1, MIS12 kinetochore complex component(Nsl1);NUF2, NDC80 kinetochore complex component(Nuf2);Opa interacting protein 5(Oip5);RAN, member RAS oncogene family(Ran);Rac GTPase-activating protein 1(Racgap1);Ras association (RalGDS/AF-6) domain family member 4(Rassf4);SET domain containing (lysine methyltransferase) 7(Setd7);SPC24, NDC80 kinetochore complex component, homolog (S. cerevisiae)(Spc24);TOPBP1-interacting checkpoint and replication regulator(Ticrr);TPX2, microtubule-associated(Tpx2);asp (abnormal spindle)-like, microcephaly associated (Drosophila)(Aspm);aurora kinase A(Aurka)aurora kinase B(Aurkb);baculoviral IAP repeat-containing 5(Birc5);cAMP-regulated phosphoprotein 19(Arpp19);cell division cycle 20(Cdc20);cell division cycle associated 3(Cdca3);cell division cycle associated 5(Cdca5);cell division cycle associated 8(Cdca8);centriole, cilia and spindle associated protein(Ccsap);centromere protein E(Cenpe);centromere protein F(Cenpf);centromere protein I(Cenpi);centromere protein M(Cenpm);checkpoint kinase 1(Chek1);chromatin assembly factor 1, subunit B (p60)(Chaf1b);chromosome alignment maintaining phosphoprotein 1(Champ1);cyclin A2(Ccna2);cyclin B1(Ccnb1);cyclin B2(Ccnb2);cyclin-dependent kinase 1(Cdk1);cyclin-dependent kinase 4(Cdk4);cyclin-dependent kinase 7(Cdk7);cyclin-dependent kinase inhibitor 1A (P21)(Cdkn1a);cyclin-dependent kinase inhibitor 3(Cdkn3);cytoskeleton associated protein 2(Ckap2);denticleless E3 ubiquitin protein ligase(Dtl);ect2 oncogene(Ect2);extra spindle pole bodies 1, separase(Espl1);forkhead box M1(Foxm1);high mobility group box 2(Hmgb2);histone cluster 1, H2bq(Hist1h2bq);inner centromere protein(Incenp);interleukin 33(Il33);kinesin family member 20B(Kif20b);kinesin family member 23(Kif23);kinetochore associated 1(Kntc1);kinetochore-localized astrin/SPAG5 binding(Knstrn);lysyl oxidase-like 2(Loxl2);maternal embryonic leucine zipper kinase(Melk);non-SMC condensin I complex, subunit D2(Ncapd2);non-SMC condensin II complex, subunit G2(Ncapg2);nucleolar and spindle associated protein 1(Nusap1);nucleolar protein interacting with the FHA domain of MKI67(Nifk);pescadillo ribosomal biogenesis factor 1(Pes1);polo-like kinase 3(Plk3);proline rich 5 (renal)(Prr5);proline/serine-rich coiled-coil 1(Psrc1);protein phosphatase 1, catalytic subunit, gamma isoform(Ppp1cc);regulator of cell cycle(Rgcc);retinoblastoma binding protein 8(Rbbp8);serine/threonine kinase 10(Stk10);shugoshin-like 1 (S. pombe)(Sgol1);sperm associated antigen 5(Spag5);sphingomyelin phosphodiesterase 3, neutral(Smpd3);spindle and kinetochore associated complex subunit 3(Ska3);thioredoxin interacting protein(Txnip);topoisomerase (DNA) II alpha(Top2a);transforming, acidic coiled-coil containing protein 3(Tacc3);ubiquitin-conjugating enzyme E2C(Ube2c);ubiquitin-like, containing PHD and RING finger domains, 1(Uhrf1);vasohibin 1(Vash1)
		2.40E-08	cell cycle	Up_keywords	67	
		2.20E-07	cell division	Goterm_BP_direct	46	

Cluster number	Enrichment score	Adjusted P-value	Ontology		Gene count	Genes
2	4.75	2.10E-06	Glutathione metabolism	Kegg_pathway	18	SH3 domain binding glutamic acid-rich protein-like 3(Sh3bgrl3);UDP glucuronosyltransferase 1 family, polypeptide A6B(Ugt1a6b);UDP glucuronosyltransferase 2 family, polypeptide A1(Ugt2a1);UDP glucuronosyltransferase 2 family, polypeptide B34(Ugt2b34);UDP glucuronosyltransferase 2 family, polypeptide B35(Ugt2b35);UDP glycosyltransferase 1 family, polypeptide A10(Ugt1a10);alanyl (membrane) aminopeptidase(Anpep);alcohol dehydrogenase 1 (class I)(Adh1);aldehyde dehydrogenase family 1, subfamily A3(Aldh1a3);carbonyl reductase 2(Cbr2);carbonyl reductase 3(Cbr3);cystathionase (cystathionine gamma-lyase)(Cth);cytochrome P450, family 1, subfamily b, polypeptide 1(Cyp1b1);epoxide hydrolase 1, microsomal(Ephx1);ethylmalonic encephalopathy 1(Ethe1);eukaryotic translation elongation factor 1 epsilon 1(Eef1e1);gamma-glutamyl cyclotransferase(Ggct);glucose-6-phosphate dehydrogenase X-linked(G6pdx);glutaredoxin(Glrx);glutathione S-transferase, alpha 2 (Yc2)(Gsta2);glutathione S-transferase, alpha 4(Gsta4);glutathione S-transferase, mu 1(Gstm1);glutathione S-transferase, mu 3(Gstm3);glutathione S-transferase, mu 4(Gstm4)glutathione S-transferase, mu 5(Gstm5);glutathione S-transferase, mu 6(Gstm6);glutathione S-transferase, theta 3(Gstt3);glutathione peroxidase 3(Gpx3);glutathione peroxidase 7(Gpx7);glutathione peroxidase 8 (putative)(Gpx8);glutathione reductase(Gsr);phosphogluconate dehydrogenase(Pgd);predicted gene 10639(Gm10639);ribonucleotide reductase M2(Rrm2);spermidine synthase(Srm)
		2.70E-06	Metabolism of xenobiotics by cytochrome P450	Kegg_pathway	19	
		1.40E-03	Drug metabolism - CYP450	Kegg_pathway	15	
3	4.45	8.80E-05	Glycoprotein	Up-keywords	233	
		4.00E-04	Disulfide bound	Up_keywords	192	
		7.60E-03	Signal	Up_keywords	253	

Cluster number	Enrichment score	Adjusted P-value	Ontology		Gene count	Genes
4	4.41	4.20E-06	Retinol metabolism	Kegg_pathway	22	UDP glucuronosyltransferase 1 family, polypeptide A6B(Ugt1a6b);UDP glucuronosyltransferase 2 family, polypeptide A1(Ugt2a1);UDP glucuronosyltransferase 2 family, polypeptide B34(Ugt2b34);UDP glucuronosyltransferase 2 family, polypeptide B35(Ugt2b35);UDP glycosyltransferase 1 family, polypeptide A10(Ugt1a10);alcohol dehydrogenase 1 (class I)(Adh1);aldehyde dehydrogenase family 1, subfamily A1(Aldh1a1);aldehyde dehydrogenase family 1, subfamily A7(Aldh1a7);alkB homolog 1, histone H2A dioxygenase(Alkbh1);carboxylesterase 2C(Ces2c);cholesterol 25-hydroxylase(Ch25h);cytochrome P450, family 1, subfamily b, polypeptide 1(Cyp1b1);cytochrome P450, family 2, subfamily a, polypeptide 22(Cyp2a22);cytochrome P450, family 2, subfamily a, polypeptide 4(Cyp2a4);cytochrome P450, family 2, subfamily a, polypeptide 5(Cyp2a5);cytochrome P450, family 2, subfamily b, polypeptide 10(Cyp2b10);cytochrome P450, family 2, subfamily b, polypeptide 9(Cyp2b9);cytochrome P450, family 2, subfamily c, polypeptide 29(Cyp2c29);cytochrome P450, family 2, subfamily c, polypeptide 55(Cyp2c55);cytochrome P450, family 2, subfamily g, polypeptide 1(Cyp2g1);cytochrome P450, family 26, subfamily a, polypeptide 1(Cyp26a1);cytochrome P450, family 3, subfamily a, polypeptide 11(Cyp3a11);cytochrome P450, family 3, subfamily a, polypeptide 16(Cyp3a16);cytochrome P450, family 3, subfamily a, polypeptide 25(Cyp3a25)cytochrome P450, family 3, subfamily a, polypeptide 41A(Cyp3a41a);cytochrome P450, family 3, subfamily a, polypeptide 44(Cyp3a44);cytochrome P450, family 3, subfamily a, polypeptide 57(Cyp3a57);cytochrome P450, family 3, subfamily a, polypeptide 59(Cyp3a59);cytochrome P450, family 4, subfamily f, polypeptide 18(Cyp4f18);cytochrome b-245, alpha polypeptide(Cyba);cytochrome b5 type B(Cyb5b);epoxide hydrolase 1, microsomal(Ephx1);heme oxygenase 1(Hmox1);hemochromatosis(Hfe);hydroxysteroid (17-beta) dehydrogenase 6(Hsd17b6);microtubule associated monooxygenase, calponin and LIM domain containing 1(Mical1);myeloperoxidase(Mpo);myo-inositol oxygenase(Miox);nitric oxide synthase 3, endothelial cell(Nos3);phospholipase A2, group VI(Pla2g6);phospholipase A2, group XIIA(Pla2g12a);polymerase I and transcript release factor(Ptrf);procollagen lysine, 2-oxoglutarate 5-dioxygenase 2(Plod2);progesterone receptor membrane component 1(Pgrmc1);prolyl 3-hydroxylase 3(P3h3);protein phosphatase 3, catalytic subunit, gamma isoform(Ppp3cc);retinol dehydrogenase 11(Rdh11);ribonucleotide reductase M2(Rrm2);sideroflexin 3(Sfxn3);solute carrier family 25, member 37(Slc25a37);sulfotransferase family 1E, member 1(Sult1e1);tet methylcytosine dioxygenase 3(Tet3);transmembrane 7 superfamily member 2(Tm7sf2)
		2.40E-04	Microsome	Up_keywords	20	
		2.50E-04	Monooxygenase	Up_keywords	20	

Cluster number	Enrichment score	Adjusted P-value	Ontology		Gene count	Genes
5	3.55	9.10E-04	Lipid metabolism	Up_keywords	39	1-acylglycerol-3-phosphate O-acyltransferase 4 (lysophosphatidic acid acyltransferase, delta)(Agpat4);2-hydroxyacyl-CoA lyase 1(Hacl1);3-hydroxyacyl-CoA dehydratase 4(Hacd4);7-dehydrocholesterol reductase(Dhcr7);ELOVL family member 6, elongation of long chain fatty acids (yeast)(Elovl6);ER lipid raft associated 1(Erlin1);JAZF zinc finger 1(Jazf1);abhydrolase domain containing 5(Abhd5);acetyl-Coenzyme A carboxylase beta(Acacb);acyl-CoA synthetase long-chain family member 5(Acsl5);acyl-CoA synthetase medium-chain family member 1(Acsm1);acyl-CoA synthetase medium-chain family member 2(Acsm2);carboxylesterase 1D(Ces1d);ceramide synthase 2(Cers2);ceramide synthase 6(Cers6);cholesterol 25-hydroxylase(Ch25h);cytochrome b5 reductase 3(Cyb5r3);elongation of very long chain fatty acids (FEN1/Elo2, SUR4/Elo3,yeast)-like 1(Elovl1);hydroxysteroid (17-beta) dehydrogenase 6(Hsd17b6);insulin induced gene 2(Insig2);lanosterol synthase(Lss);membrane bound O-acyltransferase domain containing 1(Mboat1);neuraminidase 3(Neu3);patatin-like phospholipase domain containing 3(Pnpla3)patatin-like phospholipase domain containing 5(Pnpla5);phospholipase A2, group VI(Pla2g6);phospholipase A2, group VII (platelet-activating factor acetylhydrolase, plasma)(Pla2g7);phospholipase A2, group XIIA(Pla2g12a);phospholipase A2, group XV(Pla2g15);phospholipase B domain containing 2(Plbd2);phospholipase C, eta 2(Plch2);prosaposin(Psap);prostaglandin E synthase(Ptges);protein kinase, AMP-activated, beta 1 non-catalytic subunit(Prkab1);protein tyrosine phosphatase, mitochondrial 1(Ptpmt1);solute carrier family 16 (monocarboxylic acid transporters), member 1(Slc16a1);sortilin-related receptor, LDLR class A repeats-containing(Sorl1);sphingomyelin phosphodiesterase 3, neutral(Smpd3);sterol O-acyltransferase 2(Soat2);sulfotransferase family 1D, member 1(Sult1d1);thyroid hormone responsive(Thrsp);transmembrane 7 superfamily member 2(Tm7sf2)
		1.30E-02	Lipid biosynthesis	Up_keywords	18	

Cluster number	Enrichment score	Adjusted P-value	Ontology		Gene count	Genes
6	3.05	5.50E-06	Chemotaxis	Goterm_BP_direct	25	BMP-binding endothelial regulator(Bmper);CCAAT/enhancer binding protein (C/EBP), beta(Cebpb);FGR proto-oncogene, Src family tyrosine kinase(Fgr);FMS-like tyrosine kinase 1(Flt1);Fc receptor, IgE, high affinity I, gamma polypeptide(Fcer1g);GLI pathogenesis-related 2(Glipr2);NAD(P)H dehydrogenase, quinone 2(Nqo2);RAS-related C3 botulinum substrate 2(Rac2);Rap guanine nucleotide exchange factor (GEF) 4(Rapgef4);SH3 domain binding glutamic acid-rich protein-like 3(Sh3bgrl3);SRY (sex determining region Y)-box 9(Sox9);a disintegrin-like and metallopeptidase (reprolysin type) with thrombospondin type 1 motif, 12(Adamts12);amyotrophic lateral sclerosis 2 (juvenile)(Als2);atypical chemokine receptor 2(Ackr2);bridging integrator 2(Bin2);cardiotrophin-like cytokine factor 1(Clcf1);cathelicidin antimicrobial peptide(Camp);cathepsin S(Ctss);chemokine (C-C motif) ligand 12(Ccl12);chemokine (C-C motif) ligand 2(Ccl2);chemokine (C-C motif) ligand 24(Ccl24);chemokine (C-C motif) ligand 3(Ccl3);chemokine (C-C motif) ligand 4(Ccl4);chemokine (C-C motif) ligand 6(Ccl6)chemokine (C-C motif) ligand 9(Ccl9);chemokine (C-C motif) receptor 2(Ccr2);chemokine (C-C motif) receptor 8(Ccr8);chemokine (C-X-C motif) ligand 5(Cxcl5);chemokine (C-X3-C motif) receptor 1(Cx3cr1);complement component 5a receptor 1(C5ar1);cytochrome b-245, alpha polypeptide(Cyba);drebrin 1(Dbn1);ect2 oncogene(Ect2);endothelial cell surface expressed chemotaxis and apoptosis regulator(Ecscr);eukaryotic translation initiation factor 2B, subunit 3(Eif2b3);fatty acid binding protein 4, adipocyte(Fabp4);glucose phosphate isomerase 1(Gpi1);glycoprotein (transmembrane) nmb(Gpnmb);growth differentiation factor 15(Gdf15);heat shock protein 1 (chaperonin)(Hspd1);high mobility group box 2(Hmgb2);integrin beta 2(Itgb2);interleukin 1 alpha(Il1a);interleukin 17 receptor B(Il17rb);interleukin 33(Il33);jun proto-oncogene(Jun);leukocyte cell-derived chemotaxin 2(Lect2);lymphocyte specific 1(Lsp1);myelocytomatosis oncogene(Myc);neuroepithelial cell transforming gene 1(Net1);neutrophil cytosolic factor 1(Ncf1);nuclear factor of kappa light polypeptide gene enhancer in B cells inhibitor, beta(Nfkbib);oncostatin M(Osm);peptidoglycan recognition protein 1(Pglyrp1);phosphatidylinositol 3-kinase catalytic delta polypeptide(Pik3cd);phosphatidylinositol 3-kinase, C2 domain containing, gamma polypeptide(Pik3c2g);phospholipase A2, group VI(Pla2g6);platelet derived growth factor receptor, alpha polypeptide(Pdgfra);platelet factor 4(Pf4);prostaglandin E receptor 4 (subtype EP4)(Ptger4);regulator of G-protein signalling 10(Rgs10);regulatory factor X, 1 (influences HLA class II expression)(Rfx1);roundabout guidance receptor 1(Robo1);secreted and transmembrane 1A(Sectm1a);secreted phosphoprotein 1(Spp1);serine (or cysteine) peptidase inhibitor, clade B, member 9(Serpinb9);serine (or cysteine) peptidase inhibitor, clade E, member 1(Serpine1);suppression of tumorigenicity 5(St5);toll-like receptor 1(Tlr1);transforming growth factor, beta 1(Tgfb1);transglutaminase 2, C polypeptide(Tgm2);tumor necrosis factor (ligand) superfamily, member 14(Tnfsf14);tumor necrosis factor receptor superfamily, member 10b(Tnfrsf10b);tumor necrosis factor receptor superfamily, member 21(Tnfrsf21);vav 1 oncogene(Vav1);wingless-type MMTV integration site family, member 5A(Wnt5a)
		4.70E-05	Positive regulation of inflammatory response	Goterm_BP_direct	17	

Cluster number	Enrichment score	Adjusted P-value	Ontology		Gene count	Genes
7	2.56	2.00E-03	Collagen	Up_keywords	14	ATPase, Na+/K+ transporting, alpha 3 polypeptide(Atp1a3);C1q and tumor necrosis factor related protein 6(C1qtnf6);C1q and tumor necrosis factor related protein 7(C1qtnf7);ankyrin repeat and SOCS box-containing 4(Asb4);collagen triple helix repeat containing 1(Cthrc1);collagen, type II, alpha 1(Col2a1);collagen, type IV, alpha 1(Col4a1);collagen, type IV, alpha 2(Col4a2);collagen, type V, alpha 1(Col5a1);collagen, type V, alpha 2(Col5a2);collagen, type VI, alpha 3(Col6a3);collagen, type VIII, alpha 1(Col8a1);collagen, type XII, alpha 1(Col12a1);collagen, type XVI, alpha 1(Col16a1);collagen, type XX, alpha 1(Col20a1);mannan-binding lectin serine peptidase 1(Masp1);potassium intermediate/small conductance calcium-activated channel, subfamily N, member 4(Kcnn4);procollagen C-endopeptidase enhancer protein(Pcolce);protein S (alpha)(Pros1);pyruvate kinase, muscle(Pkm)

Supplementary Table 2: Gene enrichment analyses of upregulated genes in the liver.

Cluster number	Enrichment score	Adjusted P-value	Ontology		Gene count	Genes
1	10.1	9.70E-18	chemical carcinogenesis	Kegg_pathway	20	UDP glucuronosyltransferase 1 family, polypeptide A 6B(Ugt1a6b);UDP glucuronosyltransferase 2 family, polypeptide A 3(Ugt2a3);cytochrome P450, family 2, subfamily b, polypeptide 10(Cyp2b10);cytochrome P450, family 2, subfamily b, polypeptide 9(Cyp2b9);cytochrome P450, family 2, subfamily c, polypeptide 55(Cyp2c55);cytochrome P450, family 2, subfamily c, polypeptide 65(Cyp2c65);cytochrome P450, family 2, subfamily c, polypeptide 66(Cyp2c66);cytochrome P450, family 3, subfamily a, polypeptide 11(Cyp3a11);cytochrome P450, family 3, subfamily a, polypeptide 16(Cyp3a16);cytochrome P450, family 3, subfamily a, polypeptide 25(Cyp3a25);cytochrome P450, family 3, subfamily a, polypeptide 41A(Cyp3a41a);cytochrome P450, family 3, subfamily a, polypeptide 44(Cyp3a44);glutathione S-transferase, alpha 2 (Yc2)(Gsta2);glutathione S-transferase, alpha 4(Gsta4);glutathione S-transferase, mu 1(Gstm1);glutathione S-transferase, mu 2(Gstm2);glutathione S-transferase, mu 3(Gstm3);glutathione S-transferase, mu 4(Gstm4);glutathione S-transferase, mu 6(Gstm6);microsomal glutathione S-transferase 2(Mgst2)
		9.20E-07	Metabolism of xenobiotics by cytochrome P450	Kegg_pathway	10	
		4.20E-05	Glutathione metabolism	Kegg_pathway	8	
2	8.1	9.70E-18	Chemical carcinogenesis	Kegg_pathway	20	UDP glucuronosyltransferase 1 family, polypeptide A 6B(Ugt1a6b);UDP glucuronosyltransferase 2 family, polypeptide A 3(Ugt2a3);cytochrome P450, family 2, subfamily b, polypeptide 10(Cyp2b10);cytochrome P450, family 2, subfamily b, polypeptide 9(Cyp2b9);cytochrome P450, family 2, subfamily c, polypeptide 55(Cyp2c55);cytochrome P450, family 2, subfamily c, polypeptide 65(Cyp2c65);cytochrome P450, family 2, subfamily c, polypeptide 66(Cyp2c66);cytochrome P450, family 3, subfamily a, polypeptide 11(Cyp3a11);cytochrome P450, family 3, subfamily a, polypeptide 16(Cyp3a16);cytochrome P450, family 3, subfamily a, polypeptide 25(Cyp3a25);cytochrome P450, family 3, subfamily a, polypeptide 41A(Cyp3a41a);cytochrome P450, family 3, subfamily a, polypeptide 44(Cyp3a44);glutathione S-transferase, alpha 2 (Yc2)(Gsta2);glutathione S-transferase, alpha 4(Gsta4);glutathione S-transferase, mu 1(Gstm1);glutathione S-transferase, mu 2(Gstm2);glutathione S-transferase, mu 3(Gstm3);glutathione S-transferase, mu 4(Gstm4);glutathione S-transferase, mu
		8.40E-09	Steroid hormone biosynthesis	Kegg_pathway	13	
		2.40E-08	Monooxygenase	Up_keywords	13	

						6(Gstm6);microsomal glutathione S-transferase 2(Mgst2)

Cluster number	Enrichment score	Adjusted P-value	Ontology		Gene count	Genes
3	2	4.50E-02	Membrane	Up_keywords	78	
4	2	1.80E-02	Inflammatory response	Up-keywords	7	chemokine (C-C motif) ligand 19(Ccl19);complement component 4B (Chido blood group)(C4b) ;interleukin 1 receptor accessory protein(Il1rap);nuclear factor of kappa light polypeptide gene enhancer in B cells inhibitor, delta(Nfkbid);phosphatidylinositol 3-kinase catalytic delta polypeptide(Pik3cd);toll-like receptor 1(Tlr1) ;toll-like receptor 5(Tlr5)
		3.00E-01	Innate immunity	Up-keywords	6	
5	1.66	5.00E-02	Glycosyltransferase	Up-keywords	7	MFNG O-fucosylpeptide 3-beta-N-acetylglucosaminyltransferase(Mfng;UDP glucuronosyltransferase 1 family, polypeptide A6B(Ugt1a6b);UDP glucuronosyltransferase 2 family, polypeptide A3(Ugt2a3) ;UDP-Gal:betaGlcNAc beta 1,3-galactosyltransferase, polypeptide 5(B3galt5);UDP-GlcNAc:betaGal beta-1,3-N-acetylglucosaminyltransferase 6 (core 3 synthase)(B3gnt6);glycoprotein galactosyltransferase alpha 1, 3(Ggta1);mannoside acetylglucosaminyltransferase 4, isoenzyme A(Mgat4a)
		3.00E-01	Signal-anchor	Up_keywords	8	

Supplementary Table 3: The comprehensive effect of PCN treatment on hepatic and ileal XMEs.

			LIVER			
		GeneName	**log2FC WTPCN-WTCtl**	**log2FC PXRKOPCN-PXRKOCtl**	**adj.P.Val WTPCN-WTCtl**	**adj.P.Val PXRKOPCN-PXRKOCtl**
Phase I	Cyptochomes P450	Cyp17a1	-0.207	-0.186	0.354594684	0.552695003
		Cyp1a1	0.015	-0.297	0.954617498	0.256128505
		Cyp1a2	0.285	0.892	0.381205224	0.017437424
		Cyp1b1	0.960	0.403	0.000545541	0.214793339
		Cyp20a1	0.405	-0.021	0.071042008	0.965460249
		Cyp21a1	0.517	1.004	0.168059036	0.025826814
		Cyp26a1	1.600	-1.442	0.001357012	0.011928216
		Cyp26b1	**-2.634**	**0.610**	**0.000398851**	**0.534259276**
		Cyp27a1	0.576	0.704	0.043420983	0.040420788
		Cyp2a12	-0.044	-0.080	0.864932529	0.829474334
		Cyp2a22	**0.799**	**0.368**	**0.028228105**	**0.472005496**
		Cyp2a4	1.043	0.148	0.003186099	0.800529575
		Cyp2a5	0.633	0.060	0.00478295	0.885230963
		Cyp2b10	**6.943**	**1.618**	**1.31E-07**	**0.167757172**
		Cyp2b9	**6.591**	**1.464**	**8.19E-08**	**0.176379042**
		Cyp2c29	**1.127**	**0.401**	**5.22E-06**	**0.094661353**
		Cyp2c37	0.185	0.508	0.596006078	0.201336035
		Cyp2c38	**2.070**	**0.605**	**5.34E-09**	**0.0311444**
		Cyp2c40	-0.090	-0.031	0.772898105	0.955515244
		Cyp2c44	-0.259	0.105	0.171981523	0.736868714
		Cyp2c50	0.505	0.045	0.13333446	0.948934169
		Cyp2c53-ps	**1.258**	**0.190**	**0.003304934**	**0.787236834**
		Cyp2c54	0.333	0.555	0.284557367	0.141533412
		Cyp2c55	**6.418**	**0.587**	**2.03E-14**	**0.185230396**
		Cyp2c65				

		Cyp2c66	0.261	0.104	0.110716192	0.6923277
		Cyp2c67	-0.368	-0.259	0.114215689	0.41645564
		Cyp2c68	-0.276	-0.180	0.228870045	0.595629585
		Cyp2c69	-0.352	-0.189	0.130732056	0.585741341
		Cyp2c70	0.233	0.035	0.352547408	0.943314469
		Cyp2d10	0.098	0.007	0.553842022	0.982179407
		Cyp2d11	0.075	0.091	0.78069673	0.820511303
		Cyp2d12	0.184	0.266	0.468660244	0.413051654
		Cyp2d13	-0.393	0.084	0.092562608	0.84207906
		Cyp2d22	0.395	0.241	0.064805156	0.409705177
		Cyp2d26	0.214	0.247	0.394146507	0.459331721
		Cyp2d34	0.394	0.383	0.437010067	0.591307547
		Cyp2d37-ps	-0.203	0.121	0.346150698	0.719044505
		Cyp2d40	-0.565	0.157	0.110263791	0.795360257
		Cyp2d9	0.339	0.358	0.478004592	0.591307547
		Cyp2e1	0.071	0.286	0.741251364	0.223265676
		Cyp2f2	0.027	-0.380	0.882047443	0.02887591
		Cyp2g1	**1.238**	**-0.347**	**0.003209173**	**0.559516077**
		Cyp2j13	0.348	0.290	0.051871259	0.20010032
		Cyp2j5	0.251	0.266	0.053201236	0.095291456
		Cyp2j6	0.306	0.327	0.127051182	0.196735385
		Cyp2j8	0.295	0.247	0.040827806	0.171780994
		Cyp2j9	-0.577	-0.278	0.02195992	0.420136956
		Cyp2r1	-0.041	-0.109	0.81768424	0.623314556
		Cyp2s1	-0.073	0.668	0.911222003	0.317036881
		Cyp2t4	0.085	0.015	0.551666973	0.955967419
		Cyp2u1	**-1.077**	**-0.445**	**6.32E-07**	**0.02236629**
		Cyp2w1	0.363	0.163	0.022244414	0.459331721
		Cyp39a1	-0.474	-0.007	0.291258635	0.994971281
		Cyp3a11	**3.642**	**0.358**	**2.08E-10**	**0.451653488**
		Cyp3a13	0.222	0.214	0.220599946	0.373614877

		Cyp3a16	**3.329**	**0.285**	**1.54E-10**	**0.520463869**
		Cyp3a25	**1.585**	**0.023**	**8.26E-09**	**0.953468102**
		Cyp3a41a	**1.706**	**0.216**	**7.00E-07**	**0.569460901**
		Cyp3a44	**1.241**	**0.036**	**1.56E-06**	**0.927438575**
		Cyp3a57	**1.757**	**0.021**	**1.76E-09**	**0.957596744**
		Cyp3a59	**2.778**	**0.276**	**2.06E-11**	**0.368290271**
		Cyp46a1	-0.033	-0.277	0.928740916	0.49276261
		Cyp4a10	**-1.539**	**-0.860**	**0.001789337**	**0.139267429**
		Cyp4a12a	-0.118	-0.524	0.844262835	0.440375754
		Cyp4a12b	-0.031	-0.473	0.961398971	0.503889528
		Cyp4a14	-0.919	-0.148	0.051227515	0.864625771
		Cyp4a31	**-1.741**	**-1.063**	**0.002076411**	**0.109923899**
		Cyp4b1	**-0.623**	**-0.028**	**0.004126175**	**0.950324529**
		Cyp4f13	-0.277	-0.141	0.071566449	0.525702155
		Cyp4f14	0.335	-0.125	0.065799883	0.66172333
		Cyp4f15	**0.371**	**0.244**	**0.023104582**	**0.239940605**
		Cyp4f16	**0.558**	**0.075**	**0.001393616**	**0.787718568**
		Cyp4f17	0.235	0.175	0.066549401	0.294719193
		Cyp4f18	**0.881**	**0.379**	**2.14E-05**	**0.066217803**
		Cyp4f40				
		Cyp4f41-ps	0.224	0.042	0.096401344	0.86567057
		Cyp4v3	**-0.469**	**0.130**	**0.008742124**	**0.629074268**
		Cyp4x1				
		Cyp51	0.130	0.317	0.628337335	0.317592494
		Cyp7a1	-0.295	0.284	0.28253931	0.447240471
		Cyp7b1	-0.374	0.166	0.475688316	0.85234487
		Cyp8b1	1.210	-0.291	0.052535773	0.783625551
	Alcohol dehydrogenases	**Adh1**	**0.600**	**0.369**	**0.00375224**	**0.13703633**
		Adh4	**-0.525**	**-0.295**	**0.008465973**	**0.239073432**
		Adh5	0.196	0.195	0.152699396	0.266331759
		Adh6-ps1	**-0.843**	**-0.535**	**0.011262535**	**0.197442451**

		Adh6a	0.516	0.003	0.150450063	0.997547388
		Adh7	**0.389**	**0.156**	**0.034983167**	**0.567469789**
	Aldo-keto reductases	Akr1a1	0.152	0.068	0.237741562	0.747980181
		Akr1b10	0.380	0.141	0.135676362	0.737182478
		Akr1b3	**0.753**	**0.263**	**0.000783503**	**0.342913331**
		Akr1b7	**4.871**	**0.522**	**6.63E-10**	**0.436451105**
		Akr1b8	0.214	0.315	0.307544517	0.224195859
		Akr1c12	0.116	0.126	0.450119448	0.552246932
		Akr1c13	0.109	0.115	0.472701746	0.589416119
		Akr1c14	0.292	-0.067	0.260257246	0.889885008
		Akr1c18	0.310	-0.238	0.145502005	0.413051654
		Akr1c19	0.364	0.296	0.140156064	0.371792182
		Akr1c20	0.277	0.432	0.073671843	0.020825565
		Akr1c6	0.250	0.363	0.092819684	0.04329317
		Akr1cl	1.413	-0.059	0.260782747	0.982179407
		Akr1d1	**1.739**	**0.747**	**2.77E-06**	**0.031881594**
		Akr1e1	0.275	0.032	0.08595976	0.920261591
		Akr7a5	0.304	-0.044	0.071945043	0.889551356
	Aldehyde dehydrogenases	Aldh16a1	0.141	0.092	0.410117226	0.731866998
		Aldh18a1	**0.613**	**0.294**	**0.001247957**	**0.194223241**
		Aldh1a1	**0.875**	**0.246**	**0.000102213**	**0.343164819**
		Aldh1a2	0.539	0.651	0.072759726	0.076549889
		Aldh1a3	**1.603**	**0.565**	**1.32E-06**	**0.0646244**
		Aldh1a7	**1.111**	**0.472**	**1.13E-05**	**0.056227638**
		Aldh1b1	**1.381**	**0.149**	**0.000682648**	**0.822784187**
		Aldh1l1	0.365	0.087	0.090536001	0.818182689
		Aldh1l2				
		Aldh2	0.354	0.224	0.144393915	0.519621351
		Aldh3a1	0.078	0.004	0.542350937	0.988703678

		Aldh3a2	-0.453	-0.116	0.072028222	0.786601603
		Aldh3b1	0.264	-0.094	0.23542302	0.803556501
		Aldh3b2				
		Aldh3b3	0.113	0.137	0.383294037	0.417259047
		Aldh4a1	0.711	0.422	5.80E-05	0.020042103
		Aldh5a1	0.022	-0.217	0.907839768	0.248470208
		Aldh6a1	-0.022	-0.055	0.904953726	0.824088909
		Aldh7a1	0.391	0.131	0.022853311	0.61462553
		Aldh8a1	0.367	0.092	0.115089966	0.822250907
		Aldh9a1	0.234	0.160	0.321566748	0.65156902
	Carboxylesterases	Ces1b	0.048	0.456	0.870278156	0.111248622
		Ces1c	**0.590**	**0.272**	**0.00034409**	**0.142562802**
		Ces1d	**1.283**	**0.466**	**0.000234403**	**0.242321641**
		Ces1e	0.235	-0.463	0.415525361	0.177802511
		Ces1f	0.117	-0.048	0.460154294	0.860345771
		Ces1g	1.263	0.981	0.000235613	0.008808571
		Ces2a	3.559	0.752	3.17E-13	0.007778188
		Ces2b	**1.222**	**1.009**	**0.015457505**	**0.101222258**
		Ces2c	**1.118**	**1.013**	**0.0209954**	**0.086611671**
		Ces2e	0.094	-0.214	0.751025662	0.563394735
		Ces2f	3.044	0.527	6.12E-13	0.032993137
		Ces2g	**1.126**	**0.187**	**6.28E-07**	**0.419283812**
		Ces3a	0.105	0.072	0.35158257	0.673164911
		Ces3b	0.298	0.254	0.342654775	0.568072742
		Ces4a	-0.809	-0.385	0.055209561	0.527170292
Phase II	Glutathione S-transferases	**Gsta2**	**2.788**	**0.588**	**0.00046201**	**0.587534164**
		Gsta3	**0.537**	**-0.005**	**0.002240258**	**0.989163394**
		Gsta4	**1.343**	**-0.330**	**0.000110056**	**0.42796389**
		Gstcd	**0.376**	**-0.013**	**0.020522338**	**0.968306079**
		Gstk1	-0.095	-0.272	0.497922493	0.08823388
		Gstm1	**2.142**	**0.299**	**5.88E-08**	**0.430782343**

		Gstm2	2.597	0.831	7.33E-09	0.020318855
		Gstm3	1.756	0.308	4.91E-08	0.288645858
		Gstm4	2.638	0.383	7.43E-10	0.260598097
		Gstm5	0.590	0.157	0.000286784	0.43937882
		Gstm6	**2.354**	**0.496**	**1.58E-09**	**0.100502896**
		Gstm7	0.551	-0.015	0.008119886	0.973481687
		Gsto1	0.296	0.010	0.054417479	0.976290177
		Gsto2	0.167	0.157	0.348072149	0.525144671
		Gstp1	0.143	0.058	0.447499159	0.859162837
		Gstp2	0.049	-0.057	0.653250604	0.710843534
		Gstt1	0.297	0.007	0.065709576	0.98522723
		Gstt2	**-1.150**	**-0.819**	**0.004674929**	**0.090947951**
		Gstt3	**1.758**	**0.118**	**1.44E-06**	**0.806376748**
		Gstz1	0.064	0.058	0.662205463	0.795264416
	Sulfotransferases	**Sult1a1**	**0.579**	**0.391**	**0.020048815**	**0.214513288**
		Sult1b1	**0.532**	**0.309**	**0.020794314**	**0.303500836**
		Sult1c1	-0.224	0.166	0.212304986	0.514913513
		Sult1c2	0.294	-0.566	0.223138971	0.048616017
		Sult1d1	**0.893**	**0.410**	**0.000869292**	**0.195046478**
		Sult1e1	**1.302**	**0.691**	**0.001116758**	**0.137484215**
		Sult2a7	**2.385**	**-0.028**	**6.42E-05**	**0.979818386**
		Sult2a8	-0.428	0.127	0.11043721	0.780374755
		Sult2b1				
		Sult4a1	**0.328**	**0.004**	**0.008567473**	**0.989091557**
		Sult5a1	0.551	-0.165	0.107093977	0.775618739
	UDP glycosyltransferases	**Ugt1a10**	**1.663**	**0.070**	**0.032440178**	**0.966053868**
		Ugt1a6a	0.077	-0.204	0.826663738	0.649879758
		Ugt1a6b	**0.927**	**0.343**	**8.45E-05**	**0.178423037**
		Ugt2a1	**0.763**	**0.041**	**0.000139508**	**0.903145107**
		Ugt2a3	-0.013	-0.098	0.945800485	0.682471496

		Ugt2b1	0.443	-0.632	0.13019971	0.077548112
		Ugt2b34	**0.843**	**0.047**	**0.000112842**	**0.898381451**
		Ugt2b35	**0.933**	**0.006**	**5.93E-05**	**0.98975358**
		Ugt2b36	0.186	-0.128	0.249642745	0.587303954
		Ugt2b37	0.016	-0.221	0.955988947	0.478430785
		Ugt2b38	-0.050	-0.224	0.810548106	0.331294432
		Ugt2b5	0.023	-0.180	0.932388795	0.547467398
		Ugt3a1	-0.002	0.170	0.991727773	0.499360517
		Ugt3a2	0.132	0.199	0.473132178	0.390165436
Phase III	ATP-binding cassettes	**Abca1**	**0.441**	**0.309**	**0.014420766**	**0.16670699**
		Abca12				
		Abca14				
		Abca17	0.055	0.178	0.85460872	0.63585783
		Abca2	0.287	-0.350	0.165204162	0.175615159
		Abca3	0.114	-0.006	0.439806524	0.983433163
		Abca4	0.160	0.095	0.356233155	0.728618069
		Abca5	-0.075	-0.287	0.790830001	0.366340841
		Abca6	0.200	0.215	0.226545878	0.316096111
		Abca7	-0.235	-0.101	0.086994599	0.630066325
		Abca8a	-0.133	0.366	0.546097581	0.14604884
		Abca8b	0.274	0.313	0.282626697	0.345116039
		Abca9	0.302	0.173	0.101987854	0.514407311
		Abcb10	-0.203	-0.494	0.225739383	0.014140284
		Abcb11	**0.545**	**0.090**	**0.006981563**	**0.788490603**
		Abcb1a	**1.442**	**-0.129**	**0.000277031**	**0.840097555**
		Abcb1b	**0.618**	**0.487**	**0.011612536**	**0.101237526**
		Abcb4	-0.569	-0.654	0.000180635	0.000458236
		Abcb6	-0.087	0.051	0.552760396	0.831791839
		Abcb7	0.055	0.017	0.7166416	0.95053373
		Abcb8	**0.384**	**-0.016**	**0.042919393**	**0.967784066**
		Abcb9	-0.214	-0.253	0.355091294	0.402014972

		Abcc1	-0.370	-0.291	0.003252886	0.046685918
		Abcc10	-0.089	-0.228	0.59356963	0.234738913
		Abcc12	-0.200	0.069	0.533917326	0.904928088
		Abcc2	**0.475**	**0.075**	**0.004657993**	**0.786601603**
		Abcc3	1.597	0.428	2.78E-09	0.040420788
		Abcc4	0.296	0.337	0.055654358	0.074362511
		Abcc5	0.194	0.114	0.298651162	0.69535162
		Abcc6	-0.149	-0.009	0.289362498	0.97643671
		Abcc8				
		Abcc9	0.067	0.147	0.77392958	0.626040888
		Abcd1	**0.524**	**0.376**	**0.02928331**	**0.218320755**
		Abcd2	1.151	-0.581	0.055342641	0.49793098
		Abcd3	-0.168	-0.023	0.359705926	0.951057252
		Abcd4	0.208	0.224	0.328295197	0.428448926
		Abce1	0.314	0.142	0.063060541	0.570330469
		Abcf1	0.506	0.379	0.078593279	0.31694254
		Abcf2	0.175	0.109	0.525794173	0.803587644
		Abcf3	**0.387**	**0.247**	**0.014995834**	**0.218746914**
		Abcg1	0.410	0.391	0.065678849	0.159118045
		Abcg2	0.184	0.135	0.352568376	0.646381839
		Abcg3	0.346	0.046	0.224526693	0.93643713
		Abcg4	**0.880**	**-0.115**	**0.000975509**	**0.785899795**
		Abcg5	**0.301**	**-0.112**	**0.04811495**	**0.629271906**
		Abcg8	-0.019	-0.219	0.928458194	0.301611537

			ILEUM			
		GeneName	**log2FC WTPCN-WTCtl**	**log2FC PXRKOPCN-PXRKOCtl**	**adj.P.Val WTPCN-WTCtl**	**adj.P.Val PXRKOPCN-PXRKOCtl**
Phase I	Cyptochomes P450	Cyp17a1	0.154	-0.144	7.80E-01	6.56E-01
		Cyp1a1				
		Cyp1a2				
		Cyp1b1	0.396	0.521	1.25E-01	1.39E-02
		Cyp20a1	0.088	0.045	7.25E-01	7.87E-01
		Cyp21a1	-0.534	-0.097	5.07E-01	8.89E-01
		Cyp26a1				
		Cyp26b1	-0.323	0.502	7.30E-01	3.34E-01
		Cyp27a1	0.290	0.340	4.39E-01	1.73E-01
		Cyp2a12				
		Cyp2a22				
		Cyp2a4				
		Cyp2a5	0.207	0.337	8.20E-01	4.70E-01
		Cyp2b10	**4.566**	**0.706**	**1.00E-07**	**2.49E-01**
		Cyp2b9	**4.052**	**0.280**	**4.74E-08**	**6.22E-01**
		Cyp2c29	0.479	0.408	3.47E-01	2.61E-01
		Cyp2c37				
		Cyp2c38	-0.048	-0.084	9.01E-01	6.32E-01
		Cyp2c40	0.522	0.455	2.90E-01	2.08E-01
		Cyp2c44	0.242	0.513	6.24E-01	7.83E-02
		Cyp2c50				
		Cyp2c53-ps				
		Cyp2c54				
		Cyp2c55	**3.478**	**1.312**	**1.40E-04**	**9.10E-02**
		Cyp2c65	**1.295**	**0.681**	**7.69E-03**	**1.11E-01**
		Cyp2c66	**1.311**	**0.611**	**9.35E-03**	**1.69E-01**

		Cyp2c67	0.198	0.245	6.86E-01	3.95E-01
		Cyp2c68	0.167	0.258	7.79E-01	4.25E-01
		Cyp2c69	0.209	0.196	6.98E-01	5.57E-01
		Cyp2c70	-0.137	-0.075	6.13E-01	6.86E-01
		Cyp2d10	-0.250	0.982	8.20E-01	6.16E-02
		Cyp2d11	-0.202	0.685	8.23E-01	1.13E-01
		Cyp2d12	-0.259	0.775	7.57E-01	7.86E-02
		Cyp2d13	-0.087	0.080	6.97E-01	5.61E-01
		Cyp2d22	-0.114	-0.020	7.40E-01	9.39E-01
		Cyp2d26	-0.279	0.937	7.76E-01	6.32E-02
		Cyp2d34	-0.067	0.148	9.11E-01	5.66E-01
		Cyp2d37-ps	-0.606	0.171	2.90E-01	7.27E-01
		Cyp2d40	0.081	1.461	9.61E-01	1.33E-02
		Cyp2d9	-0.208	0.102	6.35E-01	7.38E-01
		Cyp2e1	0.058	0.609	9.86E-01	5.68E-01
		Cyp2f2	-0.303	0.037	4.98E-01	9.27E-01
		Cyp2g1				
		Cyp2j13	0.133	0.303	8.26E-01	3.02E-01
		Cyp2j5				
		Cyp2j6	0.258	0.261	4.24E-01	2.31E-01
		Cyp2j8	0.211	0.495	5.56E-01	2.74E-02
		Cyp2j9	-0.027	0.261	9.64E-01	2.20E-01
		Cyp2r1	0.183	0.091	5.53E-01	6.78E-01
		Cyp2s1	0.196	0.426	6.52E-01	8.92E-02
		Cyp2t4	-0.155	-0.176	6.81E-01	4.36E-01
		Cyp2u1	-0.181	0.469	7.41E-01	1.10E-01
		Cyp2w1	0.048	-0.278	9.34E-01	1.95E-01
		Cyp39a1	0.115	0.047	8.27E-01	8.87E-01
		Cyp3a11	**3.495**	**-0.048**	**1.62E-06**	**9.51E-01**
		Cyp3a13	**0.462**	**0.082**	**5.54E-02**	**7.27E-01**
		Cyp3a16	**3.727**	**-0.031**	**2.10E-06**	**9.73E-01**

		Cyp3a25	**2.217**	**0.776**	**2.51E-03**	**2.39E-01**
		Cyp3a41a	**3.918**	**-0.101**	**8.31E-06**	**9.15E-01**
		Cyp3a44	**3.211**	**0.119**	**7.25E-05**	**8.97E-01**
		Cyp3a57	**2.308**	**0.671**	**1.36E-03**	**3.01E-01**
		Cyp3a59	**2.432**	**0.614**	**3.95E-04**	**3.16E-01**
		Cyp46a1	-0.198	0.260	7.16E-01	4.08E-01
		Cyp4a10	-0.103	-0.655	9.24E-01	1.10E-01
		Cyp4a12a				
		Cyp4a12b				
		Cyp4a14				
		Cyp4a31	-0.076	-0.135	8.73E-01	5.52E-01
		Cyp4b1	0.394	0.068	3.82E-01	8.68E-01
		Cyp4f13	-0.029	0.119	9.59E-01	5.85E-01
		Cyp4f14	0.028	0.183	9.56E-01	3.06E-01
		Cyp4f15				
		Cyp4f16	-0.336	0.246	4.40E-01	4.16E-01
		Cyp4f17	-0.140	0.162	7.11E-01	4.68E-01
		Cyp4f18	**0.456**	**0.254**	**2.04E-02**	**1.36E-01**
		Cyp4f40	-0.136	-0.133	7.74E-01	6.31E-01
		Cyp4f41-ps	-0.003	-0.136	9.95E-01	4.23E-01
		Cyp4v3	-0.339	0.269	4.12E-01	3.45E-01
		Cyp4x1	0.098	0.193	8.05E-01	3.39E-01
		Cyp51	0.225	-0.328	3.99E-01	6.87E-02
		Cyp7a1				
		Cyp7b1	0.413	0.669	8.79E-02	2.14E-03
		Cyp8b1				
	Alcohol dehydrogenases	Adh1	0.409	0.277	2.44E-01	2.96E-01
		Adh4	-0.225	-0.337	6.33E-01	2.28E-01
		Adh5	-0.002	0.049	9.96E-01	7.26E-01
		Adh6-ps1				

		Adh6a	0.231	-0.648	8.63E-01	2.86E-01
		Adh7				
	Aldo-keto reductases	Akr1a1	0.014	-0.051	9.65E-01	6.92E-01
		Akr1b10	0.110	0.059	6.20E-01	6.97E-01
		Akr1b3	-0.094	-0.050	8.71E-01	8.82E-01
		Akr1b7	**0.856**	**-0.528**	**3.56E-03**	**4.32E-02**
		Akr1b8	0.381	0.108	5.75E-01	8.40E-01
		Akr1c12	0.308	0.249	1.79E-01	1.60E-01
		Akr1c13	0.348	0.356	2.43E-01	1.06E-01
		Akr1c14	0.561	0.821	1.73E-01	1.31E-02
		Akr1c18	0.162	0.058	6.99E-01	8.49E-01
		Akr1c19	0.876	0.853	7.54E-02	3.65E-02
		Akr1c20				
		Akr1c6				
		Akr1cl	0.118	-0.165	7.33E-01	4.00E-01
		Akr1d1				
		Akr1e1	-0.144	0.004	6.95E-01	9.88E-01
		Akr7a5	-0.073	-0.025	8.51E-01	9.17E-01
	Aldehyde dehydrogenases	Aldh16a1	0.236	-0.084	5.91E-01	7.96E-01
		Aldh18a1	**-0.346**	**-0.053**	**2.78E-02**	**7.43E-01**
		Aldh1a1	0.426	0.533	1.36E-01	2.00E-02
		Aldh1a2	0.150	0.424	6.00E-01	1.57E-02
		Aldh1a3	0.388	0.422	1.97E-01	6.40E-02
		Aldh1a7	0.383	0.182	2.11E-01	4.58E-01
		Aldh1b1	-0.112	0.030	7.79E-01	9.14E-01
		Aldh1l1	-0.459	-0.469	9.65E-02	3.72E-02
		Aldh1l2	0.261	0.214	1.25E-01	1.13E-01
		Aldh2	-0.126	-0.074	6.72E-01	7.09E-01
		Aldh3a1	-0.014	-0.040	9.75E-01	8.26E-01
		Aldh3a2	0.170	0.078	5.76E-01	7.17E-01
		Aldh3b1	0.201	0.087	3.49E-01	6.04E-01

		Aldh3b2	0.105	-0.033	8.11E-01	9.08E-01
		Aldh3b3	0.072	-0.177	8.84E-01	4.18E-01
		Aldh4a1	0.032	-0.438	9.85E-01	4.15E-01
		Aldh5a1	-0.332	-0.181	2.60E-01	4.30E-01
		Aldh6a1	-0.099	0.018	6.43E-01	9.14E-01
		Aldh7a1	0.129	0.226	6.40E-01	1.62E-01
		Aldh8a1				
		Aldh9a1	-0.100	0.080	7.16E-01	6.45E-01
	Carboxylesterases	Ces1b				
		Ces1c	0.024	0.214	9.85E-01	6.23E-01
		Ces1d	0.417	0.185	4.11E-01	6.33E-01
		Ces1e	0.109	-0.005	8.95E-01	9.93E-01
		Ces1f	-0.517	-0.617	1.11E-01	1.93E-02
		Ces1g	0.003	0.032	9.99E-01	9.61E-01
		Ces2a	**2.486**	**0.568**	**1.00E-07**	**8.57E-02**
		Ces2b	0.556	0.450	9.94E-03	1.93E-02
		Ces2c	0.505	0.414	4.32E-02	4.92E-02
		Ces2e	0.188	0.209	5.00E-01	2.53E-01
		Ces2f	**1.215**	**0.163**	**1.15E-05**	**4.97E-01**
		Ces2g	0.076	-0.244	8.86E-01	2.84E-01
		Ces3a	0.627	0.778	3.32E-01	8.71E-02
		Ces3b				
		Ces4a				
Phase II	Glutathione S-transferases	**Gsta2**	**1.847**	**0.204**	**7.54E-04**	**7.17E-01**
		Gsta3	0.487	-0.003	3.43E-01	9.96E-01
		Gsta4	**0.980**	**0.032**	**2.04E-02**	**9.52E-01**
		Gstcd	-0.172	-0.132	6.91E-01	6.31E-01
		Gstk1	0.533	0.159	9.74E-02	5.83E-01
		Gstm1	**0.801**	**-0.145**	**2.83E-03**	**5.86E-01**
		Gstm2	0.562	0.058	2.47E-02	8.33E-01
		Gstm3	2.040	-0.116	1.44E-05	8.07E-01

		Gstm4	**0.720**	**-0.165**	**7.44E-03**	**5.19E-01**
		Gstm5	-0.086	-0.171	8.33E-01	3.94E-01
		Gstm6	**0.983**	**-0.099**	**7.60E-05**	**6.82E-01**
		Gstm7	-0.198	-0.286	5.19E-01	1.45E-01
		Gsto1	0.085	0.185	7.34E-01	1.72E-01
		Gsto2	0.208	0.229	3.13E-01	1.20E-01
		Gstp1	-0.081	0.011	7.38E-01	9.55E-01
		Gstp2	-0.042	-0.016	8.77E-01	9.23E-01
		Gstt1	0.028	0.225	9.51E-01	1.52E-01
		Gstt2	-0.139	-0.042	5.38E-01	8.13E-01
		Gstt3	0.127	-0.001	5.37E-01	9.97E-01
		Gstz1	-0.165	-0.081	4.06E-01	5.90E-01
	Sulfotransferases	Sult1a1	0.120	0.430	8.62E-01	1.62E-01
		Sult1b1	0.100	0.122	7.25E-01	4.59E-01
		Sult1c1	-0.028	-0.037	9.62E-01	8.93E-01
		Sult1c2	0.244	0.157	6.18E-01	6.34E-01
		Sult1d1	**0.830**	**0.207**	**4.31E-04**	**3.28E-01**
		Sult1e1				
		Sult2a7				
		Sult2a8	-0.178	-0.074	5.18E-01	7.22E-01
		Sult2b1	-0.067	-0.012	8.50E-01	9.59E-01
		Sult4a1	-0.026	-0.023	9.69E-01	9.45E-01
		Sult5a1	0.142	0.472	6.68E-01	1.54E-02
	UDP glycosyltransferases	Ugt1a10	0.053	0.030	9.25E-01	9.17E-01
		Ugt1a6a	0.291	0.161	3.04E-01	4.57E-01
		Ugt1a6b	**0.569**	**0.195**	**7.34E-03**	**3.07E-01**
		Ugt2a1	0.529	0.191	6.53E-02	4.46E-01
		Ugt2a3	**1.571**	**0.073**	**1.70E-03**	**9.02E-01**
		Ugt2b1				
		Ugt2b34	**0.487**	**0.368**	**2.55E-03**	**1.34E-02**
		Ugt2b35	0.142	-0.125	4.55E-01	3.36E-01

		Ugt2b36	0.259	0.366	5.89E-01	2.10E-01
		Ugt2b37	0.331	0.353	2.37E-01	8.86E-02
		Ugt2b38	0.251	0.349	5.82E-01	2.12E-01
		Ugt2b5	0.335	0.419	2.69E-01	5.86E-02
		Ugt3a1				
		Ugt3a2				
Phase III	ATP-binding cassettes	Abca1	0.846	0.489	4.67E-04	2.24E-02
		Abca12	-0.144	0.285	9.10E-01	6.12E-01
		Abca14	0.041	-0.140	9.10E-01	3.30E-01
		Abca17	0.011	0.020	9.85E-01	9.36E-01
		Abca2	-0.046	-0.041	8.92E-01	8.14E-01
		Abca3	0.153	0.191	4.62E-01	1.66E-01
		Abca4	0.278	0.147	4.80E-01	6.10E-01
		Abca5	-0.088	0.103	7.13E-01	4.69E-01
		Abca6				
		Abca7	0.051	-0.359	8.98E-01	2.96E-02
		Abca8a	-0.092	0.142	8.59E-01	5.84E-01
		Abca8b	-0.535	0.503	3.86E-02	2.38E-02
		Abca9	-0.039	0.230	9.41E-01	2.30E-01
		Abcb10	-0.064	-0.158	7.85E-01	1.89E-01
		Abcb11	-0.022	0.041	9.72E-01	8.80E-01
		Abcb1a	1.468	1.057	2.14E-05	9.36E-04
		Abcb1b	1.581	0.953	1.14E-05	2.44E-03
		Abcb4	1.497	1.107	4.13E-05	1.24E-03
		Abcb6	0.001	0.001	9.99E-01	9.96E-01
		Abcb7	-0.123	-0.076	6.93E-01	7.10E-01
		Abcb8	-0.188	-0.186	4.52E-01	2.69E-01
		Abcb9	0.103	0.118	7.09E-01	4.68E-01
		Abcc1	0.084	-0.015	8.71E-01	9.63E-01
		Abcc10	0.069	-0.102	8.68E-01	6.16E-01
		Abcc12				
		Abcc2	**1.351**	**0.701**	**1.70E-03**	**6.40E-02**

		Abcc3	0.373	-0.421	4.43E-01	1.94E-01
		Abcc4	-0.060	0.198	8.84E-01	2.68E-01
		Abcc5	0.274	0.358	3.83E-01	9.57E-02
		Abcc6	0.305	0.453	4.62E-01	9.77E-02
		Abcc8	-0.030	0.074	9.50E-01	6.99E-01
		Abcc9	0.422	0.438	3.15E-01	1.45E-01
		Abcd1	-0.178	-0.293	6.85E-01	2.43E-01
		Abcd2				
		Abcd3	0.125	0.272	6.49E-01	8.72E-02
		Abcd4	-0.053	0.061	8.98E-01	7.62E-01
		Abce1	-0.278	-0.310	4.13E-01	1.77E-01
		Abcf1	0.089	-0.033	7.49E-01	8.65E-01
		Abcf2	-0.146	-0.298	7.08E-01	1.69E-01
		Abcf3	-0.120	-0.094	4.05E-01	3.50E-01
		Abcg1	0.094	0.126	7.36E-01	4.25E-01
		Abcg2	-0.170	-0.399	5.18E-01	1.94E-02
		Abcg3	-0.122	0.210	6.59E-01	1.88E-01
		Abcg4	**0.530**	**0.042**	**2.14E-05**	**7.25E-01**
		Abcg5	**0.520**	**-0.067**	**1.60E-02**	**7.68E-01**
		Abcg8	0.723	0.364	6.56E-02	2.69E-01

Supplementary Table 4: Gene enrichment analyses of downregulated genes upon *Pxr* activation in the liver.

Cluster number	Enrichment score	Adjusted P-value	Ontology		Gene count	Genes
1	1.77	1.80E-03	Lipid metabolic process	Goterm_BP_direct	12	acetyl-Coenzyme A acyltransferase 1B (Acaa1b); acyl-CoA thioesterase 1 (Acot1); acyl-Co A thioesterase 3 (Acot3); carnitine O-octanoyl transferase (); peroxisome proliferator activated receptor alpha (Ppara); similar to DNA-directed RNA polymerase II 7.6k Da polypeptide (RPB10)(RPB7.6)(RPABC5); hypothetical protein LOC100044218; predicted gene 13015; polymerase (RNA) II (DNA); directed polypeptide L (); cytochrome P450 family 4 subfamily a polypeptide 31 (Cyp4a31); cytochrome P450 family 4 subfamily a polypeptide 32 (Cyp4a32); predicted gene 1077;cytochrome P450 family 4 subfamily a polypeptide 10 (Cyp4a10)
		5.20E-02	Lipid metabolism	Up_keywords	8	
2	1.5	1.90E-02	Biological rhythms	Up_keywords	5	D site albumin promoter binding protein (Dbp); hepatic leukemia factor (Hlf); CCR4 carbon catabolite repression 4-like (CCrn4l); thyrotroph embryonic factor (Tef)
		2.30E-02	Rhythmic process	Goterm_BP_direct	5	
3	1.44	8.30E-03	TGF-beta signaling pathway	Kegg_pathway	5	MAD homolog 7 (); MAD homolog 9 (); follistatin (Fst); inhibin beta E (Inhbe); inhibin beta-C (Inhbc)
4	1.35	2.60E-03	Glucose metabolic process	Goterm_BP_direct	5	peroxisome proliferator activated receptor alpha (Ppara); cytosolic phosphoenolpyruvate carboxykinase 1 (Pck1); phosphoglucomutase 2-like 1; phosphorylase kinase alpha 2 (Phka2); lactate dehydrogenase A (Ldha)
5	1.29	1.10E-02	Cytochrome P450	Interpro	5	cytochrome P450 family 4 subfamily a polypeptide 31 (Cyp4a31); cytochrome P450 family 4 subfamily a polypeptide 32 (Cyp4a32); ;cytochrome P450 family 4 subfamily a polypeptide 10 (Cyp4a10); cytochrome P450 family 2 subfamily u polypeptide 1 (Cyp2u1); cytochrome P450 family 26 subfamily b polypeptide 1 (Cyp26b1); cytochrome P450 family 4 subfamily b polypeptide 1 (Cyp4b1)
		2.20E-02	Monooxygenase	Up_keywords	5	

Chapter 3.3

Pregnane X receptor is a major sexually dimorphic hepatic sensor of the gut microbiota that controls the host xenobiotic metabolism in male mice

Context: Xenobiotics act as ligands for PXR which plays a central role in the transcriptional control of genes encoding rate-limiting enzymes in detoxication. Several groups have also recently reported that microbial metabolites can act as ligands for this nuclear receptor. These recent findings led us to investigate whether the gut microbiota may influence the hepatic functions that we previously identified as PXR-dependent and whether PXR may influence the composition of gut microbiota. This body of work which aims at establishing the importance of the bi-directional interaction of PXR and gut microbiota is subject to a publication in preparation.

Pregnane X receptor is a sexually dimorphic hepatic sensor of gut microbiota that controls the host xenobiotic metabolism

Barretto S, Lasserre F *et al.*

INTRODUCTION

The liver is the heaviest organ in the human body with a wide array of functions that can be divided into immunological activity, intermediary metabolism (including a central role in carbohydrate, lipid and nitrogen metabolism), secretion of bile, synthesis of various serum proteins, degradation of hormones, and detoxification of xenobiotics. The hepatic portal vein transports nutrients and xenobiotics present in food from the gastrointestinal tract to the liver and ensures that these are processed in the liver before they reach the rest of the organism. The liver therefore stands at the crossroad between the portal blood flow coming from the intestine and the rest of the organism. In the liver, transcription factors from the nuclear receptor superfamily can sense fluctuating levels of nutrients and xenobiotics and promptly adapt hepatic metabolism by modulating the transcription of genes. Among these, 2 nuclear receptors, the pregnane X receptor (PXR) and the constitutive androstane receptor (CAR), and one ligand-activated transcription factor from the helix-loop-helix Per-Arnt-Sim family, the aryl hydrocarbon receptor (AhR), are commonly described as xenobiotic sensors. They are known to regulate the expression of phase 1 xenobiotic metabolizing enzymes (XMEs) from the cytochrome p450 family (CYPs), thereby facilitating the elimination of xenobiotics. Although the list of their target genes overlaps, it is usually described that AhR regulates the expression of CYP1, while CAR and PXR regulate the expression of CYP2 and CYP3. Recently, several new natural

AhR ligands have been discovered, including kynurenine and planar indoles resulting from the microbial metabolism of dietary tryptophan (reviewed in [1]). Microbial ligand-driven activation of AhR is thought to limit intestinal inflammation and intestinal permeability and may be dysfunctional in inflammatory bowel disease (IBD) [2] and in metabolic diseases [3]. These studies have raised the awareness that factors involved in xenobiotic metabolism could be intimate partners with the gut microbiota.

The nuclear receptor PXR (systematic name NR1I2) is highly expressed in the liver and intestine of mammals [4] and was characterized as a xenosensor [5]. Regulation of XMEs by PXR is of high clinical and toxicological relevance since its first described target gene was CYP3A4 in humans [6], which represents 10% of all clinically relevant drug-metabolizing CYPs in the human liver and up to 75-85% in the intestine [7] and is responsible for the metabolization of 60% of marketed drugs [8]. Beside its role as a master regulator of xenobiotic metabolism, recent studies have also unveiled roles of PXR in intermediary metabolism such as control of hepatic glucose [9-11] and lipid metabolism [9,12,13]. Moreover, we have recently reported that PXR might also be involved in the control of hepatokine secretion [14].

Because of an unusually large and flexible binding pocket, PXR can be activated by a variety of structurally diverse chemicals including pharmaceutical drugs, dietary supplements, herbal medicines, and environmental pollutants [15]. In the intestine, indole-3-propionic acid (IPA), a bacterial metabolite produced from tryptophan, was recently shown to activate PXR, thereby impacting the intestinal permeability of the host [16]. In the liver, others, and we, have observed that PXR activity was strongly decreased in germ-free

(GF) male mice compared to specific-pathogen-free (SPF) animals [17-19]. Therefore, PXR has emerged as a potential sensor of gut microbiota signals.

Here, we aimed to gain insights into the bidirectional relationships between PXR and the gut microbiota. Our results show that PXR is a broad sensor of gut microbial signals in the liver and the small intestine, but not in the colon. Focusing on the liver, we demonstrate that, in male mice, the lack of PXR reduces transcriptional regulations upon microbiota depletion. PXR-dependent regulations of microbial signals were mostly involved in controlling xenobiotic metabolism, and to a lower extent fatty acid metabolism in male mice. Conversely, PXR was involved in shaping the gut microbiota. Interestingly, this PXR-mediated gut-liver dialogue was strongly sexually dimorphic. Altogether our results identify PXR as a central hepatic sensor of gut microbial signals that controls the host's hepatic xenobiotic capacities in a sexually dimorphic way.

MATERIALS AND METHODS

In vivo studies

In vivo studies were performed in accordance with European guidelines for the use and care of laboratory animals, and were approved by an independent Ethics Committee. All mice were housed at the Toxalim-INRA rodent facility (Toulouse, France). The room where the mice were housed was kept at a temperature of 21-23°C on a 12-hour light (ZT0-ZT12) 12-hour dark (ZT12-ZT24) cycle and mice were allowed free access to the diet (Teklad Global 18% Protein Rodent Diet) and tap water. ZT stands for Zeitgeber time; ZT0 is defined as the time when the lights are turned on and ZT12 as the time when lights are turned off.

In the first set of experiments, forty-six-week old C57BL/6J male mice were purchased from Charles River, kept for two weeks of acclimatization and then randomly allocated to the different experimental groups: control (CONT, n=8), ampicillin-treated (A, n=8), neomycin-treated (N, n=8), vancomycin-treated (V, n=8), wild-type ANV cocktail-treated (ANV, n=8). The individual antibiotics [1g/L ampicillin (Euromedex, Souffelweyersheim, France), 1 g/L neomycin (Sigma Aldrich, Steinheim, Germany), 0.5 g/L vancomycin (MP Biomedicals, Illkirch, France)] or a combination of these 3 antibiotics were dissolved in tap water and were provided in the animal bottles. Supplementary Table 1 gives an overview of the antibiotics used. The antibiotic solutions were prepared fresh every 3 days. After 2 weeks of antibiotic treatment, mice were sacrificed at ZT6.

In the second set of experiments, twelve six-week-old wild-type (WT) C57BL/ 6J male mice were purchased from Charles River and 12 *Pxr*$^{-/-}$ mice were used in this experiment. The *Pxr*$^{-/-}$ mice were backcrossed on the C57Bl/ 6J background and were engineered in Pr. Meyer's laboratory [20] and were bred for 10 years in our animal facility. Mice were acclimatized for two weeks, then randomly allocated to the different experimental groups: wild-type control (WT CONT n=6), wild-type PCN-treated (WT PCN, n=6), *Pxr*$^{-/-}$ control (*Pxr*$^{-/-}$ CONT, n=6), *Pxr*$^{-/-}$ PCN-treated (*Pxr*$^{-/-}$ PCN, n=6). Mice were treated for 2 weeks with antibiotics (ANV cocktail) in their drinking water or with water only as previously described. The last 4 days, PCN-treated mice received a daily intraperitoneal injection of PCN (100 mg/ kg) in corn oil while control mice received corn oil only. Mice were sacrificed at ZT6, 6 hours after the last PCN injection.

In the last set of experiments, thirty-four six-week old *Pxr*$^{+/+}$ (18 males, 16 females) and 36 *Pxr*$^{-/-}$ (16 males, 20 females) littermate mice were derived from *Pxr*$^{+/-}$ dams and

bred at Toxalim-INRA's rodent facility. At 6 weeks, mice were randomly allocated to the different experimental groups in males: *Pxr*$^{+/+}$ control (*Pxr*$^{+/+}$ CONT, n=10), *Pxr*$^{+/+}$ ATB-treated (*Pxr*$^{+/+}$ ATB, n=8), *Pxr*$^{-/-}$ control (*Pxr*$^{-/-}$ CONT, n=8), *Pxr*$^{-/-}$ ATB-treated (*Pxr*$^{-/-}$ ATB, n=8); and in females: *Pxr*$^{+/+}$ control (*Pxr*$^{+/+}$ CONT, n=8), *Pxr*$^{+/+}$ ATB-treated (*Pxr*$^{+/+}$ ATB, n=8), *Pxr*$^{-/-}$ control (*Pxr*$^{-/-}$ CONT, n=10), *Pxr*$^{-/-}$ ATB-treated males (*Pxr*$^{-/-}$ ATB, n=10). Mice were kept in cages of 5-6 animals. After 2 weeks of antibiotic treatment, mice were sacrificed at ZT6.

Bacterial Cultivation of Feces

Feces were collected at the beginning and after 14 days of experiment under sterile conditions. Fecal samples from antibiotic-treated mice were diluted at 10^{-3}, 10^{-4}, and 10^{-5} then cultured on Schaedler C blood medium anaerobically. Untreated mice samples were diluted at 10^{-5}, 10^{-6}, and 10^{-7} before being spread on the same culture media. Colonies forming unit were counted after 24 h of incubation in an anaerobic jar at 37°C.

Blood and tissue sampling

Body weight was monitored at the beginning and at the end of each experimental period. Blood was collected at the submandibular vein into lithium heparin-coated tubes (BD Microtainer, Franklin Lake, NJ, USA). Plasma was prepared by centrifugation (1500 g, 15 min, 4°C) and stored at -80°C. Following euthanasia by cervical dislocation, liver, ileum, and colon were removed, weighed, dissected, and snap-frozen in liquid nitrogen and stored at -80°C until used for RNA extraction.

Plasma Analysis

Alanine transaminase (ALT), high- or low-density lipoprotein (HDL-LDL), total cholesterol, triglycerides and free fatty acids (FFA) were determined using a Pentra 400 biochemical analyzer (Anexplo facility, Toulouse, France).

Liver neutral lipids

Hepatic samples were homogenized in 2:1 (v/v) methanol/ethylene glycol-bis(B-aminoethyl ether)-N,N,N′, N′-tetraacetic acid (EGTA; 5mM), lipids corresponding to an equivalent of 2 mg of tissue were extracted (Bligh and Dryer,1959) in chloroform : methanol : water (2.5:2.5:2.1,v/v/v) in the presence of internal standards glyceryl trinonadecanoate, stigmasterol, and cholesteryl heptadecanoate (Sigma). TGs, free cholesterol, and cholesterol esters were analyzed by gas chromatography on a Focus Thermo Electron system using a Zebron-1 Phenomenex (Phenomenex Zebron-1, England) fused-silica capillary column [5 m; 0:32 mm internal diameter (i.d.); 0:50 lm film thickness]. The oven temperature was programmed from 200 to 350°C at a rate of 5 C=min, and the carrier gas was hydrogen (0.5 bar). The injector and detector were at 315°C and 345°C, respectively.

Liver Fatty Acid Analysis

To measure all hepatic fatty acid methyl ester (FAME) molecular species, lipids that corresponded to an equivalent of 1 mg of liver were extracted in the presence of the internal standard glyceryl tri- heptadecanoate (2 μg). The lipid extract was transmethylated with 1 mL boron trifluoride (BF3) in methanol (14% solution; Sigma) and 1 mL heptane for 60 min at 80°C and evaporated to dryness. The FAMEs were extracted with heptane/water

(2:1). The organic phase was evaporated to dryness and dissolved in 50 lL ethyl acetate. A sample (1 μL) of total FAME was analyzed with gas–liquid chromatography [Clarus 600 system (PerkinElmer), with FAMEWAX fused silica capillary columns (Restek), 30 m × 0:32 mm i.d., 0:25 lm film thickness]. Oven temperature was programmed to increase from 110°C to 220°C at a rate of 2 C=min, and the carrier gas was hydrogen [7.25 pounds per square inch (psi)]. Injector and detector temperatures were 225°C and 245°C, respectively.

Gene expression

Total RNA was extracted with with TRI Reagent® (Molecular Research Center, Cincinnati, Ohio, USA). RNAs were quantified using nanodrop (NanoDropTM 1000; Thermo Scientific). Two micrograms of total RNA were reverse transcribed using the High-Capacity cDNA Reverse Transcription Kit (Applied BiosystemsTM). The SYBR Green (Applied Biosystems, California) assay primers are presented in supplementary table 1. Amplification was performed using an ABI Prism 7300 Real-Time PCR System (Applied Biosystems™). Quantitative real-time polymerase chain reaction (qPCR) data were normalized to TATA-box-binding protein mRNA levels and analyzed with LinRegPCR (version 2015.3; Jan Ruijter) to get mean efficiency (NO), which is calculated as follows: NO = threshold=ðEff mean^{Cq} Þ with Eff mean: mean PCR efficiency and CQ: quantification cycle. Primers used are described in Supplementary Table 2.

Microarrays

Total RNA was extracted with TRIzol reagent (Invitrogen, Carlsbad, CA, USA). Gene expression profiles were obtained at the GeT-TRiX facility (GénoToul, Génopole Toulouse Midi-Pyrénées, France) using Sureprint G3 Mouse GE v2 microarrays (8 x 60 K; design;

074,809; Agilent Technologies, Santa Clara, CA, USA) following the manufacturer's instructions. Microarray data and experimental details are available in NCBI's Gene Expression Omnibus (Edgar, Domrachev, & Lash, 2002) and will be made accessible through GEO Series. Microarray data were processed using R (http://www.r-project.org) and Bioconductor packages (www.bioconductor.org, v3.0). Raw data (median signal intensity) were filtered, log2 transformed, corrected for batch effects (microarray washing bath), and normalized using CrossNorm method [21]. The linear model was fitted using the limma lmFit function [22]. Pair-wise comparisons between biological conditions were applied using specific contrasts. A correction for multiple testing was applied using the Benjamini–Hochberg procedure for false discovery rate (FDR). Probes with FDR ≤ 0.05 and |fold-change| > 1.5 were considered to be differentially expressed between conditions. Gene-annotation enrichment analysis and functional annotation clustering were evaluated using DAVID [23].

Testosterone hydroxylation assay

Chemicals

Acetic acid, ethanol, sodium chloride, potassium dihydrogen phosphate, dibasic potassium phosphate, monobasic sodium phosphate, dibasic heptahydrate sodium phosphate, potassium sodium tartrate tetrahydrate, glycerol, Folin & Ciocalteu's phenol reagent, albumin from bovine serum, anhydrous sodium carbonate, NADP, D-glucose 6-phosphate sodium salt, glucose-6-phosphate dehydrogenase, magnesium chloride, 1-chloro-2,4-dinitrobenzene, reduced L-glutathione and testosterone were purchased from Sigma-Aldrich Merck (Saint Quentin Fallavier, France). Acetonitrile and methanol (HPLC grade) were purchased from Thermo Fisher Scientific (Waltham, MA, USA). Ammonium

acetate, sodium hydroxide and copper sulfate were purchased from VWR (Fontenay-sous-Bois, France). Flo-Scint™ II and Ultima Gold™ liquid scintillation cocktails were purchased from PerkinElmer (Courtabœuf, France). Ultrapure water produced by a Milli-Q system (Millipore, Saint-Quentin-en-Yvelines, France) was used for the preparation of HPLC mobile phases.

[^{14}C]-testosterone (specific activity: 2.18 GBq/mmol) was purchased from PerkinElmer and its radiopurity was 98.8 %, as determined by radio-HPLC. Standards of testosterone metabolites were purchased from Steraloids (Newport, RI, USA): 15β-hydroxytestosterone, 6α-hydroxytestosterone, 6β-hydroxytestosterone, 19-hydroxytestostérone, 15α-hydroxytestosterone, 11α-hydroxytestosterone, 6β-hydroxyandrostenedione, 11α-hydroxyandrostenedione, 16β-hydroxytestosterone, 4-androsten-16α-ol-3,17-dione, 2α-hydroxytestosterone, 2α-hydroxyandrostenedione, 4,6-androstadien-17β-ol-3-one, 7α-hydroxytestosterone and from Sigma-Aldrich: dihydroandrosterone, androstanolone, 16α-hydroxytestosterone, 11β-hydroxytestosterone, 2β-hydroxytestosterone, 11β-hydroxyandrost-4-ene-3,17-dione, 1-dehydrotestosterone, androstenedione, epitestosterone, androsterone, estradiol and estrone.

Sub-cellular fraction preparation and protein content

Following mice euthanasia, livers were collected, immediately perfused using NaCl 0.9 %. They were weighed and frozen in liquid nitrogen until sub-cellular fraction preparation, which was carried out within a month. Livers were thawed and homogenized at 4°C using a Potter-Elvehjem Teflon glass homogenizer in 4 volumes/g of ice-cold

sodium/phosphate buffer 0.1 M pH 7.4. Microsomal and cytosolic hepatic fractions were obtained after two centrifugation steps at 4°C (20 min at 9 000 *g* and 70 min at 105 000 *g*) using a Beckman Optima XPN-80 ultracentrifuge (Villepinte, France). Microsomes were resuspended with gentle homogenization in 1 mL/g of ice-cold sodium/phosphate buffer 0.1 M pH 7.4 with 20 % glycerol (v/v). Sub-cellular fractions were stored at 80°C in cryotubes until use. The protein content of sub-cellular fractions was determined using the Lowry et al. (1951) method {Lowry:vb}, which was adapted for microplate reading, using a Tecan Infinite 200 (Männedorf, Switzerland).

[^{14}C]-testosterone incubations

Mice hepatic microsomes (0.5 mg proteins/mL) were incubated at 37°C under shaking with 10 µM [^{14}C]-testosterone (3.58 kBq per incubation in 5 µL ethanol) fortified with unlabelled testosterone. Incubations were performed in a final volume of 0.5 mL in 0.1 M sodium/phosphate buffer pH 7.4 with 5 mM $MgCl_2$. Incubations were initiated using a NADPH generating system: 1.3 mM NADP, 5 mM glucose-6-phosphate, 1 IU glucose-6-phosphate dehydrogenase. The kinetic of testosterone metabolites formation was established between 10 min and 60 min. An incubation time of 20 min was selected in order to ensure a linear formation of testosterone metabolites. Incubations were stopped with 1.5 mL methanol, kept 30 min on ice and centrifuged 10 min at 6 500 *g*, 4°C (3MK Sigma centrifuges, Newtown Wem Shropshire, UK). Radioactivity measurements (10 µL) were performed before storage at -20°C, pending further radio-HPLC analysis. Radioactivity measurements were carried out using a Tri-Carb 2910TR (PerkinElmer) liquid scintillation analyzer, using Ultima Gold™ as the scintillation cocktail (PerkinElmer).

Sample quenching was compensated by the use of quench curves and external standardization.

For the LC-MS confirmation of major testosterone's metabolites structure, additional incubations were carried out using unlabeled testosterone (50 µM) and pooled microsomes (1 mg proteins/mL, pool of 10 PXR control mice) during 30 min, in the same conditions.

Radio-HPLC profiling and quantification

Incubation media were individually analyzed by radio-HPLC for testosterone metabolites profiling and quantification. Reversed-phase high-performance liquid chromatography (R-HPLC) analysis were performed on an Ultimate-3000 system (Thermo Fisher Scientific) coupled with a flow scintillation analyzer Flo-One Radiomatic™ 610TR (PerkinElmer). The HPLC system consisted of Nucleoshell RP18 column (250 x 4.6 mm, 5 µm, Macherey-Nagel, Hoerdt, France) coupled to a C18 guard precolumn (Nucleoshell RP18 5 µm EC 4/3, Macherey-Nagel), maintained at 35°C. Mobile phases were A: ammonium acetate buffer (20 mM, adjusted to pH 3.5 with acetic acid) and B: acetonitrile. The flow rate was 1 mL/min and the injection volume was 500 µL. The gradient was as follow: 0-35 min A:B from 80:20 to 60:40 (v/v); 35-45 min from 60:40 to 40:60; 45-48 min from 40:60 to 100 % B. The system returned to the initial condition at 51 min and held for another 4 min. Flo-Scint™ II (PerkinElmer) was used as scintillation cocktail, at a flow rate of 2 mL/min, and with a 500-µL detection cell. Each incubation media (800 µL, corresponding to *ca.* 1.5 kBq) was evaporated to dryness and reconstituted in mobile phase A:B 80:20 (v/v) prior to HPLC injection.

In this system, the retention time (RT) of testosterone was 29.8 min. R-HPLC profiles were processed with the A500 software (PerkinElmer) using a background suppression of 20 cpm (counts per minute) and an efficiency correction (80 % for [^{14}C]). Metabolites were quantified by integrating the area under the peaks monitored by radioactivity detection. All peaks above 4 % of the detected radioactivity were quantified for each animal.

Mass spectrometry analysis

Unlabeled testosterone incubation media were analyzed by LC-MS using the same chromatographic conditions. Testosterone metabolites structure was established based on their mass and on the similarity of their retention time with authentic standards. Media were analyzed by LC-MS using a RSLC3000 HPLC system (Thermo Fisher Scientific) coupled to a HRMS system LTQ Orbitrap XL mass spectrometer (Thermo Fisher Scientific) with a post-column split (0.2 mL/min in the source) using positive electrospray ionization (ESI). The injection volume was 50 µL, the source voltage was 1.80 kV, the capillary voltage was 30V, the capillary temperature was 350°C, the sheath gas (N_2) flow (arbitrary unit) was 50, the auxiliary gas (N_2) flow (arbitrary unit) was 40, the sweep gas (N_2) flow (arbitrary unit) was 0 and the tube lens offset was 115 V.

GSTs activity assay

Glutathione S-transferases (GSTs) specific activities were assessed in cytosolic fractions in 96-well plates. The assay is based on the GST-catalyzed reaction between GSH and the probe substrate CDNB (1-chloro-2,4-dinitrobenzene) which is metabolized by a broad range of GST isozymes. Protein content was between 0.6-1.6 µg proteins per incubation (controls: 0), to allow a linear measurement of the formation of CDNB-GSH.

Incubations were performed in potassium phosphate buffer 0.1 M pH 6.5, using 2.5 mM reduced L-glutathione. The reaction was initiated by the addition of ice-cold CDNB (2.5 µM final). CDNB-GSH formation was measured by the change in absorbance at 340 nm, recorded every min over 10 min, using a Tecan Infinite 200. Mean GSTs specific activities (n=5 mice per group) were expressed in nmol of product formed per min per mg of proteins (nmol/min/mg).

Proton Nuclear Magnetic Resonance (^{1}H-NMR) Based Metabolomics

Liver polar and lipid extracts and caecal content water were prepared for NMR analysis as described previously [24,25]. All ^{1}H-NMR spectra were obtained on a Bruker DRX-600-Avance NMR spectrometer (Bruker) using the AXIOM metabolomics platform (MetaToul) operating at 600:13MHz for ^{1}H resonance frequency using an inverse detection 5-mm ^{1}H-^{13}C-^{15}N cryoprobe attached to a cryoplatform (the preamplifier cooling unit). The ^{1}H-NMR spectra were acquired at 300 K using a standard one-dimensional noesypr1D pulse sequence with water presaturation and a total spin-echo delay (2 ns) of 100 ms. Data were analyzed by applying an exponential window function with a 0.3-Hz line broadening prior to Fourier transformation. The resulting spectra were phased, baseline-corrected, and calibrated to trimethylsilylpropanoic acid (TSP) (0:00 ppm) manually using Mnova NMR (version 9.0; Mestrelab Research S.L.). The spectra were subsequently imported into MatLab (R2014a; MathsWorks, Inc.). All data were analyzed using full-resolution spectra. The region containing the water resonance (4:6– 5:2 ppm) was removed, and the spectra were normalized to the probabilistic quotient [26] and aligned using a previously published function [27].

Data were mean-centered and scaled using the unit variance scaling prior to analysis with orthogonal projection on latent structure-discriminant analysis (O-PLS-DA). The O-PLS derived model was evaluated for goodness of prediction (Q^2Y value) using n-fold cross-validation, where n depends on the sample size. The parameters of the final models are indicated in the figure legends. Metabolite identification and discrimination between the groups were done by calculating the O-PLS-DA correlation coefficients (r^2) for each variable and back-scaled into a spectral domain so that the shapes of the NMR spectra and the signs of the coefficients were preserved [28]. The weights of the variables were color-coded according to the square of the O-PLS-DA correlation coefficients. Correlation coefficients extracted from significant models were filtered so that only significant correlations above the threshold defined by Pearson's critical correlation coefficient ($p < 0:05$; $r > 0.55$; for $n = 6$ per group) were considered significant. For illustration purposes, the area under the curve of several signals of interest was integrated and significance tested with a univariate test.

High-throughput Sequencing of Bacterial content

DNA extraction and sequencing of 16S rRNA gene regions.

The microbial population present in the samples has been determined using next generation high throughput sequencing of variable regions of the 16S rRNA bacterial gene. The workflow was established by Vaiomer (Labège, France) [29]. *Library construction and sequencing***:** The PCR amplification was performed using 16S universal primers targeting the V3-V4 regions of the bacterial 16S ribosomal gene (Vaiomer universal 16S primers). For each sample, a sequencing library was generated by addition of sequencing adapters. The detection of the sequencing fragments was performed with

the MiSeq Illumina technology using the 2 x 300 paired-end MiSeq kit. *Bioinformatics pipeline:* The targeted metagenomic sequences from microbiota were analyzed using the bioinformatics pipeline established by Vaiomer from the FROGS guidelines [30]. Briefly, after demultiplexing of the barcoded Illumina paired reads, single read sequences were cleaned and paired for each sample independently into longer fragments. Operational taxonomic units (OTUs) were produced via single-linkage clustering and taxonomic assignment is performed in order to determine community profiles.

Data Analysis

Reads obtained from the MiSeq sequencing system have been processed using the Vaiomer bioinformatics pipeline. The steps included quality-filtering, clustering into OTUs with the Swarm algorithm and taxonomic affiliation. Alpha diversity was analyzed with different methods (median + interquartile), 1) Observed, 2) Chao1, 3) Shannon, 4) Simpson, and 5) Inverse Simpson. Beta diversity (β-diversity) was measured with numeric values for the "all against all" with Jaccard, Bray-Curtis, Unifrac and Weighted Unifrac. Graphical representations of the relative proportion of taxa were made at each taxonomic level (Phylum, Class, Order, Family, and Genus) for all study samples. "Linear discriminant analysis Effect Size" (LEfSe) [31] was the algorithm used to identify taxonomic groups characterizing the differences between two or more biological conditions. LEfSe was run using default values (alpha value of 0.5 for both the factorial Kruskal-Wallis test among classes and the pairwise Wilcoxon-Mann-Whitney test between subclasses, threshold of 2.0 for the logarithmic LDA score for discriminative features) and the strategy for multi-class analysis set to 'all-against-all'. The LEfSe analysis was performed on the complete

sequence data (no OTU abundance threshold) for identifying genotype effect on either males or females and sex effect on either *Pxr*$^{+/+}$ or *Pxr*$^{-/-}$ mice.

Statistical Analysis

Statistical analyses were performed using GraphPad Prism for Mac OS X (version 7.00; GraphPad Software). One-way or two-way analysis of variance (ANOVA) was performed, followed by appropriate posthoc tests (Bonferroni) when differences were found statistically significant. When only two groups were compared, the Wilcoxon-Mann Whitney test was used; $p < 0:05$ was considered significant.

RESULTS

PXR is a broad sensor of the gut microbiota in the liver and small intestine

We first treated C57Bl6/J male mice with several individual antibiotics (ampicilin, neomycin and vancomycin) or a combination of these (ANV cocktail) for 2 weeks and monitored *Pxr* and its prototypical target genes mRNA expression in the liver, small and large intestine (Figure 1). To avoid a direct effect of the drugs on PXR activity in the liver, we tested antibiotics that are described as poorly absorbed (Supplementary Table 1). We confirm that none of the antibiotic treatments affected *Pxr* expression, whereas its activity, as assessed by the expression of its target genes, was significantly decreased. In the liver, ampicilin, vancomycin and the ANV cocktail significantly decreased *Cyp3a11* and *Cyp2c55* expression. Neomycin alone failed to decrease hepatic PXR activity, but this treatment did not significantly increased caecum weight either, suggesting a limited impact on the gut microbiota (Supplementary figure 1). In the ileum, all treatments almost

completely abolished *Cyp3a11*, *Cyp2c55*, *Cyp3a41a* and *Cyp3a44* expression. Interestingly, in the colon, CYP expression was not significantly affected by any antibiotic treatment, demonstrating that PXR is not responsive to gut microbiota-derived signals in this intestinal section.

Gut microbiota suppression does not interfere with the pharmacological activation of PXR

Next, we wondered if gut microbiota suppression could interfere with PXR's capacity to bind and respond to its ligands. To test this hypothesis, we used WT and *Pxr*$^{-/-}$ male mice treated with antibiotics (ATB), PCN (the pharmacological agonist of PXR) or a combination of both (Figure 2). As expected, PCN treatment significantly affected liver weight in a PXR-dependent way and ATB treatment increased caecum weight (**Figure 2A**). Plasma alanine amino-transferase and cholesterol levels were significantly changed upon PCN treatment, to a similar extent in the PCN and PCN+ATB groups (**Figure 2B**). In the liver, PCN treatment increased triglyceride and cholesterol ester accumulation in a PXR-dependent manner both in the PCN and PCN+ATB groups (**Figure 2C**). O-PLS-DA modeling of the ^{1}H-NMR metabolic profiling of the hepatic lipidic extracts of WT mice shows a significant discrimination between the control and PCN groups *vs*. ATB and ATB+PCN groups (**Figure 2D**). PCA modeling of the aqueous extracts shows a significant discrimination between the PCN-treated groups and the control groups, independently of the ATB treatment (**Figure 2E**). As expected, in *Pxr*$^{-/-}$ mice, these PCN-dependant effects were not observed (**Supplementary Figure 3**). Finally, induction of *Cyp3a11* and *Cyp2c55* was similar in the PCN and PCN+ATB groups in the liver (**Figure 2F**) or ileum (**Figure 2G**).

Altogether these results show that gut microbiota depletion does not prevent or decrease the extent of PXR activation upon pharmacological activation.

Gut microbiota is altered in *Pxr*$^{-/-}$ mice

To determine whether PXR conversely affected the gut microbiota, we used *Pxr*$^{+/+}$ *vs*. *Pxr*$^{-/-}$ littermate mice and compared their caecal microbiota using 16S rRNA sequencing (**Figure 3**). No differences were observed regarding biodiversity in males or in females (**Figure 3A & B**). Hierarchical clustering and Principal Coordinate Analysis (PcoA) at the OTU level demonstrated significant clustering of *Pxr*$^{+/+}$ *vs*. *Pxr*$^{-/-}$ mice (**Figure 3C-F**). This clustering seems stronger in male mice since discrimination was seen on the first PCoA axis that represents 20.8% of the variance (**Figure 3D**) than in females, for which discrimination between Pxr+/+ and Pxr-/- mice was seen on the second PCoA axis that represents 12.5% of the variance (**Figure 3F**). Using the linear discriminant analysis (LDA) effect size (LEfSe) pipeline, we confirmed significant differences in the baseline caecal microbiota composition of *Pxr*$^{-/-}$ mice, as compared to that in *Pxr*$^{+/+}$ mice (Figure 3G&H). *Pxr*$^{-/-}$ male mice had a decreased relative abundance of *Acetitafactor*, (*Eubacterieum*) *ruminantium* group, *Papillibacter*, *Variovax* and increased relative abundance of *Blautia*, *Bradyrhizobium*, *Intestinomonas,* l*achnoclostridium*, *Ruminococcaceae UCG-010* compared to *Pxr*$^{+/+}$ mice (**Figure 3G, Supplementary Figure 4A**). *Pxr*$^{-/-}$ females had a decreased relative abundance of *Desulfovibrio* and increased relative abundance of *Akkermansia* and *Mucispirillum* compared to *Pxr*$^{+/+}$ mice (**Figure 3H, Supplementary Figure 4B**).

We next investigated the metabolic profiles of caecal content in *Pxr*$^{+/+}$ *vs*. *Pxr*$^{-/-}$ mice using ^{1}H-NMR profiling (**Figure 4**). A typical ^{1}H-NMR metabolic profile of caecal content

can be found in Supplementary Figure 2. O-PLS-DA coefficient plots highlighted several peaks that were increased in *Pxr*$^{-/-}$ compared to *Pxr*$^{+/+}$ males (**Figure 4A**): one triplet at 7.006 ppm and two doublets at 6.9 and 6.87 ppm respectively. O-PLS-DA models between caecal content profiles of *Pxr*$^{+/+}$ *vs*. *Pxr*$^{-/-}$ females did not highlight any significant differences between the 2 groups (**Figure 4B**). Integration of the area under the curve for the peaks at 7.006 ppm followed by univariate statistics confirmed a significant increase of this metabolite in *Pxr*$^{-/-}$ male mice (**Figure 4C**). Searches in the literature and in metabolomics databases did not allow us to unravel a relevant candidate for the formal identification of this metabolite. However, based on the structural information we had (summarized in **Supplementary Figure 6A & B**), we hypothesized that this metabolite originated from the gut microbiota metabolism of one of the aromatic amino acid tyrosine or phenylalanine. We fed male and female mice with tyrosine by gavage and confirmed that all the peaks corresponding to the unknown metabolite were significantly increased upon tyrosine gavage in male mice only (**Supplementary Figure 5E-H**). Moreover, we confirmed that this metabolite completely disappeared from the caecal content of ATB-treated mice (**Supplementary Figure 5C & D**). Therefore, we demonstrated that this metabolite is a gut-microbial derivative of tyrosine metabolism.

Altogether, these data demonstrate that PXR has a role in shaping the gut microbiota in a sexually-dimorphic manner and that this PXR-dependent microbiota might play a role in the metabolism of aromatic amino acids.

Gut microbiota suppression decreases PXR activity in the liver and in the ileum of male mice

To further investigate this potential sexual dimorphism in the gut microbiota-PXR interactions, we depleted the gut microbiota of the *Pxr*$^{+/+}$ *vs*. *Pxr*$^{-/-}$ male and female littermate mice with antibiotics. Supplementary Figure 4 confirms the successful depletion of the gut microbiota. In these littermate mice, we confirmed a significant decrease in PXR activity upon microbiota depletion in male liver (**Figure 5A**) and small intestine (**Figure 5C**). However, surprisingly, in both the liver (**Figure 5B**) and the ileum (**Figure 5D**), gut microbiota suppression did not impact PXR activity in females.

PXR is a major hepatic sensor of the gut microbiota

Our results suggest that the PXR-gut microbiota interaction is strongly sexually dimorphic and that it affects the liver physiology of the host. To further characterize the impact of gut microbiota sensing by PXR on the host's hepatic physiology, we obtained transcriptomic profiles of the liver of *Pxr*$^{+/+}$ *vs*. *Pxr*$^{-/-}$ littermates treated or not with ATB. Using a fold-change cut-off of 1.2 and a corrected p-value < 0.05, we observed that gut microbiota depletion using ATB significantly affected the expression of 679 genes in *Pxr*$^{+/+}$ vs. 109 in *Pxr*$^{-/-}$ male mice (**Supplementary Figure 7C**). Using a more stringent fold-change cut-off of 1.5, the same proportion holds with 144 genes affected by ATB in *Pxr*$^{+/+}$ vs. 44 in *Pxr*$^{-/-}$ male mice (**Supplementary Figure 7A**). Fifty-seven genes were up-regulated (FC>1.5) upon ATB treatment in *Pxr*$^{+/+}$ males only, for which pathway enrichment analyses highlighted one significantly enriched gene cluster for genes involved in sterol biosynthesis and lipid metabolism (**Figure 6A & C**). Forty-five genes were down regulated (FC>1.5) upon ATB treatment in *Pxr*$^{+/+}$ males only, which clustered in 3 significantly

enriched biological pathways: peroxisome, acyl-CoA thioesterases, and CYPs (**Figure 6B & D**). PCA plots confirmed these results by illustrating a significant discrimination between the ATB and control groups in *Pxr*$^{+/+}$ male mice (Figure 6E) but not in *Pxr*$^{-/-}$ male mice (**Figure 6G**). The volcano plots highlight the genes that were the most significantly impacted upon ATB treatment (**Figure 4F & H**), among which many PXR-target genes involved in xenobiotic metabolism such as *Cyp3a11*, *Cyp3a16*, *Cyp3a41a* and *Cyp3a59*, but also several genes involved in lipid metabolism such as *Acot5* and *Vnn1*.

The much lower number of genes affected by ATB treatment in *Pxr*$^{-/-}$ compared to *Pxr*$^{+/+}$ male mice suggests that PXR is one of the major sensors of gut microbiota signals in the liver. We took advantage of one of our previously published datasets in which the hepatic transcriptome of *Pxr*$^{-/-}$ male mice was compared to that of WT, non-littermate, male mice (Barretto *et al*., 2019) to quantify the impact on PXR deletion in non-littermate *vs*. littermate mice. In mice in which the gut microbiota is tightly controlled (littermates), PXR deletion induced 4 to 5 times less changes in the hepatic transcriptome than in mice in which the gut microbiota strongly differs (non-littermates) (**Supplementary Figure 8**), thus confirming a major role for hepatic PXR in gut microbiota sensing.

In females, ATB treatment significantly impacted the expression of 449 genes (FC>1.2) in *Pxr*$^{+/+}$ animals vs. 274 in *Pxr*$^{-/-}$ animals. With a more stringent FC>1.5, 90 genes were changed upon ATB in *Pxr*$^{+/+}$ vs. 45 in *Pxr*$^{-/-}$ females (**Supplementary Figure 7B & D**). Pathway enrichment analysis did not unravel any significant PXR-dependent biological pathway affected upon microbiota depletion in females (**Figure 7A & B**).

Classical hepatic PXR-dependent pathways are controlled by the gut microbiota in a sexually dimorphic way

Our results suggested a strong sexually dimorphic impact of the gut microbiota on the liver physiology, in which PXR might play a role. We wondered if this sexual dimorphism was also seen in another model of gut microbiota depletion and analyzed a previously published RNA-seq dataset obtained in the liver of GF *vs* SPF male and female mice [32]. In GF mice, the impact of gut microbiota depletion on the liver transcriptome was highly sexually dimorphic with only 15 to 25% of genes that were significantly regulated in both males and females (**Supplementary Figure 9A & B**). In females, absence of gut microbiota did not impact metabolic pathways but rather biological functions linked to the cell cycle and cellular structures (see pathway-enrichment analyses in **Supplementary Figure 9C & D**). In males, absence of the gut microbiota affected few metabolic pathways mostly involved in sterol synthesis, lipid metabolism and CYP (**Supplementary Figure 9C & D**). In our ATB-treated mice, as expected, the number of hepatic genes affected by the gut microbiota depletion was much lower than in GF mice. However, the same sexual dimorphism held with only 9-11% of genes affected in both males and females (**Supplementary Figure 9E & F**). Moreover, the metabolic pathways affected in males were similar to those seen in GF males (**Supplementary Figure 9G & H**). Interestingly, the same biological pathways are classically disrupted upon PXR activation via different ligands [14].

PXR sensing of the gut microbiota is moderately involved in hepatic fatty acid metabolism in male mice

Our previous data suggest that, at least in male mice, PXR sensing of the gut microbiota might be involved in fatty acid metabolism. We measured neutral lipids and

characterized individual fatty acids in the liver of the *Pxr*$^{+/+}$ *vs* *Pxr*$^{-/-}$ littermate mice. ATB treatment did not change cholesterol or cholesterol ester levels, but slightly decreased triglyceride content in the liver of *Pxr*$^{+/+}$ but not *Pxr*$^{-/-}$ male mice (**Figure 8A**). This was confirmed by a PXR-dependent decrease in the relative content of two of the most abundant hepatic fatty acids (FA) (C16:0 and C16:1w7) upon ATB treatment (**Figure 8B**). Finally, qPCR analyses confirmed that ATB decreased the expression of genes involved in fatty acid-elongation and β-oxidation in the liver of *Pxr*$^{+/+}$ male mice (**Figure 8C**).

In females, ATB treatment did not significantly impact cholesterol, cholesterol esters and triglycerides in *Pxr*$^{+/+}$ mice, but surprisingly decreased triglycerides in *Pxr*$^{-/-}$ mice (**Figure 9A**). Individual FA measurement showed a PXR-dependant decrease in the abundance of C16:1w7 but not C16:0 upon ATB treatment (**Figure 9B**). RT-qPCR analyses did not clearly show a PXR-dependant impact of ATB treatment on FA-related genes (**Figure 9C**).

PXR sensing of the gut microbiota controls the host's hepatic xenobiotic capacities in male mice

Another interesting finding of our microarray data is the strong enrichment of the xenobiotic metabolism-related pathways in the PXR-dependent genes that were down regulated upon ATB treatment (**Figure 6B**). **Figure 10** illustrates the fold-changes in the Phase I (**Figure 10A**) and Phase II (**Figure 10C**) XMEs upon ATB treatment in *Pxr*$^{+/+}$ and *Pxr*$^{-/-}$ male mice. We observed that microbiota depletion moderately affected Phase II XMEs but strongly affected the expression of CYP belonging to the CYP3 family in a PXR-dependent way. This was not the case in females (**Supplementary Figure 10**). In order to test the consequence of the downregulation of these CYPs at a more physiological level,

the oxidative metabolism of [4-^{14}C] testosterone in male liver microsomes was measured as a reflection of the global ability of these enzymes to metabolize sterol compounds (**Figure 10C, Supplementary Figure 11**). This analysis showed that peaks at a retention time of 4.4, 8 and 12.5 min were significantly different between *Pxr*$^{-/-}$ and *Pxr*$^{+/+}$ mice, but were not affected by ATB treatment, while peaks with a retention time at 10.5 and 14.7 min were significantly decreased upon microbiota suppression in a PXR-dependent way. Several structural hypotheses could be made based (1) on RT comparison with authentic testosterone metabolites standards, for those commercially available (LC-MS experiments), and (2) on the confirmation of the m/z ions detected in LC-MS (ESI, positive mode) when analyzing incubation media from incubations carried out with non-radio labeled testosterone (**Supplementary Table 3**). The 10.5 min peak was formally identified as 6β-testosterone. The peak with a RT of 14.7 min was identified as a HO-Δ-testosterone (m/z: 303.1955), but no formal identification of the hydroxylation position could be achieved. Of note, this metabolite was clearly found to be distinct from 16α-HO-Δ-testosterone, for which the authentic standard is available. Finally, glutathione transferase-specific activity was also tested in the hepatic cytosolic fraction and showed a PXR-dependent decrease in this enzymatic activity upon ATB treatment in male mice (**Figure 10D**).

DISCUSSION

In this study, we report that microbiota depletion by various antibiotic procotols decreased PXR activity in the liver and ileum of male mice, but did not seem to impact PXR

activity in the colon. This confirmed several previously published results that evaluated the expression of PXR targets in the liver of GF [17,18,33] or ATB-treated [34] mice. The lack of decrease of PXR activity in the colon upon microbiota depletion seems counterintuitive with the facts that PXR's expression is not significantly different between the liver, the small and the large intestine (data not shown) and that gut microbiota load is higher in the colon than in the ileum. However, many previous studies have shown that the gut microbiota modulates the expression of a much larger set of genes in the small intestine than in the colon in mice [35-37]. Therefore, our observation is consistent with a role of PXR as a gut microbiota sensor and transcriptional regulator of gut microbiota effects.

Next, we use a combination of a classical pharmacological approach and antibiotic treatment and we report that, in the absence of gut microbiota, PXR is still able to bind and respond to its ligand. Therefore, we conclude that the ATB-driven decrease in PXR activity is not due to a change in the transcriptional machinery of the intestinal epithelial cells or of the hepatocytes, but rather to a decrease of microbial-derived ligands. Indeed, recent studies on the mechanisms that link the body microbial communities to immune education, protection against pathogens or metabolism point to microbiota-derived metabolites as key players during the microbe-host interactions. The 3 currently most studied class of metabolites involved in the microbiota-host cross-talk are (i) short-chain fatty acids that are produced by the microbiota from the fermentation of dietary fibers, (ii) tryptophan metabolites [1] and (iii) bile acids, produced in the liver and transformed by the microbiota: (i) Not much is known about the interactions between short-chain fatty acids and PXR. However, butyrate has been shown to strongly induce the expression of PXR upon differentiation of Caco-2 intestinal epithelial cells [38]. (ii) Tryptophan can be

converted directly in the gut by microorganisms into indole derivatives, such as indole-3-propionic acid (IPA*). In vitro*, IPA has been shown to activate both the mPXR and the hPXR, however IPA was a much more potent agonist of the mPXR [16]. *In vivo*, oral gavage with IPA has been shown to decrease intestinal permeability in the small intestine in a PXR-dependent way [16]. In distant organs, such as the vascular epithelium, IPA has been shown to regulate endothelium-dependent vasodilation in vivo, and in vitro experiments point to PXR as a potential effector of IPA effects [39]. However, *in vivo* evidence using physiological concentrations of circulating IPA were lacking. Indoxyl-3-sulfate is another by product of the microbiota-host tryptophan co-metabolism [40] and has been demonstrated to be a direct AhR ligand, however, it failed to activate CAR or PXR in cell lines [41]. Therefore, indoles, and IPA in particular, might represent potential microbial ligands for PXR that could explain our results in the intestine and in the liver. However, it is not clear whether these indoles could reach the liver at a sufficient concentration to activate PXR. (iii) Bile acids interact with PXR directly [20,42] or indirectly via regulation of the farnesoid X receptor [43]. The secondary bile acid litocholic acid and its 3-keto derivative have been shown to bind directly to PXR [20], whereas chenodeoxycholic acid, deoxycholic acid and cholic acid only mildly activate PXR [42]. Several other bile acid derivatives have been shown to directly bind to PXR using reporter assays [44,45]. Conversely, PXR plays a role in the regulation of bile acid metabolism and detoxication by inducing genes involved in bile acid synthesis [43,46], conjugation and transport in order to enhance their elimination [20,47]. Therefore, bile acids represent putative metabolites that could definitely play a role in the microbiota-PXR crosstalk described in our results. Conversely, we also observed that PXR had a moderate, but significant role in shaping the

microbiota composition, in which differential bile acid metabolism between *Pxr*$^{+/+}$ and *Pxr*$^{-/-}$ mice might be implicated.

Our hepatic transcriptomic analysis of the effect of ATB treatment in male and female *Pxr*$^{+/+}$ *vs* *Pxr*$^{-/-}$ littermate mice revealed first a strong sexually dimorphic impact of ATB treatment, independently of PXR. Indeed, we observed that only 5-10% of the hepatic genes were commonly regulated in males and females upon ATB-treatment. Our results were further confirmed by re-analyzing a previously published dataset that aimed to compare liver genes with altered rhythmicity in male and female GF mice [32]. Recent studies have highlighted strong sexually dimorphic relationships between the gut microbiota and its host. The gut microbes modulate the entero-hepatic recirculation of estrogens and androgens, thereby affecting local and systemic levels of sex steroid hormones (reviewed in [48]), while estrogens have been shown to directly influence the composition of the gut microbiota and contribute to influence the sexual-dimorphism in diet-induced metabolic syndrome [49]. The liver is a highly sexually dimorphic organ [50], and the gut microbiota is critical for maintaining hepatic sex-biased gene expression [32]. Most gene expression studies that have investigated the gut microbes-liver dialogue have used male animals [32,33,35,51] and consistently observed that xenobiotic metabolism, steroid biosynthesis and lipid metabolism were the most down-regulated pathways in the liver of GF mice [32,33,51]. We replicated these findings in our own analysis of the dataset of GF mice of Weger *et al*. and in our ATB-model of gut microbiota depletion. This corroborates that our results are mainly driven by a gut microbiota dependent effect on the liver and not by a direct effect of antibiotics. It also raises the more general question about how much of the current knowledge about the gut microbial impact on the host's

liver and metabolism holds in females. Several recent human studies have indeed observed sex-specific associations between gut microbiome and fat distribution [52].

Strikingly, PXR has been known for long to control the expression of genes involved in the metabolic pathways described previously as the most affected upon microbial depletion [9,14]. By comparing the number of genes affected by ATB treatment in *Pxr*$^{+/+}$ vs *Pxr*$^{-/-}$ mice, we were surprised to observe that 60-80% of ATB-induced gene changes were dependent of PXR. By comparison, it was found that less than 5% of the colonic gene expression changes induced by the absence of gut microbiota required MyD88 signaling, a major adaptor from the Toll-like receptors signaling [36]. Our result therefore demonstrates that PXR is, at least quantitatively, a major sensor or gut microbial signals in the liver of both male and female mice. It would be interesting to see whether this proportion of microbially-regulated PXR-controlled genes also holds in GF mice deleted or not for PXR, and in models of hepatic-specific deletion of PXR.

Our pathway enrichment analysis of the microbial-driven PXR-dependent hepatic function highlighted lipid metabolism. The gut microbiota has been previously shown to promote hepatic lipid accumulation in mice via controlling fatty acid desaturation by the stearoyl-CoA desaturase (Scd1) [51,53] and fatty acid elongation by fatty acid elongases (Elovl) [51]. Acetate originating from the microbial degradation of dietary fibers serves as a precursor for the hepatic synthesis of C16 and C18 fatty acids [51]. In our experiment, short-term ATB treatment was sufficient to slightly decrease hepatic triglyceride content in males, as well as the relative abundance of C16:0 fatty acid. Interestingly, these findings were dependent on PXR. Gene expression analysis did not show any impact of ATB-treatment on FA synthesis, however, this might be due to the time of sacrifice of our

animals that was not optimal to observe FA anabolic pathways. At ZT6, food intake is indeed usually low. However, we confirm significant effect of gut microbiota depletion on fatty acid elongases such as *Elovl2, 3* and *5*. Interestingly, PXR might play a role in the gut microbiota control of FA elongation since these genes were not affected by ATB in *Pxr*$^{-/-}$ mice. Moreover, we observed a significant PXR-dependent decrease in the expression of genes involved in FA oxidation upon ATB-treatment. These findings are counter-intuitive with the observed decrease in hepatic triglycerides and are not consistent with the findings of others that compared Cyp4 expression in GF vs SPF mice [19,54]. However, our findings could be explained by the decrease in microbial folate production upon ATB therapy that would decrease hepatic PPARα activation, therefore leading to decrease FA oxidation [55] but this deserves further investigation.

Finally, we observed that both in GF, and in ATB-treated male animals, xenobiotic metabolism is strongly affected by the gut microbiota. This corroborates many previous transcriptomics [19,51], as well as proteomics [51] studies, in which *Cyp3a11* is systematically one of the top down regulated genes and proteins in GF male mice. We add to these previous studies by demonstrating that PXR is the key mediator of these perturbations. At the gene level, PXR-dependent sensing of the gut microbiota controlled the expression of several CYP3 genes. Our *ex-vivo* assays also demonstrated that all of the significant ATB-induced perturbations in the ability of liver microsomes to oxidize testosterone were controlled by PXR, at least in male mice. Testosterone hydroxylation is a widely recognized assay that measures the global ability of microsomal enzymes, mostly CYP, to metabolize sterol compounds. In particular, we observed the formation of a lower amount of 6β-testosterone, a reaction that is primarily performed by CYP3A11 [17]. Our

results therefore bring new strong evidence that the gut microbiota controls the host's xenobiotic metabolism. In recent years, the gut microbiota has emerged as a key player in clinics and in toxicology with evidences showing that the efficacy and toxicity of orally administered drugs [56,57] and/or food pollutants [58] can be strongly affected by gut microbial metabolism. However, our findings, and those from others [19,54] shed light on another potential mechanism underlying food-drug or drug-drug interactions. In humans, CYP3A4, PXR's prototypical target gene, metabolizes the vast majority of clinically administrated drugs [59] and induction or repression of its activity is considered as the main risk factor for drug-drug interaction by pharmaceutical companies and regulatory agencies [60,61]. Our results indicate that gut microbe may represent an underestimated factor that controls part of the interindividual pharmacokinetics and may be relevant especially in cases of medications with narrow therapeutic index or potential life-threatening toxicity, e.g., the non-steroidal anti-inflammatory drugs, opioid analgesics, cardiovascular medications, warfarin, anticancer drugs and immunosuppressants [62]. Finally, it should be noted that more and more environmental and/or food contaminants such as pesticides [63,64], artificial sweeteners [65] or food additives [66] are found to perturbate of the gut microbiota composition and metabolism, with toxicological consequences for the host. Whether these chronic exposure to microbiota perturbing chemicals also interfere with PXR and the host's xenobiotic capacities remains to be determined but might also represent a risk for unexpected food-drug interactions.

In conclusion, our study identifies PXR as a sensor for gut microbiota-derived signals that control the host's hepatic lipid and xenobiotic metabolism in a sexually dimorphic manner. The effectors of these bidirectional PXR-gut microbiota interactions,

namely the specific gut bacterial species and metabolites that can activate PXR in the liver, as well as the PXR-derived metabolites controlling the gut microbiota composition, remain to be determined. These results open a new metagenomic perspective on the sexually dimorphic and interindividual differences in pharmacokinetics and sensitivity to environmental toxicity.

REFERENCES

1. Agus A, Planchais J, Sokol H. Gut Microbiota Regulation of Tryptophan Metabolism in Health and Disease. Cell Host Microbe. 2018;23:716–24.

2. Lamas B, Richard ML, Leducq V, Pham H-P, Michel M-L, da Costa G, et al. CARD9 impacts colitis by altering gut microbiota metabolism of tryptophan into aryl hydrocarbon receptor ligands. Nat Med. Nature Publishing Group; 2016;22:598–605.

3. Natividad JM, Agus A, Planchais J, Lamas B, Jarry AC, Martin R, et al. Impaired Aryl Hydrocarbon Receptor Ligand Production by the Gut Microbiota Is a Key Factor in Metabolic Syndrome. Cell Metab. 2018.

4. Bookout AL, Jeong Y, Downes M, Yu RT, Evans RM, Mangelsdorf DJ. Anatomical profiling of nuclear receptor expression reveals a hierarchical transcriptional network. Cell. 2006;126:789–99.

5. Kliewer SA, Moore JT, Wade L, Staudinger JL, Watson MA, Jones SA, et al. An orphan nuclear receptor activated by pregnanes defines a novel steroid signaling pathway. Cell. 1998;92:73–82.

6. Guengerich FP. Cytochrome P-450 3A4: regulation and role in drug metabolism. Annu Rev Pharmacol Toxicol. 1999;39:1–17.

7. Drozdzik M, Busch D, Lapczuk J, Müller J, Ostrowski M, Kurzawski M, et al. Protein Abundance of Clinically Relevant Drug-Metabolizing Enzymes in the Human Liver and Intestine: A Comparative Analysis in Paired Tissue Specimens. Clinical Pharmacology & Therapeutics. 2018;104:515–24.

8. Yu J, Petrie ID, Levy RH, Ragueneau-Majlessi I. Mechanisms and Clinical Significance of Pharmacokinetic-based Drug-drug Interactions with Drugs Approved by the U.S. Food and Drug Administration in 2017. Drug Metab. Dispos. 2018;:dmd.118.084905.

9. Hakkola J, Rysä J, Hukkanen J. Regulation of hepatic energy metabolism by the nuclear

receptor PXR. Biochim Biophys Acta. 2016.

10. Rysä J, Buler M, Savolainen MJ, Ruskoaho H, Hakkola J, Hukkanen J. Pregnane X receptor agonists impair postprandial glucose tolerance. Clinical Pharmacology & Therapeutics. Wiley-Blackwell; 2013;93:556–63.

11. Kodama S, Koike C, Negishi M, Yamamoto Y. Nuclear receptors CAR and PXR cross talk with FOXO1 to regulate genes that encode drug-metabolizing and gluconeogenic enzymes. Mol. Cell. Biol. 2004;24:7931–40.

12. Bitter A, Rümmele P, Klein K, Kandel BA, Rieger JK, Nüssler AK, et al. Pregnane X receptor activation and silencing promote steatosis of human hepatic cells by distinct lipogenic mechanisms. Arch. Toxicol. Springer Berlin Heidelberg; 2015;89:2089–103.

13. Gwag T, Meng Z, Sui Y, Helsley RN, Park S-H, Wang S, et al. Non-nucleoside reverse transcriptase inhibitor efavirenz activates PXR to induce hypercholesterolemia and hepatic steatosis. J Hepatol. 2019;70:930–40.

14. Barretto SA, Lasserre F, Fougerat A, Smith L, Fougeray T, Lukowicz C, et al. Gene Expression Profiling Reveals that PXR Activation Inhibits Hepatic PPARα Activity and Decreases FGF21 Secretion in Male C57Bl6/J Mice. Int J Mol Sci. Multidisciplinary Digital Publishing Institute; 2019;20:3767.

15. Hernandez JP, Mota LC, Baldwin WS. Activation of CAR and PXR by Dietary, Environmental and Occupational Chemicals Alters Drug Metabolism, Intermediary Metabolism, and Cell Proliferation. Curr Pharmacogenomics Person Med. 2009;7:81–105.

16. Venkatesh M, Mukherjee S, Wang H, Li H, Sun K, Benechet AP, et al. Symbiotic bacterial metabolites regulate gastrointestinal barrier function via the xenobiotic sensor PXR and Toll-like receptor 4. Immunity. 2014;41:296–310.

17. Claus SP, Ellero SL, Berger B, Krause L, Bruttin A, Molina J, et al. Colonization-induced host-gut microbial metabolic interaction. MBio. 2011;2:e00271–10.

18. Montagner A, Korecka A, Polizzi A, Lippi Y, Blum Y, Canlet C, et al. Hepatic circadian clock oscillators and nuclear receptors integrate microbiome-derived signals. Sci Rep. 2016;6:20127.

19. Fu ZD, Selwyn FP, Cui JY, Klaassen CD. RNA-Seq Profiling of Intestinal Expression of Xenobiotic Processing Genes in Germ-Free Mice. Drug Metab. Dispos. American Society for Pharmacology and Experimental Therapeutics; 2017;45:1225–38.

20. Staudinger JL, Goodwin B, Jones SA, Hawkins-Brown D, MacKenzie KI, LaTour A, et al. The nuclear receptor PXR is a lithocholic acid sensor that protects against liver toxicity. Proc Natl Acad Sci USA. 2001;98:3369–74.

21. Cheng L, Lo L-Y, Tang NLS, Wang D, Leung K-S. CrossNorm: a novel normalization strategy for microarray data in cancers. Sci Rep. Nature Publishing Group; 2016;6:18898.

22. Smyth GK. Linear models and empirical bayes methods for assessing differential expression in microarray experiments. Stat Appl Genet Mol Biol. 2004;3:Article3–25.

23. Huang DW, Sherman BT, Lempicki RA. Bioinformatics enrichment tools: paths toward the comprehensive functional analysis of large gene lists. Nucleic Acids Res. 2009;37:1–13.

24. Beckonert O, Keun HC, Ebbels TMD, Bundy J, Holmes E, Lindon JC, et al. Metabolic profiling, metabolomic and metabonomic procedures for NMR spectroscopy of urine, plasma, serum and tissue extracts. Nat Protoc. 2007;2:2692–703.

25. Martin OCB, Olier M, Ellero-Simatos S, Naud N, Dupuy J, Huc L, et al. Haem iron reshapes colonic luminal environment: impact on mucosal homeostasis and microbiome through aldehyde formation. Microbiome. 2019;7:72.

26. Dieterle F, Ross A, Schlotterbeck G, Senn H. Probabilistic quotient normalization as robust method to account for dilution of complex biological mixtures. Application in 1H NMR metabonomics. Anal Chem. 2006;78:4281–90.

27. Veselkov KA, Lindon JC, Ebbels TMD, Crockford D, Volynkin VV, Holmes E, et al. Recursive segment-wise peak alignment of biological (1)h NMR spectra for improved metabolic biomarker recovery. Anal Chem. 2009;81:56–66.

28. Cloarec O, Dumas ME, Trygg J, Craig A, Barton RH, Lindon JC, et al. Evaluation of the orthogonal projection on latent structure model limitations caused by chemical shift variability and improved visualization of biomarker changes in 1H NMR spectroscopic metabonomic studies. Anal Chem. 2005;77:517–26.

29. Lluch J, Servant F, Païssé S, Valle C, Valière S, Kuchly C, et al. The Characterization of Novel Tissue Microbiota Using an Optimized 16S Metagenomic Sequencing Pipeline. Heimesaat MM, editor. PLoS ONE. Public Library of Science; 2015;10:e0142334.

30. Escudié F, Auer L, Bernard M, Mariadassou M, Cauquil L, Vidal K, et al. FROGS: Find, Rapidly, OTUs with Galaxy Solution. Berger B, editor. Bioinformatics. 2018;34:1287–94.

31. Segata N, Izard J, Waldron L, Gevers D, Miropolsky L, Garrett WS, et al. Metagenomic biomarker discovery and explanation. Genome Biol. BioMed Central; 2011;12:R60.

32. Weger BD, Gobet C, Yeung J, Martin E, Jimenez S, Betrisey B, et al. The Mouse Microbiome Is Required for Sex-Specific Diurnal Rhythms of Gene Expression and Metabolism. Cell Metab. 2018.

33. Björkholm B, Bok CM, Lundin A, Rafter J, Hibberd ML, Pettersson S. Intestinal microbiota regulate xenobiotic metabolism in the liver. PLoS ONE. 2009;4:e6958.

34. Oh HYP, Ellero-Simatos S, Manickam R, Tan NS, Guillou H, Wahli W. Depletion of Gram-Positive Bacteria Impacts Hepatic Biological Functions During the Light Phase. Int J Mol Sci. Multidisciplinary Digital Publishing Institute; 2019;20:812.

35. Mardinoglu A, Shoaie S, Bergentall M, Ghaffari P, Zhang C, Larsson E, et al. The gut

microbiota modulates host amino acid and glutathione metabolism in mice. Mol Syst Biol. 2015;11:834.

36. Larsson E, Tremaroli V, Lee YS, Koren O, Nookaew I, Fricker A, et al. Analysis of gut microbial regulation of host gene expression along the length of the gut and regulation of gut microbial ecology through MyD88. Gut. 2012;61:1124–31.

37. Sommer F, Nookaew I, Sommer N, Fogelstrand P, Bäckhed F. Site-specific programming of the host epithelial transcriptome by the gut microbiota. Genome Biol. BioMed Central; 2015;16:62–15.

38. Ranhotra HS, Flannigan KL, Brave M, Mukherjee S, Lukin DJ, Hirota SA, et al. Xenobiotic Receptor-Mediated Regulation of Intestinal Barrier Function and Innate Immunity. Nucl Receptor Res. 2016;3.

39. Venu VKP, Saifeddine M, Mihara K, Tsai Y-C, Nieves K, Alston L, et al. The pregnane X receptor and its microbiota-derived ligand indole 3-propionic acid regulate endothelium-dependent vasodilation. American Journal of Physiology Endocrinology and Metabolism. American Physiological Society Bethesda, MD; 2019;317:E350–61.

40. Wikoff WR, Anfora AT, Liu J, Schultz PG, Lesley SA, Peters EC, et al. Metabolomics analysis reveals large effects of gut microflora on mammalian blood metabolites. Proc Natl Acad Sci USA. 2009;106:3698–703.

41. Schroeder JC, DiNatale BC, Murray IA, Flaveny CA, Liu Q, Laurenzana EM, et al. The Uremic Toxin 3-Indoxyl Sulfate Is a Potent Endogenous Agonist for the Human Aryl Hydrocarbon Receptor. Biochemistry. American Chemical Society; 2009;49:393–400.

42. Krasowski MD, Yasuda K, Hagey LR, Schuetz EG. Evolution of the pregnane x receptor: adaptation to cross-species differences in biliary bile salts. Mol. Endocrinol. 2005;19:1720–39.

43. Jung D, Mangelsdorf DJ, Meyer UA. Pregnane X receptor is a target of farnesoid X receptor. The Journal of Biological Chemistry. American Society for Biochemistry and Molecular Biology; 2006;281:19081–91.

44. Goodwin B, Gauthier KC, Umetani M, Watson MA, Lochansky MI, Collins JL, et al. Identification of bile acid precursors as endogenous ligands for the nuclear xenobiotic pregnane X receptor. PNAS. National Academy of Sciences; 2003;100:223–8.

45. Carazo A, Hyrsova L, Dusek J, Chodounska H, Horvatova A, Berka K, et al. Acetylated deoxycholic (DCA) and cholic (CA) acids are potent ligands of pregnane X (PXR) receptor. Toxicol Lett. 2017;265:86–96.

46. Li T, Chen W, Chiang JYL. PXR induces CYP27A1 and regulates cholesterol metabolism in the intestine. The Journal of Lipid Research. American Society for Biochemistry and Molecular Biology; 2007;48:373–84.

47. Schaap FG, Trauner M, Jansen PLM. Bile acid receptors as targets for drug

development. Nat Rev Gastroenterol Hepatol. Nature Publishing Group; 2014;11:55–67.

48. Cross T-WL, Kasahara K, Rey FE. Sexual dimorphism of cardiometabolic dysfunction: Gut microbiome in the play? Mol Metab. Elsevier; 2018;15:70–81.

49. Kaliannan K, Robertson RC, Murphy K, Stanton C, Kang C, Wang B, et al. Estrogen-mediated gut microbiome alterations influence sexual dimorphism in metabolic syndrome in mice. Microbiome. BioMed Central; 2018;6:205–22.

50. Rando G, Wahli W. Sex differences in nuclear receptor-regulated liver metabolic pathways. Biochim Biophys Acta. 2011;1812:964–73.

51. Kindt A, Liebisch G, Clavel T, Haller D, Hörmannsperger G, Yoon H, et al. The gut microbiota promotes hepatic fatty acid desaturation and elongation in mice. Nat Commun. Nature Publishing Group; 2018;9:3760.

52. Min Y, Ma X, Sankaran K, Ru Y, Chen L, Baiocchi M, et al. Sex-specific association between gut microbiome and fat distribution. Nat Commun. Nature Publishing Group; 2019;10:2408–9.

53. Singh V, Chassaing B, Zhang L, San Yeoh B, Xiao X, Kumar M, et al. Microbiota-Dependent Hepatic Lipogenesis Mediated by Stearoyl CoA Desaturase 1 (SCD1) Promotes Metabolic Syndrome in TLR5-Deficient Mice. Cell Metab. Cell Press; 2015;22:983–96.

54. Selwyn FP, Cheng SL, Klaassen CD, Cui JY. Regulation of Hepatic Drug-Metabolizing Enzymes in Germ-Free Mice by Conventionalization and Probiotics. Drug Metab. Dispos. 2016;44:262–74.

55. Hasan AU, Rahman A, Kobori H. Interactions between Host PPARs and Gut Microbiota in Health and Disease. Int J Mol Sci. Multidisciplinary Digital Publishing Institute; 2019;20:387.

56. Koppel N, Maini Rekdal V, Balskus EP. Chemical transformation of xenobiotics by the human gut microbiota. Science. 2017;356.

57. Carmody RN, Turnbaugh PJ. Host-microbial interactions in the metabolism of therapeutic and diet-derived xenobiotics. J Clin Invest. 2014;124:4173–81.

58. Claus SP, Guillou H, Ellero-Simatos S. The gut microbiota: a major player in the toxicity of environmental pollutants? npj Biofilms and Microbiomes. 2016.

59. Yu J, Petrie ID, Levy RH, Ragueneau-Majlessi I. Mechanisms and Clinical Significance of Pharmacokinetic-based Drug-drug Interactions with Drugs Approved by the U.S. Food and Drug Administration in 2017. Drug Metab. Dispos. 2018;:dmd.118.084905.

60. Jones BC, Rollison H, Johansson S, Kanebratt KP, Lambert C, Vishwanathan K, et al. Managing the Risk of CYP3A Induction in Drug Development: A Strategic Approach. Drug Metab. Dispos. American Society for Pharmacology and Experimental Therapeutics;

2017;45:35–41.

61. Prueksaritanont T, Tatosian DA, Chu X, Railkar R, Evers R, Chavez-Eng C, et al. Validation of a microdose probe drug cocktail for clinical drug interaction assessments for drug transporters and CYP3A. Clinical Pharmacology & Therapeutics. 2017;101:519–30.

62. Mouly S, Lloret-Linares C, Sellier P-O, Sene D, Bergmann JF. Is the clinical relevance of drug-food and drug-herb interactions limited to grapefruit juice and Saint-John's Wort? Pharmacological Research. Academic Press; 2017;118:82–92.

63. Motta EVS, Raymann K, Moran NA. Glyphosate perturbs the gut microbiota of honey bees. Proc Natl Acad Sci USA. 2018;115:10305–10.

64. Mao Q, Manservisi F, Panzacchi S, Mandrioli D, Menghetti I, Vornoli A, et al. The Ramazzini Institute 13-week pilot study on glyphosate and Roundup administered at human-equivalent dose to Sprague Dawley rats: effects on the microbiome. Environ Health. BioMed Central; 2018;17:50.

65. Suez J, Korem T, Zeevi D, Zilberman-Schapira G, Thaiss CA, Maza O, et al. Artificial sweeteners induce glucose intolerance by altering the gut microbiota. Nature. 2014;514:181–6.

66. Chassaing B, Koren O, Goodrich JK, Poole AC, Srinivasan S, Ley RE, et al. Dietary emulsifiers impact the mouse gut microbiota promoting colitis and metabolic syndrome. Nature. Nature Publishing Group; 2015;519:92–6.

FIGURE LEGENDS

Figure 1: Effect of individual antibiotic treatments on PXR expression and activity. C57Bl6/J male mice were treated with individual treatments of ampicillin, neomycin, vancomycin or a cocktail of the three antibiotics (ANV) for 2 weeks in their drinking water. RT-qPCR results are presented as mean±SEM for n=8 per group. *p≤0.05, **p≤0.01, ***p≤0.005 compared to control group. P-values were derived from 1-way ANOVA and Bonferroni's post-tests.

Figure 2: Effect of microbiota depletion on PXR activation by a pharmacological agonist. WT and *Pxr*$^{-/-}$ male mice were treated with an antibiotic cocktail of ampicillin, neomycin and vancomycin (ATB), the pharmacological agonist of PXR (PCN) or a combination of both (ATB+PCN). Impact on (A) liver and cecum weight, (B) plasma biochemistry, (C) liver lipid content, (D) ^{1}H-NMR-based metabolic profiling of the hepatic lipid phase, (E) ^{1}H-NMR-based metabolic profiling of the hepatic aqueous phase, (F) PXR's target gene expression in the liver (G) PXR's target gene expression in the ileum. Data are mean±SEM of n=5-6 per group. $p≤0.05, $$p≤0.01, $$$p≤0.001 for PCN effect, #p≤0.05 ##p≤0.01, ###p≤0.005 for genotype effect using 2-way ANOVA and Bonferroni's post-tests.

Figure 3: Gut microbiota composition in *Pxr*$^{-/-}$ and *Pxr*$^{+/+}$ mice. (A&B): Alpha-diversity measures in feces of *Pxr*$^{-/-}$ vs *Pxr*$^{+/+}$ (A) male and (B) female littermate mice. (C-F): Beta-diversity represented by hierarchical clustering based on the Jaccard distances of *Pxr*$^{-/-}$ (blue) *vs*. *Pxr*$^{+/+}$ (red) (C) male or (F) female mice and by PCA analysis based on the Jaccard distances in (D) male and (F) female mice. (G&H): Circular cladograms generated from LEFSe analysis showing the most differentially abundant taxa enriched in fecal microbiota from *Pxr*$^{+/+}$ (red) or *Pxr*$^{-/-}$ (green) (G) male or (H) female mice. Log(LDA scores)>2 and significance of α<0.05 determined using Wilcoxon-Mann Whitney test.

Figure 4: Caecal content metabolomics in Pxr-/- and Pxr+/+ mice. (A&B) Coefficient plots related to the orthogonal projection on latent structure-discriminant analysis (O-PLS-DA) models derived from the caecal extract ^{1}H-NMR-based spectra of (A) male and (B) female *Pxr*$^{+/+}$ vs *Pxr*$^{-/-}$ mice. Metabolites are color-coded according to their correlation coefficient (R), red indicating a very strong positive correlation. The direction of the metabolite indicates the group with which it is positively associated as labeled on the diagram. (C&D) Area under the curve of the ^{1}H-NMR spectra was integrated for the unknown metabolite signal (triplet at 7.006 ppm) in (C) males and (D) females. Data are presented as the mean±SEM. *p<0.05 ***p<0.001 determined using a Kruskall-Wallis test**.**

Figure 5: PXR activity upon microbiota depletion in male and female *Pxr*$^{-/-}$ *and Pxr*$^{+/+}$ littermate mice. C57Bl6/J *Pxr*$^{+/+}$ and *Pxr*$^{-/-}$ male and female littermate mice were treated with an antibiotic cocktail of ampicillin, neomycin and vancomycin (ATB) for 2 weeks. RT-qPCR gene expression of *Pxr, Cyp3a11, Cyp2c55, Cyp2b9, and Fgf21* in the liver of (A) male mice and (B) female mice; and the ileum of (C) male mice (D) female mice. Data are mean±SEM of n=8-10 per group. *p≤0.05, **p≤0.01, ***p≤0.005 for ATB effect, #p≤0.05 ##p≤0.01, ###p≤0.005 for genotype effect using 2-way ANOVA and Bonferroni's post-tests.

Figure 6: Impact of gut microbiota depletion on the hepatic transcriptome in male *Pxr*$^{-/-}$ vs *Pxr*$^{+/+}$ mice. (A&B) Venn diagram representing the number of genes affected by ATB treatment. (C & D) Gene ontology pathway analysis of the 57 and 45 gene significantly up- and down-regulated upon ATB in *Pxr*$^{+/+}$ males only, respectively. Histograms show the enrichment score for each identified pathway. Gene number is indicated to the right of the histograms and the corresponding p-value in shown inside the bars. (E&G) Principal component analysis (PCA) score plots of transcriptomic dataset of (E) *Pxr*$^{+/+}$ control vs *Pxr*$^{+/+}$ ATB and (G) *Pxr*$^{-/-}$ control vs *Pxr*$^{-/-}$ ATB male mice. (F&H) Volcano plots showing the 30 genes with the highest fold-changes upon ATB treatment in (F) *Pxr*$^{+/+}$ control vs *Pxr*$^{+/+}$ ATB (H) *Pxr*$^{-/-}$ control vs *Pxr*$^{-/-}$ ATB male mice.

Figure 7: Impact of gut microbiota depletion on the hepatic transcriptome in female *Pxr*$^{-/-}$ vs *Pxr*$^{+/+}$ mice. (A & B) Venn diagram representing the number of genes affected by ATB treatment. (C&E) Principal component analysis (PCA) score plots of the transcriptomic dataset of (C) *Pxr*$^{+/+}$ control vs *Pxr*$^{+/+}$ ATB and (E) *Pxr*$^{-/-}$ control vs *Pxr*$^{-/-}$ ATB female mice. (D&F) Volcano plot showing the 30 genes with the highest fold changes upon ATB treatment in (D) *Pxr*$^{+/+}$ control vs *Pxr*$^{+/+}$ ATB (F) *Pxr*$^{-/-}$ control vs *Pxr*$^{-/-}$ ATB female mice.

Figure 8: Impact of microbiota depletion on hepatic lipid metabolism in$^{Pxr-/-\ vs\ Pxr+/+}$ male mice. (A) Hepatic neutral lipid content and (B) relative abundance of fatty acids in the liver of male mice. (C) Fold changes (ATB vs control) in the relative expression of selected genes involved in fatty acid (FA) synthesis, FA elongation, peroxisomal FA oxidation and microsomal FA oxidation in *Pxr*$^{-/-}$ (blue) and *Pxr*$^{+/+}$ (red) male mice. Expression of genes involved in FA synthesis and elongation was derived from complementary RT-qPCR expression using n=8-10 mice per group, while expression of genes involved in FA oxidation was derived from microarray measurements (n=5-6 per group). Data are mean±SEM. *p≤0.05, **p≤0.01, ***p≤0.005 for ATB effect using Student t-tests for qPCR data and corrected p-values from linear models for microarray data. #p≤0.05 ##p≤0.01, ###p≤0.005 for genotype effect using 2-way ANOVA and Bonferroni's post-tests.

Figure 9: Impact of microbiota depletion on hepatic lipid metabolism in $^{Pxr-/-\ vs\ Pxr+/+}$ female mice. (A) Hepatic neutral lipid content and (B) relative abundance of fatty acids in the liver of female mice. (C) Fold changes (ATB vs control) in the relative expression of selected genes involved in fatty acid (FA) synthesis, FA elongation, peroxisomal FA oxidation and microsomal FA oxidation in *Pxr*$^{-/-}$ (blue) and *Pxr*$^{+/+}$ (red) male mice. Expression of genes involved in FA synthesis and elongation was derived from complementary RT-qPCR expression using n=8-10 mice per group, while expression of genes involved in FA oxidation was derived from microarray measurements (n=5-6 per group). Data are mean±SEM. *p≤0.05, **p≤0.01, ***p≤0.005 for ATB effect using Student t-tests for qPCR data and corrected p-values from linear models for microarray data. #p≤0.05 ##p≤0.01, ###p≤0.005 for genotype effect using 2-way ANOVA and Bonferroni's post-tests.

Figure 10: Impact of gut microbiota depletion on hepatic xenobiotic metabolism in *Pxr*$^{-/-}$ *vs Pxr*$^{+/+}$ male mice. (A&C) Fold change (ATB vs control) in the relative expression of genes involved in phase I (A) and phase II (C) xenobiotic metabolism in *Pxr*$^{-/-}$ vs *Pxr*$^{+/+}$ male mice. Data are derived from microarrays and are presented as mean±SEM for n=5-6 per group.

*p≤0.05, **p≤0.01, ***p≤0.005 for ATB effect using corrected p-values from linear models. (B) Profiles of oxidized metabolites of testosterone after incubation with liver microsomes of male mice. (D) Specific glutathione transferase activity after incubation with liver cytosolic fraction of male mice. Data are mean±SEM of n=5 per group. *p≤0.05, **p≤0.01, ***p≤0.005 for ATB effect, #p≤0.05 ##p≤0.01, ###p≤0.005 for genotype effect using 1 or 2-way ANOVA and appropriate post-tests.

SUPPLEMENTARY FIGURE LEGENDS:

Supplementary Figure 1: Impact of antibiotic treatment on physiological parameters. C57Bl6/J male mice were treated with individual treatments of ampicillin, neomycin, vancomycin or a cocktail of the three antibiotics (ANV) for 2 weeks in their drinking water Impact on (A) body, (B) liver, (C) caecum weights, and (D) fecal microbial count of anaerobic colonies. Results are presented as mean±SEM for n=8 per group. *p≤0.05, **p≤0.01, ***p≤0.005 compared to control group. P-values were derived from 1-way ANOVA analyses and Bonferroni's post-tests.

Supplementary Figure 2: Typical ^{1}H-NMR spectra of liver and caecal mouse extracts. (A) Typical 1H-NMR spectra of caecal content extracts. The 5 to 9 ppm region was vertically expended 6 times compared to the 0 to 4.5 ppm region. Keys: 1: bile acids (mixed), 2: butyrate, 3: leucine, 4: isoleucine, 5: valine, 6: propionate, 7: α-ketoisovalerate, 8: ethanol, 9: β-hydroxybutyrate, 10: lipids, 11: lactate, 12: alanine, 13: lysine, 14: acetate, 15: N-acetyl groups, 16: glutamate, 17: succinate, 18: α-ketoglutarate, 19: aspartate, 20: choline, 21: taurine, 22: β-xylose, 23: β-galactose, 24: β-glucose, 25: α-arabinose, 26: α-xylose, 27: α-glucose, 28: α-galactose, 29: uracil, 30: tyrosine, 31: phenylalanine, 32: adenine, 33: hypoxanthine, 34: formate. (B) Typical 1H-NMR spectra liver aqueous extracts. Keys: 1: bile acids (mixed), 2: bile acids (tauroconjugated, mixed), 4: leucine, 5: valine, 6: isoleucine, 10: 3-hydroxyburyrate, 12: lactate, 13: threonine, 15: alanine, 16: ornithine, 17: putrescine, 19: acetate, 21: glutamate, 22: glutamine, 24: oxidized glutathion, 25: reduced glutathion, 27: succinate, 30: asparate, 31: dimethylamine, 34: dimethylglycine, 35: creatine, 37: choline, 38: o-phosphocholine, 40: betaine, 41: taurine, 43: methanol, 45: glucose, 50: glycine, 52: UDP-glucose, 53: UDP-glucuronate, 55: uridine, 56: NADP+, 57: NAD+, 60: fumarate, 64: tyrosine, 66: phenylalanine, 69: nicotinurate**.**

Supplementary Figure 3: ^{1}H-NMR analysis of liver extracts in *Pxr*$^{-/-}$ mice treated with ATB, PCN or a combination of both. *Pxr*$^{-/-}$ male mice were treated with an antibiotic cocktail of ampicillin, neomycin and vancomycin (ATB), the pharmacological agonist of PXR (PCN) or a combination of both (ATB+PCN). (A) O-PLS-DA score plots derived from NMR-based metabolic profiling of the hepatic lipid phase and (B) PCA analysis derived from NMR-based metabolic profiling of the hepatic aqueous phase.

Supplementary Figure 4: Effect of *Pxr* deletion on caecal microbiota community distribution. Relative abundance per phylum (%). Data represent 5-95% boxplots. #p≤0.05 ##p≤0.01, ###p≤0.005 for genotype effect using Kruskall-Wallis test.

Supplementary Figure 5: Effect of ATB treatment on body parameters and microbiota depletion in *Pxr*$^{+/+}$ vs. *Pxr*$^{-/-}$ mice. *Pxr*$^{+/+}$ and *Pxr*$^{-/-}$ male and female mice were treated with an antibiotic cocktail of ampicillin, neomycin and vancomycin (ATB) for 2 weeks in their drinking water. (A) Body weight, (B) water consumption, (C) % body weights of liver and spleen, (D) % body weight of caecum and fecal microbial count in male mice. (E) Body weight, (F) water consumption, (G) % body weights of liver and spleen, (H) % body weight of caecum and fecal microbial count in female mice. Data are mean±SEM of n=8-10 per group. *p≤0.05, **p≤0.01,***p≤0.005 for ATB effect, #p≤0.05 ##p≤0.01, ###p≤0.005 for genotype effect using 2-way ANOVA and Bonferroni's post-tests.

Supplementary Figure 6: Tentative identification of unknown caecal metabolite discriminating *Pxr*$^{-/-}$ vs *Pxr*$^{+/+}$ males. (A) Structural information derived from various 1D and 2D NMR sequences (NOESY, J-RES, COSY, HSQC, TOCSY). (B) Statistical total correlation spectroscopy (STOCSY) analysis with triplet at 7.006 ppm as driving peak. (C&D) Area under the curve for the ^{1}H-NMR peaks at 7.006 ppm in males (C) and females (D). (E-H): Mice were gavaged for 4 days with corn-oil (control) or tyrosine and 1H-NMR metabolomic profiling was performed in their caecal content. O-PLS-DA analysis derived from caecal content spectra from tyrosine vs control male (E) or (F) female mice showing a significant increase in the peaks corresponding to tyrosine and in the 7.006 ppm peaks corresponding to the unknown metabolite. Area under the curve for the 7.006 ppm triplet in this experiment in males (G) and females (H).

Supplementary Figure 7: Microarray analysis in liver of *Pxr*$^{-/-}$ vs *Pxr*$^{+/+}$ mice. Venn diagram representing the number of genes affected by ATB treatment in (A) male and (B) female *Pxr*$^{+/+}$ and *Pxr*$^{-/-}$ littermate mice.

Supplementary Figure 8: Hepatic impact of *Pxr* deletion in littermate vs. non-littermate male mice.
Venn diagrams representing the number of genes affected by *Pxr* deletion *Pxr*$^{+/+}$ *vs* *Pxr*$^{-/-}$ littermate (green) or WT *vs*. *Pxr*$^{-/-}$ non-littermate male mice (purple). Data originate from two independent animal experiments conducted in the same animal facility and two independent microarray experiments conducted in the same facility using n=5-6 mice per groups. Genes were selected as significantly regulated using a non-corrected p-value<0.01 (A) or non-corrected p-value<0.001 (B).

Supplementary Figure 9: Sexually-dimorphic impact of gut microbiota depletion on the liver transcriptome. (A&B) Venn diagram representing the number of genes significantly up- (A) and down-regulated (B) in the liver of GF vs Conv males vs. female mice. Data were obtained from {Weger:2018dl}. (C&D) Gene ontology pathway analyses. Histograms show the enrichment score for each identified pathway. Gene number is indicated in parenthesis and the corresponding q-value in shown on the left for each significant cluster. (E&F) Venn diagram representing the number of genes significantly up- (E) and down-regulated (F) in the liver of ATB-treated *vs.* Control males and female mice. (G&H) Gene ontology pathway analyses. Histograms show the enrichment score for each identified pathway. Gene number is indicated in parenthesis and the corresponding q-value in shown on the left for each significant cluster.

Supplementary Figure 10: Impact of gut microbiota depletion on hepatic xenobiotic metabolism in *Pxr*$^{-/-}$ vs *Pxr*$^{+/+}$ female mice. (A&B) Fold change (ATB vs control) in the relative expression of genes involved in phase II (A) and phase I (B) xenobiotic metabolism in *Pxr*$^{-/-}$ vs *Pxr*$^{+/+}$ female mice. Data are derived from microarrays and are presented as mean±SEM for n=5-6 per group. *p≤0.05, **p≤0.01, ***p≤0.005 for ATB effect using corrected p-values from linear models.

Supplementary Figure 11: Representative radio-chromatograms obtained from microsomal hepatic incubation (0.5 mg proteins, 20 min) of a (A) *Pxr*$^{+/+}$+ ATB animal and a *Pxr*$^{-/-}$ Control animal (B) with 10 µM [^{14}C]-testosterone.

SUPPLEMENTARY TABLE LEGENDS

Supplementary Table 1: List of antibiotics (ATB) used and their properties (source: www.drugbank.ca).

Supplementary Table 2: List of qPCR primers

Supplementary Table 3: [^{14}C]-testosterone metabolites structure hypotheses based on their mass and on the similarity of their retention time with authentic standards.

Figure 1: Effect of individual antibiotic treatments on PXR expression and activity.

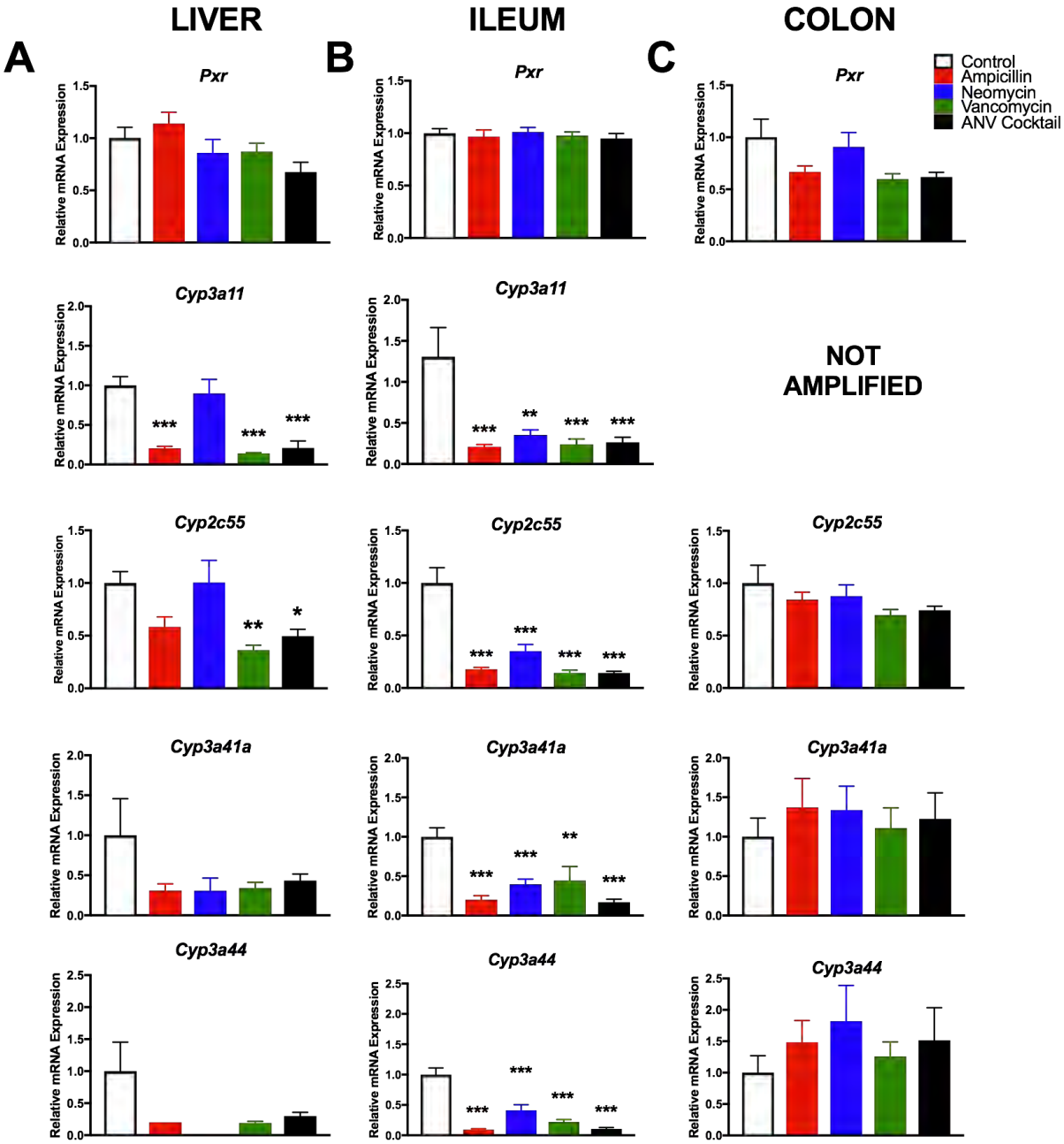

Figure 2: Effect of microbiota depletion on PXR activation by a pharmacological agonist.

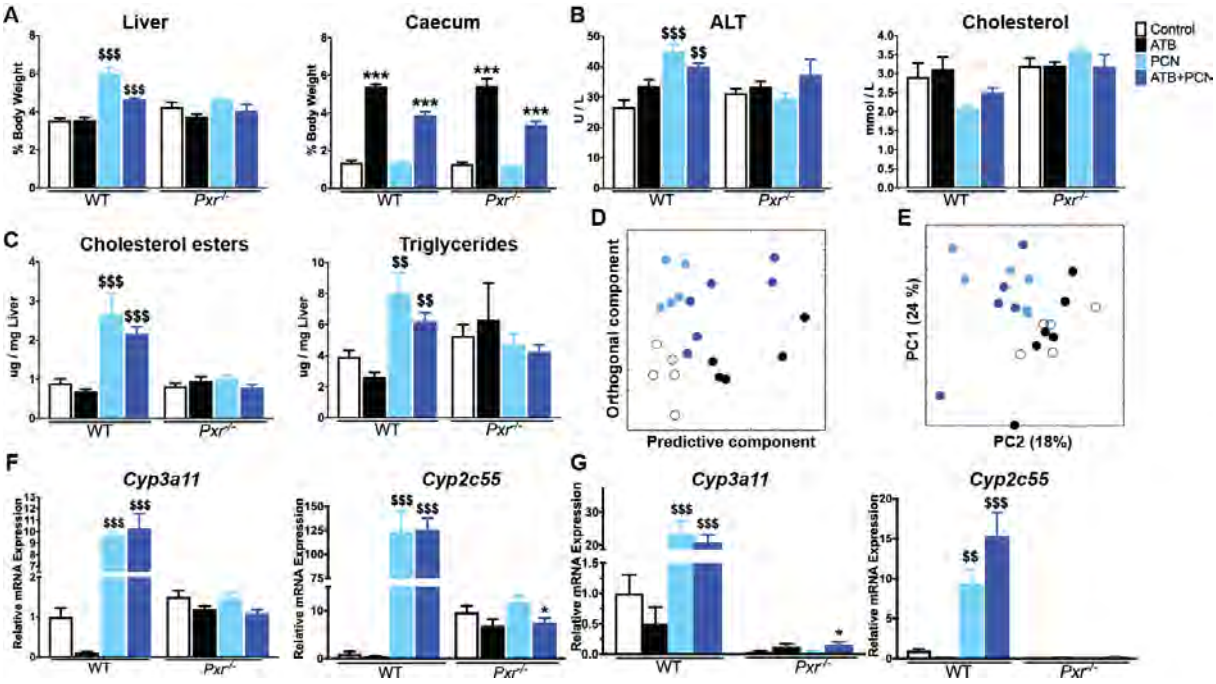

Figure 3: Gut microbiota composition in Pxr$^{-/-}$ and Pxr$^{+/+}$ mice.

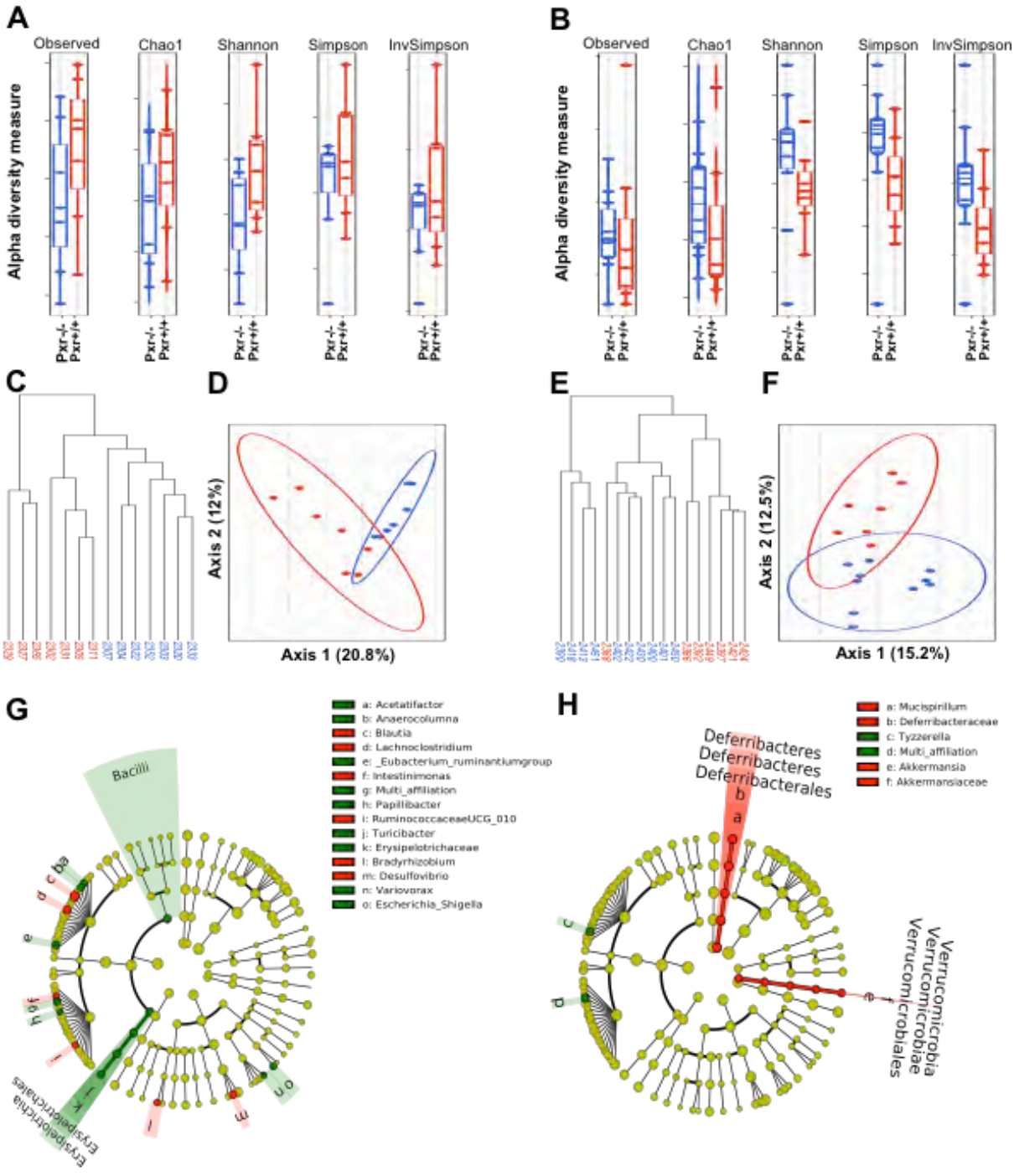

Figure 4: Caecal content metabolomics in $Pxr^{-/-}$ and $Pxr^{+/+}$ mice.

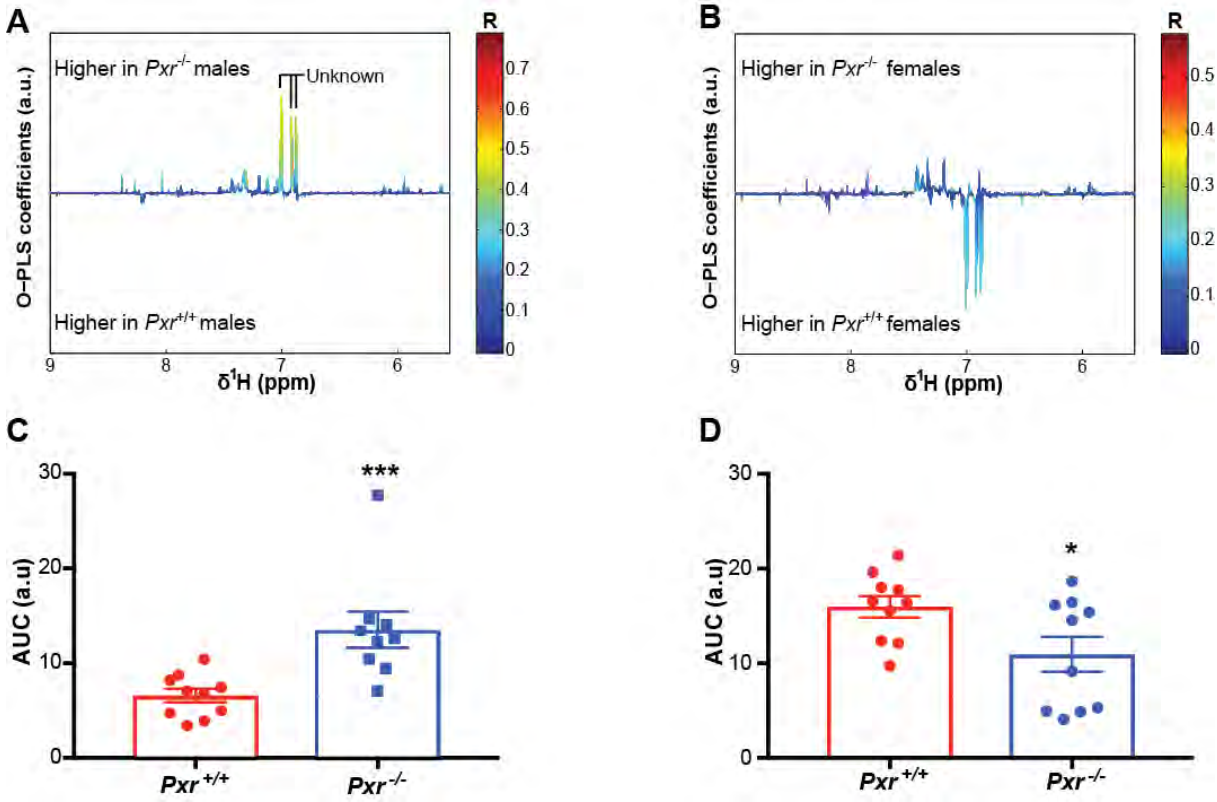

Figure 5: PXR activity upon microbiota depletion in male and female $Pxr^{-/-}$ and $Pxr^{+/+}$ mice.

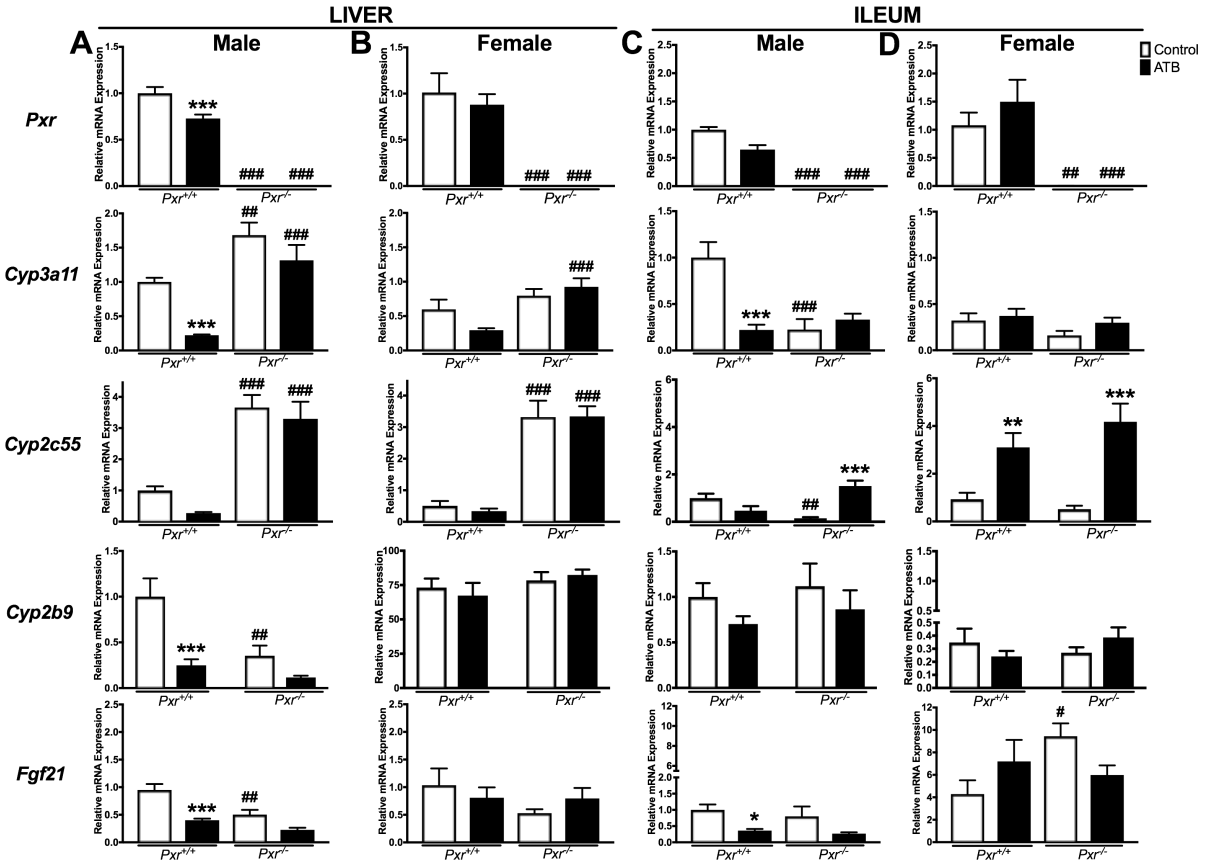

Figure 6: Impact of gut microbiota depletion on the hepatic transcriptome in male $Pxr^{-/-}$ vs $Pxr^{+/+}$ mice.

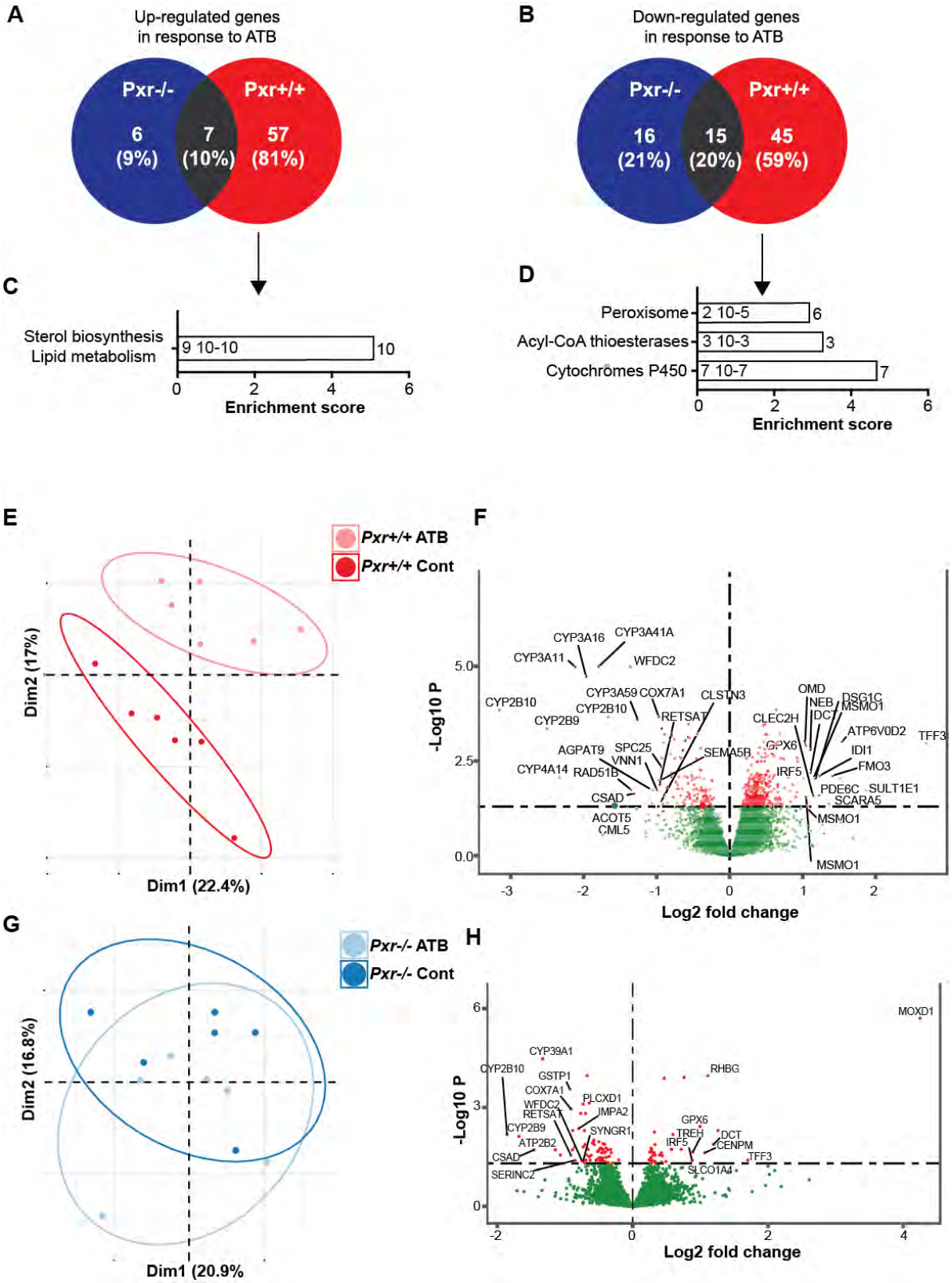

Figure 7: Impact of gut microbiota depletion on the hepatic transcriptome in female $Pxr^{-/-}$ vs $Pxr^{+/+}$ mice.

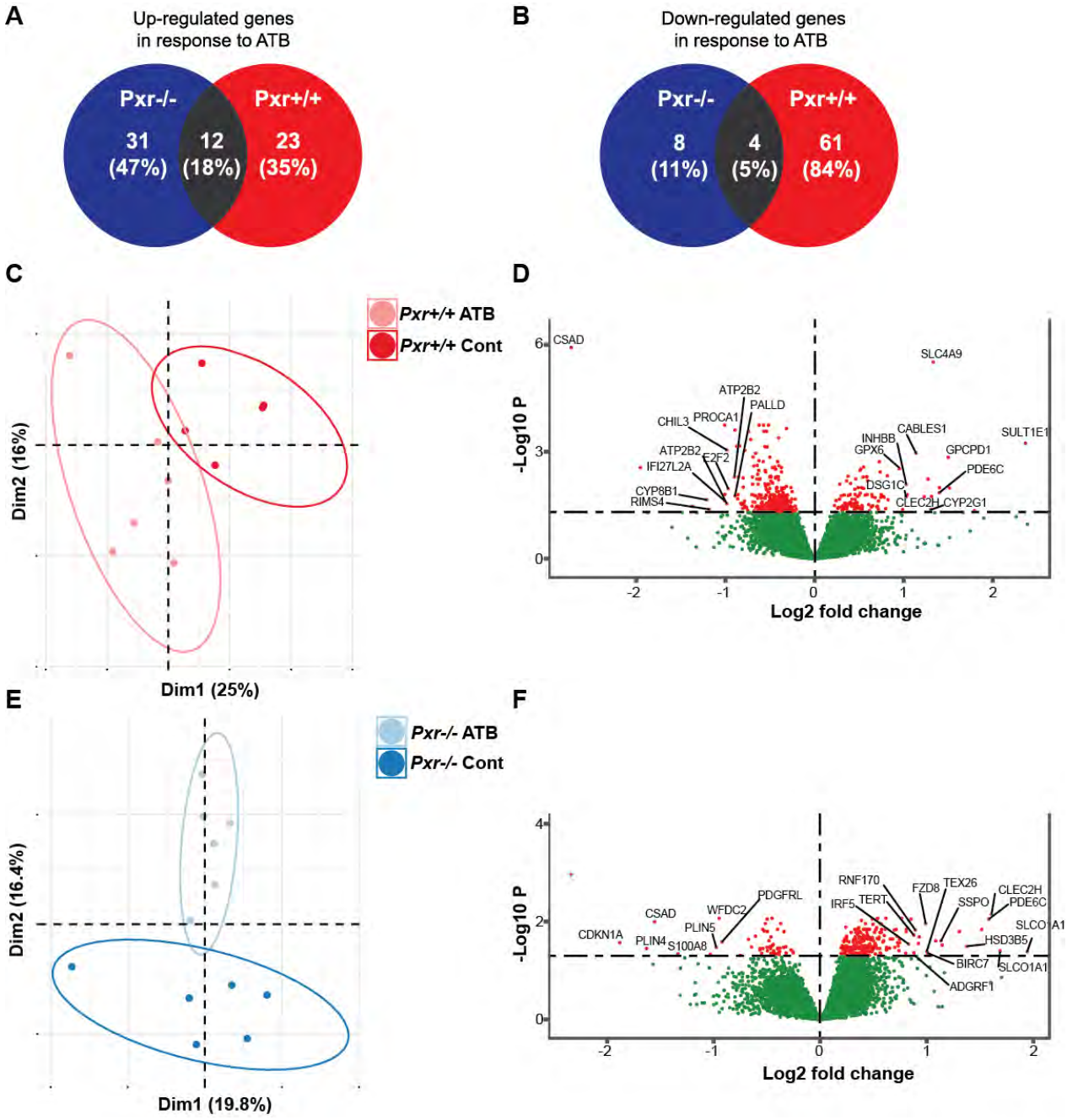

Figure 8: Impact of microbiota depletion on hepatic lipid metabolism in $Pxr^{-/-}$ vs $Pxr^{+/+}$ male mice.

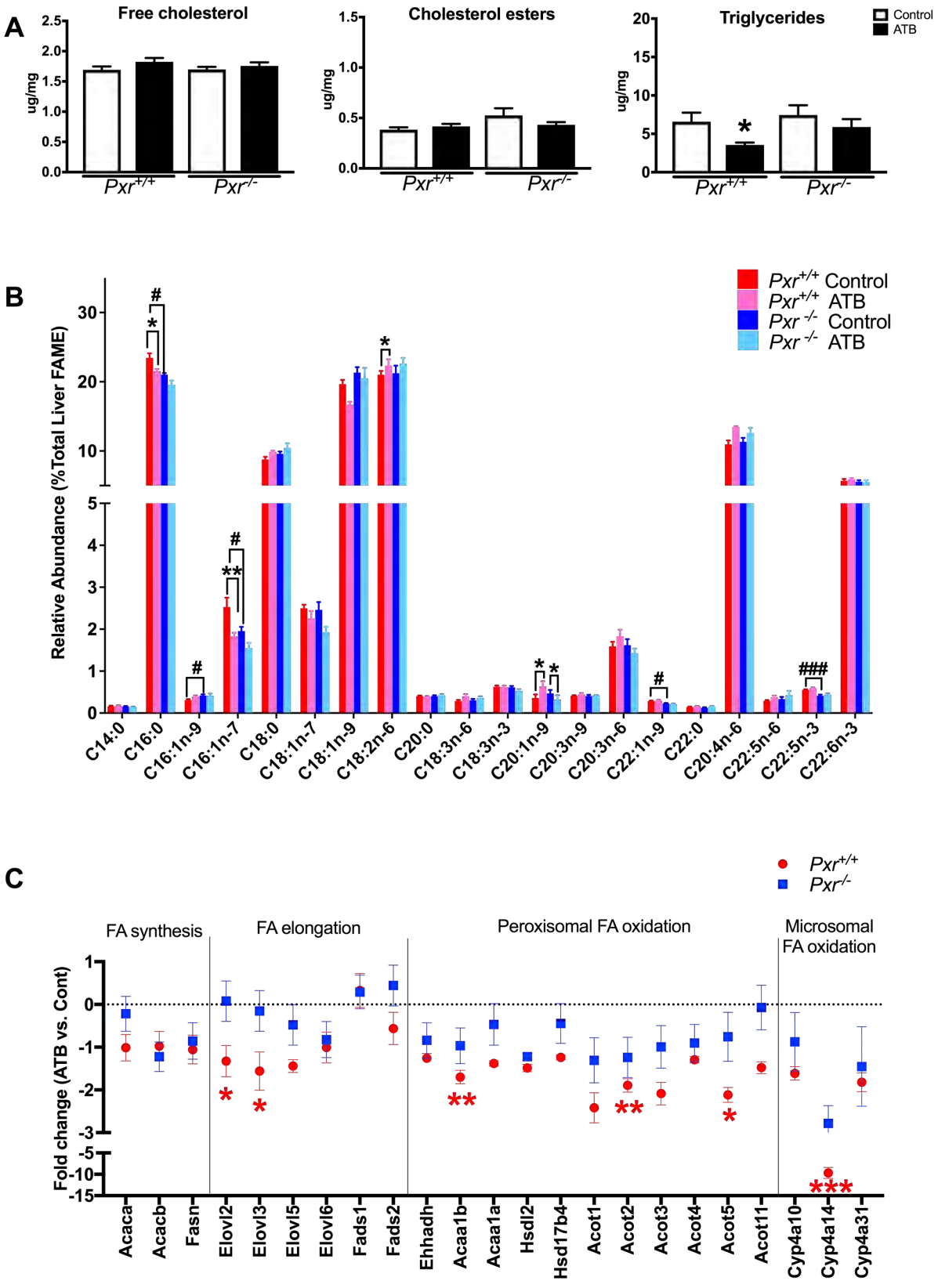

Figure 9: Impact of microbiota depletion on hepatic lipid metabolism in $Pxr^{-/-}$ vs $Pxr^{+/+}$ female mice.

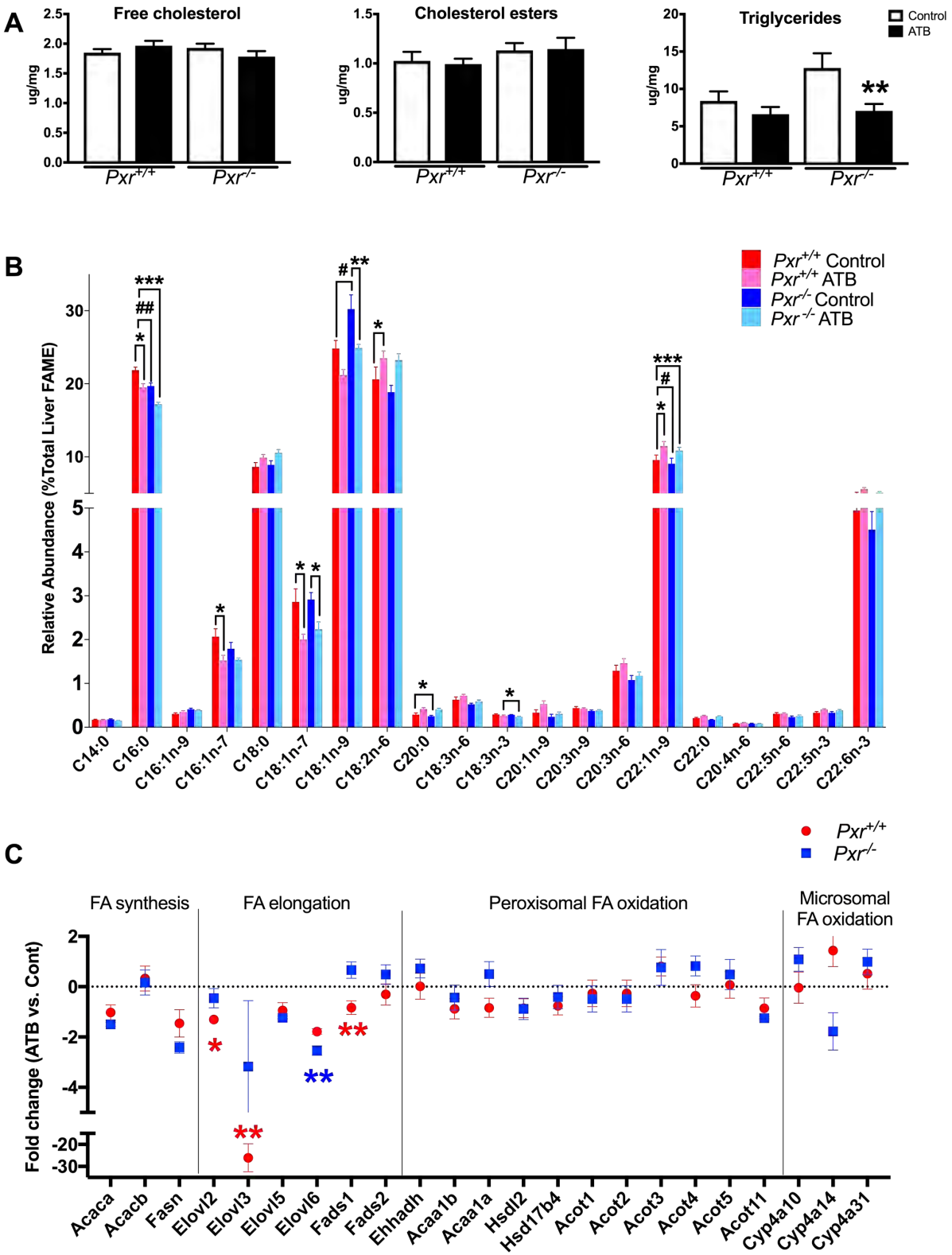

Figure 10: Impact of gut microbiota depletion on hepatic xenobiotic metabolism in $Pxr^{-/-}$ vs $Pxr^{+/+}$ male mice.

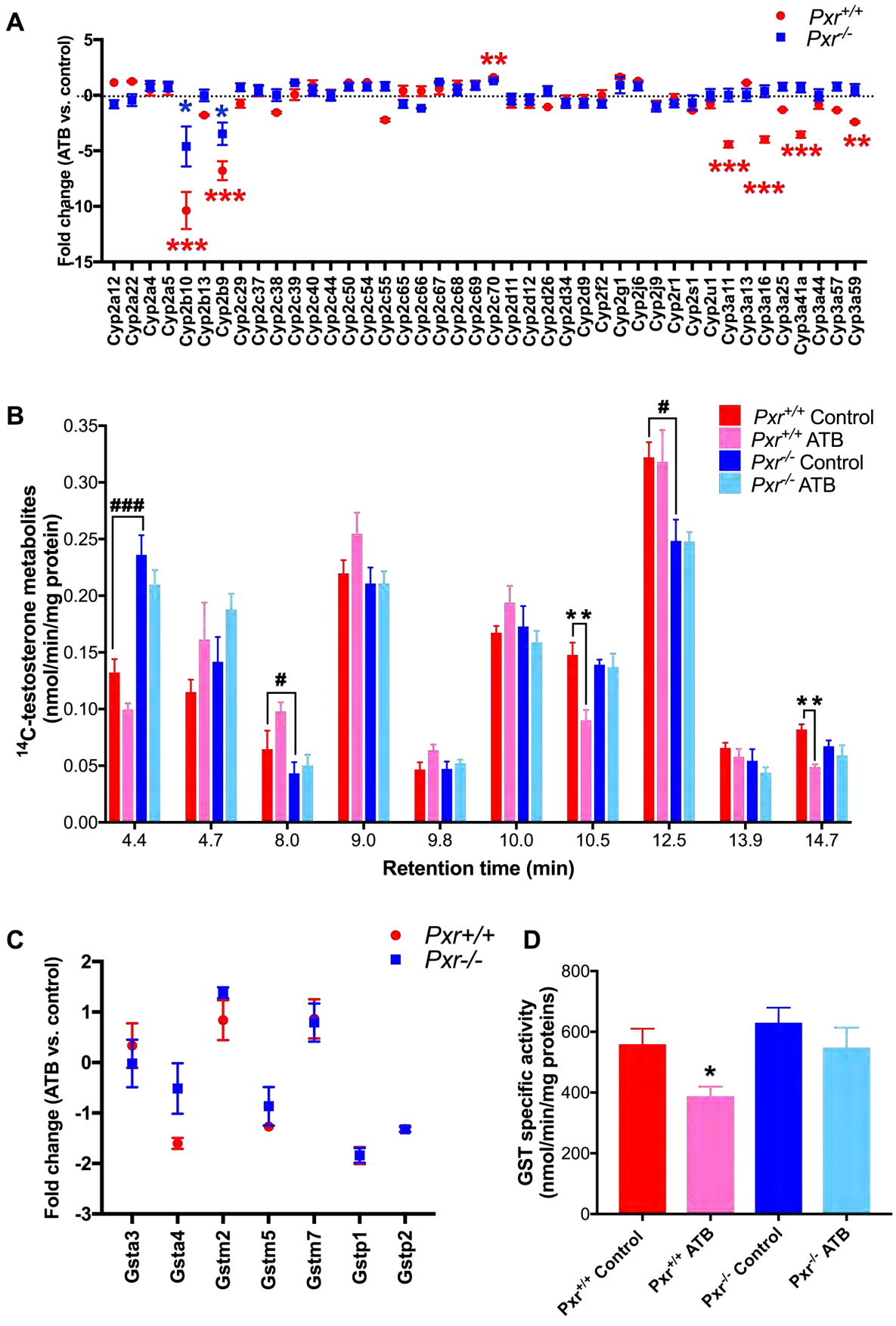

SUPPLEMENTARY FIGURES

Supplementary Figure 1: Impact of antibiotic treatment on physiological parameters.

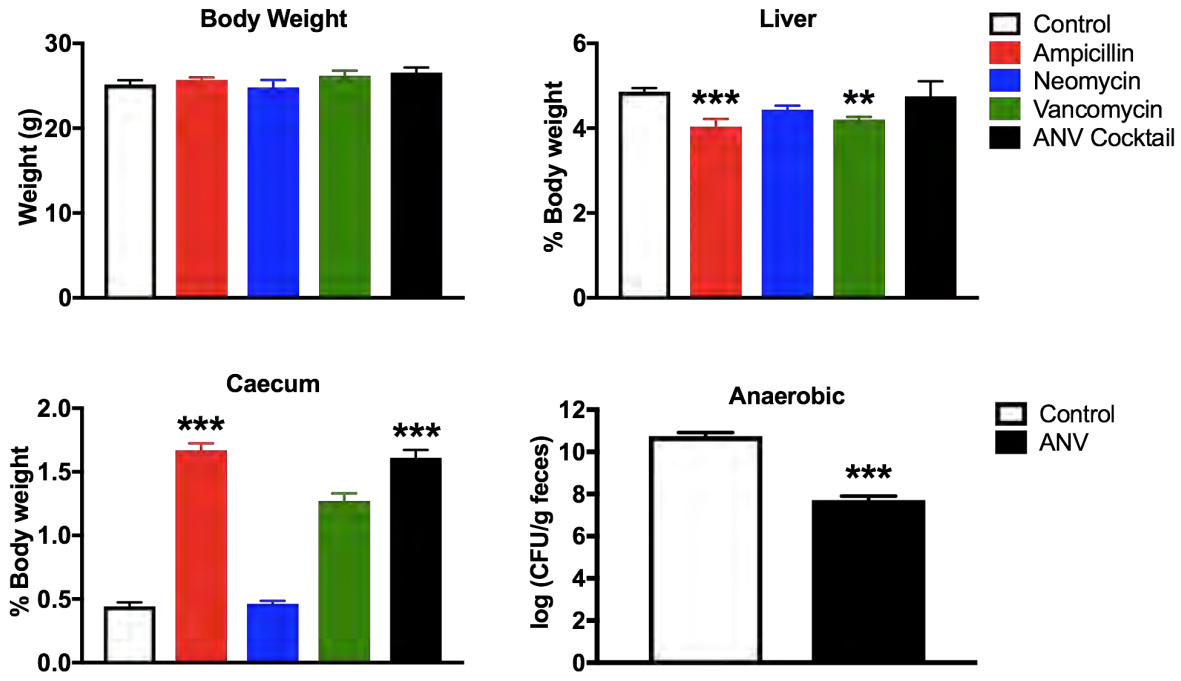

Supplementary Figure 2: Partially assigned typical ^{1}H-NMR spectra.

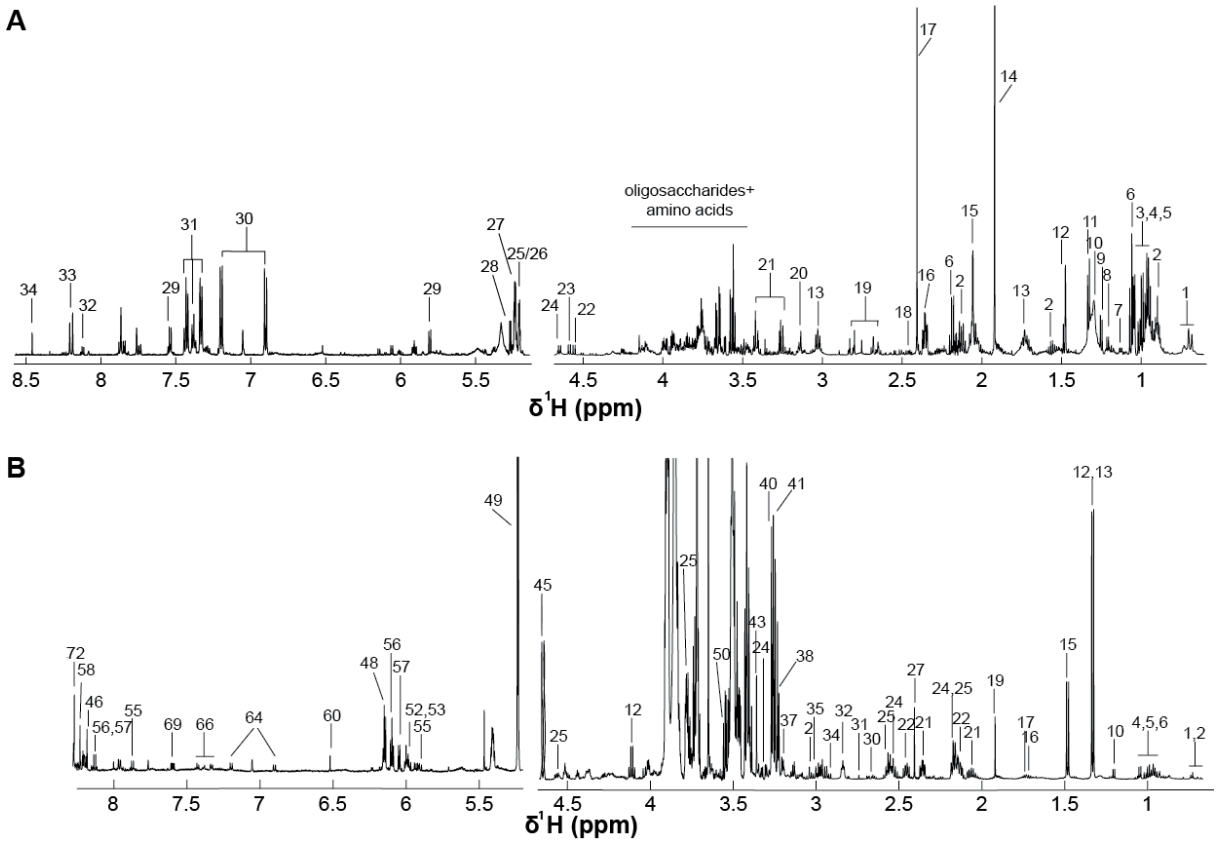

Supplementary Figure 3: ^{1}H-NMR based metabolomics analysis in liver extracts of Pxr$^{-/-}$ male mice treated with ATB, PCN or a combination of both.

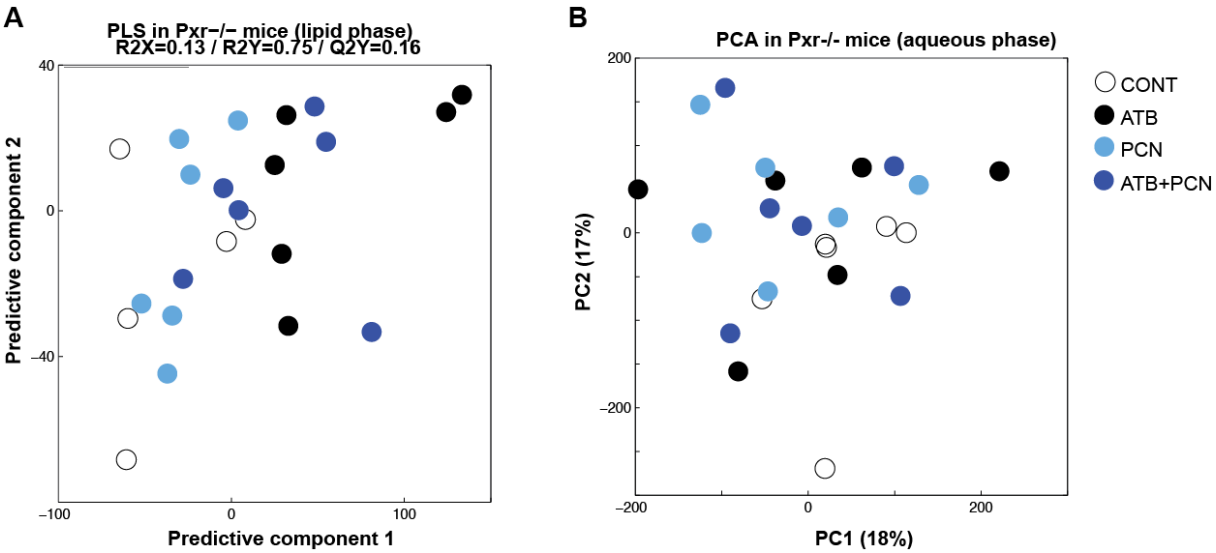

Supplementary Figure 4: Effect of Pxr deletion on caecal microbiota community distribution.

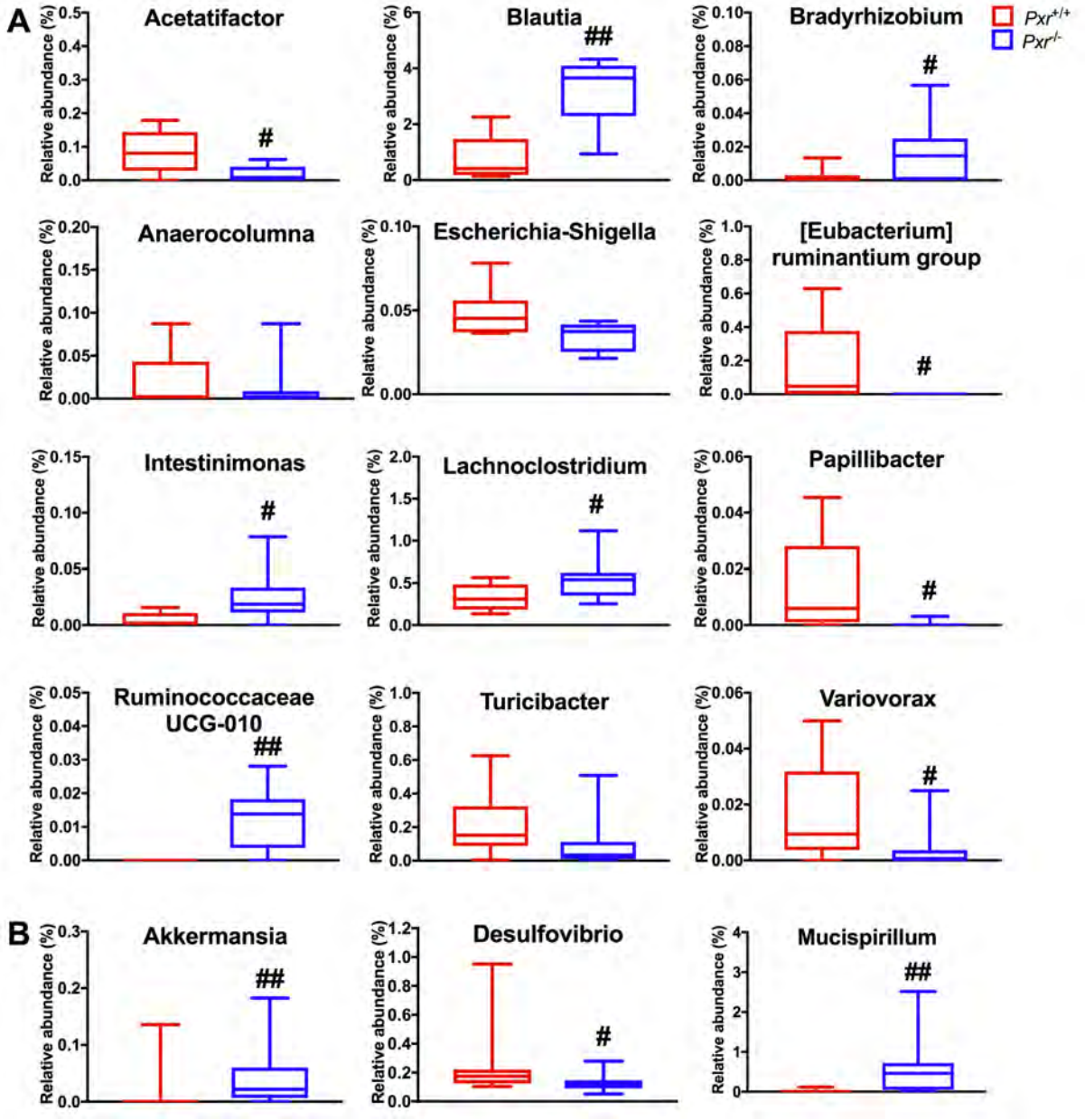

Supplementary Figure 5: Effect of ATB treatment on physiological parameters in $Pxr^{-/-}$ vs $Pxr^{+/+}$ mice.

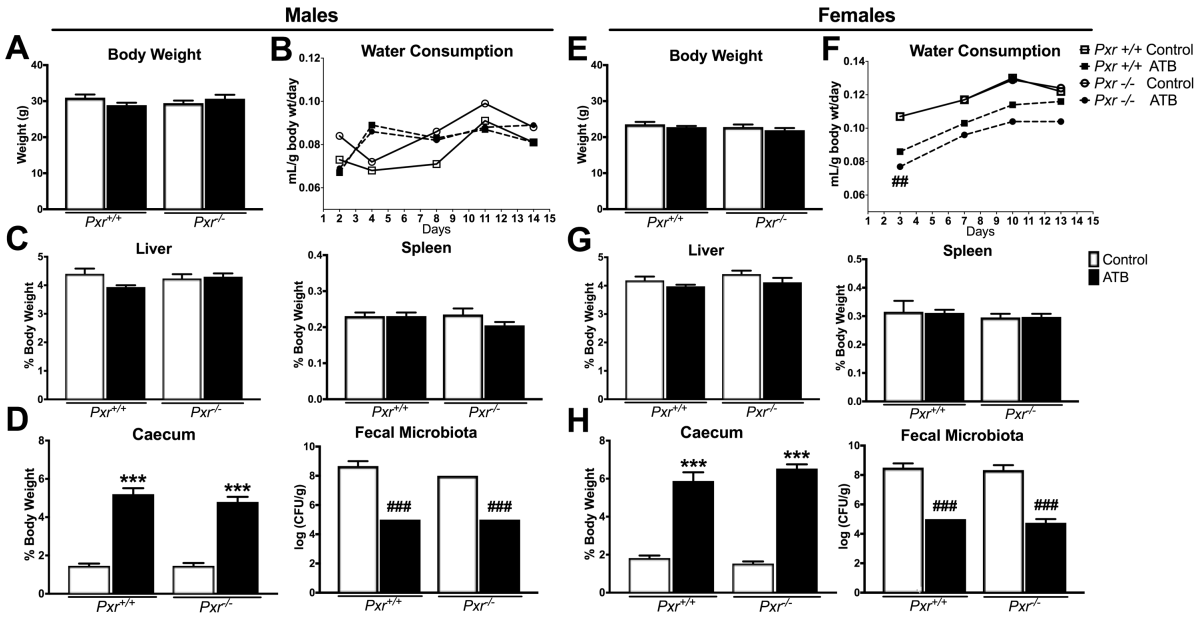

Supplementary Figure 6: Tentative identification of unknown caecal metabolite.

A

δ^{1}H (ppm)	Multiplicity	J (Hz)	δ ^{13}C (ppm)
7.006	t	7.6	123.6
6.9	d (?)		115.9
6.87	d	8	115.6
2.91	d	16 - 236	37.3
2.62	d	16 - 236	37.3

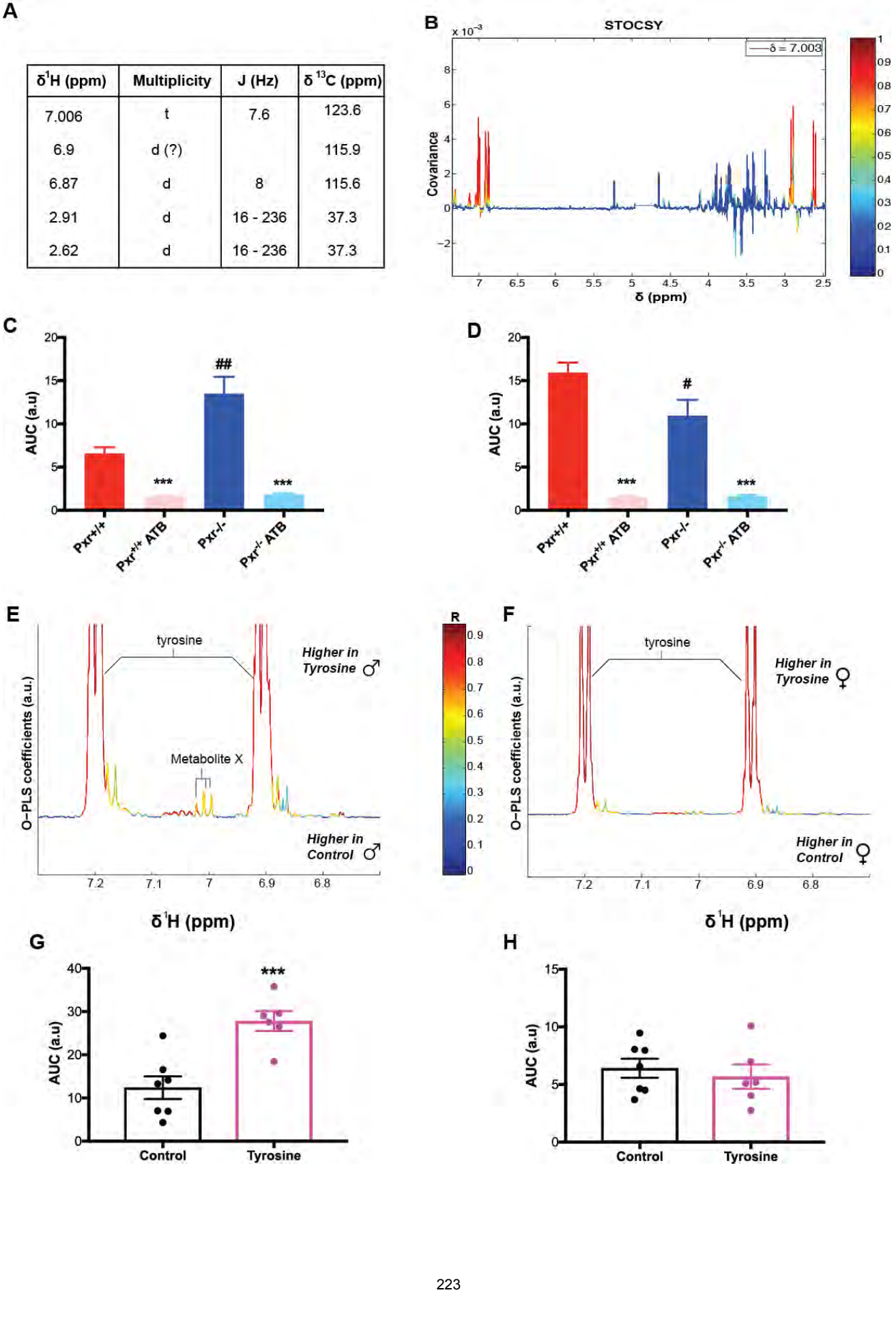

Supplementary Figure 7: Microarray analysis in liver of $Pxr^{-/-}$ vs $Pxr^{+/+}$ mice.

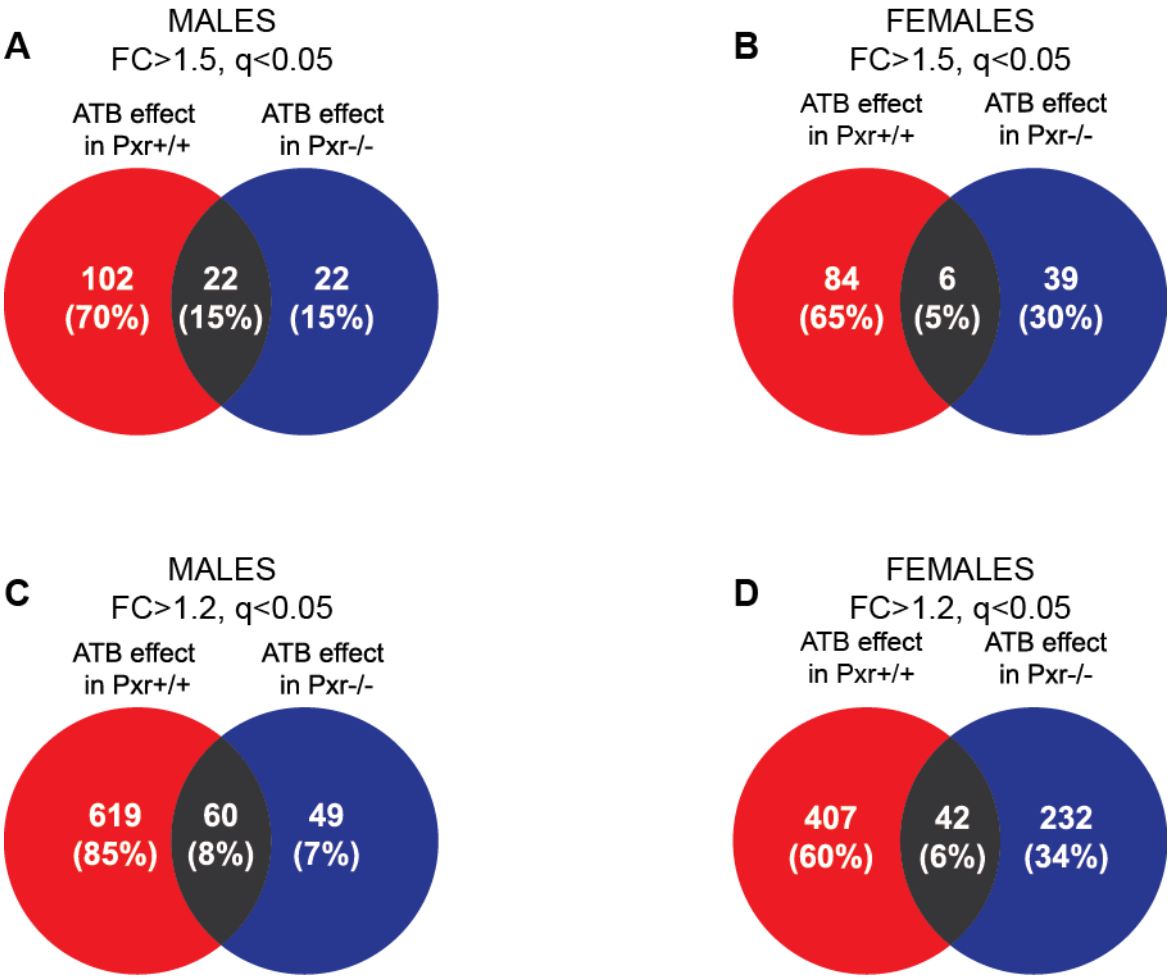

Supplementary Figure 8: Hepatic impact of Pxr deletion in littermate vs. non-littermate male mice.

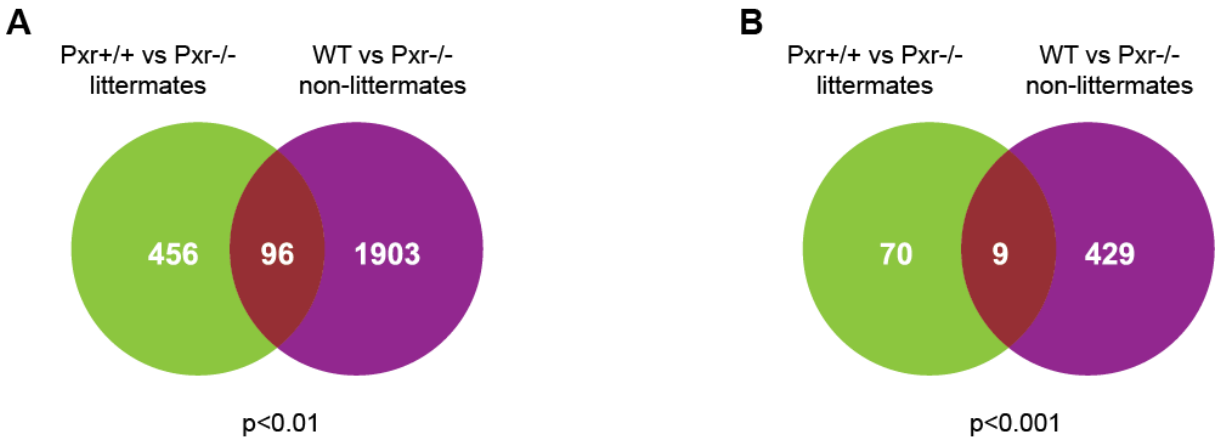

Supplementary Figure 9: Sexually dimorphic impact of gut microbiota depletion on the liver transcriptome.

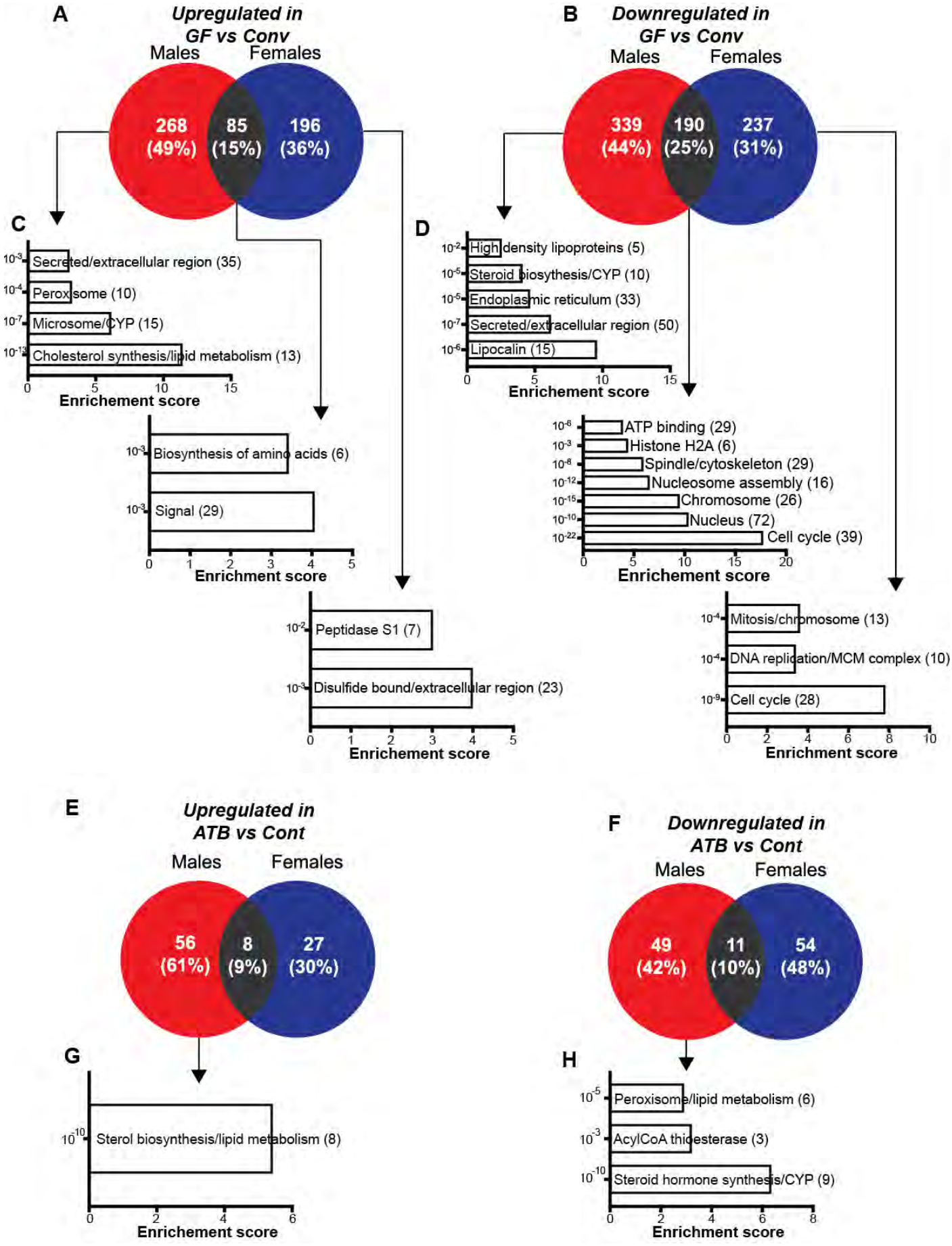

Supplementary Figure 10: Impact of gut microbiota depletion on hepatic xenobiotic metabolism in $Pxr^{-/-}$ vs $Pxr^{+/+}$ female mice.

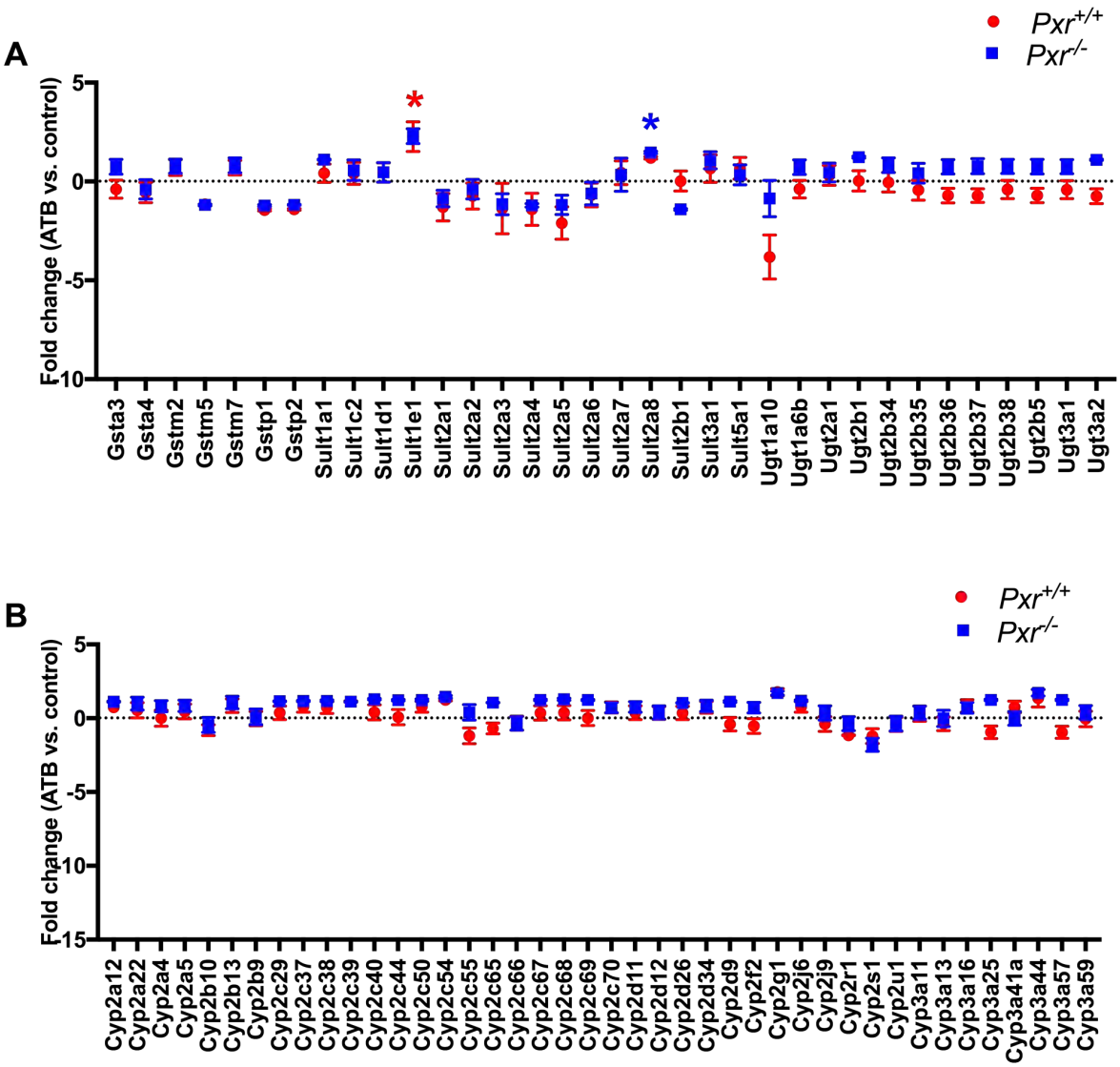

Supplementary Figure 11: Representative radio-chromatograms.

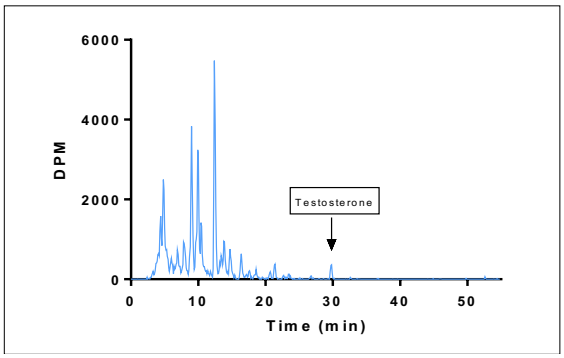

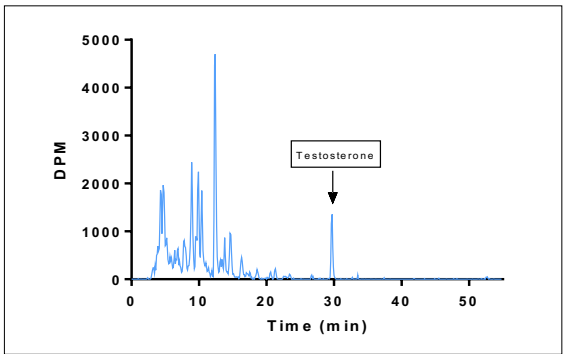

SUPPLEMENTARY TABLES

Supplementary Table 1: List of antibiotics and their properties.

Antibiotics	Quantity	Category	Mechanism	Spectrum	Intestinal absorption	Effect on CYP/NR
Ampicillin	1 gram / L	Beta-lactam	Inhibition of cell wall synthesis	Broad spectrum: excellent for gram-negative	Partial	Almost not metabolized
Neomycin	1 gram / L	Aminoglycoside	Binds to duplex RNA with high affinity; Inhibition of protein synthesis in bacteria	Broad spectrum: excellent for gram-negative	Poor absorption : 3% intact intestinal mucosa	*Low CYP450 inhibitory promiscuity
Vancomycin	0.5 gram / L	Glycopeptide	Inhibition of cell wall synthesis in bacteria	Narrow:spectrum; gram-positive	Poor	*Substrate : CYP450 3A4 Low CYP450 inhibitory promiscuity

Supplementary Table 2: Oligonucleotide sequences for real-time PCR

Gene	NCBI Refseq	Forward primer (5'-3')	Reverse primer (5'-3')
Acaca	NM_133360	TTACAGGATGGTTTGGCCTTTC	CAAATTCTGCTGGAGAAGCCAC
Cyp2b9	NM_010000	CTTTGCTGGAACTGAGACCACA	GATCTGAAAATCTCTGAATCTCATGG
Cyp2c55	AY206875	TTGTGGAAGAGCTAAGAAAAGCAAAT	GAGCACAGCTCAGGATGAATGT
Cyp3a11	NM_007818	TCACACACACAGTTGTAGGCAGAA	GTTTACGAGTCCCATATCGGTAGAG
Cyp3a41a	NM_017396.3	CCTACAGAGAGTCACACACACACATC	GGTTCATCCCTGCTTGTCTGTC
Cyp3a44	NM_177380.3	CCTACAGAGAGTCACACATACATC	CCTGCTTGTCTGTCTGCAATTT
Elovl2	NM_019423	GCAGAAGGAAGGCGGCTAC	CGCGAACTCGAGAATCTCGT
Elovl3	NM_007703	GCCTCTCATCCTCTGGTCCT	TGCCATAAACTTCCACATCCT
Elovl5	NM_134255	TCGATGCGTCACTCAGTACCTATT	ATTTTGGTCCCAGCCATACAAT
Elovl6	NM_130450	TCTGATGAACAAGCGAGCCA	TGGTCATCAGAATGTACAGCATGT
Fads1	NM_146094	TCAACATGCACCCCCTCTTC	GATGGTTGTATGGCATGTGCTT
Fads2	NM_019699	TCCAGTACCAGATCATCATGACAA	GGTGTAGAAGAAACGCATATAGTAGCTG
Fasn	NM_007988	AGTCAGCTATGAAGCAATTGTGGA	CACCCAGACGCCAGTGTTC
Fgf21	NM_020013	AAAGCCTCTAGGTTTCTTTGCCA	CCTCAGGATCAAAGTGAGGCG
Pxr	NM_010936	AGAGATCATCCCTCTTCTGCCAC	GATCTGGTCCTCAATAGGCAGGT

Supplementary Table 3: [^{14}C]-testosterone metabolites structure hypotheses based on their mass and on the similarity of their retention time with authentic standards.

LC-MS Retention time (min)	Corresponding radio-HPLC Retention time (min)	Metabolites		m/z
7.22	7.9	hydroxytestosterone	OH-Testo	305.2111
7.71			OH-Δ4-dione	303.1955
8.2	8.8	15β-hydroxytestosterone	15β-OH-Testo	305.2111
8.25		6α-hydroxytestosterone	6α-OH-Testo	305.2111
8.27			Δ-Testo	287.2006
8.44			OH-Δ4-dione	303.1955
8.9		hydroxytestosterone	OH-Testo	305.2111
9.2	9.7	7α-hydroxytestosterone	7α-OH-Testo	305.2111
9.21			Δ-Testo	287.2006
9.66	10.2	6β-hydroxytestosterone	6β-OH-Testo	305.2111
10.18			OH-Δ4-dione	303.1955
11.59	12.2	16α-hydroxytestosterone	16α-OH-Testo	305.2111
12.65	13.5	11α-hydroxytestosterone	11α-OH-Testo	305.2111
12.67			Δ-Testo	287.2006
13.0			OH-Δ4-dione	303.1955
13.72	14.4		OH-Δ4-dione	303.1955
15.42	16.0	16β-hydroxytestosterone	16β-OH-Testo	305.2111
16.15		4-Androsten-16α-ol-3,17-dione	16α-OH-Δ4-dione	303.1955
25.7	26.3	4,6-androstadien-17β-ol-3-one	Δ6-Testo	287.2006
28.63	29.8	Testosterone	Testo	289.2162
32.34	33	Androstenedione = 4-androsten-3,17-dione	Δ4-Testo	287.2006

Chapter 3.4

Constitutive androstane receptor is a sexually dimorphic hepatic sensor of gut microbiota that controls the host xenobiotic and lipid metabolism

Context: The Constitutive Androstane Receptor (CAR) is a second transcription factor of the nuclear receptor superfamily that acts as a xenosensor and controls the transcription of key genes involved in detoxification. While CAR and PXR share common ligands and regulate the expression of overlapping sets of gene in the liver, little is known regarding the activity of CAR in the gut and its putative role in the sensing of microbial metabolites. In this chapter, we report data from a set of experiments paralleled to those developed in the first three chapters on PXR. Overall, this body of work initiates a project regarding the importance of the bi-directional interaction of CAR and gut microbiota that requires further experimentation. Therefore, this chapter is not yet presented as a publication.

Constitutive androstane receptor is a sexually dimorphic hepatic sensor of gut microbiota that controls the host xenobiotic and lipid metabolism

Barretto S, Lasserre F *et al.*

INTRODUCTION

Over the past decade, research on the impact of the gut microbiota on its host has tremendously progressed. To date these studies have mainly investigated the local effects of the gut microbiota-host interactions in the intestine, targeting the various components of the intestinal barrier function as a means to understand and treat a variety of diseases including metabolic disorders and inflammatory bowel diseases. Symbiotic bacterial metabolites in the form of indoles (indole 3-propionic acid, IPA) have for example been shown to regulate gastrointestinal barrier function via the nuclear receptor pregnane X receptor (PXR, NR1I2) and Toll-like Receptor 4 (Venkatesh *et a*l., 2014).

CAR, is highly similar to PXR and is another well-described xenobiotic receptor (Gao & Xie, 2010). Both PXR and CAR are referred to as a xenobiotic sensor with a broad range of endogenous and exogenous ligands with varying chemical structures. Upon ligand-binding, CAR mainly regulates the expression of genes involved in xenobiotic metabolism and energy metabolism (Chai *et al*., 2016). CAR expression is modulated by other nuclear receptors, such as hepatocyte nuclear factor 4 alpha (HNF4α), peroxisome proliferator-activated receptor alpha (PPARα), glucocorticoid receptor (GR), farensoid X receptor (FXR) (Björkholm *et al.*, 2009), liver X receptor (LXR) (Gao & Xie, 2010). Aside from their role in xenobiotic metabolism, CAR and PXR regulate homeostasis of bile acids, sterol lipids, heme and other endogenous hydrophobic molecules (Björkholm *et al.*,

2009). In germ-free mice, it has been shown that lack of intestinal bacteria leads to the decreased availability of CAR ligands and therefore of CAR activity (Claus *et al*., 2011; Montagner *et al*., 2016)

Although numerous studies show this strong relationship between CAR, energy metabolism and the gut microbiota, the key mechanisms are still lacking.

We aimed to investigate the bidirectional relationships between CAR and the gut microbiota. Our results show that CAR is a broad sensor of the gut microbiota in the liver and small intestine. We have also demonstrated that gut microbiota does not interfere with the capacity of CAR to bind to its pharmacological ligand. Microbiota depletion decreased CAR activity in the liver and ileum of male mice. In the liver, microbiota depletion decreased hypotaurine levels, a precursor for glutathione metabolism, and decreased several microsomal testosterone hydroxylation activities in a CAR- and sex-dependent way. Conversely, CAR deletion impacted the gut microbiota composition and metabolism in male mice only, while long-term deletion of CAR influenced divergent phenotypes, where *Car*$^{-/-}$ males accumulated white adipose tissue while *Car*$^{-/-}$ females developed a slightly pro-inflammatory intestinal and systemic phenotype. Altogether, we have presented here preliminary results suggesting that CAR might be a microbial sensor in the liver that controls the host xenobiotic and lipid metabolism in a sexually dimorphic way.

MATERIALS AND METHODS

In vivo studies

In vivo studies were performed in accordance with European guidelines for the use and care of laboratory animals, and were approved by an independent Ethics Committee.

All mice were housed at the Toxalim-INRA rodent facility (Toulouse, France). The room where the mice were housed was kept at a temperature of 21-23°C on a 12-hour light (ZT0-ZT12) 12-hour dark (ZT12-ZT24) cycle and mice were allowed free access to the diet (Teklad Global 18% Protein Rodent Diet) and tap water. ZT stands for Zeitgeber time; ZT0 is defined as the time when the lights are turned on and ZT12 as the time when lights are turned off.

In the first set of experiments, forty male six-week old C57BL/6J mice were purchased from Charles River, kept for two weeks of acclimatization and then randomly allocated to the different experimental groups: control (CONT, n=8), ampicillin-treated (A, n=8), neomycin-treated (N, n=8), vancomycin-treated (WT A, n=8), wild-type ANV cocktail-treated (WT ANV, n=8). The individual antibiotics [1g/L ampicillin (Euromedex, Souffelweyersheim, France), 1 g/L neomycin (Sigma Aldrich, Steinheim, Germany), 0.5 g/L vancomycin (MP Biomedicals, Illkirch, France)] and the ANV cocktail were dissolved to their corresponding treatment groups in tap water and was distributed accordingly per bottle per cage. The antibiotic treatments were changed every 3 days. Each mouse belonging to the antibiotic groups had free access to the antibiotic mixture via their drinking water for 14 days. After 2 weeks of antibiotic treatment, mice were then sacrificed at ZT6 or ZT18.

In the second set of experiments, twelve six-week-old wild-type (WT) C57BL/ 6J male mice were purchased from Charles River and 12 *Car*$^{-/-}$ mice were used in this experiment. The *Car*$^{-/-}$ mice were backcrossed on the C57Bl/ 6J background and were engineered in Pr. Meyer's laboratory (Staudinger et al., 2001) and were bred for 10 years in our animal facility. Mice were acclimatized for two weeks, then randomly allocated to

the different experimental groups: Wild-type control (WT CONT n= 6), wild-type TCPOBOP-treated (WT TCPOBOP, n = 6), *Car*$^{-/-}$ control (*Car*$^{-/-}$ CONT, n = 6), *Car*$^{-/-}$ TCPOBOP-treated (*Car*$^{-/-}$ TCPOBOP, n= 6). TCPOBOP-treated mice received a daily intraperitoneal injection of PCN (100 mg/ kg) in corn oil for 4 days while control mice received corn oil only. Mice were sacrificed at ZT18, 18 hours after the last TCPOBOP injection.

In the third set of experiments, forty-six-week old *Car*$^{+/+}$ (20 males, 20 females) and 39 *Car*$^{-/-}$ (19 males, 20 females) littermate mice were bred at Toxalim-INRA's rodent facility. They were then kept for two weeks of acclimatization. After which, mice were randomly allocated to the different experimental groups in males: *Car*$^{+/+}$ control (*Car*$^{+/+}$ CONT, n=10), *Car*$^{+/+}$ ATB-treated (*Car*$^{+/+}$ ATB, n=10), *Car*$^{-/-}$ control (*Car*$^{-/-}$ CONT, n=10), *Car*$^{-/-}$ ATB-treated (*Car*$^{-/-}$ ATB, n=9); and in females : *Car*$^{+/+}$ control (*Car*$^{+/+}$ CONT, n=10), *Car*$^{+/+}$ ATB-treated (*Car*$^{+/+}$ ATB, n=10), *Car*$^{-/-}$ control (*Car*$^{-/-}$ CONT, n=10), *Car*$^{-/-}$ ATB-treated males (*Car*$^{-/-}$ ATB, n=10). After 2 weeks of antibiotic treatment, mice were then sacrificed at ZT18.

In the last set of experiments, twenty six-week old *Car*$^{+/+}$ (9 males, 11 females) and 22 *Car*$^{-/-}$ (12 males, 10 females) littermate mice were bred at Toxalim-INRA's rodent facility. They were then kept for two weeks of acclimatization. After which, mice were randomly allocated to the different experimental groups in males: *Car*$^{+/+}$ control (*Car*$^{+/+}$ CONT, n=9), *Car*$^{-/-}$ control (*Car*$^{-/-}$ CONT, n=12); and in females: *Car*$^{+/+}$ control (*Car*$^{+/+}$ CONT, n=11), *and* *Car*$^{-/-}$ control (*Car*$^{-/-}$ CONT, n=10). After aging the mice for 37 weeks, mice were then sacrificed at ZT18.

Bacterial Cultivation of Feces

Feces were collected at the beginning, at 7 days, and at 14 days of experimental diets under sterile conditions. Fecal samples from antibiotic-treated rats were diluted at 10^{-3}, 10^{-4}, and 10^{-5} then cultured on plate count agar medium aerobically and on Schaedler C blood medium anaerobically. Untreated mice samples were diluted at 10^{-5}, 10^{-6}, and 10^{-7} before being spread on the same culture media. Colonies forming unit were counted after 24 h at 37°C.

Blood and tissue sampling

Body weight was monitored at the beginning and at the end of each experimental period. Blood was collected at the submandibular vein into lithium heparin-coated tubes (BD Microtainer, Franklin Lake, NJ, USA) as described in Golde *et al*. (2005). Plasma was prepared by centrifugation (1500 g, 15 min, 4°C) and stored at -80°C. Following euthanasia by cervical dislocation, liver, ileum, and colon were removed, weighed, dissected, and snap-frozen in liquid nitrogen and stored at -80°C until used for RNA extraction.

Plasma Analysis

Alanine transaminase (ALT), high- or low-density lipoprotein (HDL-LDL), total cholesterol, triglycerides and free fatty acids (FFA) were determined using a Pentra 400 biochemical analyzer (Anexplo facility, Toulouse, France).

Gene expression Studies

Total RNA was extracted with with TRI Reagent® (Molecular Research Center). RNAs were quantified using nanodrop (NanoDropTM 1000; Thermo Scientific). Two micrograms of total RNA were reverse transcribed using the High-Capacity cDNA Reverse Transcription Kit (Applied BiosystemsTM). The SYBR Green (Applied Biosystems, California) assay primers are presented in supplementary table 1. Amplification was performed using an ABI Prism 7300 Real-Time PCR System (Applied Biosystems™). Quantitative real-time polymerase chain reaction (qPCR) data were normalized to TATA-box-binding protein mRNA levels and analyzed with LinRegPCR (version 2015.3; Jan Ruijter) to get mean efficiency (NO), which is calculated as follows: NO = threshold=ðEff mean^{Cq} Þ with Eff mean: mean PCR efficiency and CQ: quantification cycle.

Testosterone hydroxylation assay

Chemicals

Acetic acid, ethanol, sodium chloride, potassium dihydrogen phosphate, dibasic potassium phosphate, monobasic sodium phosphate, dibasic heptahydrate sodium phosphate, potassium sodium tartrate tetrahydrate, glycerol, Folin & Ciocalteu's phenol reagent, albumin from bovine serum, anhydrous sodium carbonate, NADP, D-glucose 6-phosphate sodium salt, glucose-6-phosphate dehydrogenase, magnesium chloride, 1-chloro-2,4-dinitrobenzene, reduced L-glutathione and testosterone were purchased from Sigma-Aldrich Merck (Saint Quentin Fallavier, France). Acetonitrile and methanol (HPLC grade) were purchased from Thermo Fisher Scientific (Waltham, MA, USA). Ammonium acetate, sodium hydroxide and copper sulfate were purchased from VWR (Fontenay-sous-Bois, France). Flo-Scint™ II and Ultima Gold™ liquid scintillation cocktails were purchased

from PerkinElmer (Courtabœuf, France). Ultrapure water produced by a Milli-Q system (Millipore, Saint-Quentin-en-Yvelines, France) was used for the preparation of HPLC mobile phases.

[^{14}C]-testosterone (specific activity: 2.18 GBq/mmol) was purchased from PerkinElmer and its radiopurity was 98.8 %, as determined by radio-HPLC. Standards of testosterone metabolites were purchased from Steraloids (Newport, RI, USA): 15β-hydroxytestosterone, 6α-hydroxytestosterone, 6β-hydroxytestosterone, 19-hydroxytestostérone, 15α-hydroxytestosterone, 11α-hydroxytestosterone, 6β-hydroxyandrostenedione, 11α-hydroxyandrostenedione, 16β-hydroxytestosterone, 4-androsten-16α-ol-3,17-dione, 2α-hydroxytestosterone, 2α-hydroxyandrostenedione, 4,6-androstadien-17β-ol-3-one, 7α-hydroxytestosterone and from Sigma-Aldrich: dihydroandrosterone, androstanolone, 16α-hydroxytestosterone, 11β-hydroxytestosterone, 2β-hydroxytestosterone, 11β-hydroxyandrost-4-ene-3,17-dione, 1-dehydrotestosterone, androstenedione, epitestosterone, androsterone, estradiol and estrone.

Sub-cellular fraction preparation and protein content

Following mice euthanasia, livers were collected, immediately perfused using NaCl 0.9 %. They were weighed and frozen in liquid nitrogen until sub-cellular fraction preparation, which was carried out within a month. Livers were thawed and homogenized at 4°C using a Potter-Elvehjem Teflon glass homogenizer in 4 volumes/g of ice-cold sodium/phosphate buffer 0.1 M pH 7.4. Microsomal and cytosolic hepatic fractions were obtained after two centrifugation steps at 4°C (20 min at 9 000 *g* and 70 min at 105 000 *g*)

using a Beckman Optima XPN-80 ultracentrifuge (Villepinte, France). Microsomes were resuspended with gentle homogenization in 1 mL/g of ice-cold sodium/phosphate buffer 0.1 M pH 7.4 with 20 % glycerol (v/v). Sub-cellular fractions were stored at 80°C in cryotubes until use. The protein content of sub-cellular fractions was determined using the Lowry et al. (1951) method, which was adapted for microplate reading, using a Tecan Infinite 200 (Männedorf, Switzerland) (Lowry *et al.*, 1951).

[^{14}C]-testosterone incubations

Mice hepatic microsomes (0.5 mg proteins/mL) were incubated at 37°C under shaking with 10 µM [^{14}C]-testosterone (3.58 kBq per incubation in 5 µL ethanol) fortified with unlabelled testosterone. Incubations were performed in a final volume of 0.5 mL in 0.1 M sodium/phosphate buffer pH 7.4 with 5 mM $MgCl_2$. Incubations were initiated using a NADPH generating system: 1.3 mM NADP, 5 mM glucose-6-phosphate, 1 IU glucose-6-phosphate dehydrogenase. The kinetic of testosterone metabolites formation was established between 10 min and 60 min. An incubation time of 20 min was selected in order to ensure a linear formation of testosterone metabolites. Incubations were stopped with 1.5 mL methanol, kept 30 min on ice and centrifuged 10 min at 6 500 *g*, 4°C (3MK Sigma centrifuges, Newtown Wem Shropshire, UK). Radioactivity measurements (10 µL) were performed before storage at -20°C, pending further radio-HPLC analysis. Radioactivity measurements were carried out using a Tri-Carb 2910TR (PerkinElmer) liquid scintillation analyzer, using Ultima Gold™ as the scintillation cocktail (PerkinElmer). Sample quenching was compensated by the use of quench curves and external standardization.

For the LC-MS confirmation of major testosterone's metabolites structure, additional incubations were carried out using unlabeled testosterone (50 µM) and pooled microsomes (1 mg proteins/mL, pool of 10 PXR control mice) during 30 min, in the same conditions.

Radio-HPLC profiling and quantification

Incubation media were individually analyzed by radio-HPLC for testosterone metabolites profiling and quantification. Reversed-phase high-performance liquid chromatography (R-HPLC) analysis were performed on an Ultimate-3000 system (Thermo Fisher Scientific) coupled with a flow scintillation analyzer Flo-One Radiomatic™ 610TR (PerkinElmer). The HPLC system consisted of Nucleoshell RP18 column (250 x 4.6 mm, 5 µm, Macherey-Nagel, Hoerdt, France) coupled to a C18 guard precolumn (Nucleoshell RP18 5 µm EC 4/3, Macherey-Nagel), maintained at 35°C. Mobile phases were A: ammonium acetate buffer (20 mM, adjusted to pH 3.5 with acetic acid) and B: acetonitrile. The flow rate was 1 mL/min and the injection volume was 500 µL. The gradient was as follow: 0-35 min A:B from 80:20 to 60:40 (v/v); 35-45 min from 60:40 to 40:60; 45-48 min from 40:60 to 100 % B. The system returned to the initial condition at 51 min and held for another 4 min. Flo-Scint™ II (PerkinElmer) was used as scintillation cocktail, at a flow rate of 2 mL/min, and with a 500-µL detection cell. Each incubation media (800 µL, corresponding to *ca.* 1.5 kBq) was evaporated to dryness and reconstituted in mobile phase A:B 80:20 (v/v) prior to HPLC injection.

In this system, the retention time (RT) of testosterone was 29.8 min. R-HPLC profiles were processed with the A500 software (PerkinElmer) using a background suppression of 20 cpm (counts per minute) and an efficiency correction (80 % for [^{14}C]). Metabolites were

quantified by integrating the area under the peaks monitored by radioactivity detection. All peaks above 4 % of the detected radioactivity were quantified for each animal. Mean results were expressed in nmol/min/mg protein ± SEM (n=5 mice per group).

Mass spectrometry analysis

Unlabeled testosterone incubation media were analyzed by LC-MS using the same chromatographic conditions. Testosterone metabolites structure was established based on their mass and on the similarity of their retention time with authentic standards. Media were analyzed by LC-MS using a RSLC3000 HPLC system (Thermo Fisher Scientific) coupled to a HRMS system LTQ Orbitrap XL mass spectrometer (Thermo Fisher Scientific) with a post-column split (0.2 mL/min in the source) using positive electrospray ionization (ESI). The injection volume was 50 µL, the source voltage was 1.80 kV, the capillary voltage was 30V, the capillary temperature was 350°C, the sheath gas (N_2) flow (arbitrary unit) was 50, the auxiliary gas (N_2) flow (arbitrary unit) was 40, the sweep gas (N_2) flow (arbitrary unit) was 0 and the tube lens offset was 115 V.

Proton Nuclear Magnetic Resonance (^{1}H-NMR) Based Metabolomics

Liver and caecal content polar extracts were prepared for NMR analysis as described previously (Beckonert *et al.*, 2007; Martin *et al*., 2019). All ^{1}H-NMR spectra were obtained on a Bruker DRX-600-Avance NMR spectrometer (Bruker) using the AXIOM metabolomics platform (MetaToul) operating at 600:13MHz for ^{1}H resonance frequency using an inverse detection 5-mm ^{1}H-^{13}C-^{15}N cryoprobe attached to a cryoplatform (the preamplifier cooling unit). The ^{1}H-NMR spectra were acquired at 300 K using a standard one-dimensional noesypr1D pulse sequence with water presaturation and a total spin-

echo delay (2 ns) of 100 ms. Data were analyzed by applying an exponential window function with a 0.3-Hz line broadening prior to Fourier transformation. The resulting spectra were phased, baseline-corrected, and calibrated to trimethylsilylpropanoic acid (TSP) (0:00 ppm) manually using Mnova NMR (version 9.0; Mestrelab Research S.L.). The spectra were subsequently imported into MatLab (R2014a; MathsWorks, Inc.). All data were analyzed using full-resolution spectra. The region containing the water resonance (4:6– 5:2 ppm) was removed, and the spectra were normalized to the probabilistic quotient [26] and aligned using a previously published function (Veselkov *et al.*, 2009).

Data were mean-centered and scaled using the unit variance scaling prior to analysis with orthogonal projection on latent structure-discriminant analysis (O-PLS-DA). The O-PLS derived model was evaluated for goodness of prediction (Q^2Y value) using n-fold cross-validation, where n depends on the sample size. The parameters of the final models are indicated in the figure legends. Metabolite identification and discrimination between the groups were done by calculating the O-PLS-DA correlation coefficients (r^2) for each variable and back-scaled into a spectral domain so that the shapes of the NMR spectra and the signs of the coefficients were preserved [28]. The weights of the variables were color-coded according to the square of the O-PLS-DA correlation coefficients. Correlation coefficients extracted from significant models were filtered so that only significant correlations above the threshold defined by Pearson's critical correlation coefficient ($p < 0:05$; $r > 0.55$; for $n = 6$ per group) were considered significant. For illustration purposes, the area under the curve of several signals of interest was integrated and significance tested with a univariate test.

High-throughput Sequencing of Bacterial content

DNA extraction and sequencing of 16S rRNA gene regions.

The microbial population present in the samples has been determined using next generation high throughput sequencing of variable regions of the 16S rRNA bacterial gene. The workflow was established by Vaiomer (Lluch *et al.*, 2015). (*1)Library construction and sequencing***:** The PCR amplification was performed using 16S universal primers targeting the V3-V4 regions of the bacterial 16S ribosomal gene (Vaiomer universal 16S primers). For each sample, a sequencing library was generated by addition of sequencing adapters. The detection of the sequencing fragments was performed with the MiSeq Illumina technology using the 2 x 300 paired-end MiSeq kit. *(2) Bioinformatics pipeline:* The targeted metagenomic sequences from microbiota were analyzed using the bioinformatics pipeline established by Vaiomer from the FROGS guidelines (Escudié *et al.*, 2018). Briefly, after demultiplexing of the barcoded Illumina paired reads, single read sequences were cleaned and paired for each sample independently into longer fragments. Operational taxonomic units (OTUs) were produced via single-linkage clustering and taxonomic assignment is performed in order to determine community profiles.

Data Analysis

Reads obtained from the MiSeq sequencing system have been processed using the Vaiomer bioinformatics pipeline. The steps included quality-filtering, clustering into OTUs with the Swarm algorithm and taxonomic affiliation. Alpha diversity was analyzed with different methods (median + interquartile), 1) Observed, 2) Chao1, 3) Shannon, 4) Simpson, and 5) Inverse Simpson. Beta diversity (β-diversity) was measured with numeric

values for the "all against all" with Jaccard, Bray-Curtis, Unifrac and Weighted Unifrac. Graphical representations of the relative proportion of taxa were made at each taxonomic level (Phylum, Class, Order, Family, and Genus) for all study samples. "Linear discriminant analysis Effect Size" (LEfSe) (Segata *et al*., 2011) was the algorithm used to identify taxonomic groups characterizing the differences between two or more biological conditions. LEfSe was run using default values (alpha value of 0.5 for both the factorial Kruskal-Wallis test among classes and the pairwise Wilcoxon-Mann-Whitney test between subclasses, threshold of 2.0 for the logarithmic LDA score for discriminative features) and the strategy for multi-class analysis set to 'all-against-all'. The LEfSe analysis was performed on the complete sequence data (no OTU abundance threshold) for identifying genotype effect on either males or females and sex effect on either $Car^{+/+}$ or $Car^{-/-}$ mice.

Statistical Analysis

Statistical analyses were performed using GraphPad Prism for Mac OS X (version 7.00; GraphPad Software). One-way or two-way analysis of variance (ANOVA) was performed, followed by appropriate posthoc tests (Bonferroni) when differences were found statistically significant. When only two groups were compared, the student's t-test was used; $p < 0:05$ was considered significant.

RESULTS

Car is a broad sensor of the gut microbiota in the liver and small intestine

We treated C57Bl6/J male mice with several individual antibiotics (ampicillin, neomycin and vancomycin) or the combination of these (ANV cocktail) for 2 weeks and

sacrificed them at ZT6 or ZT18 (**Figure 1A-C, Supplementary Figure 1**). Female C57Bl6/J mice were treated with the ANV cocktail for 2 weeks and sacrificed at ZT18 (Figure 1D-F, Supplementary Figure 1). We monitored CAR's prototypical target genes' (*Cyp2b10* and *Cyp2c55*) mRNA expression in the liver, small and large intestine (**Figure 1**). To avoid a direct effect of the drugs on CAR activity in the liver, we tested only antibiotics that are described as poorly absorbed (**Supplementary Table 1**).

In the liver at ZT6, vancomycin significantly decreased *Cyp2c55* expression, while the ANV cocktail decreased both *Cyp2b10* and *Cyp2c55* expression. At ZT18, *Cyp2b10* expression was 3 times higher than at ZT6, and ANV cocktail significantly decreased *Cyp2b10* and *Cyp2c55* expression in both males and females (**Figure 1A & D**).

In the ileum, *Cyp2b10* expression at ZT18 was 4 times higher than at ZT6 while the antibiotic-treated groups did not significantly differ from their controls. *Cyp2c55* expression was significantly decreased across all treatments at both ZT6 and ZT18 in males and females (**Figure 1B & E**).

Interestingly, in the colon, CYP expression was not significantly affected by any antibiotic treatment in males. In females, we observed a slight decrease in *Cyp2c55* expression.

Altogether, these results first show that CAR activity is sensitive to circadian rhythm and is higher at ZT18, confirming previous studies (Montagner *et al.*, 2016). Moreover, CAR seems less responsive to gut microbiota-derived signals in the colon than in the small intestine and the liver, at least in males.

Gut microbiota suppression does not interfere with the pharmacological activation of CAR

To determine if gut microbiota suppression could interfere with CAR's capacity to bind and respond to its ligands, we used WT and *Car*$^{-/-}$ male mice treated with antibiotics (ATB), with 1,4-Bis-[2-(3,5-dichloropyridyloxy)]benzene, 3,3′,5,5′-Tetrachloro-1,4-bis(pyridyloxy)benzene (TCPOBOP, the pharmacological agonist of CAR) or a combination of both (**Figure 2**). TCPOBOP treatment significantly increased liver weight in a CAR-dependent way, but to a similar extent in the TCPOBOP and TCPOBOP+ATB groups. ATB treatment increased caecum weight, but to a similar extent in the ATB and ATB+TCPOBOP groups (**Figure 2A**). The CAR-dependent induction of *Cyp2b10* and *Cyp2c55* mRNA expression was similar in the TCPOBOP and TCPOBOP+ATB groups in the liver (**Figure 2B**) and ileum (**Figure 2C**). These results show that gut microbiota depletion does not interfere with CAR's capacity to bind and respond to its pharmacological ligand.

Gut microbiota is altered in Car-/- male mice

To determine whether CAR conversely affected the gut microbiota, we used *Car*$^{+/+}$ *vs Car*$^{-/-}$ littermate mice and compared their cecal microbiota using 16S rRNA sequencing (**Figure 3**). In males, CAR depletion significantly increased alpha-diversity (observed and chao1 indexes) (**Figure 3A**), while no significant difference in biodiversity was observed in females (**Figure 3B**). At the OTU level, significant clustering is seen in the hierarchical clustering and Principal Coordinate Analysis (PcoA) of *Car*$^{+/+}$ *vs Car*$^{-/-}$ male mice but not in females (**Figure 3C-F**). This clustering in male mice is evident in the first PCoA axis that represents 27.8% of the variance (**Figure 3D**). Using the linear discriminant analysis (LDA)

effect size (LEfSe) pipeline, we confirmed significant differences in the baseline caecal microbiota composition of *Car*$^{-/-}$ male mice, as compared to that in *Car*$^{+/+}$ mice (**Figure 3G & H**). *Car*$^{-/-}$ male mice had a decreased relative abundance of *Akkermansia*, *Anaerostipes*, *Lachnoclostridium*, and *Parabacteroides* and a decreased relative abundance of *Ruminococcus 1*, (*Eubacterium) ventrosium* group, (*Eubacterium) xylanophilum* group, *Ruminococcaceae UCG-014, Coprococcus 2, and Odoribacter* (**Supplementary Figure 2A**). There were no differences found between *Car*$^{+/+}$ vs *Car*$^{-/-}$ females (**Supplementary figure 2B, Supplementary Figure 3**).

We then investigated the metabolic profiles of caecal content in *Car*$^{+/+}$ *vs Car*$^{-/-}$ mice using ^{1}H-NMR-based profiling (**Figure 4**). The discrimination between the caecal content metabolic profiles of *Car*$^{+/+}$ *vs Car*$^{-/-}$ males was significant (**Figure 4A**, parameters of the O-PLS-DA model: $Q^2Y=0.65$, $p=0.001$), but not that of *Car*$^{+/+}$ *vs Car*$^{-/-}$ females (**Figure 4D**, $Q2Y<0$, $p>0.05$).,The O-PLS-DA coefficient plots illustrate several peaks contributing to the significant separation of *Car*$^{+/+}$ *vs Car*$^{-/-}$ males (highlighted in red in **Figure 4B**): one doublet of doublet at 8.12 ppm, two singulets at 6.13 and 6.15 ppm and one triplet at 5.99 ppm that were higher in *Car*$^{-/-}$ mice, while 2 singulets at 8.38 and 8.03 ppm and five doublets at 7.91, 7.86, 6.07, 5.95 and 5.91 ppm were higher in *Car*$^{+/+}$ male mice. Statistical total correlation spectroscopy (STOCSY) analyses and additional 2D-NMR experiments (COSY and TOCSY) confirmed that these 2 groups of peaks belonged to 2 metabolites. Spike in experiments of pure standard confirmed that the metabolite higher in *Car*$^{-/-}$ mice could be assigned to uridine monophosphate (UMP) (data not shown), while available structural information did not allow us to formally identify the other discriminating metabolite. O-PLS-DA models between caecal content profiles of *Car*$^{+/+}$ *vs*

Car$^{-/-}$ females (**Figure 4E**) did not highlight any significant differences between the 2 groups. Integration of the area under the curve for the discriminating peaks, followed by univariate statistics confirmed a higher caecal UMP content and a lower level of the unknown metabolite in *Car*$^{-/-}$ males compared to Car+/+ males (**Figure 4C**). Interestingly, caecal content metabolomics of ATB-treated mice confirmed that the caecal levels of both UMP and of this unidentified metabolite depend on the gut microbiota since they were lower in ATB-treated mice compared to the control mice (data not shown).

Collectively, these data demonstrate that CAR plays a role in shaping the gut microbiota in a sexually-dimorphic manner, and that the male-specific CAR-dependant microbiota might display significant differences in nucleotide metabolism.

Gut microbiota suppression decreases CAR activity in the liver and in the ileum of male mice

To further investigate the gut microbiota-CAR interactions, we depleted the gut microbiota of the *Car*$^{+/+}$ *vs* *Car*$^{-/-}$ male and female littermate mice with ATB. **Supplementary Figure 4** confirms the successful depletion of the gut microbiota. We observed a significant decrease in CAR activity upon microbiota depletion in the liver of male (**Figure 5A**) and female mice (**Figure 5B**). The same decrease in CAR activity is extended in the ileum of male mice (**Figure 5C**) but surprisingly no difference is seen in females (**Figure 5D**).

Gut microbiota-CAR interaction influences host's hepatic metabolism

To determine if these changes in the microbiota could in turn affect the host metabolism, we first investigated the effect of ATB on plasma biochemistry in *Car*$^{+/+}$ *vs* *Car*$^{-/-}$ mice (**Supplementary Figure 5**). CAR deletion significantly influenced circulating

cholesterol, HDL and LDL levels. However, no significant effect of ATB was observed in male or female *Car*$^{+/+}$ mice.

We next focused on the liver and first conducted ^{1}H-NMR profiling of liver tissue (**Figure 6**). O-PLS-DA coefficient plots highlighted several peaks (2 triplets at 2.66 and 3.37 ppm respectively) that were higher in *Car*$^{+/+}$ compared to *Car*$^{-/-}$ male mice (**Figure 6A**). This difference was not observed in ATB-treated males (**Figure 6B**). No significant differences were observed between *Car*$^{+/+}$ and *Car*$^{-/-}$ females (**Figure 6D & E**). Integration of the area under the curve for the hypotaurine signals, followed by univariate statistics confirmed that hepatic hypotaurine levels were significantly affected by both ATB and CAR deletion in males (**Figure 6C**). Moreover, ATB-induced decrease in hypotaurine level was CAR-dependent, since no significant decrease was observed in ATB-treated *Car*$^{-/-}$ males (**Figure 6C**). In females, hypotaurine levels were also lower upon ATB treatment, but were not influenced by CAR deletion (**Figure 6F**). Hypotaurine is known for its antioxidant activity and is a precursor to glutathione metabolism (Aruoma *et al*., 1988).

We next investigated the oxidative metabolism of [4-^{14}C] testosterone in male liver microsomes. This measurement shows the global ability of CYPs to metabolize sterol compounds (**Figure 7**). Peak at retention time (RT) of 13.9 minutes was significantly different between *Car*$^{-/-}$ and *Car*$^{+/+}$ mice, but was not affected by ATB treatment. Upon microbiota suppression, the peak with RT at 14.7 min was significantly decreased in a CAR-dependent way, while the peak with RT of 10.0 minutes was significantly increased in a CAR-dependent way. Several structural hypotheses could be made based (1) on RT comparison with authentic testosterone metabolites standards, for those commercially available (LC-MS experiments), and (2) on the confirmation of the m/z ions detected in LC-

MS (ESI, positive mode) when analyzing incubation media from incubations carried out with non-radio labeled testosterone. The peak with a RT of 14.7 min was identified as a HO-Δ-testosterone (m/z: 303.1955), but no formal identification of the hydroxylation position could be achieved. Of note, this metabolite was clearly found to be distinct from 16α-HO-Δ-testosterone, for which the authentic standard is available.

Long-term CAR deletion induces a sexually dimorphic phenotype: preliminary evidence

Since we observed a significant gut microbiota dysbiosis upon CAR-deletion in male mice, we then investigated the long-term consequences of CAR deletion in male and female mice. *Car*$^{+/+}$ and *Car*$^{-/-}$ male and female littermate mice were aged until 37 weeks with free access to a standard rodent chow and tap water. Body weight was monitored on a weekly basis and no difference was observed between *Car*$^{+/+}$ and *Car*$^{-/-}$ groups in males (**Figure 8A**) and females (Figure 8C). At age 32 weeks, an oral glucose tolerance test (OGTT) was conducted, and no differences were found (**Figure 8B & J**). Upon sacrifice at 37 weeks, no significant difference was observed in plasmatic ALT, HDL, LDL, triglyceride, cholesterol and FFA levels in males (**Figures 8C-H**) and females (**Figures 8K-P**).

At sacrifice, the liver, caecum and spleen were significantly heavier, while colon length was significantly shorter in *Car*$^{-/-}$ compared to *Car*$^{+/+}$ females, while no differences were found in brown adipose tissue (BAT), perigonadal and subcutaneous white adipose tissue (WAT) weights (**Figure 9**). In males, the perigonadal and subcutaneous WAT were heavier in *Car*$^{-/-}$ mice compared to *Car*$^{+/+}$ mice (**Figure 9**). Thus, a sexually dimorphic phenotype was observed on the physiological impact of CAR deletion in littermate mice:

in females, CAR deletion induced a slight pro-inflammatory intestinal and systemic phenotype, while in males, CAR deletion promoted WAT accumulation. The potential role of the CAR-induced gut microbiota dysbiosis in this dimorphic phenotype remains to be investigated.

DISCUSSION

This work is ongoing and still requires several complementary experiments. Discussion about perspectives of this work will be found in the next general discussion chapter.

REFERENCES

Beckonert, O., Keun, H. C., Ebbels, T. M. D., Bundy, J., Holmes, E., Lindon, J. C., & Nicholson, J. K. (2007). Metabolic profiling, metabolomic and metabonomic procedures for NMR spectroscopy of urine, plasma, serum and tissue extracts. *Nature Protocols*, *2*(11), 2692–2703. https://doi.org/10.1038/nprot.2007.376

Björkholm, B., Bok, C. M., Lundin, A., Rafter, J., Hibberd, M. L., & Pettersson, S. (2009). Intestinal Microbiota Regulate Xenobiotic Metabolism in the Liver. *PLOS ONE*, *4*(9), e6958. https://doi.org/10.1371/journal.pone.0006958

Chai, S. C., Cherian, M. T., Wang, Y.-M., & Chen, T. (2016). Small-molecule modulators of PXR and CAR. *Biochimica Et Biophysica Acta*, *1859*(9), 1141–1154. https://doi.org/10.1016/j.bbagrm.2016.02.013

Claus, S. P., Ellero, S. L., Berger, B., Krause, L., Bruttin, A., Molina, J., … others. (2011). Colonization-induced host-gut microbial metabolic interaction. *MBio*, *2*(2), e00271–10.

Escudié, F., Auer, L., Bernard, M., Mariadassou, M., Cauquil, L., Vidal, K., … Pascal, G. (2018). FROGS: Find, Rapidly, OTUs with Galaxy Solution. *Bioinformatics*, *34*(8), 1287–1294. https://doi.org/10.1093/bioinformatics/btx791

Gao, J., & Xie, W. (2010). Pregnane X Receptor and Constitutive Androstane Receptor at the Crossroads of Drug Metabolism and Energy Metabolism. *Drug Metabolism and Disposition*, *38*(12), 2091–2095. https://doi.org/10.1124/dmd.110.035568

Lluch, J., Servant, F., Païssé, S., Valle, C., Valière, S., Kuchly, C., … Lelouvier, B. (2015). The Characterization of Novel Tissue Microbiota Using an Optimized 16S Metagenomic Sequencing Pipeline. *PLOS ONE*, *10*(11), e0142334. https://doi.org/10.1371/journal.pone.0142334

Lowry, O. H., Rosebrough, N. J., Farr, A. L., & Randall, R. J. (1951). Protein measurement with the Folin phenol reagent. *The Journal of Biological Chemistry*, *193*(1), 265–275.

Martin, O. C. B., Olier, M., Ellero-Simatos, S., Naud, N., Dupuy, J., Huc, L., … Pierre, F. H. F. (2019). Haem iron reshapes colonic luminal environment: Impact on mucosal homeostasis and microbiome through aldehyde formation. *Microbiome*, *7*(1), 72. https://doi.org/10.1186/s40168-019-0685-7

Montagner, A., Korecka, A., Polizzi, A., Lippi, Y., Blum, Y., Canlet, C., … Wahli, W. (2016). Hepatic circadian clock oscillators and nuclear receptors integrate microbiome-derived signals. *Scientific Reports*, *6*, 20127. https://doi.org/10.1038/srep20127

Segata, N., Izard, J., Waldron, L., Gevers, D., Miropolsky, L., Garrett, W. S., & Huttenhower, C. (2011). Metagenomic biomarker discovery and explanation. *Genome Biology*, *12*(6), R60. https://doi.org/10.1186/gb-2011-12-6-r60

Staudinger, J. L., Goodwin, B., Jones, S. A., Hawkins-Brown, D., MacKenzie, K. I., LaTour, A., … Kliewer, S. A. (2001). The nuclear receptor PXR is a lithocholic acid sensor that protects against liver toxicity. *Proceedings of the National Academy of Sciences of the United States of America*, *98*(6), 3369–3374. https://doi.org/10.1073/pnas.051551698

Venkatesh, M., Mukherjee, S., Wang, H., Li, H., Sun, K., Benechet, A. P., … Mani, S. (2014). Symbiotic Bacterial Metabolites Regulate Gastrointestinal Barrier Function via the Xenobiotic Sensor PXR and Toll-like Receptor 4. *Immunity*, *41*(2), 296–310. https://doi.org/10.1016/j.immuni.2014.06.014

Veselkov, K. A., Lindon, J. C., Ebbels, T. M. D., Crockford, D., Volynkin, V. V., Holmes, E., … Nicholson, J. K. (2009). Recursive Segment-Wise Peak Alignment of Biological 1H NMR Spectra for Improved Metabolic Biomarker Recovery. *Analytical Chemistry*, *81*(1), 56–66. https://doi.org/10.1021/ac8011544

FIGURE LEGENDS

Figure 1: Effect of individual antibiotic treatments on CAR target genes. C57Bl6/J male mice were treated with individual treatments of ampicillin, neomycin, vancomycin or a cocktail of the three antibiotics (ANV) for 2 weeks in their drinking water and sacrificed at ZT6 or ZT18, while females were treated with the ANV cocktail and sacrificed at ZT18. RT-qPCR results are presented as mean±SEM for n=8 per group. *p≤0.05, **p≤0.01, ***p≤0.005 for ATB effect compared to control group; # p≤0.05 for ZT effect; $ p≤0.05, $$ p≤0.01, $$$ p≤0.005 for sex effect. P-values were derived from 1-way or 2-way ANOVA and Bonferroni's post-tests.

Figure 2: Effect of microbiota depletion on CAR activation via its pharmacological agonist. WT and *Car*$^{-/-}$ male mice were treated with an antibiotic cocktail of ampicillin, neomycin and vancomycin (ATB), the pharmacological agonist of CAR (TCPOBOP) or a combination of both (ATB+TCPOBOP). Impact on (A) liver and cecum weight, RT-qPCR expression of CAR's target genes in the (B) liver and (C) ileum. Data are mean±SEM of n=5-6 per group. $p≤0.05, $$p≤0.01, $$$p≤0.001 for PCN effect; *p≤0.05, **p≤0.01, ***p≤0.005 for genotype effect using 2-way ANOVA and Bonferroni's post-tests

Figure 3: Gut microbiota composition in *Car*$^{-/-}$ vs *Car*$^{+/+}$ mice. Alpha-diversity measures in caecal content of *Car*$^{-/-}$ vs *Car*$^{+/+}$ (A) male and (B) female littermate mice. Beta-diversity represented by hierarchical clustering based on the Bray distances of *Car*$^{+/+}$ (red) *vs*. *Car*$^{-/-}$ (blue) (C) male or (E) female mice and by PCoA analysis based on the Bray distances in (D) male and (F) female mice. Circular cladograms generated from LEFSe analysis showing the most differentially abundant taxa enriched in fecal microbiota from *Car*$^{+/+}$ (green) or *Car*$^{-/-}$ (red) (G) male mice. Log(LDA scores)>2 and significance of $\alpha<0.05$ determined using Wicoxon-Mann Whitney test.

Figure 4: 1H-NMR based metabolomics analysis of caecal content extracts in *Car*$^{-/-}$ and *Car*$^{+/+}$ mice. Score plots related to the O-PLS-DA models derived from the ^{1}H-NMR spectra of caecal content extract from (A) *Car*$^{+/+}$ *vs* *Car*$^{-/-}$ males and (D) *Car*$^{+/+}$ *vs* *Car*$^{-/-}$ females. Coefficient plots related to the O-PLS-DA models from (B) *Car*$^{+/+}$ *vs* *Car*$^{-/-}$ males and (E) *Car*$^{+/+}$ *vs* *Car*$^{-/-}$ females. Metabolites are color-coded according to their correlation coefficient (R), red indicating a very strong positive correlation. The direction of the metabolite indicates the group with which it is positively associated: metabolites pointing upward are higher in *Car*$^{-/-}$ mice and metabolites pointing downward are higher in *Car*$^{+/+}$ mice. Area under the curve of the ^{1}H-NMR spectra was integrated for the uridine monophosphate (UMP) signal (doublet at 8.12 ppm) and the unknown metabolite signals (2 singulets at 8.38 and 8.03 ppm and five doublets at 7.91, 7.86, 6.07, 5.95 and 5.91 ppm) in (C) male and (F) female mice. Data are mean±SEM of n=8-10 per group. *p≤0.05, **p≤0.01, ***p≤0.005 for genotype effect using Wilcoxon tests.

Figure 5: CAR activity upon microbiota depletion in male and female *Car*$^{-/-}$ vs *Car*$^{+/+}$ littermate mice. C57Bl6/J *Car*$^{+/+}$ and *Car*$^{-/-}$ male and female littermate mice were treated with an antibiotic cocktail of ampicillin, neomycin and vancomycin (ATB) for 2 weeks. RT-qPCR gene expression of *Car, Cyp2b10 and Cyp2c55* in the liver of (A) male mice and (B) female mice; and the ileum of (C) male mice (D) female mice. Data are mean±SEM of n=8-10 per group. *p≤0.05, **p≤0.01, ***p≤0.005 for ATB effect, #p≤0.05 ##p≤0.01, ###p≤0.005 for genotype effect using 2-way ANOVA and Bonferroni's post-tests.

Figure 6: 1H-NMR based metabolomics analysis of hepatic extracts in *Car*$^{-/-}$ and *Car*$^{+/+}$ mice. Coefficient plots related to the O-PLS-DA models derived from the 1H-NMR spectra of hepatic extract from (A) *Car*$^{+/+}$ *vs Car*$^{-/-}$ males, (B) *Car*$^{+/+}$+ ATB *vs Car*$^{-/-}$ + ATB males, (C) *Car*$^{+/+}$ *vs Car*$^{-/-}$ females, (D) *Car*$^{+/+}$+ ATB *vs*. *Car*$^{-/-}$ + ATB females. Metabolites are color-coded according to their correlation coefficient (R), red indicating a very strong positive correlation. The direction of the metabolite indicates the group with which it is positively associated: metabolites pointing upward are higher in *Car*$^{+/+}$ mice and metabolites pointing downward are higher in *Car*$^{-/-}$ mice. Area under the curve of the 1H-NMR spectra was integrated for the hypotaurine signals (triplet at 2.65 ppm) in (C) males and (F) females. Data are mean±SEM of n=8-10 per group. *p≤0.05, **p≤0.01, ***p≤0.005 for ATB effect; #p≤0.05 ##p≤0.01, ###p≤0.005 for genotype effect; §§§ p≤0.005 for gender effect using 2-way ANOVA and Bonferroni's post-tests.

Figure 7: Impact of gut microbiota depletion on hepatic xenobiotic metabolism in *Car*$^{-/-}$ vs *Car*$^{+/+}$ male mice. Profile of ^{14}C metabolites of testosterone after incubation with liver microsomes from male mice. Data are mean±SEM of n=5 per group. *p≤0.05, **p≤0.01, ***p≤0.005 for ATB effect, #p≤0.05 ##p≤0.01, ###p≤0.005 for genotype effect using 2-way ANOVA and Bonferroni's post-tests.

Figure 8: Impact of long-term CAR deletion on metabolic parameters and plasma biochemistry in *Car*$^{-/-}$ vs *Car*$^{+/+}$ littermate mice. *Car*$^{+/+}$ and *Car*$^{-/-}$ male and female littermate mice were aged until 37 weeks with free access to a standard rodent chow and water. Body weight in (A) male and (I) female mice, OGTT values and area under the curve (AUC) in 32 week-old (B) males and (J) females. Plasmatic alanine aminotransferase (ALT), high density lipoprotein (HDL), low density lipoprotein (LDL), triglyceride, cholesterol, and free fatty acid levels in male (C-H) and female mice (K-P).

Figure 9: Effect of long-term CAR deletion on organ weights. *Car*$^{+/+}$ and *Car*$^{-/-}$ male and female littermate mice were kept until 37 weeks of age with free access to a standard rodent chow and water. (A) Body weight, (B) liver weight (C) spleen weight, (D) Brown adipose tissue (BAT) weight, (E) perigonadal and subcutaneous white adipose tissue (WAT) weights, (F) caecum weight and colon length in male mice. (A) Body weight, (B) liver weight (C) spleen weight, (D) BAT weight, (E) perigonadal and subcutaneous WAT weights, (F) caecum weight and colon length in female mice. Data are mean±SEM of n=8-

10 per group. #p≤0.05, ##p≤0.01,###p≤0.005 for genotype effect using unpaired student test.

SUPPLEMENTARY FIGURE LEGENDS

Supplementary Figure 1: Effect of various ATB treatment on physiological parameters. (A) Body, (B) liver, and (C) caecum weight of male mice sacrificed at ZT6 and ZT18. (D) Body and (E) caecum, weight of male and female mice sacrificed at ZT18. Anaerobic fecal microbial count after 2 weeks of ANV cocktail treatment of male mice sacrificed at ZT18.

Supplementary Figure 2: Effect of *Car* deletion on caecal microbiota community distribution. Graphical representations of the relative proportion of taxa at the Genus level between *Car*$^{+/+}$ vs *Car*$^{-/-}$ (A) male and (B) female mice from the LEfSe analysis. Data are mean±SEM of n=8-10 per group. #p≤0.05, ##p≤0.01, ###p≤0.005 for genotype effect using unpaired student test.

Supplementary Figure 3: Circular cladograms generated from LEFSe analysis showing the most differentially abundant taxa enriched in fecal microbiota from *Car*$^{+/+}$ (green) or *Car*$^{-/-}$ (red) female mice. Log(LDA scores)>2 and significance of α<0.05 determined using Wicoxon-Mann Whitney test.

Supplementary Figure 4: Effect of ATB treatment on physiological parameters in *Car*$^{-/-}$ vs *Car*$^{+/+}$ mice. *Car*$^{+/+}$ and *Car*$^{-/-}$ male and female mice were treated with an antibiotic cocktail of ampicillin, neomycin and vancomycin (ATB) for 2 weeks in their drinking water. (A) Body weight, (B) water consumption, (C) % body weights of liver and spleen, (D) % body weight of caecum and fecal microbial count in male mice. (E) Body weight, (F) water consumption, (G) % body weights of liver and spleen, (H) % body weight of caecum and fecal microbial count in female mice. Data are mean±SEM of n=8-10 per group. *p≤0.05, **p≤0.01, ***p≤0.005 for ATB effect, #p≤0.05 ##p≤0.01, ###p≤0.005 for genotype effect using 2-way ANOVA and Bonferroni's post-tests.

Supplementary Figure 5: Impact of microbiota depletion on plasma biochemistry in *Car*$^{-/-}$ vs *Car*$^{+/+}$ mice. Effect of ATB treatment in (A) male and (B) female mice. Data are mean±SEM of n=8-10 per group. *p≤0.05, **p≤0.01, ***p≤0.005 for ATB effect; #p≤0.05 ##p≤0.01, ###p≤0.005 for genotype effect using 2-way ANOVA and Bonferroni's post-tests.

SUPPLEMENTARY TABLES

Supplementary Table 1: List of antibiotics and their properties.

Supplementary Table 2. Oligonucleotide sequences for real-time PCR

Figure 1: Effect of individual antibiotic treatments on CAR target genes.

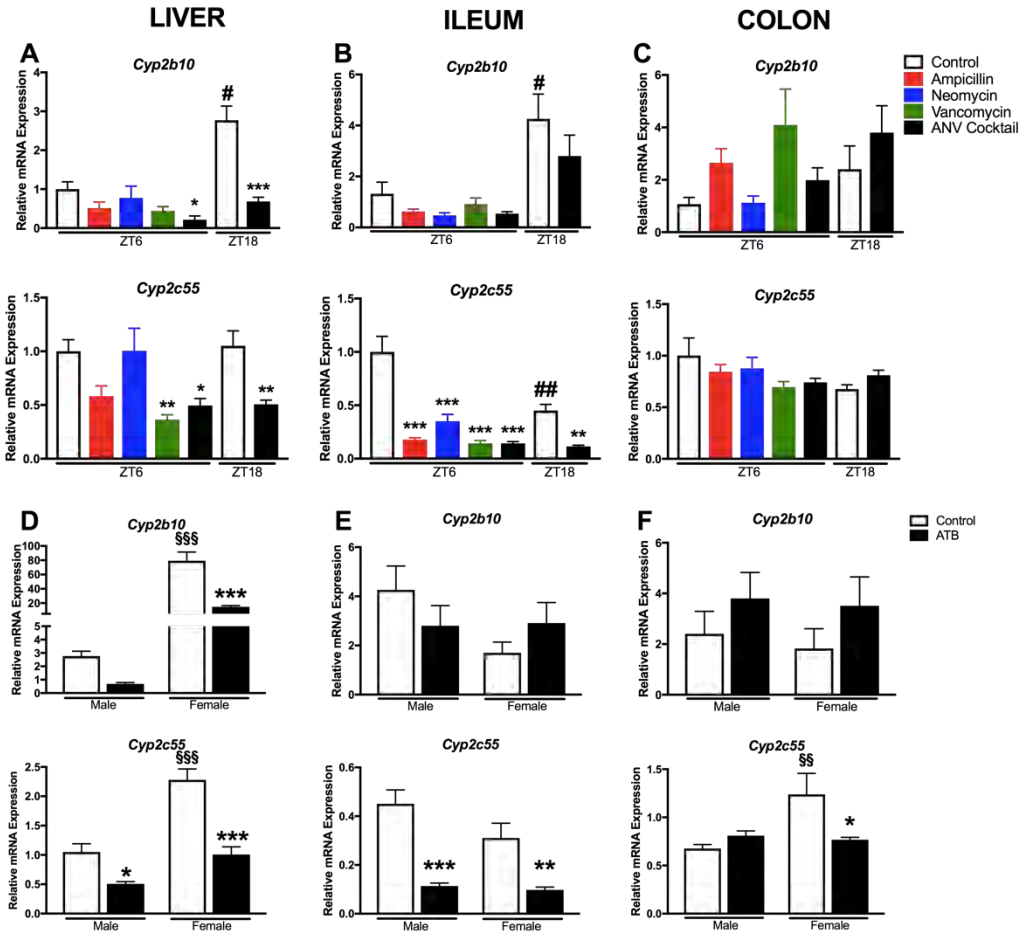

Figure 2: Effect of microbiota depletion on CAR activation via its pharmacological agonist.

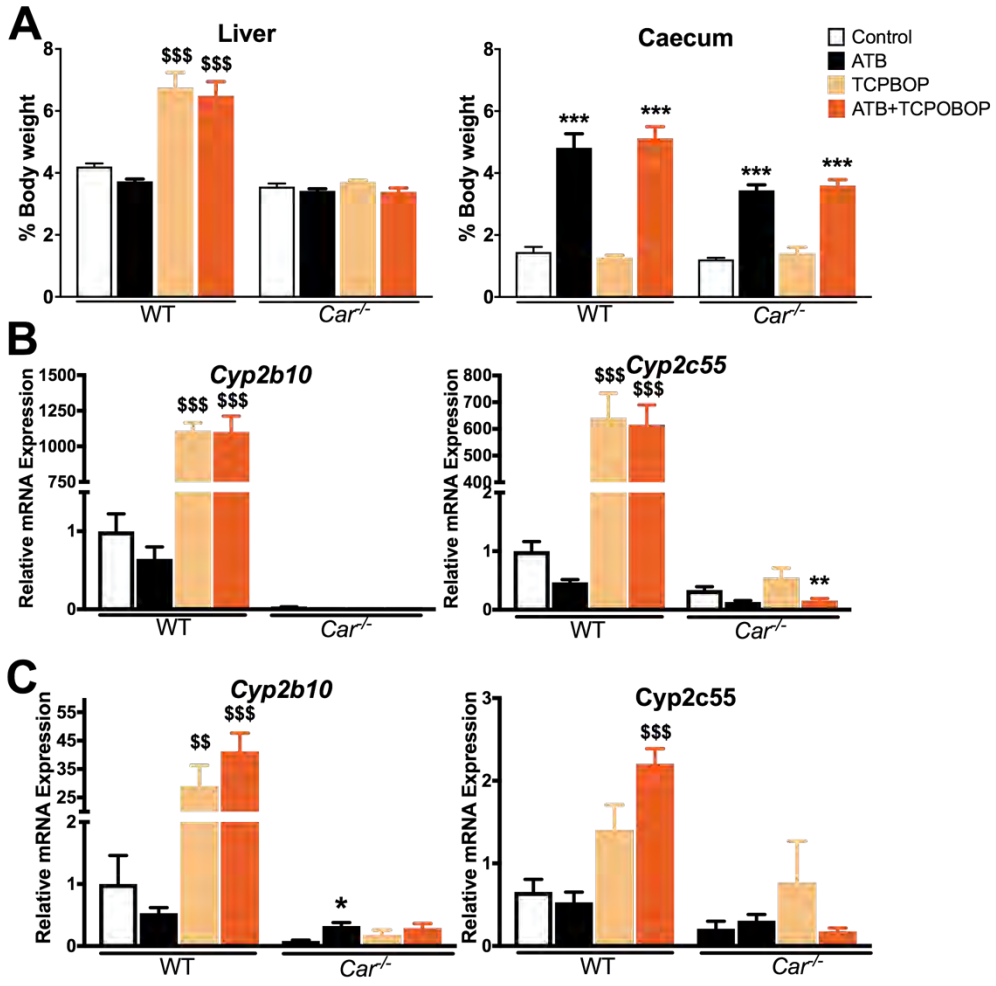

Figure 3: Gut microbiota composition in *Car*$^{-/-}$ *vs Car*$^{+/+}$ mice.

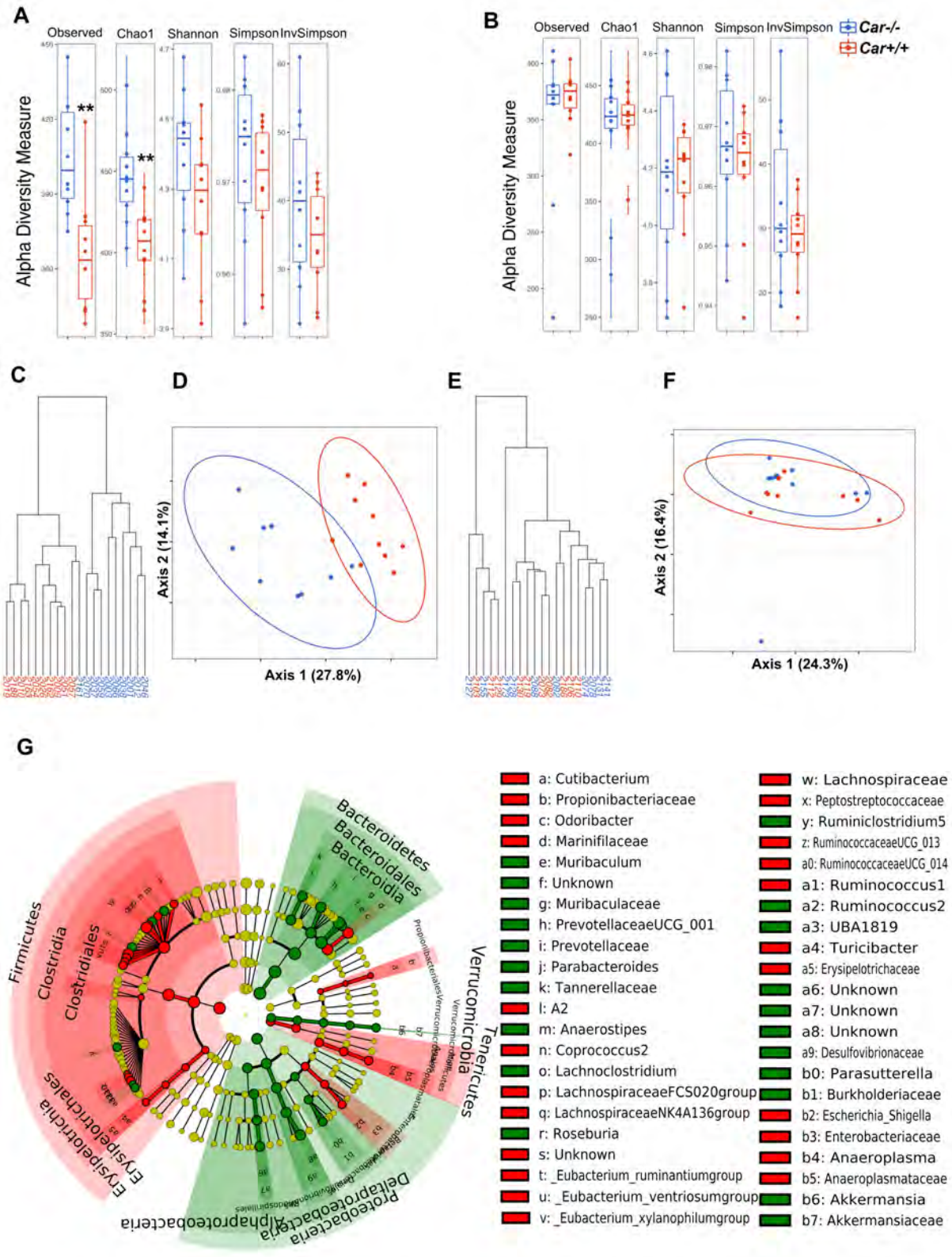

Figure 4: 1H-NMR based metabolomics analysis of caecal content extracts in *Car*$^{-/-}$ and *Car*$^{+/+}$ mice.

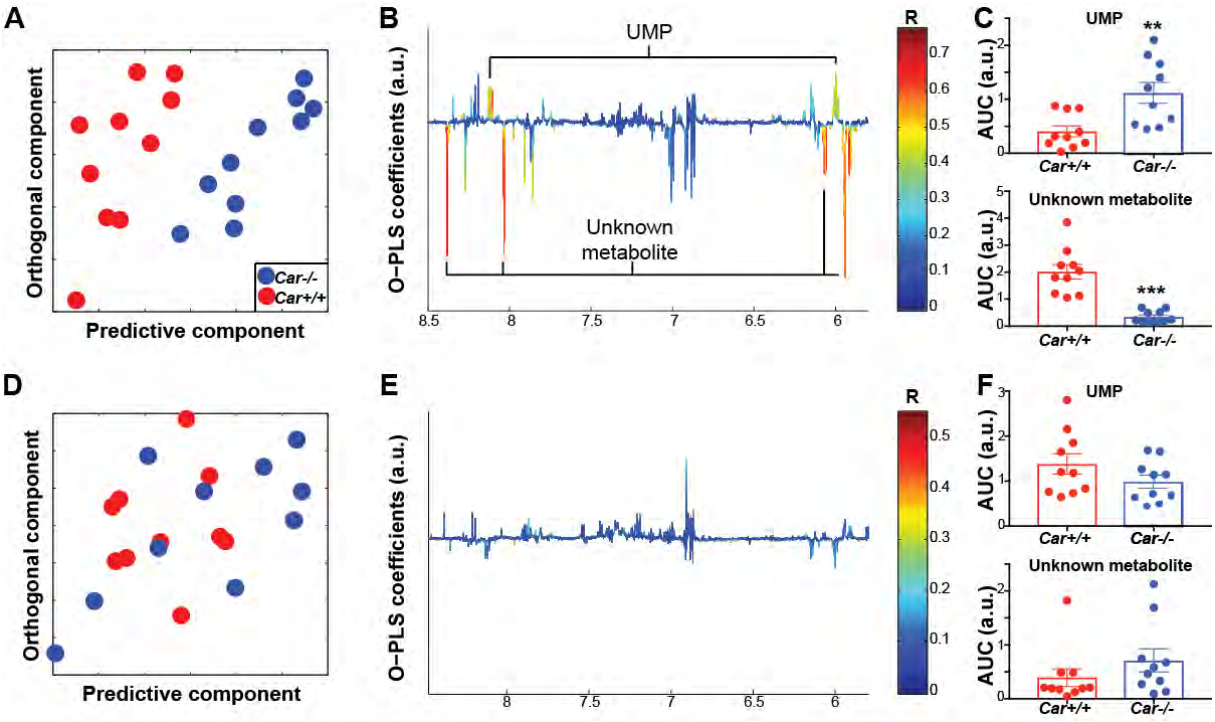

Figure 5: CAR activity upon microbiota depletion in male and female *Car*$^{-/-}$ vs *Car*$^{+/+}$ littermate mice.

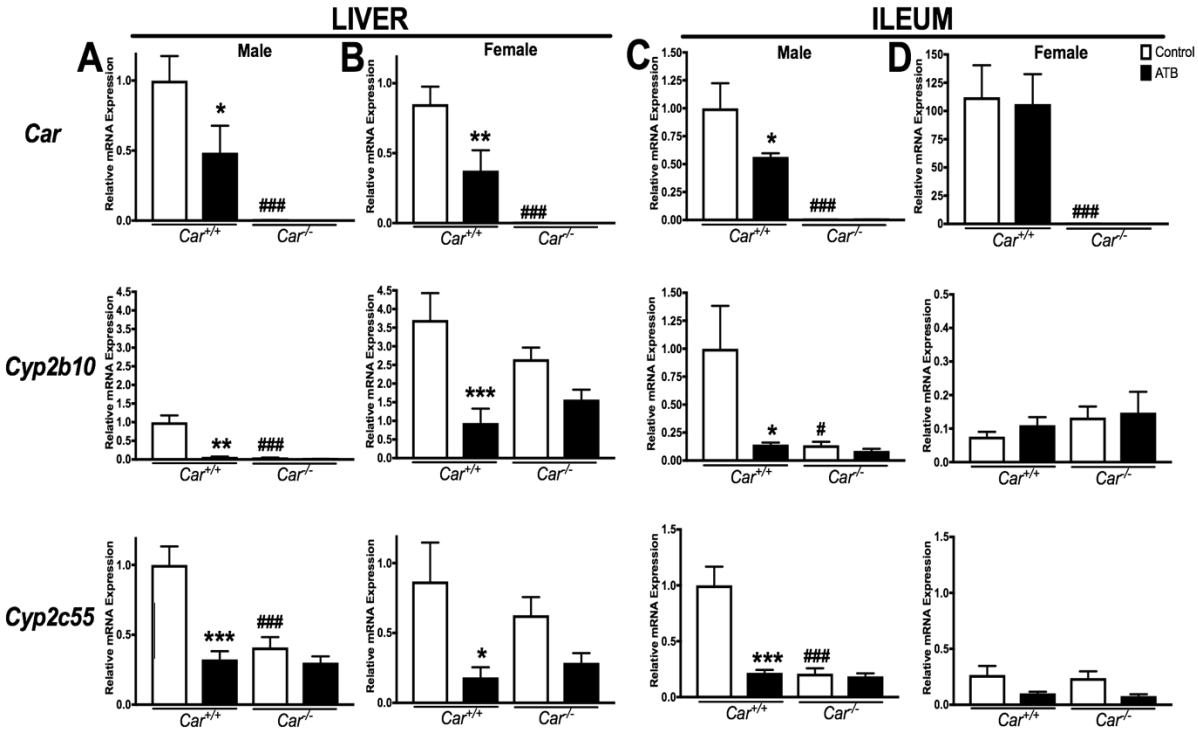

Figure 6: 1H-NMR based metabolomics analysis of hepatic extracts in *Car*$^{+/+}$ and *Car*$^{-/-}$ mice.

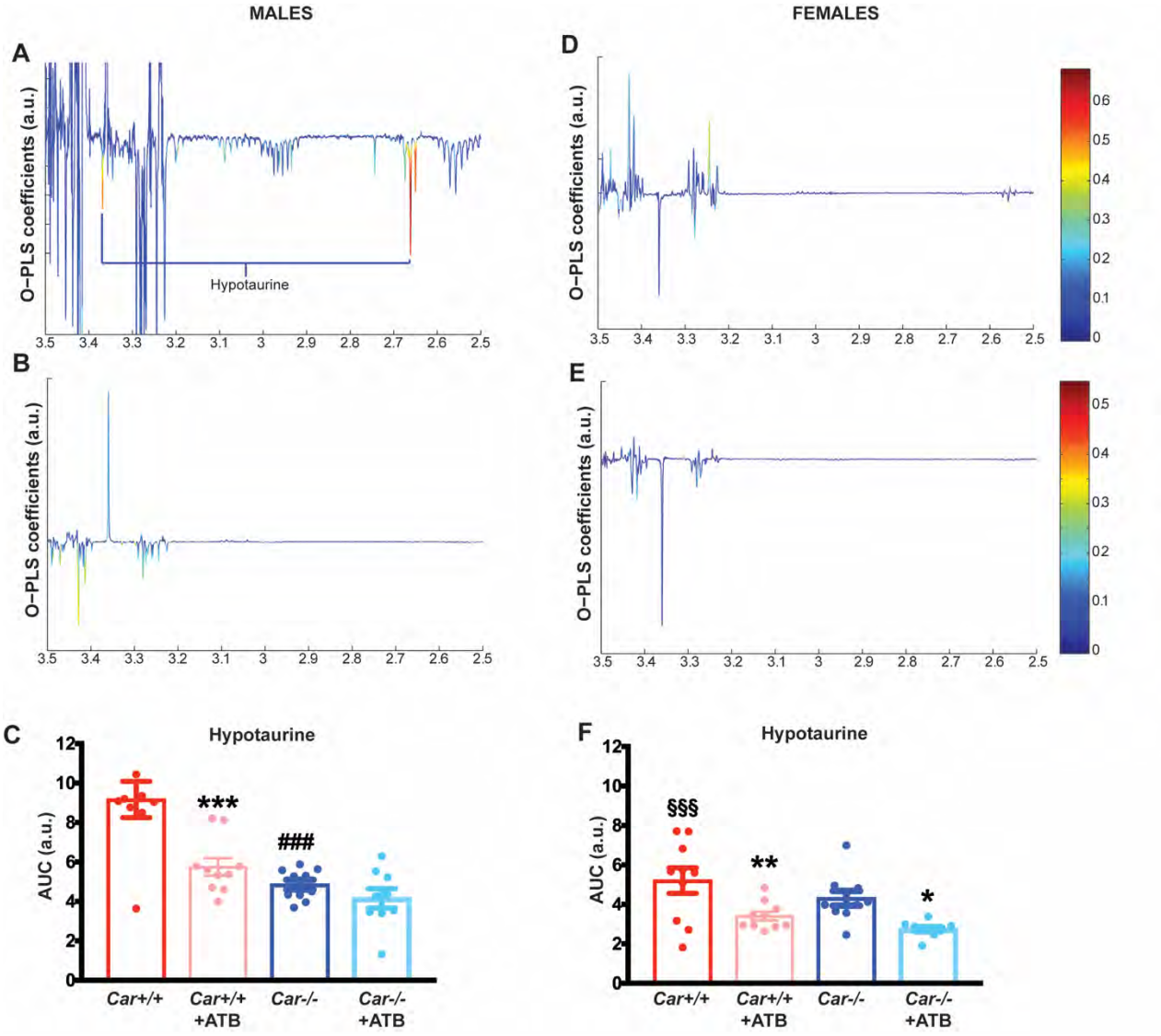

Figure 7: Impact of gut microbiota depletion on hepatic xenobiotic metabolism in *Car*$^{+/+}$ vs *Car*$^{-/-}$ male mice.

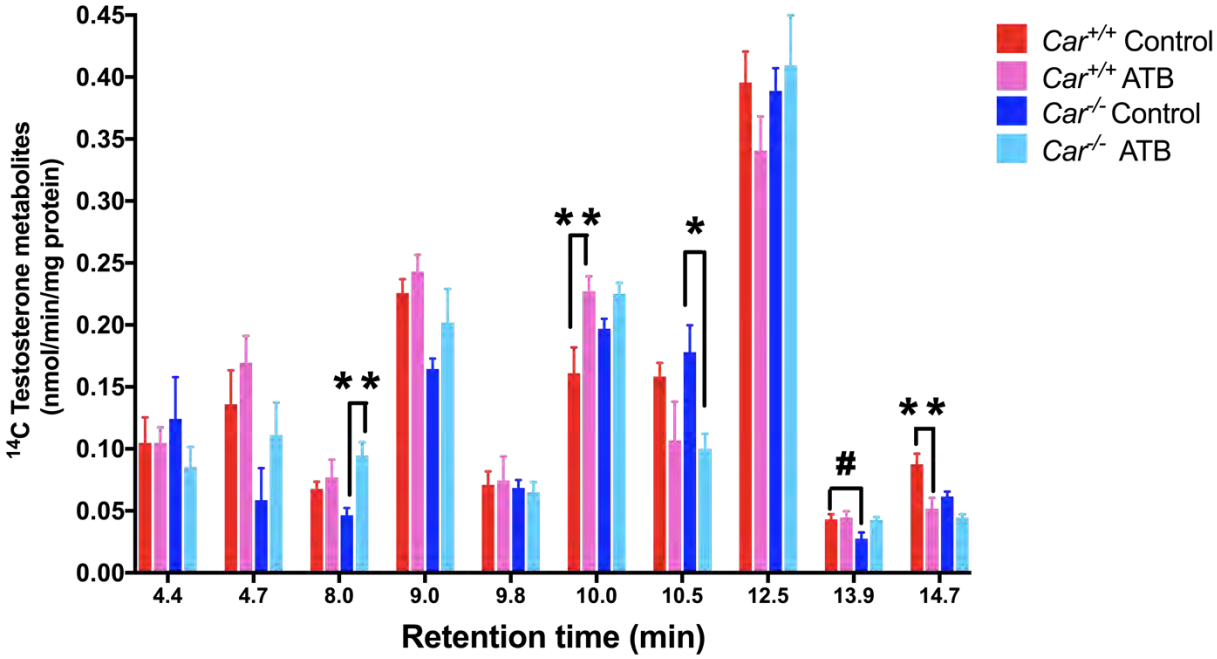

Figure 8: Impact of long-term CAR deletion on metabolic parameters and plasma biochemistry in *Car*$^{-/-}$ vs *Car*$^{+/+}$ littermate mice.

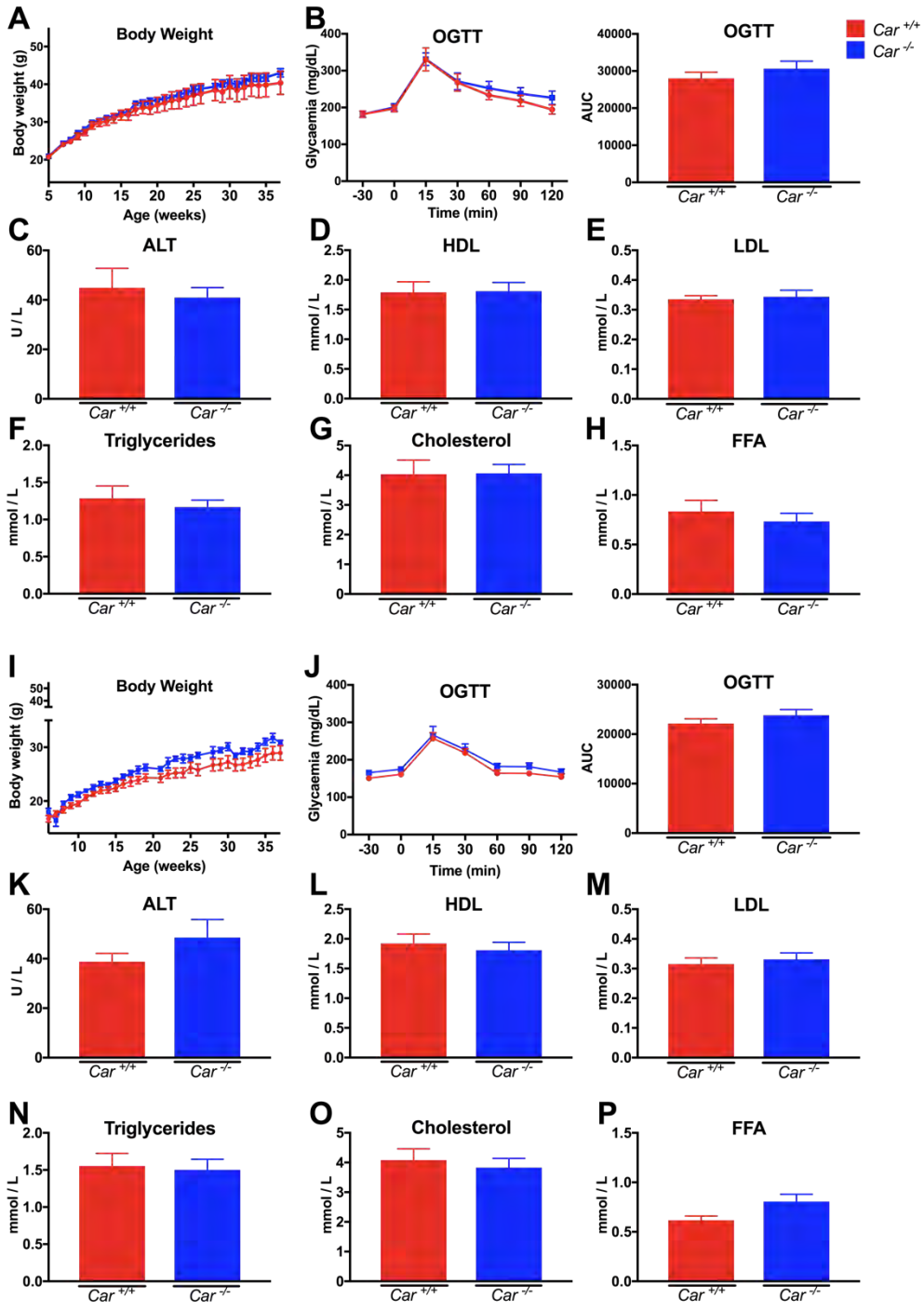

Figure 9: Effect of long-term CAR deletion on organ weights.

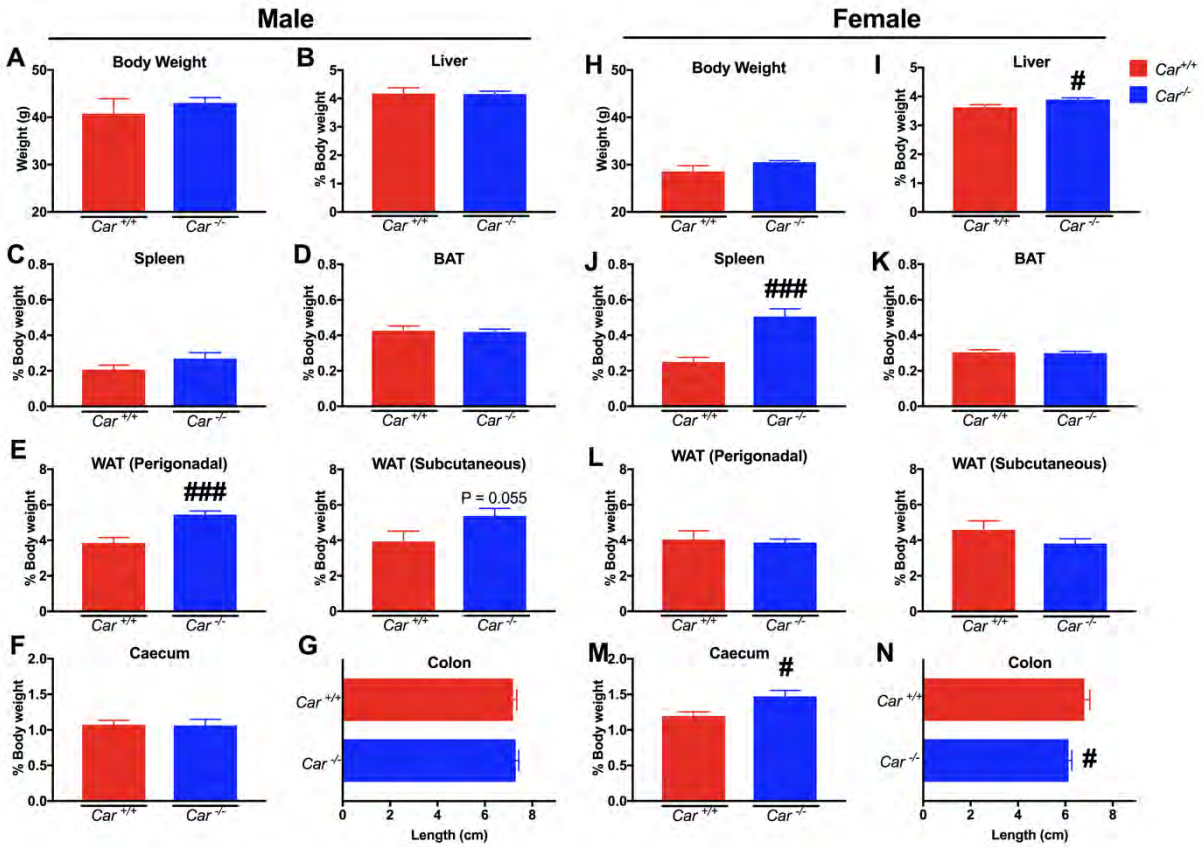

Supplementary Figure 1: Effect of various ATB treatment on physiological parameters.

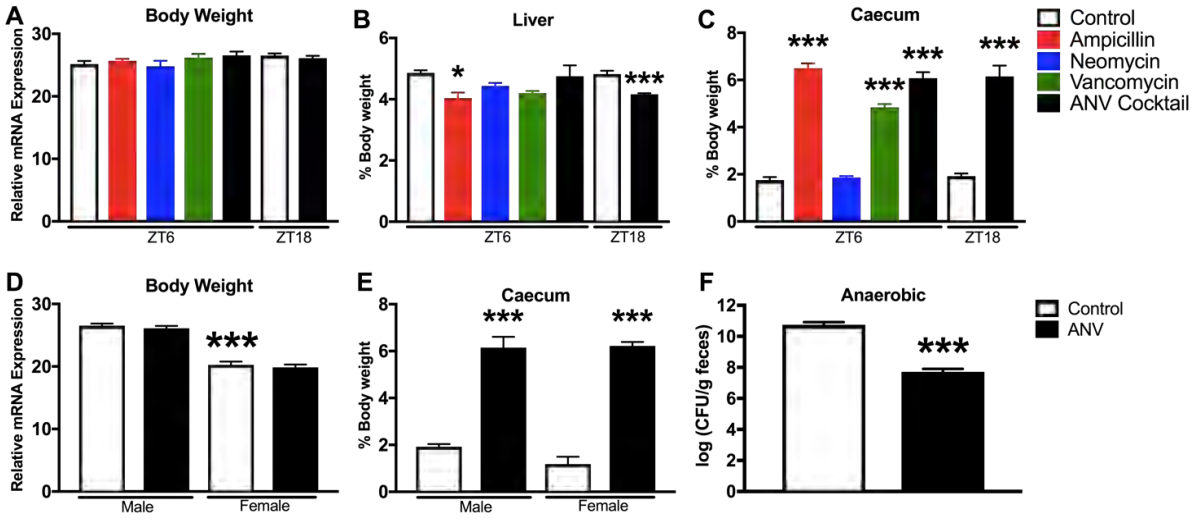

Supplementary Figure 2: Effect of *Car* deletion on caecal microbiota community distribution.

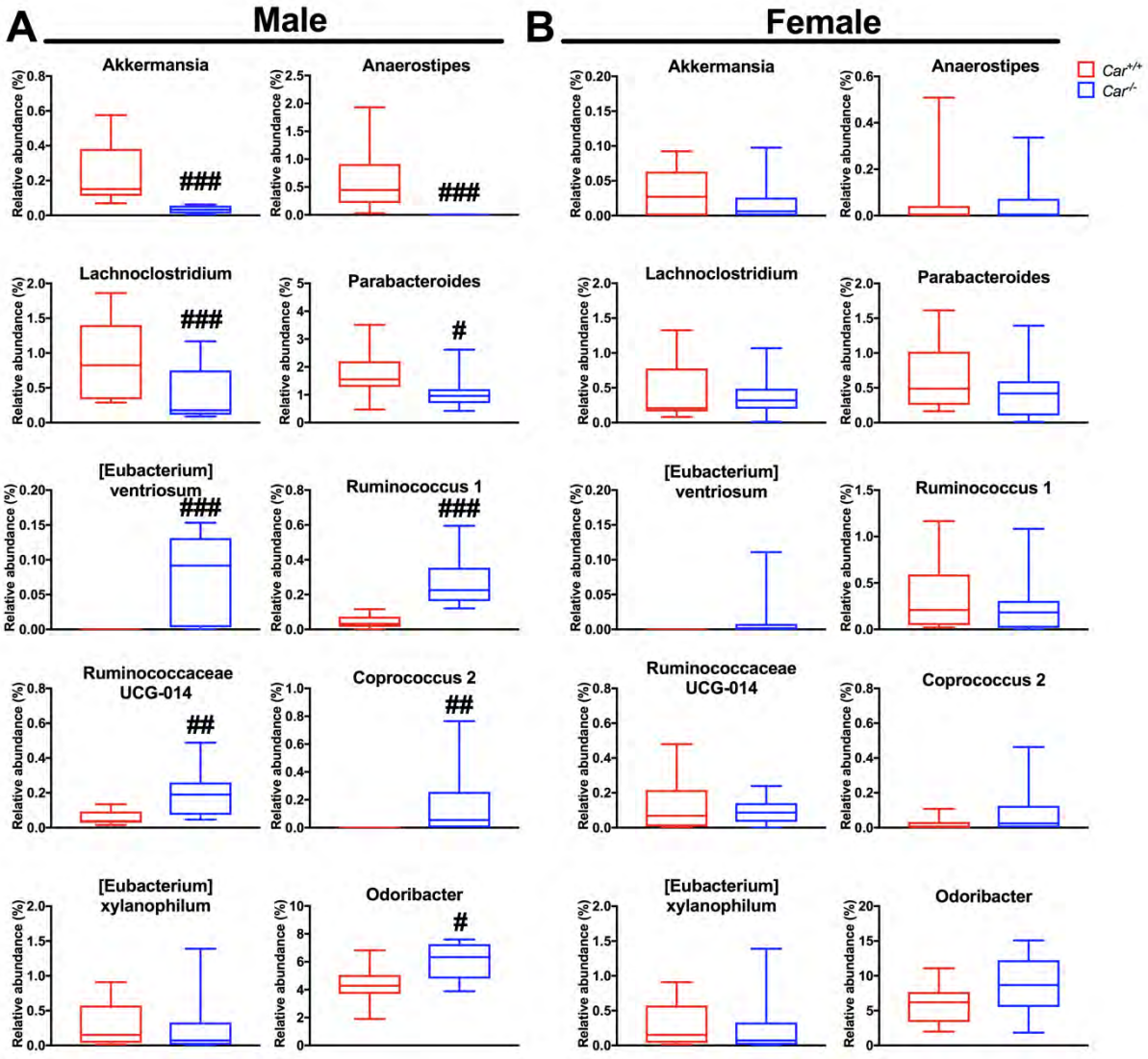

Supplementary Figure 3: Circular cladograms generated from LEFSe analysis showing the most differentially abundant taxa enriched in fecal microbiota from *Car*$^{+/+}$ (green) or *Car*$^{-/-}$ (red) female mice.

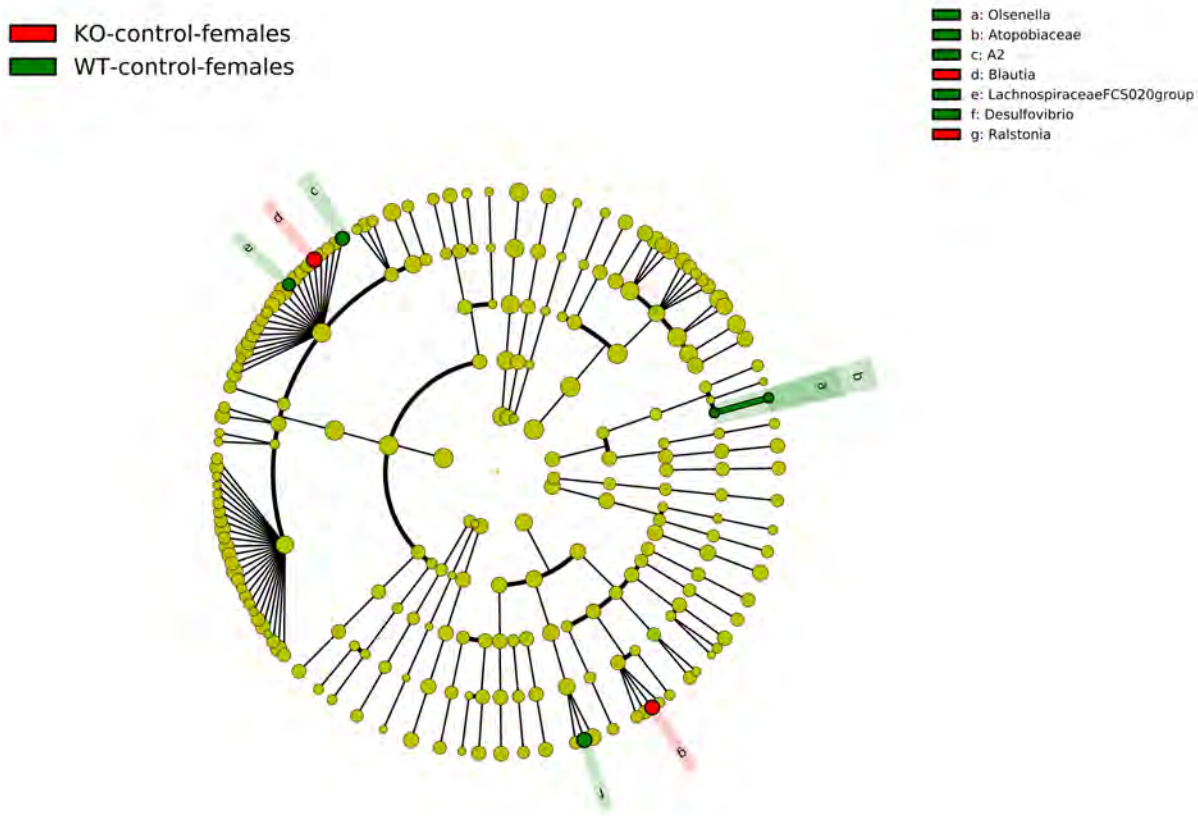

Supplementary Figure 4: Effect of ATB treatment on physiological parameters in *Car*$^{-/-}$ vs *Car*$^{+/+}$ mice.

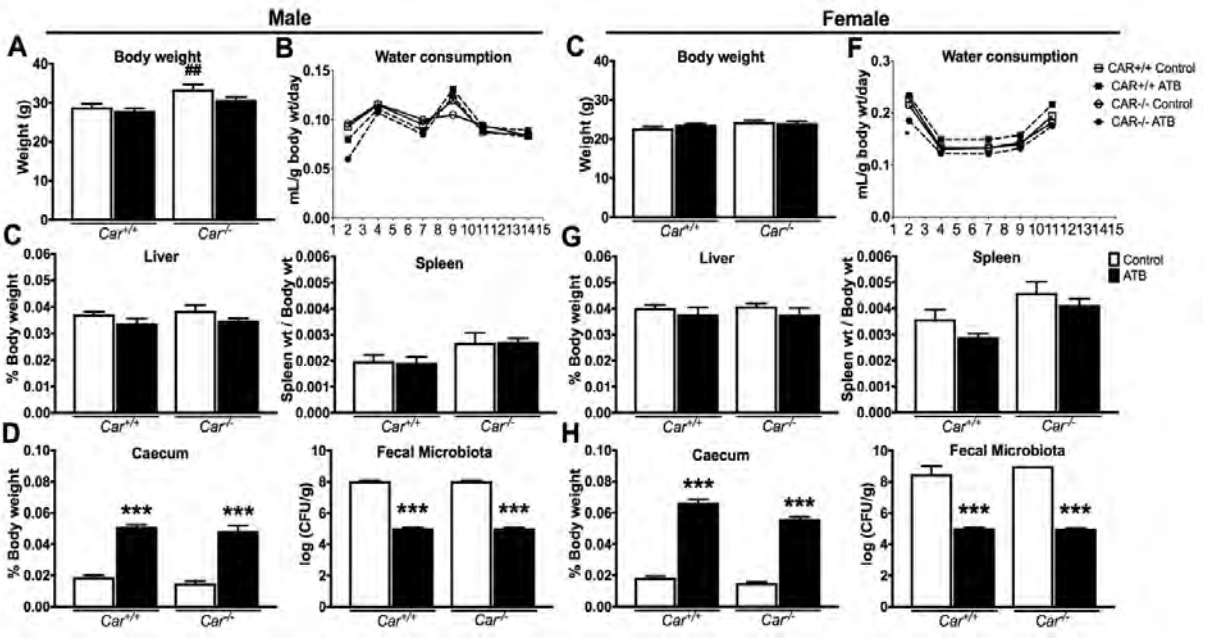

Supplementary Figure 5: Impact of microbiota depletion on plasma biochemistry in *Car*$^{+/+}$ vs *Car*$^{-/-}$ mice.

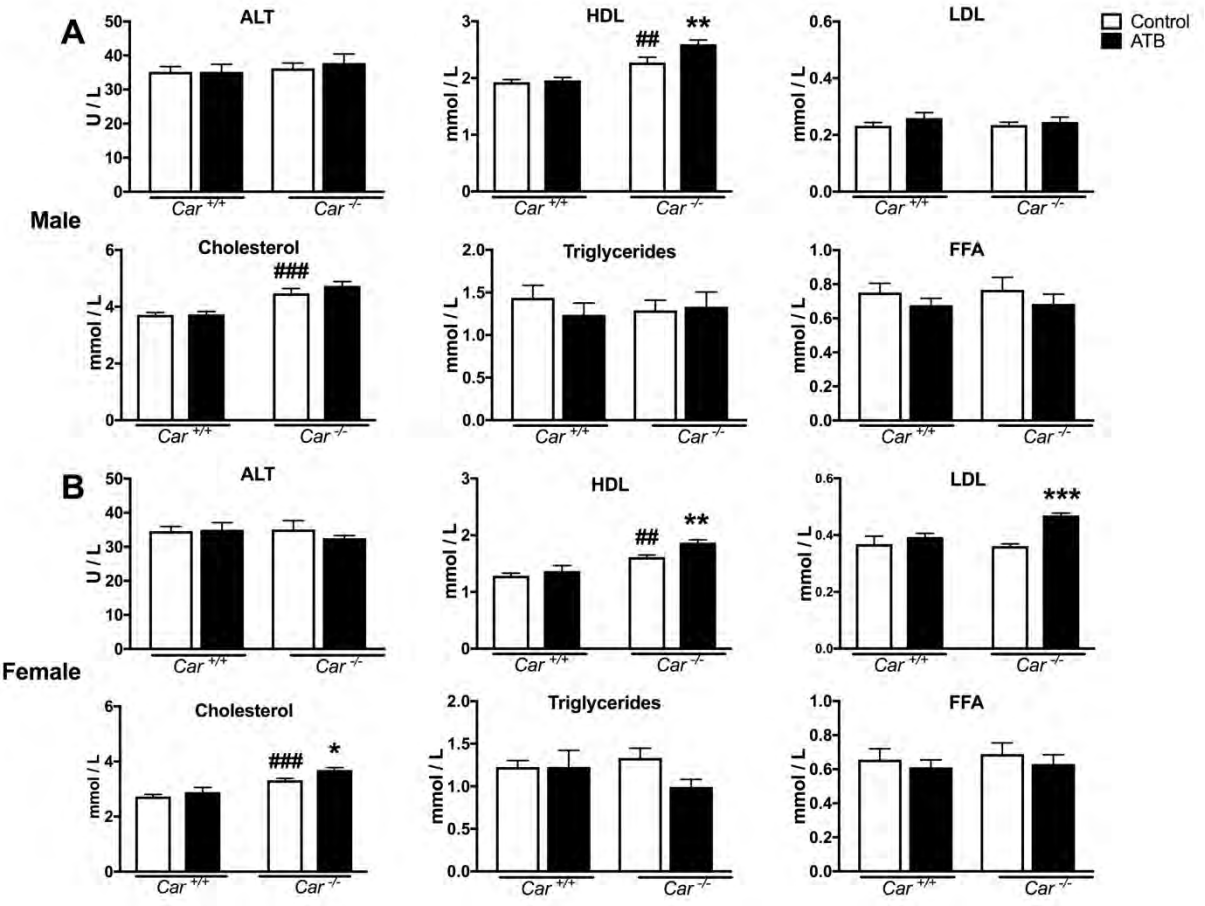

SUPPLEMENTARY TABLE

Supplementary Table 1: List of antibiotics (ATB) used and their properties (source: www.drugbank.ca).

Antibiotics	Quantity	Category	Mechanism	Spectrum	Intestinal absorption	Effect on CYP/NR
Ampicillin	1 gram / L	Beta-lactam	Inhibition of cell wall synthesis	Broad spectrum: excellent for gram-negative	Partial	Almost not metabolized
Neomycin	1 gram / L	Aminoglycoside	Binds to duplex RNA with high affinity; Inhibition of protein synthesis in bacteria	Broad spectrum: excellent for gram-negative	Poor absorption : 3% intact intestinal mucosa	*Low CYP450 inhibitory promiscuity
Vancomycin	0.5 gram / L	Glycopeptide	Inhibition of cell wall synthesis in bacteria	Narrow:spectrum; gram-positive	Poor	*Substrate : CYP450 3A4 Low CYP450 inhibitory promiscuity

Supplementary Table 2. Oligonucleotide sequences for real-time PCR

Gene	NCBI Refseq	Forward primer (5'-3')	Reverse primer (5'-3')
Cyp2b10	NM_009999	TTTCTGCCCTTCTCAACAGGAA	ATGGACGTGAAGAAAAGGAACAAC
Cyp2c55	AY206875	TTGTGGAAGAGCTAAGAAAAGCAAAT	GAGCACAGCTCAGGATGAATGT

GENERAL DISCUSSION AND PERSPECTIVES

General Discussion and Perspectives

In the last two decades, research in the field of gut microbiota has progressed from correlation-based studies between microbiota composition and diseases to investigating molecular pathways of interactions between specific bacterial strains, their metabolites and the host. Current knowledge states that gut microbiota composition is variable subject to the host's genetic background complemented with dietary and environmental factors. Of note, gut microbiota metabolites also influence the composition and activity of microbial communities in the gut (Cani, 2018). Concomitantly, nuclear receptors (NRs) play a primordial role by regulating numerous physiological processes in response to endocrine, metabolic and environmental stimuli (Evans & Mangelsdorf, 2014). In the liver, the nuclear receptors CAR and PXR primarily regulate xenobiotic metabolism and are considered as the master regulators of drug metabolism and transport (Gao & Xie, 2010). In the recent years, numerous studies have also demonstrated that CAR and PXR play a role in energy homeostasis through the regulation of glucose (Kodama *et al.* , 2004; Miao *et al.*, 2006; Zhou *et al.*, 2006) and lipid metabolism (Dong *et al*., 2009; Gao *et al*., 2009).

CAR and PXR are broad sensors of the gut microbiota in the liver and ileum

In this work, we have first demonstrated in several independent experiments that microbial depletion by different antibiotic protocols decreased CAR and PXR activity in the liver and ileum but not in the colon. This confirmed several previously published results that evaluated the expression of PXR and CAR targets in the liver of germ free (GF) male mice (Banerjee, Robbins, & Chen, 2013; Björkholm *et al*., 2009; Claus *et al*., 2011; Kawamoto *et al.*, 2000; Lundin *et al*., 2008) and mice treated with antibiotics (ATB) (Oh *et*

al., 2019). This also confirms the few existing studies that have shown that xenobiotic enzyme expression is lower in the small intestine of GF vs. conventional mice (Fu *et al.*, 2017). The colon results were surprising, since we have confirmed that PXR expression is not significantly different between the liver, the small and the large intestine (**Chapter 4**). However, CAR expression has been described to be low in the colon (Lundin *et al.*, 2008). It was also surprising since gut microbiota load is higher in the colon than in the ileum (Eckburg *et al*., 2005). However, previous studies have already shown that gut microbiota affects the expression of a much larger set of genes in the small intestine than in the colon in mice (Larsson *et al*., 2012; Mardinoglu *et al*., 2015; Sommer *et al*.,2015). Therefore, our results are consistent with the hypothesis that CAR and PXR are indeed gut microbiota (GM) sensors and transcriptional regulators of GM effects in the liver and in the ileum (**Chapter 3.3, Figure10B; Chap 3.4, Figure1**).

Impact of circadian rhythm and sex

We have observed that the activity of PXR in the basal state and in response to gut microbiota was not significantly affected by the circadian rhythm (**Chapter 3.3, Figure1A-C & 5; Chap 3.2, Figure1**). This confirms previous results from our team that showed that PXR activity in GF mice was almost completely depleted at all times (Montagner *et al*., 2016) (**Figure 16**).

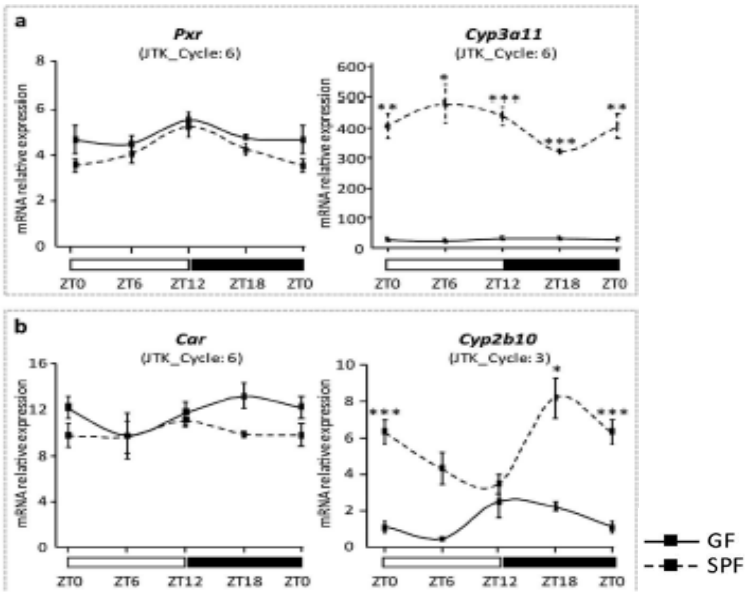

Figure 16. Circadian Oscillations of xenosensors in mouse. (A) PXR and target gene *Cyp3a11*, (B) CAR and target gene *Cyp2b10* (Montagner *et al*., 2016).

On the contrary, mice (Montagner *et al*., 2016) and rat (Kanno, *et al*., 2004) studies have previously observed that CAR activity has a circadian oscillation that peaks at ZT18-ZT20 in the liver. This could explain the weak inhibition of CAR activity to the antibiotic treatments that we observed at ZT6 contrasting with the significant decreased expression of *Cyp2b10* and *Cyp2c55* at ZT18 (**Chapter 3.4, Figure1A-D & 5**). Interestingly, upon ATB treatment, both *Cyp2b10* and *Cyp2c55* mRNA levels decreased in the liver and only *Cyp2c55* mRNA decreased in the ileum. Though there is the tendency to decrease, it is rather striking to observe the difference between these two classical CAR target genes. CAR and PXR are known to regulate the expression of a number of overlapping or distinct set of genes in xenobiotic metabolism, thus, it is noteworthy to know the difference between *Cyp2b10* from *Cyp2c55*. *Cyp2b10* is strongly induced by a class of xenobiotics known as 'phenobarbital like inducers', such as phenobarbital or TCPOBOP, which are ligands specific to CAR activation (Wei *et al*., 2002). Conversely, the transcriptional regulation of murine *Cyp2c* genes is poorly understood and are identified to be

differentially regulated by CAR or PXR. Of note, *Cyp2c55*, initially identified to be regulated by PXR, is also regulated by CAR in mouse liver and kidney (Konno *et al*., 2010).

Furthermore, CAR activity in the liver was particularly sexually dimorphic: *Cyp2b10* expression was 80 times higher and Cyp2c55 two times higher in females compared to males (**Chapter 3.4, Figure1D**). As explained in **Chapter 1.6.4.**, CAR expression itself is higher in females compared to males (Petrick & Klaassen, 2007). Moreover, previous studies have also shown that when mice were treated with the CAR ligands TCPOBOP (Ledda-Columbano *et al*., 2003), and Zoxozolamine (Hernandez *et al*., 2009), CAR activity was significantly more increased in females compared to males. Therefore, CAR is thought to be more active and more inducible in females than in males (Petrick & Klaassen, 2007; Wei *et a*l., 2002). This sexually dimorphic activity could due to three main reasons: (1) the inhibition of CAR activity in males by androstane (testosterone metabolite), which acts as an inverse agonist of CAR. The androgen levels result from the metabolism of testosterone via several steps of hydroxylation. Hydroxylase 6α activity is more significant in females than the hydroxylase 15α in males. In consequence, the ratio of 6α/15α hydroxylase is decreased in CAR deficient females contributing to the masculinization of these mice (Hernandez *et al*., 2009). This ratio is considered a biomarker of androgen levels and perturbations (Wilson, *et al*., 1999). (2) Estrogen mediated CAR activity (Kawamoto *et al.*, 2000); (3) the significant contribution of HNF4α in females (Kamiyama et al., 2007; Wiwi, Gupte, & Waxman, 2004; Wortham *et al.* , 2007).

Altogether, our results are in line with recent data highlighting that circadian rhythm and sex are two important parameters to take into consideration when one

investigates the gut microbiota-host interaction, and in our case, the gut microbiota-nuclear receptor interaction (Kuang et al., 2019; Weger et al., 2019).

Gut microbiota depletion does not interfere with the capacity of CAR and PXR to induce transcription upon pharmacological binding

CAR /PXR activity can be inhibited by the displacement of an agonist or the binding of an antagonist that may block the recruitment of RXR or co-activators thereby strengthening the interactions of a co-repressor. In addition, post-translational modifications may also interfere with CAR/PXR activity. Generally, there have been large number of inhibitors reported but it is believed that only a few of these bind at the ligand binding pocket (Chai *et al.*, 2016). **Figure 1** shows several classes of chemicals found to inhibit CAR and PXR activity.

Having previously demonstrated the microbial sensing capacity of CAR and PXR, we proceeded to investigate if the gut microbiota could interfere with the ligand-binding function of CAR and PXR. We have shown that, when mice are exposed to their pharmaceutical ligands (PCN for PXR and TCPOBOP for CAR) and/or the ATB treatment, these xenosensors consistently and robustly responded to their ligands (**Chapter 3.3, Figure2F & G; Chapter 3.3, Figure2B & C**). This demonstrates that gut microbiota depletion does not prevent or decrease the extent of CAR and PXR activity upon pharmacological activation. Therefore, we conclude that the antibiotic-driven decrease in PXR and CAR activity is not due to a change in the transcriptional machinery of the intestinal epithelial cells or of the hepatocytes, but rather to a decrease of microbial-derived ligands.

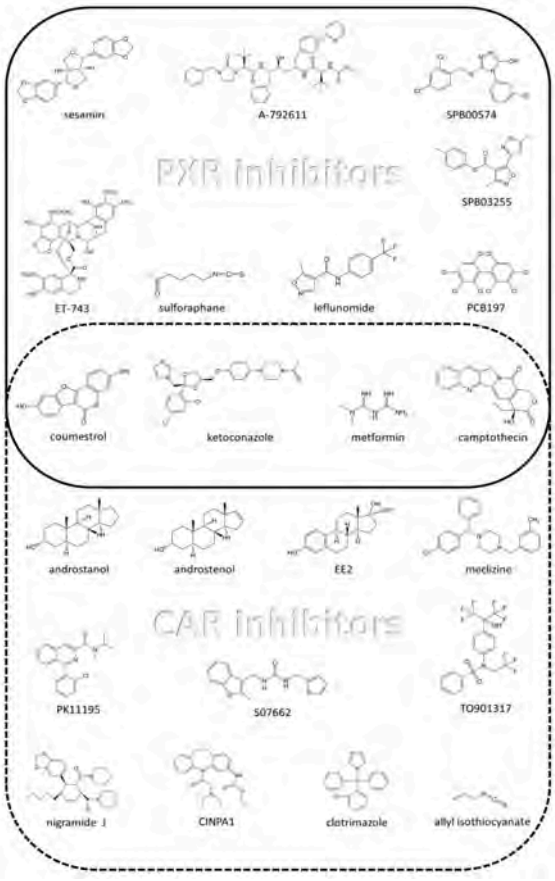

Figure 1 . Reported PXR (top) and CAR (bottom) inhibitors. Compounds described as inhibiting both NRs are enclosed in the center (Chai *et al*., 2016)

The gut microbiota-xenosensor interaction's impact on the host hepatic xenobiotic metabolism and beyond

In **Chapters 3 and 4** of this work, we have extensively investigated the primary metabolic pathway showing that upon pharmacological activation of PXR, the most sensitive genes were related to xenobiotic metabolism and that this regulation was shared between the liver and intestine. Consistently, we demonstrated in **Chapter 3** that the gut microbiota-PXR interaction mainly controls the expression and the activity of xenobiotic metabolizing enzymes. This corroborates many previous transcriptome (Fu *et al.*, 2017; Kindt *et al*., 2018), as well as proteome (Kindt *et al*., 2018) analysis, in which *Cyp3a11* is systematically one of the top down regulated genes and proteins in GF male mice. We add to these previous studies by demonstrating that PXR is the key mediator of these

perturbations. No microarray analysis was done on the *Car*$^{+/+}$ vs *Car*$^{-/-}$ littermates treated with antibiotics. However, previous data from our lab were obtained from hepatic transcriptomes of 16-week old WT vs *Car*$^{-/-}$ mice (Lukowicz *et al*., submitted for publication). Females had a greater number of differentially expressed genes (487 upregulated, 106 downregulated) than males (100 upregulated, 62 downregulated). In males, significant biological functions involved in oxidation and reduction processes (including CYPs), cholesterol transport and endoplasmic reticulum were upregulated, while genes linked to steroid hormone biosynthesis were downregulated. In females, genes specifically involved in the hepatic immune system were upregulated, while genes related to steroid hormone biosynthesis, cell junction, transmembrane region, and carboxylic ester hydroxylase were down-regulated. Although the mice used by Lukowicz *et al*. were not littermates, the transcriptomic data corroborates with the PXR profile, where dysregulated functions were sexually dimorphic and xenobiotic metabolism oriented. It would be interesting to see the transcriptomic signature from CAR littermates treated or not with ATB, where the confounding effects of microbiota variation between strains are controlled (Robertson *et al*., 2019). In *Car*$^{+/+}$ vs *Car*$^{-/-}$ littermates, antibiotic treatment reduced *Cyp2b10* expression in the liver and testosterone hydroxylation assays also demonstrated functional CAR-dependent alterations of xenobiotic metabolism. CAR is recognized to be a regulator of *Cyp2* gene family (Bae, Kemper, & Kemper, 2004). Thus, we hypothesize that the gut microbiota-CAR interaction also controls mainly xenobiotic metabolism through *Cyp2* gene family, but further transcriptomic analysis is needed to confirm this.

Sexual dimorphism

It would also be intriguing to further investigate the mechanisms of sexual dimorphism in the hepatic profile of these mice. We have observed with PXR littermate mice that the microbiota depletion by ATB has impacted the transcriptomic profile, independently from PXR. It has been previously described that gut microbes can impact the entero-hepatic recirculation of estrogens and androgens, thereby affecting local and systemic levels of sex steroid hormones (Cross, Kasahara, & Rey, 2018). In addition, estrogen can directly influence gut microbiota composition and consequently influence the sexual-dimorphism in diet-induced metabolic syndrome (Kailannan *et al.,* 2018). Furthermore, estrogen receptors have also been shown to either have an inhibitory or activating effect on CAR depending on the presence of ligands (Min *et al.*, 2002). With already differences in CAR basal expression and activity in the liver, it would be important to understand more, especially on a mechanistic level, how these sex hormones affect CAR's hepatic activity.

Lipid metabolism

In **Chapters 1 & 3**, our results on pathway enrichment analysis from the PXR microarray data has also confirmed that lipid metabolism is another PXR-dependent hepatic function. In **Chapter 1**, we confirmed the pro-steatotic effect of PXR activation from both induction of lipogenesis and repression of β-oxidation, and that this repression is certainly partly mediated through inhibition of PPARα. These data reinforce existing studies describing that PXR promotes lipogenesis (Gao *et al.*, 2009) and is associated with the induction of fatty acid translocase (FAT/CD36), peroxisome proliferator-activated receptor γ2 (PPARγ2), and stearoyl-CoA desaturase-1(SCD1) (Zhou *et al*., 2006).

Interestingly, we also highlighted possible new pleiotropic effects of PXR through its involvement in the regulation of hepatokines such as GDF15 and FGF21. Both GDF15 and FGF21 are liver-derived hormones of the hepatokine family. These proteins have been described as playing many key endocrine roles. For example, GDF15 (Tsai, *et al.*, 2018) and FGF21 (Kliewer & Mangelsdorf, 2019) have both been reported to influence whole body metabolic homeostasis as well as behavioral responses. Therefore, our data raises the interesting hypothesis that drugs and other xenobiotics that act as potent regulator of PXR activity may induce side effects and endocrine disruption through the modulation of hepatokine expression. Further work is required to analyze whether PXR mediated regulation of GDF15 and FGF21 occurs through a direct control of gene expression and whether the changes we observed in response to a pharmacological agonist may also occur in response to other drugs and other xenobiotics.

In **Chapter 3**, we extended our results on the moderate impact that gut microbiota contributes in hepatic fatty acid metabolism, at least in male mice. Various studies have described that gut microbiota can control the profile of the lipids in the gut-liver axis by affecting cholesterol-derived compounds and their hepatic recirculation, thereby affecting the consequences of liver metabolism (Bitter et al., 2015; Björkholm *et al.*, 2009; Hakkola, Rysä, & Hukkanen, 2016; Kodama & Negishi, 2013). Inferring from these results, our data provides additional insights into how PXR might play a role in liaison with gut microbiota in fatty acid elongation (Kindt *et al.*, 2018)

CAR also plays a role in hepatic lipid homeostasis. CAR activation results in the inhibition of hepatic lipogenic genes and alleviate hepatic steatosis by inhibiting LXRα to the Srebp-1c gene promoter (Björkholm *et al.*, 2009). In another study, CAR or PXR

reduced the level of SREBP-1c by inducing Insig-1, a protein with antilipogenic properties (Roth *et al*., 2008). CAR activation also results in the inhibition of fatty acid synthesis and gluconeogenesis (Björkholm *et al.*, 2009), as well as the increase of energy expenditure in brown adipose tissue (Gao *et al*., 2009). With the equal importance of CAR's impact on lipid metabolism, it would be of timely opportunity to take further steps in completing the transcriptional profile with microarray and more gene expression experiments. In addition investigating the relative abundance of fatty acids in the liver from littermate mice would complement and provide better understanding of the CAR-gut microbiota impact on lipid metabolism.

Altogether, our data provide evidence that the interaction of the gut microbiota with CAR and PXR modulates the host' hepatic xenobiotic metabolism in a sexually dimorphic way, which then perturbs the profile of circulating lipids via the gut-liver axis thereby affecting pathways important in hepatic lipid metabolism.

CAR and PXR alters gut microbiota

The gut microbiota contributes to a wide array of functions, including dietary digestion and absorption of nutrients and immunity. The gut has a protective layer of epithelial cells of which its integrity is affected by resident microbial metabolites. When this layer is compromised, chronic inflammation occurs. This dysfunction of the protective layer has been the epicenter of recent research implicating a variety of diseases linked to innate immunity and homeostasis in the intestine (Ranhotra *et al*., 2016). PXR has been recently studied and recognized for its role in regulating intestinal mucosal homeostasis by xenobiotic and endobiotic sensing of intestinal microbial metabolites (Ranhotra et al., 2016; Venkatesh *et al.*, 2014).

In **Chapter 3**, our results initially showed no differences between the biodiversity in males or in females, but detected significant differences in the baseline caecal microbiota composition of *Pxr*$^{-/-}$ compared to that in *Pxr*$^{+/+}$ male mice. Then, we detected a change in the profile of a tyrosine-based metabolite demonstrating that PXR has a role in shaping the gut microbiota in a sexually-dimorphic manner and that this PXR-dependent microbiota might play a role in the metabolism of aromatic amino acids. *In vivo* cardioprotection studies on rat (Lam *et al*., 2016) have shown that the catabolism of aromatic amino acids is a prevalent response of changes in the abundance of specific bacterial groups in the rat intestine. Alterations in the abundance of individual groups of bacteria (namely *Clostridia, Bacilli* and *Proteobacteria*) were not responsible for the cardioprotection in rats but the corresponding changes in aromatic amino acid metabolites link the intestinal microbiota responsible for this cardioprotective phenotype. Amino acid catabolism was by far the most affected pathway, of which metabolites of the aromatic amino acids phenylalanine, tryptophan, and tyrosine constituted the majority (33 of 50) of the affected metabolites. Tryptophan catabolism via specific bacterial strains (e.g.,indole positive *Clostridium sporogenes*) results in the production of indoles. This has been demonstrated in mice treated with clindamycin, in which, enteric bacterial metabolites of tryptophan (but not host metabolites) decreased compared to untreated mice (Jump *et al*., 2014). Similar results have been seen in germ-free versus conventional mice (Wikoff *et al*., 2009). Tryptophan can be converted directly in the gut by microorganisms into indole derivatives, such as indole-3-propionic acid (IPA*). In vitro*, IPA has been shown to activate both the mPXR and the hPXR, however IPA was a much more potent agonist of the mPXR (Venkatesh *et al*., 2014). *In vivo*, oral gavage with IPA has been

shown to decrease intestinal permeability in the small intestine in a PXR-dependent way (Venkatesh *et al.*, 2014). In distant organs, such as the vascular epithelium, IPA has been shown to regulate endothelium-dependent vasodilation in vivo, and in vitro experiments point to PXR as a potential effector of IPA effects (Venu *et al.*, 2019). However, there is lacking *in vivo* evidence using physiological concentrations of circulating IPA. Indoxyl-3-sulfate is another by product of the microbiota-host tryptophan co-metabolism (Wikoff *et al.*, 2009). and has been demonstrated to be a direct AhR ligand, however, it failed to activate CAR or PXR in cell lines (Schroeder *et al.*, 2010). Therefore, indoles, and IPA in particular, might represent potential microbial ligands for PXR that could explain our results in the intestine and in the liver. However, it is not clear whether these indoles could reach the liver at a sufficient concentration to activate PXR.

Conversely, CAR is reportedly involved in modulating hepatic xenobiotic metabolism without direct contact to the liver via CAR-ligands (Björkholm *et al.*, 2009). In **Chapter 4**, our results show that CAR depletion significantly increased alpha-diversity in males but not in females. We also observed a significant increase in caecal UMP concentrations, and a significant decrease of an unidentified metabolite in *Car*$^{-/-}$ mice compared to *Car*$^{+/+}$ mice. Interestingly, this unidentified metabolite is gut microbiota and CAR dependent in males and is 4 times higher than in females. In addition, hypotaurine level in the liver of males was CAR and gut micorbiota-dependent, but in females, only gut microbiota-dependent. These results demonstrate that CAR shapes the gut microbiota in a sexually-dimorphic manner, and that the male-specific CAR-dependent microbiota might display significant differences in nucleotide metabolism. In a previous study in our team, CAR induced sexually dimorphic changes in hepatic metabolites. CAR deletion

significantly decreased glutathione precursors glycine and hypotaurine in males, while all bile signals were decreased in females (Lukowicz *et al*., submitted for publication). It is known that levels of bile acids, steroid hormones and bilirubin are regulated by gut microbiota (Chu, Duan *et al.*, 2019; Vítek *et al*., 2005). In many cases, these cholesterol-derived metabolites in their unmodified form, act as ligands or activators of NRs in the liver to control the endogenous metabolism of the compounds. These studies validate our results on the involvement of the CAR-gut microbiota interaction, as well as affecting gluthatione metabolism in the liver of males. Finding studies correlating CAR-dependent microbiota to its metabolites is a challenge. However, in one study by Björkholm *et al*. (2009), bile acids and steroids have been proposed. Constitutively higher CAR expression in the intestine of GF mice was associated with elevated levels of the CAR activators bilirubin, bile acids and steroid hormones, although the relative contributions of these are so far unknown. This might be a result of the increased levels of cholesterol, and/or the direct biochemical effects of the microbiota on these compounds. It is important to highlight, though, that these mice were challenged with phenobarbital. Bile acids interact with PXR directly (Krasowski *et al.*, 2005; Staudinger *et al.*, 2001) or indirectly via regulation of the farnesoid X receptor (Björkholm *et a*l., 2009; Jung, Mangelsdorf, & Meyer, 2006). Bile acids and their metabolites help maintain hepatic glucose, cholesterol and triglyceride homeostasis.

Preclinical studies suggest that bile acids can contribute to the development of non-alcoholic fatty liver (NAFL) and non-alcoholic steatohepatitis (NASH). In patients with Crohn's disease or ulcerative colitis with active mild or moderate inflammation, as well as in tissues isolated from colitis mice, CAR gene expression is reduced in intestinal mucosal

biopsies. Selective activation of CAR enhances wound healing in intestinal epithelial cells in culture, an effect driven by enhanced cell migration. Finally, inhibition of CAR delays mucosal healing after the induction of experimental colitis, while its pharmacological activation accelerates recovery (Hudson *et al*, 2017). Thus, CAR alters the natural milieu of the microbiota (Duszka & Wahli, 2018). CAR in the intestine and in the liver depends on the presence of the microbiota (Lundin *et al*., 2008; Björkholm *et a*l., 2009). Again, because CAR and PXR can be activated by the same ligands, upregulation of overlapping sets of genes allows for coordinated clearance and detoxification of harmful compounds like bile, for example.

It would be interesting to further explore this fertile area of research, where there has been no solid evidence linking CAR dependent metabolites with phenotypes associated with inflammation, NAFLD and NASH. The mice used in our results were first of all, unchallenged in their diet regimes, thus having milder phenotypes than what is described in literature. Next, the microbial depletion implemented with littermate mice was only short term. Long-term depletion of gut microbiota via GF models would be an interesting perspective to observe long-term effects of this interaction. With the 37-week aging of CAR-depleted mice, there were already differing phenotypes where males accumulated adipose tissues while females developed a slightly pro-inflammatory phenotype. Changes in the microbiota are associated with the development of non-alcoholic fatty liver (NAFLD) (Le Roy *et al*, 2013, Bäckhed *et al.,* 2004). Moreover, epididymal fat weight, hepatic steatosis, multifocal necrosis and infiltration of liver by inflammatory cells were significantly increased in GF mice colonized with faeces from patients with NASH and then fed a high-fat diet (HFD) (Chiu *et al*., 2017). These results

indicate that risk of NAFL and NASH can be transmitted by the faecal microbiota (Chu *et al.*, 2018). Thus, it would also be very interesting to feed *Car*$^{-/-}$ and *Car*$^{+/+}$ mice with a western diet (WD, high carbohydrate and high-fat diet) or HFD to study the impact of the CAR-gut microbiota interaction on NAFL and NASH.

In conclusion, PXR and CAR interact with microbiota and are required for the proper functioning of the liver and intestine in xenobiotic and lipid metabolism. Importantly, these xenosensors are interconnected (**Figure 18**) and show a high level of coordination and, thus, future research may show that they embody an essential pathway in the gut–liver axis and its role in gender specific sensitivity to gastro-intestinal responses to microbiota derived metabolites.

These investigations may help us understand gender specific susceptibility to xenobiotic exposure and chronic pathologies such as NAFLD. It will not only be critical to design appropriated preventive strategies, as well as personalized medication.

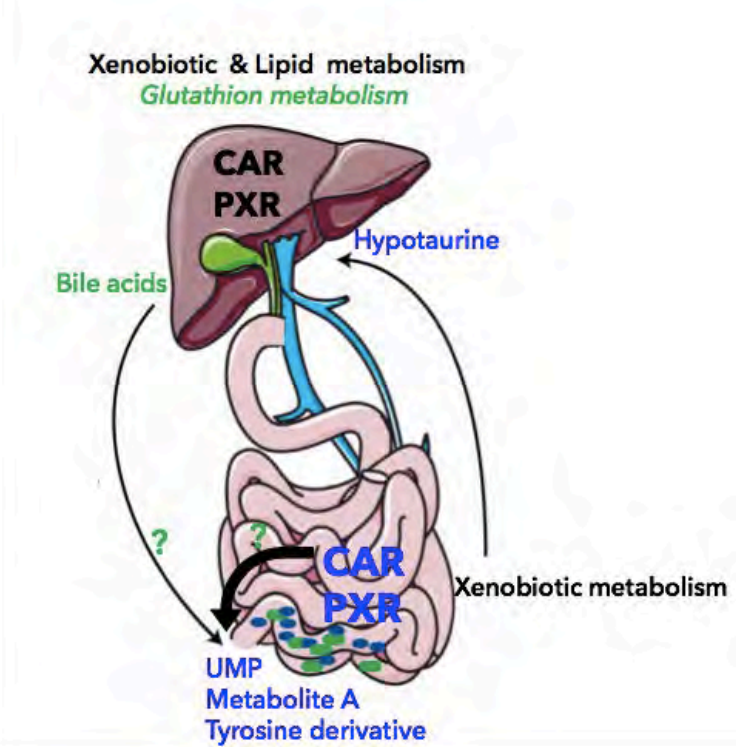

Figure 18. Bi-directional interactions of CAR and PXR and the gut microbiota in the liver and intestine. CAR /PXR-gut microbiota interaction modulates xenobiotic metabolism pathways (e.g. glutathione metabolism via a PXR-gut microbiota dependent-change in the hypotaurine profile) in a sexually dimorphic way, which then perturbs the profile of circulating lipids via the gut-liver axis thereby affecting important pathways in hepatic lipid metabolism. PXR in the intestine changed a tyrosine-based metabolite caused by sexually-dimorphic and PXR-dependent alterations in the GM composition. CAR significantly alters gut microbiota composition in males but not in females, thereby significantly changing the UMP profile in *Car*$^{-/-}$ male mice and the profile of metabolite A in *Car*$^{+/+}$ male mice. Thus, inducing a male-specific impact gut microbiota metabolism. Altogether, PXR and CAR interact with microbiota and are required for the proper functioning of the liver and intestine in xenobiotic and lipid metabolism.

BIBLIOGRAPHIC REFERENCES

Bibliographic references

Abdel-Misih, S. R. Z., & Bloomston, M. (2010). Liver anatomy. *The Surgical Clinics of North America*, *90*(4), 643–653. https://doi.org/10.1016/j.suc.2010.04.017

Abdul Rahim, M. B. H., Chilloux, J., Martinez-Gili, L., Neves, A. L., Myridakis, A., Gooderham, N., & Dumas, M.-E. (2019). Diet-induced metabolic changes of the human gut microbiome: Importance of short-chain fatty acids, methylamines and indoles. *Acta Diabetologica*, *56*(5), 493–500. https://doi.org/10.1007/s00592-019-01312-x

Abe, T., Takahashi, M., Kano, M., Amaike, Y., Ishii, C., Maeda, K., … Yoshinari, K. (2017). Activation of nuclear receptor CAR by an environmental pollutant perfluorooctanoic acid. *Archives of Toxicology*, *91*(6), 2365–2374. https://doi.org/10.1007/s00204-016-1888-3

Agus, A., Planchais, J., & Sokol, H. (2018). Gut Microbiota Regulation of Tryptophan Metabolism in Health and Disease. *Cell Host & Microbe*, *23*(6), 716–724. https://doi.org/10.1016/j.chom.2018.05.003

Alaynick, W. A. (2008). Nuclear receptors, mitochondria and lipid metabolism. *Mitochondrion*, *8*(4), 329–337. https://doi.org/10.1016/j.mito.2008.02.001

Archer, R. H., Chong, R., & Maddox, I. S. (1982). Hydrolysis of bile acid conjugates by Clostridium bifermentans. *European Journal of Applied Microbiology and Biotechnology*, *14*(1), 41–45. https://doi.org/10.1007/BF00508002

Atarashi, K., Nishimura, J., Shima, T., Umesaki, Y., Yamamoto, M., Onoue, M., … Takeda, K. (2008). ATP drives lamina propria T(H)17 cell differentiation. *Nature*, *455*(7214), 808–812. https://doi.org/10.1038/nature07240

Atkinson, C., Frankenfeld, C. L., & Lampe, J. W. (2005). Gut Bacterial Metabolism of the Soy Isoflavone Daidzein: Exploring the Relevance to Human Health. *Experimental Biology and Medicine*, *230*(3), 155–170. https://doi.org/10.1177/153537020523000302

Auerbach, S. S., Stoner, M. A., Su, S., & Omiecinski, C. J. (2005). Retinoid X receptor-alpha-dependent transactivation by a naturally occurring structural variant of human constitutive androstane receptor (NR1I3). *Molecular Pharmacology*, *68*(5), 1239–1253. https://doi.org/10.1124/mol.105.013417

Bacher, A., Eberhardt, S., Fischer, M., Kis, K., & Richter, G. (2000). Biosynthesis of vitamin b2 (riboflavin). *Annual Review of Nutrition*, *20*, 153–167. https://doi.org/10.1146/annurev.nutr.20.1.153

Bäckhed, F., Ding, H., Wang, T., Hooper, L. V., Koh, G. Y., Nagy, A., … Gordon, J. I. (2004). The gut microbiota as an environmental factor that regulates fat storage. *Proceedings of the National Academy of Sciences of the United States of America*, *101*(44), 15718–15723. https://doi.org/10.1073/pnas.0407076101

Bäckhed, F., Manchester, J. K., Semenkovich, C. F., & Gordon, J. I. (2007). Mechanisms underlying the resistance to diet-induced obesity in germ-free mice. *Proceedings of the National Academy of Sciences of the United States of America*, *104*(3), 979–984. https://doi.org/10.1073/pnas.0605374104

Bae, Y., Kemper, J. K., & Kemper, B. (2004). Repression of CAR-mediated transactivation of CYP2B genes by the orphan nuclear receptor, short heterodimer partner (SHP). *DNA and Cell Biology*, *23*(2), 81–91. https://doi.org/10.1089/104454904322759894

Baes, M., Gulick, T., Choi, H. S., Martinoli, M. G., Simha, D., & Moore, D. D. (1994). A new orphan member of the nuclear hormone receptor superfamily that interacts with a subset of retinoic acid response elements. *Molecular and Cellular Biology*, *14*(3), 1544–1552. https://doi.org/10.1128/mcb.14.3.1544

Baldwin, W. S., & Roling, J. A. (2009). A concentration addition model for the activation of the constitutive androstane receptor by xenobiotic mixtures. *Toxicological Sciences: An Official Journal of the Society of Toxicology*, *107*(1), 93–105. https://doi.org/10.1093/toxsci/kfn206

Banerjee, M., Robbins, D., & Chen, T. (2013). Modulation of Xenobiotic Receptors by Steroids. *Molecules*, *18*(7), 7389–7406. https://doi.org/10.3390/molecules18077389

Barrett, E., Fitzgerald, P., Dinan, T. G., Cryan, J. F., Ross, R. P., Quigley, E. M., … Stanton, C. (2012). Bifidobacterium breve with α-linolenic acid and linoleic acid alters fatty acid metabolism in the maternal separation model of irritable bowel syndrome. *PloS One*, *7*(11), e48159. https://doi.org/10.1371/journal.pone.0048159

Beck, J. A., Lloyd, S., Hafezparast, M., Lennon-Pierce, M., Eppig, J. T., Festing, M. F. W., & Fisher, E. M. C. (2000). Genealogies of mouse inbred strains. *Nature Genetics*, *24*(1), 23. https://doi.org/10.1038/71641

Beigneux, A. P., Moser, A. H., Shigenaga, J. K., Grunfeld, C., & Feingold, K. R. (2002). Reduction in cytochrome P-450 enzyme expression is associated with repression of CAR (constitutive androstane receptor) and PXR (pregnane X receptor) in mouse liver during the acute phase response. *Biochemical and Biophysical Research Communications*, *293*(1), 145–149.

Belkaid, Y., & Harrison, O. J. (2017). Homeostatic immunity and the microbiota. *Immunity*, *46*(4), 562–576. https://doi.org/10.1016/j.immuni.2017.04.008

Benson, A. K., Kelly, S. A., Legge, R., Ma, F., Low, S. J., Kim, J., … Pomp, D. (2010). Individuality in gut microbiota composition is a complex polygenic trait shaped by multiple environmental and host genetic factors. *Proceedings of the National Academy of Sciences of the United States of America*, *107*(44), 18933–18938. https://doi.org/10.1073/pnas.1007028107

Bergmark, J., Carlsson, A., Granerus, A. K., Jagenburg, R., Magnusson, T., & Svanborg, A. (1972). Decarboxylation of orally administered L-dopa in the human digestive tract. *Naunyn-Schmiedeberg's Archives of Pharmacology*, *272*(4), 437–440. https://doi.org/10.1007/bf00501249

Bitter, A., Rümmele, P., Klein, K., Kandel, B. A., Rieger, J. K., Nüssler, A. K., … Burk, O. (2015). Pregnane X receptor activation and silencing promote steatosis of human hepatic cells by distinct lipogenic mechanisms. *Archives of Toxicology*, *89*(11), 2089–2103. https://doi.org/10.1007/s00204-014-1348-x

Björkholm, B., Bok, C. M., Lundin, A., Rafter, J., Hibberd, M. L., & Pettersson, S. (2009). Intestinal Microbiota Regulate Xenobiotic Metabolism in the Liver. *PLOS ONE*, *4*(9), e6958. https://doi.org/10.1371/journal.pone.0006958

Bibliographic references

Blizard, D., Sueyoshi, T., Negishi, M., Dehal, S. S., & Kupfer, D. (2001). Mechanism of induction of cytochrome p450 enzymes by the proestrogenic endocrine disruptor pesticide-methoxychlor: Interactions of methoxychlor metabolites with the constitutive androstane receptor system. *Drug Metabolism and Disposition: The Biological Fate of Chemicals*, *29*(6), 781–785.

Bookout, A. L., Jeong, Y., Downes, M., Yu, R. T., Evans, R. M., & Mangelsdorf, D. J. (2006). Anatomical profiling of nuclear receptor expression reveals a hierarchical transcriptional network. *Cell*, *126*(4), 789–799. https://doi.org/10.1016/j.cell.2006.06.049

Bourguet, W., Ruff, M., Chambon, P., Gronemeyer, H., & Moras, D. (1995). Crystal structure of the ligand-binding domain of the human nuclear receptor RXR-alpha. *Nature*, *375*(6530), 377–382. https://doi.org/10.1038/375377a0

Breuker, C., Moreau, A., Lakhal, L., Tamasi, V., Parmentier, Y., Meyer, U., … Pascussi, J.-M. (2010). Hepatic expression of thyroid hormone-responsive spot 14 protein is regulated by constitutive androstane receptor (NR1I3). *Endocrinology*, *151*(4), 1653–1661. https://doi.org/10.1210/en.2009-1435

Brugman, S., Liu, K.-Y., Lindenbergh-Kortleve, D., Samsom, J. N., Furuta, G. T., Renshaw, S. A., … Nieuwenhuis, E. E. S. (2009). Oxazolone-induced enterocolitis in zebrafish depends on the composition of the intestinal microbiota. *Gastroenterology*, *137*(5), 1757-1767.e1. https://doi.org/10.1053/j.gastro.2009.07.069

Burk, O., Arnold, K. A., Geick, A., Tegude, H., & Eichelbaum, M. (2005). A role for constitutive androstane receptor in the regulation of human intestinal MDR1 expression. *Biological Chemistry*, *386*(6), 503–513. https://doi.org/10.1515/BC.2005.060

Burt, A. D., Lackner, C., & Tiniakos, D. G. (2015). Diagnosis and Assessment of NAFLD: Definitions and Histopathological Classification. *Seminars in Liver Disease*, *35*(3), 207–220. https://doi.org/10.1055/s-0035-1562942

Caminero, A., Nistal, E., Herrán, A. R., Pérez-Andrés, J., Ferrero, M. A., Vaquero Ayala, L., … Casqueiro, F. J. (2015). Differences in gluten metabolism among healthy volunteers, coeliac disease patients and first-degree relatives. *The British Journal of Nutrition*, *114*(8), 1157–1167. https://doi.org/10.1017/S0007114515002767

Campieri, M., & Gionchetti, P. (2001). Bacteria as the cause of ulcerative colitis. *Gut*, *48*(1), 132–135. https://doi.org/10.1136/gut.48.1.132

Cani, P. D. (2018). Human gut microbiome: Hopes, threats and promises. *Gut*, *67*(9), 1716–1725. https://doi.org/10.1136/gutjnl-2018-316723

Cerveny, L., Svecova, L., Anzenbacherova, E., Vrzal, R., Staud, F., Dvorak, Z., … Pavek, P. (2007). Valproic acid induces CYP3A4 and MDR1 gene expression by activation of constitutive androstane receptor and pregnane X receptor pathways. *Drug Metabolism and Disposition: The Biological Fate of Chemicals*, *35*(7), 1032–1041. https://doi.org/10.1124/dmd.106.014456

Chai, S. C., Cherian, M. T., Wang, Y.-M., & Chen, T. (2016). Small-molecule modulators of PXR and CAR. *Biochimica Et Biophysica Acta*, *1859*(9), 1141–1154. https://doi.org/10.1016/j.bbagrm.2016.02.013

Chandran, A., & Vishveshwara, S. (2016). Exploration of the conformational landscape in pregnane X receptor reveals a new binding pocket: Conformational Landscape in Pregnane X Receptor. *Protein Science*, *25*(11), 1989–2005. https://doi.org/10.1002/pro.3012

Chawla, A. (2001). Nuclear Receptors and Lipid Physiology: Opening the X-Files. *Science*, *294*(5548), 1866–1870. https://doi.org/10.1126/science.294.5548.1866

Chawla, Ajay, Repa, J. J., Evans, R. M., & Mangelsdorf, D. J. (2001). Nuclear Receptors and Lipid Physiology: Opening the X-Files. *Science*, *294*(5548), 1866–1870. https://doi.org/10.1126/science.294.5548.1866

Chen, W., Chen, G., Head, D. L., Mangelsdorf, D. J., & Russell, D. W. (2007). Enzymatic reduction of oxysterols impairs LXR signaling in cultured cells and the livers of mice. *Cell Metabolism*, *5*(1), 73–79. https://doi.org/10.1016/j.cmet.2006.11.012

Chen, X., Maiti, S., Zhang, J., & Chen, G. (2006). Nuclear receptor interactions in methotrexate induction of human dehydroepiandrosterone sulfotransferase (hSULT2A1). *Journal of Biochemical and Molecular Toxicology*, *20*(6), 309–317. https://doi.org/10.1002/jbt.20149

Cheng, J., Shah, Y. M., Ma, X., Pang, X., Tanaka, T., Kodama, T., … Gonzalez, F. J. (2010). Therapeutic role of rifaximin in inflammatory bowel disease: Clinical implication of human pregnane X receptor activation. *The Journal of Pharmacology and Experimental Therapeutics*, *335*(1), 32–41. https://doi.org/10.1124/jpet.110.170225

Cheng, S., Zou, M., Liu, Q., Kuang, J., Shen, J., Pu, S., … He, J. (2017). Activation of Constitutive Androstane Receptor Prevents Cholesterol Gallstone Formation. *The American Journal of Pathology*, *187*(4), 808–818. https://doi.org/10.1016/j.ajpath.2016.12.013

Cheng, X., & Klaassen, C. D. (2008). Critical Role of PPAR-α in Perfluorooctanoic Acid– and Perfluorodecanoic Acid–Induced Downregulation of Oatp Uptake Transporters in Mouse Livers. *Toxicological Sciences*, *106*(1), 37–45. https://doi.org/10.1093/toxsci/kfn161

Cherrington, N. J., Hartley, D. P., Li, N., Johnson, D. R., & Klaassen, C. D. (2002). Organ distribution of multidrug resistance proteins 1, 2, and 3 (Mrp1, 2, and 3) mRNA and hepatic induction of Mrp3 by constitutive androstane receptor activators in rats. *The Journal of Pharmacology and Experimental Therapeutics*, *300*(1), 97–104. https://doi.org/10.1124/jpet.300.1.97

Cho, C. E., & Caudill, M. A. (2017). Trimethylamine-N-Oxide: Friend, Foe, or Simply Caught in the Cross-Fire? *Trends in Endocrinology and Metabolism: TEM*, *28*(2), 121–130. https://doi.org/10.1016/j.tem.2016.10.005

Cho, H. Y., Jung, J.-Y., Park, H., Yang, J.-Y., Jung, S., An, J. H., … Shin, C. S. (2014). In vivo deletion of CAR resulted in high bone mass phenotypes in male mice. *Journal of Cellular Physiology*, *229*(5), 561–571. https://doi.org/10.1002/jcp.24478

Choi, H., Chung, M., Tzameli, I., Simha, D., Lee, Y., Seol, W., & Moore, D. (1997). Differential transactivation by two isoforms of the orphan nuclear hormone receptor CAR. - PubMed–NCBI. Retrieved June 20, 2019, from https://www-ncbi-nlm-nih-gov.gate2.inist.fr/pubmed/9295294

Chu, H., Duan, Y., Yang, L., & Schnabl, B. (2019). Small metabolites, possible big changes: A microbiota-centered view of non-alcoholic fatty liver disease. *Gut*, *68*(2), 359–370. https://doi.org/10.1136/gutjnl-2018-316307

Claus, S. P., Ellero, S. L., Berger, B., Krause, L., Bruttin, A., Molina, J., … others. (2011). Colonization-induced host-gut microbial metabolic interaction. *MBio*, *2*(2), e00271–10.

Claus, S. P., Guillou, H., & Ellero-Simatos, S. (2016). The gut microbiota: A major player in the toxicity of environmental pollutants? *NPJ Biofilms and Microbiomes*, *2*, 16003. https://doi.org/10.1038/npjbiofilms.2016.3

Clavel, T., Henderson, G., Engst, W., Doré, J., & Blaut, M. (2006). Phylogeny of human intestinal bacteria that activate the dietary lignan secoisolariciresinol diglucoside. *FEMS Microbiology Ecology*, *55*(3), 471–478. https://doi.org/10.1111/j.1574-6941.2005.00057.x

Cross, A. J., Ferrucci, L. M., Risch, A., Graubard, B. I., Ward, M. H., Park, Y., … Sinha, R. (2010). A large prospective study of meat consumption and colorectal cancer risk: An investigation of potential mechanisms underlying this association. *Cancer Research*, *70*(6), 2406–2414. https://doi.org/10.1158/0008-5472.CAN-09-3929

Cross, T.-W. L., Kasahara, K., & Rey, F. E. (2018). Sexual dimorphism of cardiometabolic dysfunction: Gut microbiome in the play? *Molecular Metabolism*, *15*, 70–81. https://doi.org/10.1016/j.molmet.2018.05.016

Cryan, J. F., & Dinan, T. G. (2012). Mind-altering microorganisms: The impact of the gut microbiota on brain and behaviour. *Nature Reviews. Neuroscience*, *13*(10), 701–712. https://doi.org/10.1038/nrn3346

Currie, R. A., Peffer, R. C., Goetz, A. K., Omiecinski, C. J., & Goodman, J. I. (2014). Phenobarbital and propiconazole toxicogenomic profiles in mice show major similarities consistent with the key role that constitutive androstane receptor (CAR) activation plays in their mode of action. *Toxicology*, *321*, 80–88. https://doi.org/10.1016/j.tox.2014.03.003

Dalile, B., Van Oudenhove, L., Vervliet, B., & Verbeke, K. (2019). The role of short-chain fatty acids in microbiota-gut-brain communication. *Nature Reviews. Gastroenterology & Hepatology*, *16*(8), 461–478. https://doi.org/10.1038/s41575-019-0157-3

Dapito, D. H., Mencin, A., Gwak, G.-Y., Pradere, J.-P., Jang, M.-K., Mederacke, I., … Schwabe, R. F. (2012). Promotion of hepatocellular carcinoma by the intestinal microbiota and TLR4. *Cancer Cell*, *21*(4), 504–516. https://doi.org/10.1016/j.ccr.2012.02.007

Darfeuille-Michaud, A., Neut, C., Barnich, N., Lederman, E., Di Martino, P., Desreumaux, P., … Colombel, J. F. (1998). Presence of adherent Escherichia coli strains in ileal mucosa of patients with Crohn's disease. *Gastroenterology*, *115*(6), 1405–1413. https://doi.org/10.1016/s0016-5085(98)70019-8

Darfeuille-Michaud, Arlette. (2002). Adherent-invasive Escherichia coli: A putative new E. coli pathotype associated with Crohn's disease. *International Journal of Medical Microbiology: IJMM*, *292*(3–4), 185–193. https://doi.org/10.1078/1438-4221-00201

David, L. A., Maurice, C. F., Carmody, R. N., Gootenberg, D. B., Button, J. E., Wolfe, B. E., … Turnbaugh, P. J. (2014). Diet rapidly and reproducibly alters the human gut microbiome. *Nature*, *505*(7484), 559–563. https://doi.org/10.1038/nature12820

Day, C. P. (2010). Genetic and environmental susceptibility to non-alcoholic fatty liver disease. *Digestive Diseases (Basel, Switzerland)*, *28*(1), 255–260. https://doi.org/10.1159/000282098

De Vadder, F., Kovatcheva-Datchary, P., Goncalves, D., Vinera, J., Zitoun, C., Duchampt, A., … Mithieux, G. (2014). Microbiota-generated metabolites promote metabolic benefits via gut-brain neural circuits. *Cell*, *156*(1–2), 84–96. https://doi.org/10.1016/j.cell.2013.12.016

DeKeyser, J. G., Stagliano, M. C., Auerbach, S. S., Prabhu, K. S., Jones, A. D., & Omiecinski, C. J. (2009). Di(2-ethylhexyl) phthalate is a highly potent agonist for the human constitutive androstane receptor splice variant CAR2. *Molecular Pharmacology*, *75*(5), 1005–1013. https://doi.org/10.1124/mol.108.053702

Deloménie, C., Fouix, S., Longuemaux, S., Brahimi, N., Bizet, C., Picard, B., … Dupret, J.-M. (2001). Identification and Functional Characterization of Arylamine N-Acetyltransferases in Eubacteria: Evidence for Highly Selective Acetylation of 5-Aminosalicylic Acid. *Journal of Bacteriology*, *183*(11), 3417–3427. https://doi.org/10.1128/JB.183.11.3417-3427.2001

den Besten, G., van Eunen, K., Groen, A. K., Venema, K., Reijngoud, D.-J., & Bakker, B. M. (2013). The role of short-chain fatty acids in the interplay between diet, gut microbiota, and host energy metabolism. *Journal of Lipid Research*, *54*(9), 2325–2340. https://doi.org/10.1194/jlr.R036012

Deshmukh, H. S., Liu, Y., Menkiti, O. R., Mei, J., Dai, N., O'Leary, C. E., … Worthen, G. S. (2014). The microbiota regulates neutrophil homeostasis and host resistance to Escherichia coli K1 sepsis in neonatal mice. *Nature Medicine*, *20*(5), 524–530. https://doi.org/10.1038/nm.3542

Devlin, A. S., Marcobal, A., Dodd, D., Nayfach, S., Plummer, N., Meyer, T., … Fischbach, M. A. (2016). Modulation of a Circulating Uremic Solute via Rational Genetic Manipulation of the Gut Microbiota. *Cell Host & Microbe*, *20*(6), 709–715. https://doi.org/10.1016/j.chom.2016.10.021

Dingemanse, C., Belzer, C., van Hijum, S. A. F. T., Günthel, M., Salvatori, D., den Dunnen, J. T., … Robanus-Maandag, E. C. (2015). Akkermansia muciniphila and Helicobacter typhlonius modulate intestinal tumor development in mice. *Carcinogenesis*, *36*(11), 1388–1396. https://doi.org/10.1093/carcin/bgv120

Dionne, M. S., & Schneider, D. S. (2008). Models of infectious diseases in the fruit fly Drosophila melanogaster. *Disease Models & Mechanisms*, *1*(1), 43–49. https://doi.org/10.1242/dmm.000307

Doerner, K. C., Takamine, F., LaVoie, C. P., Mallonee, D. H., & Hylemon, P. B. (1997). Assessment of fecal bacteria with bile acid 7 alpha-dehydroxylating activity for the presence of bai-like genes. *Applied and Environmental Microbiology*, *63*(3), 1185–1188.

Dominianni, C., Sinha, R., Goedert, J. J., Pei, Z., Yang, L., Hayes, R. B., & Ahn, J. (2015). Sex, body mass index, and dietary fiber intake influence the human gut microbiome. *PloS One*, *10*(4), e0124599. https://doi.org/10.1371/journal.pone.0124599

Dong, B., Saha, P. K., Huang, W., Chen, W., Abu-Elheiga, L. A., Wakil, S. J., … Moore, D. D. (2009). Activation of nuclear receptor CAR ameliorates diabetes and fatty liver disease. *Proceedings of the National Academy of Sciences of the United States of America*, *106*(44), 18831–18836. https://doi.org/10.1073/pnas.0909731106

Dou, W., Zhang, J., Zhang, E., Sun, A., Ding, L., Chou, G., … Mani, S. (2013). Chrysin ameliorates chemically induced colitis in the mouse through modulation of a PXR/NF-κB signaling pathway. *The Journal of Pharmacology and Experimental Therapeutics*, *345*(3), 473–482. https://doi.org/10.1124/jpet.112.201863

Duret, C., Daujat-Chavanieu, M., Pascussi, J.-M., Pichard-Garcia, L., Balaguer, P., Fabre, J.-M., … Gerbal-Chaloin, S. (2006). Ketoconazole and miconazole are antagonists of the human glucocorticoid receptor: Consequences on the expression and function of the constitutive androstane receptor and the pregnane X receptor. *Molecular Pharmacology*, *70*(1), 329–339. https://doi.org/10.1124/mol.105.022046

Duszka, K., & Wahli, W. (2018). Enteric Microbiota−Gut−Brain Axis from the Perspective of Nuclear Receptors. *International Journal of Molecular Sciences*, *19*(8). https://doi.org/10.3390/ijms19082210

Eckburg, P. B., Bik, E. M., Bernstein, C. N., Purdom, E., Dethlefsen, L., Sargent, M., … Relman, D. A. (2005). Diversity of the human intestinal microbial flora. *Science (New York, N.Y.)*, *308*(5728), 1635–1638. https://doi.org/10.1126/science.1110591

Elcombe, C. R., Elcombe, B. M., Foster, J. R., Chang, S.-C., Ehresman, D. J., & Butenhoff, J. L. (2012). Hepatocellular hypertrophy and cell proliferation in Sprague-Dawley rats from dietary exposure to potassium perfluorooctanesulfonate results from increased expression of xenosensor nuclear receptors PPARα and CAR/PXR. *Toxicology*, *293*(1–3), 16–29. https://doi.org/10.1016/j.tox.2011.12.014

Engevik, M. A., & Versalovic, J. (2017). Biochemical features of beneficial microbes: Foundations for therapeutic microbiology. *Microbiology Spectrum*, *5*(5). https://doi.org/10.1128/microbiolspec.BAD-0012-2016

Evans, R. M., & Mangelsdorf, D. J. (2014). Nuclear Receptors, RXR, and the Big Bang. *Cell*, *157*(1), 255–266. https://doi.org/10.1016/j.cell.2014.03.012

Falany, C. N., Fortinberry, H., Leiter, E. H., & Barnes, S. (1997). Cloning, expression, and chromosomal localization of mouse liver bile acid CoA:amino acid N-acyltransferase. *Journal of Lipid Research*, *38*(6), 1139–1148.

Falany, C. N., Johnson, M. R., Barnes, S., & Diasio, R. B. (1994). Glycine and taurine conjugation of bile acids by a single enzyme. Molecular cloning and expression of human liver bile acid CoA:amino acid N-acyltransferase. *The Journal of Biological Chemistry*, *269*(30), 19375–19379.

Fennema, D., Phillips, I. R., & Shephard, E. A. (2016). Trimethylamine and Trimethylamine N-Oxide, a Flavin-Containing Monooxygenase 3 (FMO3)-Mediated Host-Microbiome Metabolic Axis Implicated in Health and Disease. *Drug Metabolism and Disposition: The Biological Fate of Chemicals*, *44*(11), 1839–1850. https://doi.org/10.1124/dmd.116.070615

Fontaine, C. A., Skorupski, A. M., Vowles, C. J., Anderson, N. E., Poe, S. A., & Eaton, K. A. (2015). How free of germs is germ-free? Detection of bacterial contamination in a germ free mouse unit. *Gut Microbes*, *6*(4), 225–233. https://doi.org/10.1080/19490976.2015.1054596

Forman, B. M., Tzameli, I., Choi, H. S., Chen, J., Simha, D., Seol, W., … Moore, D. D. (1998). Androstane metabolites bind to and deactivate the nuclear receptor CAR-beta. *Nature*, *395*(6702), 612–615. https://doi.org/10.1038/26996

Frank, C., Makkonen, H., Dunlop, T. W., Matilainen, M., Väisänen, S., & Carlberg, C. (2005). Identification of pregnane X receptor binding sites in the regulatory regions of genes involved in bile acid homeostasis. *Journal of Molecular Biology*, *346*(2), 505–519. https://doi.org/10.1016/j.jmb.2004.12.003

Frankenfeld, C. L., Atkinson, C., Wähälä, K., & Lampe, J. W. (2014). Obesity prevalence in relation to gut microbial environments capable of producing equol or O-desmethylangolensin from the isoflavone daidzein. *European Journal of Clinical Nutrition*, *68*(4), 526–530. https://doi.org/10.1038/ejcn.2014.23

Friswell, M. K., Gika, H., Stratford, I. J., Theodoridis, G., Telfer, B., Wilson, I. D., & McBain, A. J. (2010). Site and strain-specific variation in gut microbiota profiles and metabolism in experimental mice. *PloS One*, *5*(1), e8584. https://doi.org/10.1371/journal.pone.0008584

Fu, Z. D., Selwyn, F. P., Cui, J. Y., & Klaassen, C. D. (2017). RNA-Seq Profiling of Intestinal Expression of Xenobiotic Processing Genes in Germ-Free Mice. *Drug Metabolism and Disposition*, *45*(12), 1225–1238. https://doi.org/10.1124/dmd.117.077313

Fukiya, S., Arata, M., Kawashima, H., Yoshida, D., Kaneko, M., Minamida, K., … Yokota, A. (2009). Conversion of cholic acid and chenodeoxycholic acid into their 7-oxo derivatives by Bacteroides intestinalis AM-1 isolated from human feces. *FEMS Microbiology Letters*, *293*(2), 263–270. https://doi.org/10.1111/j.1574-6968.2009.01531.x

Fukumasu, H., Cordeiro, Y. G., Rochetti, A. L., Barra, C. N., Sámora, T. S., Strefezzi, R. F., & Dagli, M. L. Z. (2015). Expression of NR1I3 in mouse lung tumors induced by the tobacco-specific nitrosamine 4-(methylnitrosamino)-4-(3-pyridyl)-1-butanone. *Brazilian Journal of Medical and Biological Research = Revista Brasileira De Pesquisas Medicas E Biologicas*, *48*(3), 240–244. https://doi.org/10.1590/1414-431X20144210

Gao, Jie, He, J., Zhai, Y., Wada, T., & Xie, W. (2009). The Constitutive Androstane Receptor Is an Anti-obesity Nuclear Receptor That Improves Insulin Sensitivity. *Journal of Biological Chemistry*, *284*(38), 25984–25992. https://doi.org/10.1074/jbc.M109.016808

Gao, Jie, & Xie, W. (2010). Pregnane X Receptor and Constitutive Androstane Receptor at the Crossroads of Drug Metabolism and Energy Metabolism. *Drug Metabolism and Disposition*, *38*(12), 2091–2095. https://doi.org/10.1124/dmd.110.035568

Gao, Jie, Yan, J., Xu, M., Ren, S., & Xie, W. (2015). CAR Suppresses Hepatic Gluconeogenesis by Facilitating the Ubiquitination and Degradation of PGC1α. *Molecular Endocrinology (Baltimore, Md.)*, *29*(11), 1558–1570. https://doi.org/10.1210/me.2015-1145

Gao, Jing, Xu, K., Liu, H., Liu, G., Bai, M., Peng, C., … Yin, Y. (2018). Impact of the Gut Microbiota on Intestinal Immunity Mediated by Tryptophan Metabolism. *Frontiers in Cellular and Infection Microbiology*, *8*. https://doi.org/10.3389/fcimb.2018.00013

Garcia, M., Thirouard, L., Sedès, L., Monrose, M., Holota, H., Caira, F., … Beaudoin, C. (2018). Nuclear Receptor Metabolism of Bile Acids and Xenobiotics: A Coordinated Detoxification System with Impact on Health and Diseases. *International Journal of Molecular Sciences*, *19*(11). https://doi.org/10.3390/ijms19113630

García-Villalba, R., Beltrán, D., Espín, J. C., Selma, M. V., & Tomás-Barberán, F. A. (2013). Time course production of urolithins from ellagic acid by human gut microbiota. *Journal of Agricultural and Food Chemistry*, *61*(37), 8797–8806. https://doi.org/10.1021/jf402498b

Garg, A., Zhao, A., Erickson, S. L., Mukherjee, S., Lau, A. J., Alston, L., … Hirota, S. A. (2016). Pregnane X Receptor Activation Attenuates Inflammation-Associated Intestinal Epithelial Barrier Dysfunction by Inhibiting Cytokine-Induced Myosin Light-Chain Kinase Expression and c-Jun N-Terminal Kinase 1/2 Activation. *The Journal of Pharmacology and Experimental Therapeutics*, *359*(1), 91–101. https://doi.org/10.1124/jpet.116.234096

Gérard, P., Béguet, F., Lepercq, P., Rigottier-Gois, L., Rochet, V., Andrieux, C., & Juste, C. (2004). Gnotobiotic rats harboring human intestinal microbiota as a model for studying cholesterol-to-coprostanol conversion. *FEMS Microbiology Ecology*, *47*(3), 337–343. https://doi.org/10.1016/S0168-6496(03)00285-X

Gerbes, A., Zoulim, F., Tilg, H., Dufour, J.-F., Bruix, J., Paradis, V., … Avila, M. A. (2018). Gut roundtable meeting paper: Selected recent advances in hepatocellular carcinoma. *Gut*, *67*(2), 380–388. https://doi.org/10.1136/gutjnl-2017-315068

Germain, P., Staels, B., Dacquet, C., Spedding, M., & Laudet, V. (2006). Overview of nomenclature of nuclear receptors. *Pharmacological Reviews*, *58*(4), 685–704. https://doi.org/10.1124/pr.58.4.2

Gill, S. R., Pop, M., DeBoy, R. T., Eckburg, P. B., Turnbaugh, P. J., Samuel, B. S., … Nelson, K. E. (2006). Metagenomic Analysis of the Human Distal Gut Microbiome. *Science (New York, N.Y.)*, *312*(5778), 1355–1359. https://doi.org/10.1126/science.1124234

Goetz, A. K., Bao, W., Ren, H., Schmid, J. E., Tully, D. B., Wood, C., … Dix, D. J. (2006). Gene expression profiling in the liver of CD-1 mice to characterize the hepatotoxicity of triazole fungicides. *Toxicology and Applied Pharmacology*, *215*(3), 274–284. https://doi.org/10.1016/j.taap.2006.02.016

Goldin, B. R., Peppercorn, M. A., & Goldman, P. (1973). Contributions of host and intestinal microflora in the metabolism of L-dopa by the rat. *The Journal of Pharmacology and Experimental Therapeutics*, *186*(1), 160–166.

Gong, H., Singh, S. V., Singh, S. P., Mu, Y., Lee, J. H., Saini, S. P. S., … Xie, W. (2006). Orphan nuclear receptor pregnane X receptor sensitizes oxidative stress responses in transgenic mice and cancerous cells. *Molecular Endocrinology (Baltimore, Md.)*, *20*(2), 279–290. https://doi.org/10.1210/me.2005-0205

Gonzalez-Perez, G., Hicks, A. L., Tekieli, T. M., Radens, C. M., Williams, B. L., & Lamousé-Smith, E. S. N. (2016). Maternal Antibiotic Treatment Impacts Development of the Neonatal Intestinal Microbiome and Antiviral Immunity. *Journal of Immunology (Baltimore, Md.: 1950)*, *196*(9), 3768–3779. https://doi.org/10.4049/jimmunol.1502322

Goodwin, B., Hodgson, E., & Liddle, C. (1999). The orphan human pregnane X receptor mediates the transcriptional activation of CYP3A4 by rifampicin through a distal enhancer module. *Molecular Pharmacology*, *56*(6), 1329–1339. https://doi.org/10.1124/mol.56.6.1329

Guéguen, Y., Mouzat, K., Ferrari, L., Tissandie, E., Lobaccaro, J. M. A., Batt, A.-M., … Souidi, M. (2006). [Cytochromes P450: Xenobiotic metabolism, regulation and clinical importance]. *Annales De Biologie Clinique*, *64*(6), 535–548.

Guo, D., Sarkar, J., & Xu, Y. (2007). Induction of nuclear translocation of constitutive androstane receptor by peroxisome proliferator-activated receptor alpha synthetic ligands in mou... - PubMed—NCBI. Retrieved June 20, 2019, from https://www-ncbi-nlm-nih-gov.gate2.inist.fr/pubmed/17962186

Guo, G. L., Staudinger, J., Ogura, K., & Klaassen, C. D. (2002). Induction of rat organic anion transporting polypeptide 2 by pregnenolone-16alpha-carbonitrile is via interaction with pregnane X receptor. *Molecular Pharmacology*, *61*(4), 832–839. https://doi.org/10.1124/mol.61.4.832

Gwag, T., Meng, Z., Sui, Y., Helsley, R. N., Park, S.-H., Wang, S., … Zhou, C. (2019). Non-nucleoside reverse transcriptase inhibitor efavirenz activates PXR to induce hypercholesterolemia and hepatic steatosis. *Journal of Hepatology*, *70*(5), 930–940. https://doi.org/10.1016/j.jhep.2018.12.038

Hager, G. L., Lim, C. S., Elbi, C., & Baumann, C. T. (2000). Trafficking of nuclear receptors in living cells. *The Journal of Steroid Biochemistry and Molecular Biology*, *74*(5), 249–254.

Hakkola, J., Rysä, J., & Hukkanen, J. (2016). Regulation of hepatic energy metabolism by the nuclear receptor PXR. *Biochimica Et Biophysica Acta*, *1859*(9), 1072–1082. https://doi.org/10.1016/j.bbagrm.2016.03.012

Hardie, D. G., & Ashford, M. L. J. (2014). AMPK: Regulating energy balance at the cellular and whole body levels. *Physiology (Bethesda, Md.)*, *29*(2), 99–107. https://doi.org/10.1152/physiol.00050.2013

Haro, C., Rangel-Zúñiga, O. A., Alcalá-Díaz, J. F., Gómez-Delgado, F., Pérez-Martínez, P., Delgado-Lista, J., … Camargo, A. (2016). Intestinal Microbiota Is Influenced by Gender and Body Mass Index. *PloS One*, *11*(5), e0154090. https://doi.org/10.1371/journal.pone.0154090

Haughton, E. L., Tucker, S. J., Marek, C. J., Durward, E., Leel, V., Bascal, Z., … Wright, M. C. (2006). Pregnane X receptor activators inhibit human hepatic stellate cell transdifferentiation in vitro. *Gastroenterology*, *131*(1), 194–209. https://doi.org/10.1053/j.gastro.2006.04.01

Heinzel, T., Lavinsky, R. M., Mullen, T. M., Söderstrom, M., Laherty, C. D., Torchia, J., … Rosenfeld, M. G. (1997). A complex containing N-CoR, mSin3 and histone deacetylase mediates transcriptional repression. *Nature*, *387*(6628), 43–48. https://doi.org/10.1038/387043a0

Henao-Mejia, J., Elinav, E., Jin, C., Hao, L., Mehal, W. Z., Strowig, T., … Flavell, R. A. (2012). Inflammasome-mediated dysbiosis regulates progression of NAFLD and obesity. *Nature*, *482*(7384), 179–185. https://doi.org/10.1038/nature10809

Hernandez, J. P., Mota, L. C., & Baldwin, W. S. (2009). Activation of CAR and PXR by Dietary, Environmental and Occupational Chemicals Alters Drug Metabolism, Intermediary Metabolism, and Cell Proliferation. *Current Pharmacogenomics and Personalized Medicine*, *7*(2), 81–105. https://doi.org/10.2174/187569209788654005

Hernandez, Juan P., Huang, W., Chapman, L. M., Chua, S., Moore, D. D., & Baldwin, W. S. (2007). The environmental estrogen, nonylphenol, activates the constitutive androstane receptor. *Toxicological Sciences: An Official Journal of the Society of Toxicology*, *98*(2), 416–426. https://doi.org/10.1093/toxsci/kfm107

Hildebrand, F., Nguyen, T. L. A., Brinkman, B., Yunta, R. G., Cauwe, B., Vandenabeele, P., … Raes, J. (2013). Inflammation-associated enterotypes, host genotype, cage and inter-individual effects drive gut microbiota variation in common laboratory mice. *Genome Biology*, *14*(1), R4. https://doi.org/10.1186/gb-2013-14-1-r4

Holloway, M. G., Miles, G. D., Dombkowski, A. A., & Waxman, D. J. (2008). Liver-specific hepatocyte nuclear factor-4alpha deficiency: Greater impact on gene expression in male than in female mouse liver. *Molecular Endocrinology (Baltimore, Md.)*, *22*(5), 1274–1286. https://doi.org/10.1210/me.2007-0564

Honkakoski, P., Sueyoshi, T., & Negishi, M. (2003). Drug-activated nuclear receptors CAR and PXR. *Annals of Medicine*, *35*(3), 172–182.

Hooper, L. V., Littman, D. R., & Macpherson, A. J. (2012). Interactions between the microbiota and the immune system. *Science (New York, N.Y.)*, *336*(6086), 1268–1273. https://doi.org/10.1126/science.1223490

Howe, K., Sanat, F., Thumser, A. E., Coleman, T., & Plant, N. (2011). The statin class of HMG-CoA reductase inhibitors demonstrate differential activation of the nuclear receptors PXR, CAR and FXR, as well as their downstream target genes. *Xenobiotica; the Fate of Foreign Compounds in Biological Systems*, *41*(7), 519–529. https://doi.org/10.3109/00498254.2011.569773

Huang, W., Zhang, J., Wei, P., Schrader, W. T., & Moore, D. D. (2004). Meclizine is an agonist ligand for mouse constitutive androstane receptor (CAR) and an inverse agonist for human CAR. *Molecular Endocrinology (Baltimore, Md.)*, *18*(10), 2402–2408. https://doi.org/10.1210/me.2004-0046

Hudson, G. M., Flannigan, K. L., Erickson, S. L., Vicentini, F. A., Zamponi, A., Hirota, C. L., … Hirota, S. A. (2017). Constitutive androstane receptor regulates the intestinal mucosal response to injury. *British Journal of Pharmacology*, *174*(12), 1857–1871. https://doi.org/10.1111/bph.13787

Hugenholtz, F., & de Vos, W. M. (2018). Mouse models for human intestinal microbiota research: A critical evaluation. *Cellular and Molecular Life Sciences: CMLS*, *75*(1), 149–160. https://doi.org/10.1007/s00018-017-2693-8

Ihunnah, C. A., Jiang, M., & Xie, W. (2011). Nuclear receptor PXR, transcriptional circuits and metabolic relevance. *Biochimica Et Biophysica Acta*, *1812*(8), 956–963. https://doi.org/10.1016/j.bbadis.2011.01.014

Ingelfinger, J. R. (2008). Melamine and the Global Implications of Food Contamination. *New England Journal of Medicine*, *359*(26), 2745–2748. https://doi.org/10.1056/NEJMp0808410

Iroz, A., Montagner, A., Benhamed, F., Levavasseur, F., Polizzi, A., Anthony, E., … Postic, C. (2017). A Specific ChREBP and PPARα Cross-Talk Is Required for the Glucose-Mediated FGF21 Response. *Cell Reports*, *21*(2), 403–416. https://doi.org/10.1016/j.celrep.2017.09.065

Jackson, J. P., Ferguson, S. S., Moore, R., Negishi, M., & Goldstein, J. A. (2004). The constitutive active/androstane receptor regulates phenytoin induction of Cyp2c29. *Molecular Pharmacology*, *65*(6), 1397–1404. https://doi.org/10.1124/mol.65.6.1397

Jarukamjorn, K., Sakuma, T., & Nemoto, N. (2002). Sexual dimorphic expression of mouse hepatic CYP2B: Alterations during development or after hypophysectomy. *Biochemical Pharmacology*, *63*(11), 2037–2041.

Jones, S. A., Moore, L. B., Shenk, J. L., Wisely, G. B., Hamilton, G. A., McKee, D. D., … Moore, J. T. (2000). The pregnane X receptor: A promiscuous xenobiotic receptor that has diverged during evolution. *Molecular Endocrinology (Baltimore, Md.)*, *14*(1), 27–39. https://doi.org/10.1210/mend.14.1.0409

Jump, R. L. P., Polinkovsky, A., Hurless, K., Sitzlar, B., Eckart, K., Tomas, M., … Donskey, C. J. (2014). Metabolomics analysis identifies intestinal microbiota-derived biomarkers of colonization resistance in clindamycin-treated mice. *PloS One*, *9*(7), e101267. https://doi.org/10.1371/journal.pone.0101267

Jung, D., Mangelsdorf, D. J., & Meyer, U. A. (2006). Pregnane X receptor is a target of farnesoid X receptor. *The Journal of Biological Chemistry*, *281*(28), 19081–19091. https://doi.org/10.1074/jbc.M600116200

Kabat, A. M., Pott, J., & Maloy, K. J. (2016). The Mucosal Immune System and Its Regulation by Autophagy. *Frontiers in Immunology*, *7*. https://doi.org/10.3389/fimmu.2016.00240

Kaliannan, K., Robertson, R. C., Murphy, K., Stanton, C., Kang, C., Wang, B., … Kang, J. X. (2018). Estrogen-mediated gut microbiome alterations influence sexual dimorphism in metabolic syndrome in mice. *Microbiome*, *6*. https://doi.org/10.1186/s40168-018-0587-0

Kamiyama, Y., Matsubara, T., Yoshinari, K., Nagata, K., Kamimura, H., & Yamazoe, Y. (2007). Role of human hepatocyte nuclear factor 4alpha in the expression of drug-metabolizing enzymes and transporters in human hepatocytes assessed by use of small interfering RNA. *Drug Metabolism and Pharmacokinetics*, *22*(4), 287–298.

Kanno, Y., Otsuka, S., Hiromasa, T., Nakahama, T., & Inouye, Y. (2004). Diurnal difference in CAR mRNA expression. *Nuclear Receptor*, *2*(1), 6. https://doi.org/10.1186/1478-1336-2-6

Kasai, C., Sugimoto, K., Moritani, I., Tanaka, J., Oya, Y., Inoue, H., … Takase, K. (2015). Comparison of the gut microbiota composition between obese and non-obese individuals in a Japanese population, as analyzed by terminal restriction fragment length polymorphism and next-generation sequencing. *BMC Gastroenterology*, *15*, 100. https://doi.org/10.1186/s12876-015-0330-2

Kassam, A., Winrow, C. J., Fernandez-Rachubinski, F., Capone, J. P., & Rachubinski, R. A. (2000). The peroxisome proliferator response element of the gene encoding the peroxisomal beta-oxidation enzyme enoyl-CoA hydratase/3-hydroxyacyl-CoA dehydrogenase is a target for constitutive androstane receptor beta/9-cis-retinoic acid receptor-mediated transactivation. *The Journal of Biological Chemistry*, *275*(6), 4345–4350. https://doi.org/10.1074/jbc.275.6.4345

Kast, H. R., Goodwin, B., Tarr, P. T., Jones, S. A., Anisfeld, A. M., Stoltz, C. M., … Edwards, P. A. (2002). Regulation of multidrug resistance-associated protein 2 (ABCC2) by the nuclear receptors pregnane X receptor, farnesoid X-activated receptor, and constitutive androstane receptor. *The Journal of Biological Chemistry*, *277*(4), 2908–2915. https://doi.org/10.1074/jbc.M109326200

Kawamoto, T., Kakizaki, S., Yoshinari, K., & Negishi, M. (2000). Estrogen activation of the nuclear orphan receptor CAR (constitutive active receptor) in induction of the mouse Cyp2b10 gene. *Molecular Endocrinology (Baltimore, Md.)*, *14*(11), 1897–1905. https://doi.org/10.1210/mend.14.11.0547

Kellogg, T. F., Knight, P. L., & Wostmann, B. S. (1970). Effect of bile acid deconjugation on the fecal excretion of steroids. *Journal of Lipid Research*, *11*(4), 362–366.

Kellogg, T. F., & Wostmann, B. S. (1969). Fecal neutral steroids and bile acids from germfree rats. *Journal of Lipid Research*, *10*(5), 495–503.

Kennedy, E. A., King, K. Y., & Baldridge, M. T. (2018). Mouse Microbiota Models: Comparing Germ-Free Mice and Antibiotics Treatment as Tools for Modifying Gut Bacteria. *Frontiers in Physiology*, *9*. https://doi.org/10.3389/fphys.2018.01534

Kindt, A., Liebisch, G., Clavel, T., Haller, D., Hörmannsperger, G., Yoon, H., … Ecker, J. (2018). The gut microbiota promotes hepatic fatty acid desaturation and elongation in mice. *Nature Communications*, *9*(1), 3760. https://doi.org/10.1038/s41467-018-05767-4

Kisiela, M., Skarka, A., Ebert, B., & Maser, E. (2012). Hydroxysteroid dehydrogenases (HSDs) in bacteria: A bioinformatic perspective. *The Journal of Steroid Biochemistry and Molecular Biology*, *129*(1–2), 31–46. https://doi.org/10.1016/j.jsbmb.2011.08.002

Kitahara, M., Takamine, F., Imamura, T., & Benno, Y. (2000). Assignment of Eubacterium sp. VPI 12708 and related strains with high bile acid 7alpha-dehydroxylating activity to Clostridium scindens and proposal of Clostridium hylemonae sp. Nov., isolated from human faeces. *International Journal of Systematic and Evolutionary Microbiology*, *50 Pt 3*, 971–978. https://doi.org/10.1099/00207713-50-3-971

Kitahara, M., Takamine, F., Imamura, T., & Benno, Y. (2001). Clostridium hiranonis sp. Nov., a human intestinal bacterium with bile acid 7alpha-dehydroxylating activity. *International Journal of Systematic and Evolutionary Microbiology*, *51*(Pt 1), 39–44. https://doi.org/10.1099/00207713-51-1-39

Kliewer, S. A., Umesono, K., Mangelsdorf, D. J., & Evans, R. M. (1992). Retinoid X receptor interacts with nuclear receptors in retinoic acid, thyroid hormone and vitamin D3 signalling. *Nature*, *355*(6359), 446–449. https://doi.org/10.1038/355446a0

Kliewer, Steven A. (2015). Nuclear receptor PXR: Discovery of a pharmaceutical anti-target. *The Journal of Clinical Investigation*, *125*(4), 1388–1389. https://doi.org/10.1172/JCI81244

Kliewer, Steven A., & Mangelsdorf, D. J. (2019). A Dozen Years of Discovery: Insights into the Physiology and Pharmacology of FGF21. *Cell Metabolism*, *29*(2), 246–253. https://doi.org/10.1016/j.cmet.2019.01.004

Knight, R., Callewaert, C., Marotz, C., Hyde, E. R., Debelius, J. W., McDonald, D., & Sogin, M. L. (2017). The Microbiome and Human Biology. *Annual Review of Genomics and Human Genetics*, *18*, 65–86. https://doi.org/10.1146/annurev-genom-083115-022438

Kobayashi, K., Sueyoshi, T., Inoue, K., Moore, R., & Negishi, M. (2003). Cytoplasmic accumulation of the nuclear receptor CAR by a tetratricopeptide repeat protein in HepG2 cells. *Molecular Pharmacology*, *64*(5), 1069–1075. https://doi.org/10.1124/mol.64.5.1069

Kodama, S., Koike, C., Negishi, M., & Yamamoto, Y. (2004). Nuclear Receptors CAR and PXR Cross Talk with FOXO1 To Regulate Genes That Encode Drug-Metabolizing and Gluconeogenic Enzymes. *Molecular and Cellular Biology*, *24*(18), 7931–7940. https://doi.org/10.1128/MCB.24.18.7931-7940.2004

Kodama, S., & Negishi, M. (2013). PXR cross-talks with internal and external signals in physiological and pathophysiological responses. *Drug Metabolism Reviews*, *45*(3), 300–310. https://doi.org/10.3109/03602532.2013.795585

Konno, Y., Kamino, H., Moore, R., Lih, F., Tomer, K. B., Zeldin, D. C., … Negishi, M. (2010). The Nuclear Receptors Constitutive Active/Androstane Receptor and Pregnane X Receptor Activate the Cyp2c55 Gene in Mouse Liver. *Drug Metabolism and Disposition*, *38*(7), 1177–1182. https://doi.org/10.1124/dmd.110.032334

Koppel, N., Maini Rekdal, V., & Balskus, E. P. (2017). Chemical transformation of xenobiotics by the human gut microbiota. *Science (New York, N.Y.)*, *356*(6344). https://doi.org/10.1126/science.aag2770

Kostic, A. D., Howitt, M. R., & Garrett, W. S. (2013). Exploring host-microbiota interactions in animal models and humans. *Genes & Development*, *27*(7), 701–718. https://doi.org/10.1101/gad.212522.112

Kovacs, A., Ben-Jacob, N., Tayem, H., Halperin, E., Iraqi, F. A., & Gophna, U. (2011). Genotype is a stronger determinant than sex of the mouse gut microbiota. *Microbial Ecology*, *61*(2), 423–428. https://doi.org/10.1007/s00248-010-9787-2

Krasowski, M. D., Yasuda, K., Hagey, L. R., & Schuetz, E. G. (2005). Evolution of the pregnane x receptor: Adaptation to cross-species differences in biliary bile salts. *Molecular Endocrinology (Baltimore, Md.)*, *19*(7), 1720–1739. https://doi.org/10.1210/me.2004-0427

Krüger, M., Shehata, A. A., Schrödl, W., & Rodloff, A. (2013). Glyphosate suppresses the antagonistic effect of Enterococcus spp. On Clostridium botulinum. *Anaerobe*, *20*, 74–78. https://doi.org/10.1016/j.anaerobe.2013.01.005

Krych, L., Hansen, C. H. F., Hansen, A. K., van den Berg, F. W. J., & Nielsen, D. S. (2013). Quantitatively different, yet qualitatively alike: A meta-analysis of the mouse core gut microbiome with a view towards the human gut microbiome. *PloS One*, *8*(5), e62578. https://doi.org/10.1371/journal.pone.0062578

Kuang, Z., Wang, Y., Li, Y., Ye, C., Ruhn, K. A., Behrendt, C. L., … Hooper, L. V. (2019). The intestinal microbiota programs diurnal rhythms in host metabolism through histone deacetylase 3. *Science*, *365*(6460), 1428–1434. https://doi.org/10.1126/science.aaw3134

Lahtela, J. T., Arranto, A. J., & Sotaniemi, E. A. (1985). Enzyme inducers improve insulin sensitivity in non-insulin-dependent diabetic subjects. *Diabetes*, *34*(9), 911–916. https://doi.org/10.2337/diab.34.9.911

Lam, V., Su, J., Hsu, A., Gross, G. J., Salzman, N. H., & Baker, J. E. (2016). Intestinal Microbial Metabolites Are Linked to Severity of Myocardial Infarction in Rats. *PLoS ONE*, *11*(8). https://doi.org/10.1371/journal.pone.0160840

Lamba, V., Yasuda, K., Lamba, J. K., Assem, M., Davila, J., Strom, S., & Schuetz, E. G. (2004). PXR (NR1I2): Splice variants in human tissues, including brain, and identification of neurosteroids and nicotine as PXR activators. *Toxicology and Applied Pharmacology*, *199*(3), 251–265. https://doi.org/10.1016/j.taap.2003.12.027

Lamousé-Smith, E. S., Tzeng, A., & Starnbach, M. N. (2011). The intestinal flora is required to support antibody responses to systemic immunization in infant and germ free mice. *PloS One*, *6*(11), e27662. https://doi.org/10.1371/journal.pone.0027662

Larsson, E., Tremaroli, V., Lee, Y. S., Koren, O., Nookaew, I., Fricker, A., … Bäckhed, F. (2012). Analysis of gut microbial regulation of host gene expression along the length of the gut and regulation of gut microbial ecology through MyD88. *Gut*, *61*(8), 1124–1131. https://doi.org/10.1136/gutjnl-2011-301104

Laurenzana, E., Coslo, D., Vigilar, M., Roman, A., & Omieciski, C. (2012). The orphan nuclear receptor DAX-1 functions as a potent corepressor of the constitutive androstane receptor (NR1I3). - PubMed—NCBI. Retrieved June 20, 2019, from https://www-ncbi-nlm-nih-gov.gate2.inist.fr/pubmed/?term=laurenzana+2012+car

Laurenzana, E. M., Coslo, D. M., Vigilar, M. V., Roman, A. M., & Omiecinski, C. J. (2016). Activation of the Constitutive Androstane Receptor by Monophthalates. *Chemical Research in Toxicology*, *29*(10), 1651–1661. https://doi.org/10.1021/acs.chemrestox.6b00186

Lavrijsen, K., van Dyck, D., van Houdt, J., Hendrickx, J., Monbaliu, J., Woestenborghs, R., … Heykants, J. (1995). Reduction of the prodrug loperamide oxide to its active drug loperamide in the gut of rats, dogs, and humans. *Drug Metabolism and Disposition: The Biological Fate of Chemicals*, *23*(3), 354–362.

Le Roy, T., Llopis, M., Lepage, P., Bruneau, A., Rabot, S., Bevilacqua, C., … Gérard, P. (2013). Intestinal microbiota determines development of non-alcoholic fatty liver disease in mice. *Gut*, *62*(12), 1787–1794. https://doi.org/10.1136/gutjnl-2012-303816

Ledda-Columbano, G. M., Pibiri, M., Concas, D., Molotzu, F., Simbula, G., Cossu, C., & Columbano, A. (2003). Sex difference in the proliferative response of mouse hepatocytes to treatment with the CAR ligand, TCPOBOP. *Carcinogenesis*, *24*(6), 1059–1065. https://doi.org/10.1093/carcin/bgg063

Lederberg, J., & McCray, A. (2001). 'Ome Sweet 'Omics—A Genealogical Treasury of Words. Retrieved July 5, 2019, from The Scientist Magazine® website: https://www.the-scientist.com/commentary/ome-sweet-omics---a-genealogical-treasury-of-words-54889

Lehouritis, P., Cummins, J., Stanton, M., Murphy, C. T., McCarthy, F. O., Reid, G., … Tangney, M. (2015). Local bacteria affect the efficacy of chemotherapeutic drugs. *Scientific Reports*, *5*, 14554. https://doi.org/10.1038/srep14554

Lempiäinen, H., Molnár, F., Macias Gonzalez, M., Peräkylä, M., & Carlberg, C. (2005). Antagonist- and inverse agonist-driven interactions of the vitamin D receptor and the constitutive androstane receptor with corepressor protein. *Molecular Endocrinology (Baltimore, Md.)*, *19*(9), 2258–2272. https://doi.org/10.1210/me.2004-0534

Ley, R. E., Bäckhed, F., Turnbaugh, P., Lozupone, C. A., Knight, R. D., & Gordon, J. I. (2005). Obesity alters gut microbial ecology. *Proceedings of the National Academy of Sciences of the United States of America*, *102*(31), 11070–11075. https://doi.org/10.1073/pnas.0504978102

Ley, R. E., Hamady, M., Lozupone, C., Turnbaugh, P. J., Ramey, R. R., Bircher, J. S., … Gordon, J. I. (2008). Evolution of mammals and their gut microbes. *Science (New York, N.Y.)*, *320*(5883), 1647–1651. https://doi.org/10.1126/science.1155725

Li, F., Hao, X., Chen, Y., Bai, L., Gao, X., Lian, Z., … Tian, Z. (2017). The microbiota maintain homeostasis of liver-resident γδT-17 cells in a lipid antigen/CD1d-dependent manner. *Nature Communications*, *7*, 13839. https://doi.org/10.1038/ncomms13839

Li, J., Jia, H., Cai, X., Zhong, H., Feng, Q., Sunagawa, S., … Wang, J. (2014). An integrated catalog of reference genes in the human gut microbiome. *Nature Biotechnology*, *32*(8), 834–841. https://doi.org/10.1038/nbt.2942

Li, Lei, Bao, X., Zhang, Q.-Y., Negishi, M., & Ding, X. (2017). Role of CYP2B in Phenobarbital-Induced Hepatocyte Proliferation in Mice. *Drug Metabolism and Disposition: The Biological Fate of Chemicals*, *45*(8), 977–981. https://doi.org/10.1124/dmd.117.076406

Li, Linhao, Chen, T., Stanton, J. D., Sueyoshi, T., Negishi, M., & Wang, H. (2008). The peripheral benzodiazepine receptor ligand 1-(2-chlorophenyl-methylpropyl)-3-isoquinoline-

carboxamide is a novel antagonist of human constitutive androstane receptor. *Molecular Pharmacology*, *74*(2), 443–453. https://doi.org/10.1124/mol.108.046656

Li, M., Wang, B., Zhang, M., Rantalainen, M., Wang, S., Zhou, H., … Zhao, L. (2008). Symbiotic gut microbes modulate human metabolic phenotypes. *Proceedings of the National Academy of Sciences of the United States of America*, *105*(6), 2117–2122. https://doi.org/10.1073/pnas.0712038105

Littman, D. R., & Pamer, E. G. (2011). Role of the commensal microbiota in normal and pathogenic host immune responses. *Cell Host & Microbe*, *10*(4), 311–323. https://doi.org/10.1016/j.chom.2011.10.004

López-Velázquez, J. A., Carrillo-Córdova, L. D., Chávez-Tapia, N. C., Uribe, M., & Méndez-Sánchez, N. (2012). Nuclear receptors in nonalcoholic Fatty liver disease. *Journal of Lipids*, *2012*, 139875. https://doi.org/10.1155/2012/139875

Lu, Y.-F., Jin, T., Xu, Y., Zhang, D., Wu, Q., Zhang, Y.-K. J., & Liu, J. (2013). Sex differences in the circadian variation of cytochrome p450 genes and corresponding nuclear receptors in mouse liver. *Chronobiology International*, *30*(9), 1135–1143. https://doi.org/10.3109/07420528.2013.805762

Lundin, A., Bok, C. M., Aronsson, L., Björkholm, B., Gustafsson, J.-A., Pott, S., … Pettersson, S. (2008). Gut flora, Toll-like receptors and nuclear receptors: A tripartite communication that tunes innate immunity in large intestine. *Cellular Microbiology*, *10*(5), 1093–1103. https://doi.org/10.1111/j.1462-5822.2007.01108.x

Lynch, C., Pan, Y., Li, L., Heyward, S., Moeller, T., Swaan, P. W., & Wang, H. (2014). Activation of the constitutive androstane receptor inhibits gluconeogenesis without affecting lipogenesis or fatty acid synthesis in human hepatocytes. *Toxicology and Applied Pharmacology*, *279*(1), 33–42. https://doi.org/10.1016/j.taap.2014.05.009

Lyte, M. (2011). Probiotics function mechanistically as delivery vehicles for neuroactive compounds: Microbial endocrinology in the design and use of probiotics. *BioEssays: News and Reviews in Molecular, Cellular and Developmental Biology*, *33*(8), 574–581. https://doi.org/10.1002/bies.201100024

Ma, X., Idle, J. R., & Gonzalez, F. J. (2008a). The pregnane X receptor: From bench to bedside. *Expert Opinion on Drug Metabolism & Toxicology*, *4*(7), 895–908. https://doi.org/10.1517/17425255.4.7.895

Ma, X., Idle, J. R., & Gonzalez, F. J. (2008b). The pregnane X receptor: From bench to bedside. *Expert Opinion on Drug Metabolism & Toxicology*, *4*(7), 895–908. https://doi.org/10.1517/17425255.4.7.895

Ma, X., Shah, Y. M., Guo, G. L., Wang, T., Krausz, K. W., Idle, J. R., & Gonzalez, F. J. (2007). Rifaximin is a gut-specific human pregnane X receptor activator. *The Journal of Pharmacology and Experimental Therapeutics*, *322*(1), 391–398. https://doi.org/10.1124/jpet.107.121913

Macdonald, I. A., Bokkenheuser, V. D., Winter, J., McLernon, A. M., & Mosbach, E. H. (1983). Degradation of steroids in the human gut. *Journal of Lipid Research*, *24*(6), 675–700.

Macfarlane, G. T., & Macfarlane, S. (2012). Bacteria, colonic fermentation, and gastrointestinal health. *Journal of AOAC International*, *95*(1), 50–60.

Madak-Erdogan, Z., Gong, P., Zhao, Y. C., Xu, L., Wrobel, K. U., Hartman, J. A., … Helferich, W. G. (2016). Dietary licorice root supplementation reduces diet-induced weight gain, lipid deposition, and hepatic steatosis in ovariectomized mice without stimulating reproductive tissues and mammary gland. *Molecular Nutrition & Food Research*, *60*(2), 369–380. https://doi.org/10.1002/mnfr.201500445

Maglich, J. M., Watson, J., McMillen, P. J., Goodwin, B., Willson, T. M., & Moore, J. T. (2004). The Nuclear Receptor CAR Is a Regulator of Thyroid Hormone Metabolism during Caloric Restriction. *Journal of Biological Chemistry*, *279*(19), 19832–19838. https://doi.org/10.1074/jbc.M313601200

Mäkinen, J., Frank, C., Jyrkkärinne, J., Gynther, J., Carlberg, C., & Honkakoski, P. (2002). Modulation of mouse and human phenobarbital-responsive enhancer module by nuclear receptors. *Molecular Pharmacology*, *62*(2), 366–378. https://doi.org/10.1124/mol.62.2.366

Malaplate-Armand, C., Ferrari, L., Masson, C., Visvikis-Siest, S., Lambert, H., & Batt, A. M. (2005). Down-regulation of astroglial CYP2C, glucocorticoid receptor and constitutive androstane receptor genes in response to cocaine in human U373 MG astrocytoma cells. *Toxicology Letters*, *159*(3), 203–211. https://doi.org/10.1016/j.toxlet.2005.04.005

Mangelsdorf, D. J., Thummel, C., Beato, M., Herrlich, P., Schütz, G., Umesono, K., … Evans, R. M. (1995). The nuclear receptor superfamily: The second decade. *Cell*, *83*(6), 835–839.

Manichanh, C., Borruel, N., Casellas, F., & Guarner, F. (2012). The gut microbiota in IBD. *Nature Reviews. Gastroenterology & Hepatology*, *9*(10), 599–608. https://doi.org/10.1038/nrgastro.2012.152

Mardinoglu, A., Shoaie, S., Bergentall, M., Ghaffari, P., Zhang, C., Larsson, E., … Nielsen, J. (2015). The gut microbiota modulates host amino acid and glutathione metabolism in mice. *Molecular Systems Biology*, *11*(10), 834. https://doi.org/10.15252/msb.20156487

Martin, A. M., Sun, E. W., Rogers, G. B., & Keating, D. J. (2019). The Influence of the Gut Microbiome on Host Metabolism Through the Regulation of Gut Hormone Release. *Frontiers in Physiology*, *10*. https://doi.org/10.3389/fphys.2019.00428

Martin, P., Riley, R., Back, D. J., & Owen, A. (2008). Comparison of the induction profile for drug disposition proteins by typical nuclear receptor activators in human hepatic and intestinal cells. *British Journal of Pharmacology*, *153*(4), 805–819. https://doi.org/10.1038/sj.bjp.0707601

Martin, R., Nauta, A. J., Ben Amor, K., Knippels, L. M. J., Knol, J., & Garssen, J. (2010). Early life: Gut microbiota and immune development in infancy. *Beneficial Microbes*, *1*(4), 367–382. https://doi.org/10.3920/BM2010.0027

Masson, D., Qatanani, M., Sberna, A. L., Xiao, R., Pais de Barros, J. P., Grober, J., … Assem, M. (2008). Activation of the constitutive androstane receptor decreases HDL in wild-type and human

apoA-I transgenic mice. *Journal of Lipid Research*, *49*(8), 1682–1691. https://doi.org/10.1194/jlr.M700374-JLR200

Mastropasqua, F., Girolimetti, G., & Shoshan, M. (2018). PGC1α: Friend or Foe in Cancer? *Genes*, *9*(1). https://doi.org/10.3390/genes9010048

Matur, E., & Eraslan, E. (2012). The Impact of Probiotics on the Gastrointestinal Physiology. *New Advances in the Basic and Clinical Gastroenterology*. https://doi.org/10.5772/34067

McFall-Ngai, M. J., & Ruby, E. G. (1991). Symbiont recognition and subsequent morphogenesis as early events in an animal-bacterial mutualism. *Science (New York, N.Y.)*, *254*(5037), 1491–1494. https://doi.org/10.1126/science.1962208

McKenna, N. J., Cooney, A. J., DeMayo, F. J., Downes, M., Glass, C. K., Lanz, R. B., … O'Malley, B. W. (2009). Minireview: Evolution of NURSA, the Nuclear Receptor Signaling Atlas. *Molecular Endocrinology (Baltimore, Md.)*, *23*(6), 740–746. https://doi.org/10.1210/me.2009-0135

Meng, Z., Gwag, T., Sui, Y., Park, S.-H., Zhou, X., & Zhou, C. (2019). The atypical antipsychotic quetiapine induces hyperlipidemia by activating intestinal PXR signaling. *JCI Insight*, *4*(3). https://doi.org/10.1172/jci.insight.125657

Miao, J., Fang, S., Bae, Y., & Kemper, J. K. (2006). Functional inhibitory cross-talk between constitutive androstane receptor and hepatic nuclear factor-4 in hepatic lipid/glucose metabolism is mediated by competition for binding to the DR1 motif and to the common coactivators, GRIP-1 and PGC-1alpha. *The Journal of Biological Chemistry*, *281*(21), 14537–14546. https://doi.org/10.1074/jbc.M510713200

Min, G., Kim, H., Bae, Y., Petz, L., & Kemper, J. K. (2002). Inhibitory cross-talk between estrogen receptor (ER) and constitutively activated androstane receptor (CAR). CAR inhibits ER-mediated signaling pathway by squelching p160 coactivators. *The Journal of Biological Chemistry*, *277*(37), 34626–34633. https://doi.org/10.1074/jbc.M205239200

Min, Y., Ma, X., Sankaran, K., Ru, Y., Chen, L., Baiocchi, M., & Zhu, S. (2019). Sex-specific association between gut microbiome and fat distribution. *Nature Communications*, *10*(1), 2408. https://doi.org/10.1038/s41467-019-10440-5

Molly, K., Vande Woestyne, M., & Verstraete, W. (1993). Development of a 5-step multi-chamber reactor as a simulation of the human intestinal microbial ecosystem. *Applied Microbiology and Biotechnology*, *39*(2), 254–258. https://doi.org/10.1007/bf00228615

Montagner, A., Korecka, A., Polizzi, A., Lippi, Y., Blum, Y., Canlet, C., … Wahli, W. (2016). Hepatic circadian clock oscillators and nuclear receptors integrate microbiome-derived signals. *Scientific Reports*, *6*, 20127. https://doi.org/10.1038/srep20127

Montagner, A., Polizzi, A., Fouché, E., Ducheix, S., Lippi, Y., Lasserre, F., … Guillou, H. (2016). Liver PPARα is crucial for whole-body fatty acid homeostasis and is protective against NAFLD. *Gut*, *65*(7), 1202–1214. https://doi.org/10.1136/gutjnl-2015-310798

Moore, L. B., Parks, D. J., Jones, S. A., Bledsoe, R. K., Consler, T. G., Stimmel, J. B., … others. (2000). Orphan nuclear receptors constitutive androstane receptor and pregnane X receptor share xenobiotic and steroid ligands. *Journal of Biological Chemistry*, *275*(20), 15122–15127.

Mueller, S., Saunier, K., Hanisch, C., Norin, E., Alm, L., Midtvedt, T., … Blaut, M. (2006). Differences in fecal microbiota in different European study populations in relation to age, gender, and country: A cross-sectional study. *Applied and Environmental Microbiology*, *72*(2), 1027–1033. https://doi.org/10.1128/AEM.72.2.1027-1033.2006

Murray, M., Fiala-Beer, E., & Sutton, D. (2003). Upregulation of cytochromes P450 2B in rat liver by orphenadrine. *British Journal of Pharmacology*, *139*(4), 787–796. https://doi.org/10.1038/sj.bjp.0705305

Mutoh, S., Osabe, M., Inoue, K., Moore, R., Pedersen, L., Perera, L., … Negishi, M. (2009). Dephosphorylation of threonine 38 is required for nuclear translocation and activation of human xenobiotic receptor CAR (NR1I3). *The Journal of Biological Chemistry*, *284*(50), 34785–34792. https://doi.org/10.1074/jbc.M109.048108

Nakatsu, C. H., Armstrong, A., Clavijo, A. P., Martin, B. R., Barnes, S., & Weaver, C. M. (2014). Fecal Bacterial Community Changes Associated with Isoflavone Metabolites in Postmenopausal Women after Soy Bar Consumption. *PLoS ONE*, *9*(10). https://doi.org/10.1371/journal.pone.0108924

Nebert, D. W., Roe, A. L., Dieter, M. Z., Solis, W. A., Yang, Y., & Dalton, T. P. (2000). Role of the aromatic hydrocarbon receptor and [Ah] gene battery in the oxidative stress response, cell cycle control, and apoptosis. *Biochemical Pharmacology*, *59*(1), 65–85. https://doi.org/10.1016/s0006-2952(99)00310-x

Nguyen, T. L. A., Vieira-Silva, S., Liston, A., & Raes, J. (2015). How informative is the mouse for human gut microbiota research? *Disease Models & Mechanisms*, *8*(1), 1–16. https://doi.org/10.1242/dmm.017400

Ni, J., Wu, G. D., Albenberg, L., & Tomov, V. T. (2017). Gut microbiota and IBD: Causation or correlation? *Nature Reviews. Gastroenterology & Hepatology*, *14*(10), 573–584. https://doi.org/10.1038/nrgastro.2017.88

Nicholson, J. K., Holmes, E., Kinross, J., Burcelin, R., Gibson, G. R., Jia, W., & Pettersson, S. (2012). Host-gut microbiota metabolic interactions. *Science*, *336*(6086), 1262–1267. https://doi.org/10.1126/science.1223813

Nicklas, W., Keubler, L., & Bleich, A. (2015). Maintaining and Monitoring the Defined Microbiota Status of Gnotobiotic Rodents. *ILAR Journal*, *56*(2), 241–249. https://doi.org/10.1093/ilar/ilv029

Nutt, J. G., & Holford, N. H. (1996). The response to levodopa in Parkinson's disease: Imposing pharmacological law and order. *Annals of Neurology*, *39*(5), 561–573. https://doi.org/10.1002/ana.410390504

O'Callaghan, D., & Vergunst, A. (2010). Non-mammalian animal models to study infectious disease: Worms or fly fishing? *Current Opinion in Microbiology*, *13*(1), 79–85. https://doi.org/10.1016/j.mib.2009.12.005

Oh, H. Y. P., Ellero-Simatos, S., Manickam, R., Tan, N. S., Guillou, H., & Wahli, W. (2019). Depletion of Gram-Positive Bacteria Impacts Hepatic Biological Functions During the Light Phase. *International Journal of Molecular Sciences*, *20*(4). https://doi.org/10.3390/ijms20040812

O'Hara, A. M., & Shanahan, F. (2006). The gut flora as a forgotten organ. *EMBO Reports*, *7*(7), 688–693. https://doi.org/10.1038/sj.embor.7400731

O'Mahony, S. M., Clarke, G., Borre, Y. E., Dinan, T. G., & Cryan, J. F. (2015). Serotonin, tryptophan metabolism and the brain-gut-microbiome axis. *Behavioural Brain Research*, *277*, 32–48. https://doi.org/10.1016/j.bbr.2014.07.027

Oshida, K., Vasani, N., Thomas, R. S., Applegate, D., Rosen, M., Abbott, B., … Corton, J. C. (2015). Identification of Modulators of the Nuclear Receptor Peroxisome Proliferator-Activated Receptor α (PPARα) in a Mouse Liver Gene Expression Compendium. *PLoS ONE*, *10*(2). https://doi.org/10.1371/journal.pone.0112655

O'Toole, P. W., & Claesson, M. J. (2010). Gut microbiota: Changes throughout the lifespan from infancy to elderly. *International Dairy Journal*, *20*(4), 281–291. https://doi.org/10.1016/j.idairyj.2009.11.010

Pakharukova, M. Y., Smetanina, M. A., Kaledin, V. I., Kobzev, V. F., Romanova, I. V., & Merkulova, T. I. (2007). Activation of constitutive androstane receptor under the effect of hepatocarcinogenic aminoazo dyes in mouse and rat liver. *Bulletin of Experimental Biology and Medicine*, *144*(3), 338–341. https://doi.org/10.1007/s10517-007-0327-0

Pascussi, J. M., Gerbal-Chaloin, S., Fabre, J. M., Maurel, P., & Vilarem, M. J. (2000). Dexamethasone enhances constitutive androstane receptor expression in human hepatocytes: Consequences on cytochrome P450 gene regulation. *Molecular Pharmacology*, *58*(6), 1441–1450. https://doi.org/10.1124/mol.58.6.1441

Patel, R. D., Hollingshead, B. D., Omiecinski, C. J., & Perdew, G. H. (2007). Aryl-hydrocarbon receptor activation regulates constitutive androstane receptor levels in murine and human liver. *Hepatology (Baltimore, Md.)*, *46*(1), 209–218. https://doi.org/10.1002/hep.21671

Pathak, P., Xie, C., Nichols, R. G., Ferrell, J. M., Boehme, S., Krausz, K. W., … Chiang, J. Y. L. (2018). Intestine farnesoid X receptor agonist and the gut microbiota activate G-protein bile acid receptor-1 signaling to improve metabolism. *Hepatology (Baltimore, Md.)*, *68*(4), 1574–1588. https://doi.org/10.1002/hep.29857

Peet, D. J., Janowski, B. A., & Mangelsdorf, D. J. (1998). The LXRs: A new class of oxysterol receptors. *Current Opinion in Genetics & Development*, *8*(5), 571–575.

Peffer, R. C., Moggs, J. G., Pastoor, T., Currie, R. A., Wright, J., Milburn, G., … Rusyn, I. (2007). Mouse liver effects of cyproconazole, a triazole fungicide: Role of the constitutive androstane receptor. *Toxicological Sciences: An Official Journal of the Society of Toxicology*, *99*(1), 315–325. https://doi.org/10.1093/toxsci/kfm154

Peppercorn, M. A., & Goldman, P. (1972). The role of intestinal bacteria in the metabolism of salicylazosulfapyridine. *The Journal of Pharmacology and Experimental Therapeutics*, *181*(3), 555–562.

Petrick, J. S., & Klaassen, C. D. (2007). Importance of hepatic induction of constitutive androstane receptor and other transcription factors that regulate xenobiotic metabolism and transport. *Drug Metabolism and Disposition: The Biological Fate of Chemicals*, *35*(10), 1806–1815. https://doi.org/10.1124/dmd.107.015974

Pompei, A., Cordisco, L., Amaretti, A., Zanoni, S., Matteuzzi, D., & Rossi, M. (2007). Folate Production by Bifidobacteria as a Potential Probiotic Property. *Applied and Environmental Microbiology*, *73*(1), 179–185. https://doi.org/10.1128/AEM.01763-06

Presley, L. L., Wei, B., Braun, J., & Borneman, J. (2010). Bacteria Associated with Immunoregulatory Cells in Mice. *Applied and Environmental Microbiology*, *76*(3), 936–941. https://doi.org/10.1128/AEM.01561-09

Prokopec, S. D., Watson, J. D., Lee, J., Pohjanvirta, R., & Boutros, P. C. (2015). Sex-related differences in murine hepatic transcriptional and proteomic responses to TCDD. *Toxicology and Applied Pharmacology*, *284*(2), 188–196. https://doi.org/10.1016/j.taap.2015.02.012

Puchalska, P., & Crawford, P. A. (2017). Multi-dimensional Roles of Ketone Bodies in Fuel Metabolism, Signaling, and Therapeutics. *Cell Metabolism*, *25*(2), 262–284. https://doi.org/10.1016/j.cmet.2016.12.022

Pulakazhi Venu, V. K., Saifeddine, M., Mihara, K., Tsai, Y.-C., Nieves, K., Alston, L., … Hirota, S. A. (2019). The pregnane X receptor and its microbiota-derived ligand indole 3-propionic acid regulate endothelium-dependent vasodilation. *American Journal of Physiology. Endocrinology and Metabolism*, *317*(2), E350–E361. https://doi.org/10.1152/ajpendo.00572.2018

Qatanani, M., Wei, P., & Moore, D. D. (2004). Alterations in the distribution and orexigenic effects of dexamethasone in CAR-null mice. *Pharmacology, Biochemistry, and Behavior*, *78*(2), 285–291. https://doi.org/10.1016/j.pbb.2004.04.001

Quinet, E. M., Savio, D. A., Halpern, A. R., Chen, L., Miller, C. P., & Nambi, P. (2004). Gene-selective modulation by a synthetic oxysterol ligand of the liver X receptor. *Journal of Lipid Research*, *45*(10), 1929–1942. https://doi.org/10.1194/jlr.M400257-JLR200

Rafii, F., Franklin, W., & Cerniglia, C. E. (1990). Azoreductase activity of anaerobic bacteria isolated from human intestinal microflora. *Applied and Environmental Microbiology*, *56*(7), 2146–2151.

Rakoff-Nahoum, S., Paglino, J., Eslami-Varzaneh, F., Edberg, S., & Medzhitov, R. (2004). Recognition of commensal microflora by toll-like receptors is required for intestinal homeostasis. *Cell*, *118*(2), 229–241. https://doi.org/10.1016/j.cell.2004.07.002

Ranhotra, H. S., Flannigan, K. L., Brave, M., Mukherjee, S., Lukin, D. J., Hirota, S. A., & Mani, S. (2016). Xenobiotic Receptor-Mediated Regulation of Intestinal Barrier Function and Innate Immunity. *Nuclear Receptor Research*, *3*. https://doi.org/10.11131/2016/101199

Rastelli, M., Knauf, C., & Cani, P. D. (2018). Gut Microbes and Health: A Focus on the Mechanisms Linking Microbes, Obesity, and Related Disorders. *Obesity (Silver Spring, Md.)*, *26*(5), 792–800. https://doi.org/10.1002/oby.22175

Régnier, M., Polizzi, A., Lippi, Y., Fouché, E., Michel, G., Lukowicz, C., … Montagner, A. (2018). Insights into the role of hepatocyte PPARα activity in response to fasting. *Molecular and Cellular Endocrinology*, *471*, 75–88. https://doi.org/10.1016/j.mce.2017.07.035

Repa, J. J., Liang, G., Ou, J., Bashmakov, Y., Lobaccaro, J. M., Shimomura, I., … Mangelsdorf, D. J. (2000). Regulation of mouse sterol regulatory element-binding protein-1c gene (SREBP-1c) by oxysterol receptors, LXRalpha and LXRbeta. *Genes & Development*, *14*(22), 2819–2830. https://doi.org/10.1101/gad.844900

Rezen, T., Tamasi, V., Lövgren-Sandblom, A., Björkhem, I., Meyer, U. A., & Rozman, D. (2009). Effect of CAR activation on selected metabolic pathways in normal and hyperlipidemic mouse livers. *BMC Genomics*, *10*, 384. https://doi.org/10.1186/1471-2164-10-384

Ridlon, J. M., & Bajaj, J. S. (2015). The human gut sterolbiome: Bile acid-microbiome endocrine aspects and therapeutics. *Acta Pharmaceutica Sinica. B*, *5*(2), 99–105. https://doi.org/10.1016/j.apsb.2015.01.006

Ridlon, J. M., Kang, D. J., Hylemon, P. B., & Bajaj, J. S. (2014). Bile acids and the gut microbiome. *Current Opinion in Gastroenterology*, *30*(3), 332–338. https://doi.org/10.1097/MOG.0000000000000057

Ridlon, J. M., Kang, D.-J., & Hylemon, P. B. (2006). Bile salt biotransformations by human intestinal bacteria. *Journal of Lipid Research*, *47*(2), 241–259. https://doi.org/10.1194/jlr.R500013-JLR200

Roager, H. M., & Licht, T. R. (2018). Microbial tryptophan catabolites in health and disease. *Nature Communications*, *9*. https://doi.org/10.1038/s41467-018-05470-4

Robertson, S. J., Lemire, P., Maughan, H., Goethel, A., Turpin, W., Bedrani, L., … Philpott, D. J. (2019). Comparison of Co-housing and Littermate Methods for Microbiota Standardization in Mouse Models. *Cell Reports*, *27*(6), 1910-1919.e2. https://doi.org/10.1016/j.celrep.2019.04.023

Rosenfeld, M. G., & Glass, C. K. (2001). Coregulator codes of transcriptional regulation by nuclear receptors. *The Journal of Biological Chemistry*, *276*(40), 36865–36868. https://doi.org/10.1074/jbc.R100041200

Roth, A., Looser, R., Kaufmann, M., Blättler, S. M., Rencurel, F., Huang, W., … Meyer, U. A. (2008). Regulatory cross-talk between drug metabolism and lipid homeostasis: Constitutive androstane receptor and pregnane X receptor increase Insig-1 expression. *Molecular Pharmacology*, *73*(4), 1282–1289. https://doi.org/10.1124/mol.107.041012

Rothhammer, V., Mascanfroni, I. D., Bunse, L., Takenaka, M. C., Kenison, J. E., Mayo, L., … Quintana, F. J. (2016). Type I interferons and microbial metabolites of tryptophan modulate astrocyte activity and central nervous system inflammation via the aryl hydrocarbon receptor. *Nature Medicine*, *22*(6), 586–597. https://doi.org/10.1038/nm.4106

Rowland, I., Gibson, G., Heinken, A., Scott, K., Swann, J., Thiele, I., & Tuohy, K. (2018). Gut microbiota functions: Metabolism of nutrients and other food components. *European Journal of Nutrition*, *57*(1), 1–24. https://doi.org/10.1007/s00394-017-1445-8

Ruckpaul, K., Rein, H., & Blanck, J. (1985). [Regulation mechanisms of the endoplasmic cytochrome P-450 systems of the liver]. *Biomedica Biochimica Acta*, *44*(3), 351–379.

Ruddick, J. P., Evans, A. K., Nutt, D. J., Lightman, S. L., Rook, G. A. W., & Lowry, C. A. (2006). Tryptophan metabolism in the central nervous system: Medical implications. *Expert Reviews in Molecular Medicine*, *8*(20), 1–27. https://doi.org/10.1017/S1462399406000068

Russell, D. W. (2003). The Enzymes, Regulation, and Genetics of Bile Acid Synthesis. *Annual Review of Biochemistry*, *72*(1), 137–174. https://doi.org/10.1146/annurev.biochem.72.121801.161712

Saito, K., Moore, R., & Negishi, M. (2013). P38 Mitogen-activated protein kinase regulates nuclear receptor CAR that activates the CYP2B6 gene. *Drug Metabolism and Disposition: The Biological Fate of Chemicals*, *41*(6), 1170–1173. https://doi.org/10.1124/dmd.113.051623

Sampson, T. R., & Mazmanian, S. K. (2015). Control of brain development, function, and behavior by the microbiome. *Cell Host & Microbe*, *17*(5), 565–576. https://doi.org/10.1016/j.chom.2015.04.011

Santos-Marcos, J. A., Haro, C., Vega-Rojas, A., Alcala-Diaz, J. F., Molina-Abril, H., Leon-Acuña, A., … Camargo, A. (2019). Sex Differences in the Gut Microbiota as Potential Determinants of Gender Predisposition to Disease. *Molecular Nutrition & Food Research*, *63*(7), e1800870. https://doi.org/10.1002/mnfr.201800870

Saussele, T., Burk, O., Blievernicht, J. K., Klein, K., Nussler, A., Nussler, N., … Zanger, U. M. (2007). Selective induction of human hepatic cytochromes P450 2B6 and 3A4 by metamizole. *Clinical Pharmacology and Therapeutics*, *82*(3), 265–274. https://doi.org/10.1038/sj.clpt.6100138

Savary, C. C., Jossé, R., Bruyère, A., Guillet, F., Robin, M.-A., & Guillouzo, A. (2014). Interactions of endosulfan and methoxychlor involving CYP3A4 and CYP2B6 in human HepaRG cells. *Drug Metabolism and Disposition: The Biological Fate of Chemicals*, *42*(8), 1235–1240. https://doi.org/10.1124/dmd.114.057786

Sayin, S. I., Wahlström, A., Felin, J., Jäntti, S., Marschall, H.-U., Bamberg, K., … Bäckhed, F. (2013). Gut Microbiota Regulates Bile Acid Metabolism by Reducing the Levels of Tauro-beta-muricholic Acid, a Naturally Occurring FXR Antagonist. *Cell Metabolism*, *17*(2), 225–235. https://doi.org/10.1016/j.cmet.2013.01.003

Sberna, A. L., Assem, M., Gautier, T., Grober, J., Guiu, B., Jeannin, A., … Masson, D. (2011). Constitutive androstane receptor activation stimulates faecal bile acid excretion and reverse cholesterol transport in mice. *Journal of Hepatology*, *55*(1), 154–161. https://doi.org/10.1016/j.jhep.2010.10.029

Schmidt, D., Amrani, A., Verdaguer, J., Bou, S., & Santamaria, P. (1999). Autoantigen-Independent Deletion of Diabetogenic CD4+ Thymocytes by Protective MHC Class II Molecules. *The Journal of Immunology*, *162*(8), 4627–4636.

Schnabl, B., & Brenner, D. A. (2014). Interactions between the intestinal microbiome and liver diseases. *Gastroenterology*, *146*(6), 1513–1524. https://doi.org/10.1053/j.gastro.2014.01.020

Schnorr, S. L., Candela, M., Rampelli, S., Centanni, M., Consolandi, C., Basaglia, G., … Crittenden, A. N. (2014). Gut microbiome of the Hadza hunter-gatherers. *Nature Communications*, *5*, 3654. https://doi.org/10.1038/ncomms4654

Scholtens, P. A. M. J., Oozeer, R., Martin, R., Amor, K. B., & Knol, J. (2012). The early settlers: Intestinal microbiology in early life. *Annual Review of Food Science and Technology*, *3*, 425–447. https://doi.org/10.1146/annurev-food-022811-101120

Schroeder, J. C., Dinatale, B. C., Murray, I. A., Flaveny, C. A., Liu, Q., Laurenzana, E. M., … Perdew, G. H. (2010). The uremic toxin 3-indoxyl sulfate is a potent endogenous agonist for the human aryl hydrocarbon receptor. *Biochemistry*, *49*(2), 393–400. https://doi.org/10.1021/bi901786x

Schubert, A. M., Sinani, H., & Schloss, P. D. (2015). Antibiotic-Induced Alterations of the Murine Gut Microbiota and Subsequent Effects on Colonization Resistance against Clostridium difficile. *MBio*, *6*(4), e00974-15. https://doi.org/10.1128/mBio.00974-15

Selwyn, F. P., Cheng, S. L., Klaassen, C. D., & Cui, J. Y. (2016). Regulation of Hepatic Drug-Metabolizing Enzymes in Germ-Free Mice by Conventionalization and Probiotics. *Drug Metabolism and Disposition: The Biological Fate of Chemicals*, *44*(2), 262–274. https://doi.org/10.1124/dmd.115.067504

Sender, R., Fuchs, S., & Milo, R. (2016). Are We Really Vastly Outnumbered? Revisiting the Ratio of Bacterial to Host Cells in Humans. *Cell*, *164*(3), 337–340. https://doi.org/10.1016/j.cell.2016.01.013

Shah, Y. M., Ma, X., Morimura, K., Kim, I., & Gonzalez, F. J. (2007). Pregnane X receptor activation ameliorates DSS-induced inflammatory bowel disease via inhibition of NF-kappaB target gene expression. *American Journal of Physiology. Gastrointestinal and Liver Physiology*, *292*(4), G1114-1122. https://doi.org/10.1152/ajpgi.00528.2006

Shehata, A. A., Schrödl, W., Aldin, A. A., Hafez, H. M., & Krüger, M. (2013). The effect of glyphosate on potential pathogens and beneficial members of poultry microbiota in vitro. *Current Microbiology*, *66*(4), 350–358. https://doi.org/10.1007/s00284-012-0277-2

Shi, X., Cheng, Q., Xu, L., Yan, J., Jiang, M., He, J., … Xie, W. (2014). Cholesterol sulfate and cholesterol sulfotransferase inhibit gluconeogenesis by targeting hepatocyte nuclear factor 4α. *Molecular and Cellular Biology*, *34*(3), 485–497. https://doi.org/10.1128/MCB.01094-13

Shibayama, Y., Ushinohama, K., Ikeda, R., Yoshikawa, Y., Motoya, T., Takeda, Y., & Yamada, K. (2006). Effect of methotrexate treatment on expression levels of multidrug resistance protein 2, breast cancer resistance protein and organic anion transporters Oat1, Oat2 and Oat3 in rats. *Cancer Science*, *97*(11), 1260–1266. https://doi.org/10.1111/j.1349-7006.2006.00304.x

Shindo, S., Numazawa, S., & Yoshida, T. (2007). A physiological role of AMP-activated protein kinase in phenobarbital-mediated constitutive androstane receptor activation and CYP2B induction. *The Biochemical Journal*, *401*(3), 735–741. https://doi.org/10.1042/BJ20061238

Sinal, C. J., Tohkin, M., Miyata, M., Ward, J. M., Lambert, G., & Gonzalez, F. J. (2000). Targeted disruption of the nuclear receptor FXR/BAR impairs bile acid and lipid homeostasis. *Cell*, *102*(6), 731–744.

Smith, M. I., Yatsunenko, T., Manary, M. J., Trehan, I., Mkakosya, R., Cheng, J., … Gordon, J. I. (2013). Gut microbiomes of Malawian twin pairs discordant for kwashiorkor. *Science (New York, N.Y.)*, *339*(6119), 548–554. https://doi.org/10.1126/science.1229000

Sommer, F., Nookaew, I., Sommer, N., Fogelstrand, P., & Bäckhed, F. (2015). Site-specific programming of the host epithelial transcriptome by the gut microbiota. *Genome Biology*, *16*, 62. https://doi.org/10.1186/s13059-015-0614-4

Sotaniemi, E. A., Arranto, A. J., Sutinen, S., Stengård, J. H., & Sutinen, S. (1983). Treatment of noninsulin-dependent diabetes mellitus with enzyme inducers. *Clinical Pharmacology and Therapeutics*, *33*(6), 826–835. https://doi.org/10.1038/clpt.1983.113

Spiljar, M., Merkler, D., & Trajkovski, M. (2017). The Immune System Bridges the Gut Microbiota with Systemic Energy Homeostasis: Focus on TLRs, Mucosal Barrier, and SCFAs. *Frontiers in Immunology*, *8*. https://doi.org/10.3389/fimmu.2017.01353

Spor, A., Koren, O., & Ley, R. (2011). Unravelling the effects of the environment and host genotype on the gut microbiome. *Nature Reviews. Microbiology*, *9*(4), 279–290. https://doi.org/10.1038/nrmicro2540

Staudinger, J. L., Goodwin, B., Jones, S. A., Hawkins-Brown, D., MacKenzie, K. I., LaTour, A., … Kliewer, S. A. (2001). The nuclear receptor PXR is a lithocholic acid sensor that protects against liver toxicity. *Proceedings of the National Academy of Sciences of the United States of America*, *98*(6), 3369–3374. https://doi.org/10.1073/pnas.051551698

Staudinger, Jeff L., Madan, A., Carol, K. M., & Parkinson, A. (2003). Regulation of drug transporter gene expression by nuclear receptors. *Drug Metabolism and Disposition: The Biological Fate of Chemicals*, *31*(5), 523–527. https://doi.org/10.1124/dmd.31.5.523

Stedman, C. A. M., Liddle, C., Coulter, S. A., Sonoda, J., Alvarez, J. G. A., Moore, D. D., … Downes, M. (2005). Nuclear receptors constitutive androstane receptor and pregnane X receptor ameliorate cholestatic liver injury. *Proceedings of the National Academy of Sciences of the United States of America*, *102*(6), 2063–2068. https://doi.org/10.1073/pnas.0409794102

Stickel, F., & Hellerbrand, C. (2010). Non-alcoholic fatty liver disease as a risk factor for hepatocellular carcinoma: Mechanisms and implications. *Gut*, *59*(10), 1303–1307. https://doi.org/10.1136/gut.2009.199661

Sueyoshi, T., Kawamoto, T., Zelko, I., Honkakoski, P., & Negishi, M. (1999). The repressed nuclear receptor CAR responds to phenobarbital in activating the human CYP2B6 gene. *The Journal of Biological Chemistry*, *274*(10), 6043–6046. https://doi.org/10.1074/jbc.274.10.6043

Sueyoshi, Tatsuya, Moore, R., Sugatani, J., Matsumura, Y., & Negishi, M. (2008). PPP1R16A, the membrane subunit of protein phosphatase 1beta, signals nuclear translocation of the nuclear receptor constitutive active/androstane receptor. *Molecular Pharmacology*, *73*(4), 1113–1121. https://doi.org/10.1124/mol.107.042960

Sugatani, J., Kojima, H., Ueda, A., Kakizaki, S., Yoshinari, K., Gong, Q. H., … Sueyoshi, T. (2001). The phenobarbital response enhancer module in the human bilirubin UDP-glucuronosyltransferase UGT1A1 gene and regulation by the nuclear receptor CAR. *Hepatology (Baltimore, Md.)*, *33*(5), 1232–1238. https://doi.org/10.1053/jhep.2001.24172

Suino, K., Peng, L., Reynolds, R., Li, Y., Cha, J.-Y., Repa, J. J., … Xu, H. E. (2004). The nuclear xenobiotic receptor CAR: Structural determinants of constitutive activation and heterodimerization. *Molecular Cell*, *16*(6), 893–905. https://doi.org/10.1016/j.molcel.2004.11.036

Sun, L., Zhang, X., Zhang, Y., Zheng, K., Xiang, Q., Chen, N., … He, Q. (2019). Antibiotic-Induced Disruption of Gut Microbiota Alters Local Metabolomes and Immune Responses. *Frontiers in Cellular and Infection Microbiology*, *9*, 99. https://doi.org/10.3389/fcimb.2019.00099

Sutherland, J. D., & Macdonald, I. A. (1982). The metabolism of primary, 7-oxo, and 7 beta-hydroxy bile acids by Clostridium absonum. *Journal of Lipid Research*, *23*(5), 726–732.

Swales, K., & Negishi, M. (2004). CAR, driving into the future. *Molecular Endocrinology (Baltimore, Md.)*, *18*(7), 1589–1598. https://doi.org/10.1210/me.2003-0397

Swanson, P. A., Kumar, A., Samarin, S., Vijay-Kumar, M., Kundu, K., Murthy, N., … Neish, A. S. (2011). Enteric commensal bacteria potentiate epithelial restitution via reactive oxygen species-mediated inactivation of focal adhesion kinase phosphatases. *Proceedings of the National Academy of Sciences of the United States of America*, *108*(21), 8803–8808. https://doi.org/10.1073/pnas.1010042108

Teng, S., & Piquette-Miller, M. (2005). The involvement of the pregnane X receptor in hepatic gene regulation during inflammation in mice. *The Journal of Pharmacology and Experimental Therapeutics*, *312*(2), 841–848. https://doi.org/10.1124/jpet.104.076141

Terc, J., Hansen, A., Alston, L., & Hirota, S. A. (2014). Pregnane X receptor agonists enhance intestinal epithelial wound healing and repair of the intestinal barrier following the induction of experimental colitis. *European Journal of Pharmaceutical Sciences: Official Journal of the European Federation for Pharmaceutical Sciences*, *55*, 12–19. https://doi.org/10.1016/j.ejps.2014.01.007

Thomas, C., Pellicciari, R., Pruzanski, M., Auwerx, J., & Schoonjans, K. (2008). Targeting bile-acid signalling for metabolic diseases. *Nature Reviews Drug Discovery*, *7*(8), 678–693. https://doi.org/10.1038/nrd2619

Thomas, S., Izard, J., Walsh, E., Batich, K., Chongsathidkiet, P., Clarke, G., … Prendergast, G. C. (2017). The Host Microbiome Regulates and Maintains Human Health: A Primer and Perspective for Non-Microbiologists. *Cancer Research*, *77*(8), 1783–1812. https://doi.org/10.1158/0008-5472.CAN-16-2929

Thompson, P. D., Jurutka, P. W., Haussler, C. A., Whitfield, G. K., & Haussler, M. R. (1998). Heterodimeric DNA binding by the vitamin D receptor and retinoid X receptors is enhanced by 1,25-dihydroxyvitamin D3 and inhibited by 9-cis-retinoic acid. Evidence for allosteric receptor interactions. *The Journal of Biological Chemistry*, *273*(14), 8483–8491. https://doi.org/10.1074/jbc.273.14.8483

Timsit, Y. E., & Negishi, M. (2007). CAR and PXR: The Xenobiotic-Sensing Receptors. *Steroids*, *72*(3), 231–246. https://doi.org/10.1016/j.steroids.2006.12.006

Tolson, A. H., & Wang, H. (2010). Regulation of drug-metabolizing enzymes by xenobiotic receptors: PXR and CAR. *Advanced Drug Delivery Reviews*, *62*(13), 1238–1249.

Torow, N., & Hornef, M. W. (2017). The Neonatal Window of Opportunity: Setting the Stage for Life-Long Host-Microbial Interaction and Immune Homeostasis. *Journal of Immunology (Baltimore, Md.: 1950)*, *198*(2), 557–563. https://doi.org/10.4049/jimmunol.1601253

Treuting, P. M., Dintzis, S. M., Liggitt, D., & Frevert, C. W. (2011). *Comparative Anatomy and Histology: A Mouse and Human Atlas (Expert Consult)*. Academic Press.

Tsai, V. W. W., Husaini, Y., Sainsbury, A., Brown, D. A., & Breit, S. N. (2018). The MIC-1/GDF15-GFRAL Pathway in Energy Homeostasis: Implications for Obesity, Cachexia, and Other Associated Diseases. *Cell Metabolism*, *28*(3), 353–368. https://doi.org/10.1016/j.cmet.2018.07.018

Turnbaugh, P. J., Ley, R. E., Mahowald, M. A., Magrini, V., Mardis, E. R., & Gordon, J. I. (2006). An obesity-associated gut microbiome with increased capacity for energy harvest. *Nature*, *444*(7122), 1027–1031. https://doi.org/10.1038/nature05414

Turnbaugh, P. J., Ridaura, V. K., Faith, J. J., Rey, F. E., Knight, R., & Gordon, J. I. (2009). The effect of diet on the human gut microbiome: A metagenomic analysis in humanized gnotobiotic mice. *Science Translational Medicine*, *1*(6), 6ra14. https://doi.org/10.1126/scitranslmed.3000322

Turroni, S., Brigidi, P., Cavalli, A., & Candela, M. (2018). Microbiota-Host Transgenomic Metabolism, Bioactive Molecules from the Inside. *Journal of Medicinal Chemistry*, *61*(1), 47–61. https://doi.org/10.1021/acs.jmedchem.7b00244

Tzameli, I., Pissios, P., Schuetz, E. G., & Moore, D. D. (2000). The xenobiotic compound 1,4-bis[2-(3,5-dichloropyridyloxy)]benzene is an agonist ligand for the nuclear receptor CAR. *Molecular and Cellular Biology*, *20*(9), 2951–2958. https://doi.org/10.1128/mcb.20.9.2951-2958.2000

Ueda, A., Hamadeh, H. K., Webb, H. K., Yamamoto, Y., Sueyoshi, T., Afshari, C. A., … Negishi, M. (2002). Diverse roles of the nuclear orphan receptor CAR in regulating hepatic genes in response to phenobarbital. *Molecular Pharmacology*, *61*(1), 1–6. https://doi.org/10.1124/mol.61.1.1

Usui, T., Tochiya, M., Sasaki, Y., Muranaka, K., Yamakage, H., Himeno, A., … Satoh-Asahara, N. (2013). Effects of natural S-equol supplements on overweight or obesity and metabolic syndrome in the Japanese, based on sex and equol status. *Clinical Endocrinology*, *78*(3), 365–372. https://doi.org/10.1111/j.1365-2265.2012.04400.x

Uzbay, T. (2019). Germ-free animal experiments in the gut microbiota studies. *Current Opinion in Pharmacology*, *49*, 6–10. https://doi.org/10.1016/j.coph.2019.03.016

Van de Wiele, T., Van den Abbeele, P., Ossieur, W., Possemiers, S., & Marzorati, M. (2015). The Simulator of the Human Intestinal Microbial Ecosystem (SHIME®). In K. Verhoeckx, P. Cotter, I. López-Expósito, C. Kleiveland, T. Lea, A. Mackie, … H. Wichers (Eds.), *The Impact of Food Bioactives on Health: In vitro and ex vivo models* (pp. 305–317). https://doi.org/10.1007/978-3-319-16104-4_27

Venkatesh, M., Mukherjee, S., Wang, H., Li, H., Sun, K., Benechet, A. P., … Mani, S. (2014). Symbiotic Bacterial Metabolites Regulate Gastrointestinal Barrier Function via the Xenobiotic Sensor PXR and Toll-like Receptor 4. *Immunity*, *41*(2), 296–310. https://doi.org/10.1016/j.immuni.2014.06.014

Verbeke, K. A., Boobis, A. R., Chiodini, A., Edwards, C. A., Franck, A., Kleerebezem, M., … Tuohy, K. M. (2015). Towards microbial fermentation metabolites as markers for health benefits of

prebiotics. *Nutrition Research Reviews*, *28*(1), 42–66. https://doi.org/10.1017/S0954422415000037

Verdaguer, J., Schmidt, D., Amrani, A., Anderson, B., Averill, N., & Santamaria, P. (1997). Spontaneous autoimmune diabetes in monoclonal T cell nonobese diabetic mice. *The Journal of Experimental Medicine*, *186*(10), 1663–1676. https://doi.org/10.1084/jem.186.10.1663

Vernocchi, P., Del Chierico, F., & Putignani, L. (2016). Gut Microbiota Profiling: Metabolomics Based Approach to Unravel Compounds Affecting Human Health. *Frontiers in Microbiology*, *7*. https://doi.org/10.3389/fmicb.2016.01144

Visconti, A., Roy, C. I. L., Rosa, F., Rossi, N., Martin, T. C., Mohney, R. P., … Falchi, M. (2019). Interplay between the human gut microbiome and host metabolism. *Nature Communications*, *10*(1), 1–10. https://doi.org/10.1038/s41467-019-12476-z

Visser, T. J., Kaptein, E., Glatt, H., Bartsch, I., Hagen, M., & Coughtrie, M. W. (1998). Characterization of thyroid hormone sulfotransferases. *Chemico-Biological Interactions*, *109*(1–3), 279–291.

Vítek, L., Zelenka, J., Zadinová, M., & Malina, J. (2005). The impact of intestinal microflora on serum bilirubin levels. *Journal of Hepatology*, *42*(2), 238–243. https://doi.org/10.1016/j.jhep.2004.10.012

Volta, U., Bonazzi, C., Bianchi, F. B., Baldoni, A. M., Zoli, M., & Pisi, E. (1987). IgA antibodies to dietary antigens in liver cirrhosis. *La Ricerca in Clinica E in Laboratorio*, *17*(3), 235–242.

Wahlström, A., Sayin, S. I., Marschall, H.-U., & Bäckhed, F. (2016). Intestinal Crosstalk between Bile Acids and Microbiota and Its Impact on Host Metabolism. *Cell Metabolism*, *24*(1), 41–50. https://doi.org/10.1016/j.cmet.2016.05.005

Wang, Han, Geng, C., Li, J., Hu, A., & Yu, C.-P. (2014). Characterization of a novel melamine-degrading bacterium isolated from a melamine-manufacturing factory in China. *Applied Microbiology and Biotechnology*, *98*(7), 3287–3293. https://doi.org/10.1007/s00253-013-5363-2

Wang, Hongbing, Faucette, S., Moore, R., Sueyoshi, T., Negishi, M., & LeCluyse, E. (2004). Human constitutive androstane receptor mediates induction of CYP2B6 gene expression by phenytoin. *The Journal of Biological Chemistry*, *279*(28), 29295–29301. https://doi.org/10.1074/jbc.M400580200

Ward, T. G., & Trexler, P. C. (1958). Gnotobiotics: A New Discipline in Biological and Medical Research. *Perspectives in Biology and Medicine*, *1*(4), 447–456. https://doi.org/10.1353/pbm.1958.0031

Waterston, R. H., Birney, E., Rogers, J., Abril, J. F., Agarwal, P., Agarwala, R., … Lander, E. S. (2002). Initial sequencing and comparative analysis of the mouse genome. *Nature*, *420*(6915), 520–562. https://doi.org/10.1038/nature01262

Weger, B. D., Gobet, C., Yeung, J., Martin, E., Jimenez, S., Betrisey, B., … Gachon, F. (2019). The Mouse Microbiome Is Required for Sex-Specific Diurnal Rhythms of Gene Expression and

Metabolism. *Cell Metabolism*, *29*(2), 362-382.e8. https://doi.org/10.1016/j.cmet.2018.09.023

Weghorst, C. M., & Klaunig, J. E. (1989). Phenobarbital promotion in diethylnitrosamine-initiated infant B6C3F1 mice: Influence of gender. *Carcinogenesis*, *10*(3), 609–612. https://doi.org/10.1093/carcin/10.3.609

Wei, P., Zhang, J., Dowhan, D. H., Han, Y., & Moore, D. D. (2002). Specific and overlapping functions of the nuclear hormone receptors CAR and PXR in xenobiotic response. *The Pharmacogenomics Journal*, *2*(2), 117–126.

Wei, P., Zhang, J., Egan-Hafley, M., Liang, S., & Moore, D. D. (2000). The nuclear receptor CAR mediates specific xenobiotic induction of drug metabolism. *Nature*, *407*(6806), 920–923. https://doi.org/10.1038/35038112

Whiteside, S. A., Razvi, H., Dave, S., Reid, G., & Burton, J. P. (2015). The microbiome of the urinary tract—A role beyond infection. *Nature Reviews. Urology*, *12*(2), 81–90. https://doi.org/10.1038/nrurol.2014.361

Wikoff, W. R., Anfora, A. T., Liu, J., Schultz, P. G., Lesley, S. A., Peters, E. C., & Siuzdak, G. (2009). Metabolomics analysis reveals large effects of gut microflora on mammalian blood metabolites. *Proceedings of the National Academy of Sciences of the United States of America*, *106*(10), 3698–3703. https://doi.org/10.1073/pnas.0812874106

Williams, B. B., Van Benschoten, A. H., Cimermancic, P., Donia, M. S., Zimmermann, M., Taketani, M., … Fischbach, M. A. (2014). Discovery and characterization of gut microbiota decarboxylases that can produce the neurotransmitter tryptamine. *Cell Host & Microbe*, *16*(4), 495–503. https://doi.org/10.1016/j.chom.2014.09.001

Willson, T. M., & Kliewer, S. A. (2002). PXR, CAR and drug metabolism. *Nature Reviews. Drug Discovery*, *1*(4), 259–266. https://doi.org/10.1038/nrd753

Wilson, J. D. (1992). Presentation of the Southern Society for Clinical Investigation Founder's Medal to Dr. Daniel W. Foster. *The American Journal of the Medical Sciences*, *304*(1), 1–2.

Wilson, V. S., McLachlan, J. B., Falls, J. G., & LeBlanc, G. A. (1999). Alteration in sexually dimorphic testosterone biotransformation profiles as a biomarker of chemically induced androgen disruption in mice. *Environmental Health Perspectives*, *107*(5), 377–384. https://doi.org/10.1289/ehp.99107377

Wiwi, C. A., Gupte, M., & Waxman, D. J. (2004). Sexually dimorphic P450 gene expression in liver-specific hepatocyte nuclear factor 4alpha-deficient mice. *Molecular Endocrinology (Baltimore, Md.)*, *18*(8), 1975–1987. https://doi.org/10.1210/me.2004-0129

Wortham, M., Czerwinski, M., He, L., Parkinson, A., & Wan, Y.-J. Y. (2007). Expression of constitutive androstane receptor, hepatic nuclear factor 4 alpha, and P450 oxidoreductase genes determines interindividual variability in basal expression and activity of a broad scope of xenobiotic metabolism genes in the human liver. *Drug Metabolism and Disposition: The Biological Fate of Chemicals*, *35*(9), 1700–1710. https://doi.org/10.1124/dmd.107.016436

Wright, E., Vincent, J., & Fernandez, E. J. (2007). Thermodynamic characterization of the interaction between CAR-RXR and SRC-1 peptide by isothermal titration calorimetry. *Biochemistry*, *46*(3), 862–870. https://doi.org/10.1021/bi061627i

Wright, M. C. (2006). The impact of pregnane X receptor activation on liver fibrosis. *Biochemical Society Transactions*, *34*(Pt 6), 1119–1123. https://doi.org/10.1042/BST0341119

Wu, H.-J., Ivanov, I. I., Darce, J., Hattori, K., Shima, T., Umesaki, Y., … Mathis, D. (2010). Gut-residing segmented filamentous bacteria drive autoimmune arthritis via T helper 17 cells. *Immunity*, *32*(6), 815–827. https://doi.org/10.1016/j.immuni.2010.06.001

Wyde, M. E., Bartolucci, E., Ueda, A., Zhang, H., Yan, B., Negishi, M., & You, L. (2003). The environmental pollutant 1,1-dichloro-2,2-bis (p-chlorophenyl)ethylene induces rat hepatic cytochrome P450 2B and 3A expression through the constitutive androstane receptor and pregnane X receptor. *Molecular Pharmacology*, *64*(2), 474–481. https://doi.org/10.1124/mol.64.2.474

Wyde, M. E., Kirwan, S. E., Zhang, F., Laughter, A., Hoffman, H. B., Bartolucci-Page, E., … You, L. (2005). Di-n-butyl phthalate activates constitutive androstane receptor and pregnane X receptor and enhances the expression of steroid-metabolizing enzymes in the liver of rat fetuses. *Toxicological Sciences: An Official Journal of the Society of Toxicology*, *86*(2), 281–290. https://doi.org/10.1093/toxsci/kfi204

Xiao, L., Feng, Q., Liang, S., Sonne, S. B., Xia, Z., Qiu, X., … Kristiansen, K. (2015). A catalog of the mouse gut metagenome. *Nature Biotechnology*, *33*(10), 1103–1108. https://doi.org/10.1038/nbt.3353

Xie, W., Barwick, J. L., Downes, M., Blumberg, B., Simon, C. M., Nelson, M. C., … Evans, R. M. (2000). Humanized xenobiotic response in mice expressing nuclear receptor SXR. *Nature*, *406*(6794), 435–439. https://doi.org/10.1038/35019116

Xie, Wen, Yeuh, M.-F., Radominska-Pandya, A., Saini, S. P. S., Negishi, Y., Bottroff, B. S., … Evans, R. M. (2003). Control of steroid, heme, and carcinogen metabolism by nuclear pregnane X receptor and constitutive androstane receptor. *Proceedings of the National Academy of Sciences of the United States of America*, *100*(7), 4150–4155. https://doi.org/10.1073/pnas.0438010100

Xie, Y.-B., Nedumaran, B., & Choi, H.-S. (2009). Molecular characterization of SMILE as a novel corepressor of nuclear receptors. *Nucleic Acids Research*, *37*(12), 4100–4115. https://doi.org/10.1093/nar/gkp333

Xu, C., Li, C. Y.-T., & Kong, A.-N. T. (2005). Induction of phase I, II and III drug metabolism/transport by xenobiotics. *Archives of Pharmacal Research*, *28*(3), 249–268.

Yamamoto, Y., Moore, R., Hess, H. A., Guo, G. L., Gonzalez, F. J., Korach, K. S., … Negishi, M. (2006). Estrogen receptor alpha mediates 17alpha-ethynylestradiol causing hepatotoxicity. *The Journal of Biological Chemistry*, *281*(24), 16625–16631. https://doi.org/10.1074/jbc.M602723200

Yan, Jing, Herzog, J. W., Tsang, K., Brennan, C. A., Bower, M. A., Garrett, W. S., … Charles, J. F. (2016). Gut microbiota induce IGF-1 and promote bone formation and growth. *Proceedings of the National Academy of Sciences of the United States of America*, *113*(47), E7554–E7563. https://doi.org/10.1073/pnas.1607235113

Yan, Jiong, Chen, B., Lu, J., & Xie, W. (2015). Deciphering the roles of the constitutive androstane receptor in energy metabolism. *Acta Pharmacologica Sinica*, *36*(1), 62–70. https://doi.org/10.1038/aps.2014.102

Yang, H., Garzel, B., Heyward, S., Moeller, T., Shapiro, P., & Wang, H. (2014). Metformin represses drug-induced expression of CYP2B6 by modulating the constitutive androstane receptor signaling. *Molecular Pharmacology*, *85*(2), 249–260. https://doi.org/10.1124/mol.113.089763

Yang, X., Downes, M., Yu, R. T., Bookout, A. L., He, W., Straume, M., … Evans, R. M. (2006). Nuclear receptor expression links the circadian clock to metabolism. *Cell*, *126*(4), 801–810. https://doi.org/10.1016/j.cell.2006.06.050

Yi, P., & Li, L. (2012). The germfree murine animal: An important animal model for research on the relationship between gut microbiota and the host. *Veterinary Microbiology*, *157*(1), 1–7. https://doi.org/10.1016/j.vetmic.2011.10.024

Yoshinari, K., Kobayashi, K., Moore, R., Kawamoto, T., & Negishi, M. (2003). Identification of the nuclear receptor CAR:HSP90 complex in mouse liver and recruitment of protein phosphatase 2A in response to phenobarbital. *FEBS Letters*, *548*(1–3), 17–20.

Zackular, J. P., Baxter, N. T., Chen, G. Y., & Schloss, P. D. (2016). Manipulation of the Gut Microbiota Reveals Role in Colon Tumorigenesis. *MSphere*, *1*(1). https://doi.org/10.1128/mSphere.00001-15

Zeller, G., Tap, J., Voigt, A. Y., Sunagawa, S., Kultima, J. R., Costea, P. I., … Bork, P. (2014). Potential of fecal microbiota for early-stage detection of colorectal cancer. *Molecular Systems Biology*, *10*, 766. https://doi.org/10.15252/msb.20145645

Zhang, B., Xie, W., & Krasowski, M. D. (2008). PXR: A xenobiotic receptor of diverse function implicated in pharmacogenetics. *Pharmacogenomics*, *9*(11), 1695–1709. https://doi.org/10.2217/14622416.9.11.1695

Zhang, J., Huang, W., Chua, S. S., Wei, P., & Moore, D. D. (2002). Modulation of acetaminophen-induced hepatotoxicity by the xenobiotic receptor CAR. *Science (New York, N.Y.)*, *298*(5592), 422–424. https://doi.org/10.1126/science.1073502

Zhang, J., Huang, W., Qatanani, M., Evans, R. M., & Moore, D. D. (2004). The constitutive androstane receptor and pregnane X receptor function coordinately to prevent bile acid-induced hepatotoxicity. *The Journal of Biological Chemistry*, *279*(47), 49517–49522. https://doi.org/10.1074/jbc.M409041200

Zhang, X.-J., Shi, Z., Lyv, J.-X., He, X., Englert, N. A., & Zhang, S.-Y. (2015). Pyrene is a Novel Constitutive Androstane Receptor (CAR) Activator and Causes Hepatotoxicity by CAR. *Toxicological Sciences: An Official Journal of the Society of Toxicology*, *147*(2), 436–445. https://doi.org/10.1093/toxsci/kfv142

Zheng, X., Zhao, A., Xie, G., Chi, Y., Zhao, L., Li, H., … Jia, W. (2013). Melamine-induced renal toxicity is mediated by the gut microbiota. *Science Translational Medicine*, *5*(172), 172ra22. https://doi.org/10.1126/scitranslmed.3005114

Zhou, J., Febbraio, M., Wada, T., Zhai, Y., Kuruba, R., He, J., … Xie, W. (2008). Hepatic fatty acid transporter Cd36 is a common target of LXR, PXR, and PPARgamma in promoting steatosis. *Gastroenterology*, *134*(2), 556–567. https://doi.org/10.1053/j.gastro.2007.11.037

Zhou, J., Zhai, Y., Mu, Y., Gong, H., Uppal, H., Toma, D., … Xie, W. (2006). A novel pregnane X receptor-mediated and sterol regulatory element-binding protein-independent lipogenic pathway. *The Journal of Biological Chemistry*, *281*(21), 15013–15020. https://doi.org/10.1074/jbc.M511116200

Zimmer, J., Lange, B., Frick, J.-S., Sauer, H., Zimmermann, K., Schwiertz, A., … Enck, P. (2012). A vegan or vegetarian diet substantially alters the human colonic faecal microbiota. *European Journal of Clinical Nutrition*, *66*(1), 53–60. https://doi.org/10.1038/ejcn.2011.141

ANNEXES

Associated publications

Ilchmann-Diounou, H., Olier, M., Lencina, C., Riba, A., Barretto, S., Nankap, M., … Ménard, S. (2019). **Early life stress induces type 2 diabetes-like features in ageing mice.** ***Brain, Behavior, and Immunity,*** *80*, 452–463. https://doi.org/10.1016/j.bbi.2019.04.025

Zhang, X., Grosfeld, A., Williams, E., Vasiliauskas, D., Barretto, S., Smith, L., … Douard, V. (2019). **Fructose malabsorption induces cholecystokinin expression in the ileum and cecum by changing microbiota composition and metabolism.** ***The FASEB Journal*****,** *33*(6), 7126–7142. https://doi.org/10.1096/fj.201801526RR

(In review for Scientific Reports)

Céline Lukowicz[1], Sandrine Ellero-Simatos[1], Marion Régnier[1], Fabiana Oliviero[1], Frédéric Lasserre[1], Arnaud Polizzi[1], Alexandra Montagner[1], Sarra Smati[1], Frédéric Boudou[2], Françoise Lenfant[2], Laurence Guzylack[1], Sandrine Menard[1], Sharon Baretto[1], Anne Fougerat[1], Yannick Lippi[1], Claire Naylies[1], Justine Bertrand-Michel[3], Afifa Ait Belgnaoui[1], Vassilia Theodorou[1], Pierre Gourdy[2], Laurence Gamet-Payrastre[1], Nicolas Loiseau[1], Hervé Guillou[1], Laila Mselli-Lakhal[1](2019). **Constitutive androstane receptor deficiency leads to sexually dimorphic obesity, diabetes, steatosis and endocrine disruptions in mice**.

Brain, Behavior, and Immunity 80 (2019) 452–463

Contents lists available at ScienceDirect

Brain, Behavior, and Immunity

journal homepage: www.elsevier.com/locate/ybrbi

Early life stress induces type 2 diabetes-like features in ageing mice

Hanna Ilchmann-Diounou[a], Maïwenn Olier[a], Corinne Lencina[a], Ambre Riba[a], Sharon Barretto[b], Michèle Nankap[a], Caroline Sommer[c], Hervé Guillou[b], Sandrine Ellero-Simatos[b], Laurence Guzylack-Piriou[a], Vassilia Théodorou[a], Sandrine Ménard[a,*]

[a] Neuro-Gastroenterology and Nutrition Team, Toxalim (Research Centre in Food Toxicology), Université de Toulouse, INRA, ENVT, INP-Purpan, UPS, Toulouse, France
[b] Integrative Toxicology and Metabolism Team, Toxalim (Research Centre in Food Toxicology), Université de Toulouse, INRA, ENVT, INP-Purpan, UPS, Toulouse, France
[c] Experimental and Zootechnic Platform, Toxalim (Research Centre in Food Toxicology), Université de Toulouse, INRA, ENVT, INP-Purpan, UPS, Toulouse, France

ARTICLE INFO

Keywords:
Intestinal barrier
Microbiota dysbiosis
DOHaD
Non-communicable diseases

ABSTRACT

Early life stress is known to impair intestinal barrier through induction of intestinal hyperpermeability, low-grade inflammation and microbiota dysbiosis in young adult rodents. Interestingly, those features are also observed in metabolic disorders (obesity and type 2 diabetes) that appear with ageing. Based on the concept of Developmental Origins of Health and Diseases, our study aimed to investigate whether early life stress can trigger metabolic disorders in ageing mice.

Maternal separation (MS) is a well-established model of early life stress in rodent. In this study, MS increased fasted blood glycemia, induced glucose intolerance and decreased insulin sensitivity in post-natal day 350 wild type C3H/HeN male mice fed a standard diet without affecting body weight. MS also triggered fecal dysbiosis favoring pathobionts and significantly decreased IL-17 and IL-22 secretion in response to anti-CD3/CD28 stimulation in small intestine *lamina propria*. Finally, IL-17 secretion in response to anti-CD3/CD28 stimulation was also diminished at systemic level (spleen).

For the first time, we demonstrate that early life stress is a risk factor for metabolic disorders development in ageing wild type mice under normal diet.

1. Introduction

During the last century, the incidence of non-communicable diseases, including metabolic disorders, is expanding in western countries (Bach, 2002). The causes for this drastic increase are debated. The concept of Developmental Origins of Health and Disease (DOHaD) highlights the importance of early life period and raises the hypothesis that chronic diseases could find their origins in perinatal environment (Barker et al., 1989; Gluckman et al., 2016). In mice and humans, early life is important for the development of the immune system, metabolic switch, microbiota colonization (Tamburini et al., 2016) and the development of life-long beneficial host-microbe homeostasis (Hornef and Fulde, 2014). Adverse events can disturb these mechanisms of adaptation. Several observational epidemiological studies have shown an association between adverse childhood experiences and metabolic diseases in later life (Huang et al., 2015). This study aims to provide experimental data to support a link between early life stress and development of metabolic disorders with ageing.

Metabolic disorders, such as obesity and type 2 diabetes are associated with modification of intestinal barrier, microbiota dysbiosis and low grade inflammation (Brun et al., 2007; Cani et al., 2008; Osborn and Olefsky, 2012; Turnbaugh et al., 2006). In mice, several models such as diet induced obesity (high-fat or western diets) or genetic models (*ob/ob* and *db/db*, respectively deficient for leptin and leptin receptor) are used to investigate obesity associated with hyperglycemia. In those models, a defect of intestinal barrier as well as low-grade inflammation were observed, even before the onset of obesity and hyperglycemia (Araújo et al., 2017; Brun et al., 2007). Neonatal maternal separation (MS) is a stress model widely used in rodents as a paradigm of early life adverse events. We previously observed that, in male mice, MS triggers long lasting alterations of intestinal homeostasis in young adult offspring (post-natal-day (PND) 50) including a defect of intestinal barrier, microbiota dysbiosis and low-grade inflammation (Riba et al., 2018). With ageing, intestinal permeability and low-grade

Abbreviations: DOHaD, Developmental Origin of Health and Diseases; FSS, Fluorescein Sodium Salt; HRP, Horse Radish Peroxidase; IBS, Irritable Bowel Syndrome; MS, Maternal Separation; OTU, Operational Taxonomic Unit; PND, Post-Natal Day; siLP, small intestine *Lamina Propria*; TCR, T cell Receptor

* Corresponding author.
E-mail address: sandrine.menard@inra.fr (S. Ménard).

https://doi.org/10.1016/j.bbi.2019.04.025
Received 5 November 2018; Received in revised form 22 February 2019; Accepted 10 April 2019
Available online 11 April 2019

THE FASEB JOURNAL • RESEARCH • www.fasebj.org

Fructose malabsorption induces cholecystokinin expression in the ileum and cecum by changing microbiota composition and metabolism

Xufei Zhang,[*,†] Alexandra Grosfeld,[‡] Edek Williams,[§] Daniel Vasiliauskas,[¶] Sharon Barretto,[‖] Lorraine Smith,[‖] Mahendra Mariadassou,[#] Catherine Philippe,[*] Fabienne Devime,[*] Chloé Melchior,[**] Guillaume Gourcerol,[**] Nathalie Dourmap,[††] Nicolas Lapaque,[*] Pierre Larraufie,[*] Hervé Blottière,[*] Christine Herberden,[*] Philippe Gerard,[*] Jens Rehfeld,[‡‡] Ronaldo Ferraris,[§§] Christopher Fritton,[§] Sandrine Ellero-Simatos,[‖] and Veronique Douard[*,1]

[*]Micalis Institute, Institut National de la Recherche Agronomique (INRA), AgroParisTech, Université Paris–Saclay, Jouy-en-Josas, France; [†]Collège Doctoral, Sorbonne Université, Paris, France; [‡]Centre de Recherche des Cordeliers, INSERM Unité Mixte de Recherche (UMR) S1138, Sorbonne Université, Sorbonne Cités, Université Paris–Diderot (UPD), Centre National de la Recherche Scientifique (CNRS), Instituts hospitalo–universitaires (IHU), Institute of Cardiometabolism and Nutrition (ICAN), Paris, France; [§]Department of Orthopedics and [§§]Department of Pharmacology, Physiology and Neuroscience, Rutgers University, Newark, New Jersey, USA; [¶]Paris-Saclay Institute of Neuroscience, Université Paris Sud, Centre National de la Recherche Scientifique (CNRS), Université Paris–Saclay, Gif-sur-Yvette, France; [‖]Toxalim, Université de Toulouse, Institut National de la Recherche Agronomique (INRA), Toulouse, France; [#]Mathématiques et Informatique Appliquées du Génome à l'Environnement (MaIAGE), Unité de Recherche (UR) 1404, Institut National de la Recherche Agronomique (INRA), Jouy-en-Josas, France; [**]INSERM Unit 1073, University of Rouen (UNIROUEN), Normandie University, Rouen, France; [††]UNIROUEN, Inserm U1245 and Rouen University Hospital, Normandy Centre for Genomic and Personalized Medicine, Normandy University, Rouen, France; and [‡‡]Department of Clinical Biochemistry, Rigshospitalet, University of Copenhagen, Copenhagen, Denmark

ABSTRACT: Current fructose consumption levels often overwhelm the intestinal capacity to absorb fructose. We investigated the impact of fructose malabsorption on intestinal endocrine function and addressed the role of the microbiota in this process. To answer this question, a mouse model of moderate fructose malabsorption [ketohexokinase mutant (KHK)$^{-/-}$] and wild-type (WT) littermate mice were used and received a 20%-fructose (KHK-F and WT-F) or 20%-glucose diet. Cholecystokinin (*Cck*) mRNA and protein expression in the ileum and cecum, as well as preproglucagon (*Gcg*) and neurotensin (*Nts*) mRNA expression in the cecum, increased in KHK-F mice. In KHK-F mice, triple-label immunohistochemistry showed major up-regulation of CCK in enteroendocrine cells (EECs) that were glucagon-like peptide-1 (GLP-1)$^{+}$/Peptide YY (PYY^{-}) in the ileum and colon and GLP-1^{-}/PYY^{-} in the cecum. The cecal microbiota composition was drastically modified in the KHK-F in association with an increase in glucose, propionate, succinate, and lactate concentrations. Antibiotic treatment abolished fructose malabsorption-dependent induction of cecal *Cck* mRNA expression and, in mouse GLUTag and human NCI-H716 cells, *Cck* mRNA expression levels increased in response to propionate, both suggesting a microbiota-dependent process. Fructose reaching the lower intestine can modify the composition and metabolism of the microbiota, thereby stimulating the production of CCK from the EECs possibly in response to propionate.—Zhang, X., Grosfeld, A., Williams, E., Vasiliauskas, D., Barretto, S., Smith, L., Mariadassou, M., Philippe, C., Devime, F., Melchior, C., Gourcerol, G., Dourmap, N., Lapaque, N., Larraufie, P., Blottière, H., Herberden, C., Gerard, P., Rehfeld, J., Ferraris, R., Fritton, C., Ellero-Simatos, S., Douard, V. Fructose malabsorption induces cholecystokinin expression in the ileum and cecum by changing microbiota composition and metabolism. FASEB J. 33, 000–000 (2019). www.fasebj.org

KEY WORDS: CCK · KHK · propionate

ABBREVIATIONS: AB, antibiotic; CCK, cholecystokinin; EEC, enteroendocrine cell; FC, fold change; FFAR, free fatty acid receptor; FROGS, Find, Rapidly, OTUs with Galaxy Solution; GCG, preproglucagon; GIP, gastric inhibitory polypeptide; GI, gastrointestinal; GLP-1, glucagon-like peptide-1; GLUT, facilitated glucose/fructose transporter; KHK, ketohexokinase; Math1, atonal bHLH transcription factor 1; NeuroD, neuronal differentiation; Neurog, neurogenin; NTS, neurotensin; O-PLS-DA, orthogonal projection on latent structure-discriminant analysis; OTU, operational taxonomic unit; Pax, paired box; PCA, principal component analysis; PYY, peptide YY; qRT-PCR, quantitative PCR; SCFA, short-chain fatty acid; SCT, secretin; SST, somatostatin; TPH1, tryptophan hydroxylase 1; WT, wild type

[1] Correspondence: Micalis Institute, INRA, Domaine du Vilvert, 78352 Jouy-en-Josas, France. E-mail: veronique.douard@inra.fr

doi: 10.1096/fj.201801526RR

This article includes supplemental data. Please visit *http://www.fasebj.org* to obtain this information.

0892-6638/19/0033-0001 © FASEB

Constitutive androstane receptor deficiency leads to sexually dimorphic obesity, diabetes, steatosis and endocrine disruptions in mice

Céline Lukowicz[1], Sandrine Ellero-Simatos[1], Marion Régnier[1], Fabiana Oliviero[1], Frédéric Lasserre[1], Arnaud Polizzi[1], Alexandra Montagner[1], Sarra Smati[1], Frédéric Boudou[2], Françoise Lenfant[2], Laurence Guzylack[1], Sandrine Menard[1], Sharon Baretto[1], Anne Fougerat[1], Yannick Lippi[1], Claire Naylies[1], Justine Bertrand-Michel[3], Afifa Ait Belgnaoui[1], Vassilia Theodorou[1], Pierre Gourdy[2], Laurence Gamet-Payrastre[1], Nicolas Loiseau[1], Hervé Guillou[1], Laila Mselli-Lakhal[1,#]

[1] Toxalim (Research Centre in Food Toxicology), Université de Toulouse, INRA, ENVT, INP-Purpan, UPS, Toulouse, France.
[2] I2MC, Institut National de la Santé et de la Recherche Médicale (INSERM)-U 1048, Université de Toulouse 3 and CHU de Toulouse, Toulouse, France.
[3] Metatoul-Lipidomic Facility, MetaboHUB, Institut National de la Santé et de la Recherche Médicale (INSERM), UMR1048, Institute of Metabolic and Cardiovascular Diseases, Toulouse, France

Keywords: Nuclear receptor - metabolic disease - transcriptomic - metabolomic - lipidomic

Emails of authors:
Céline Lukowicz: celine.lukowicz@inra.fr, Sandrine Ellero-Simatos: sandrine.ellero--simatos@inra.fr, Marion Régnier: marion.regnier@inra.fr, Fabiana Oliviero: fabiana.oliviero@inra.fr, Frédéric Lasserre: Frederic.lasserre@inra.fr, Arnaud Polizzi: arnaud.polizzi@inra.fr, Alexandra Montagner: Alexandra.montagner@inserm.fr, Sarra Smati : sarra.smati@inra.fr, Frédéric Boudou: fréderic.boudou@inserm.fr, Françoise Lenfant: Françoise.lenfant@inserm.fr, Laurence Guzylack: Laurence.guzylack@inra.fr, Sandrine Menard: sandrine.memard@inra.fr, Sharon Baretto: sharon.baretto@inra.fr, Anne Fougerat: anne.fougerat@inra.fr, Yannick Lippi: Yannick.lippi@inra.fr, Claire Naylies: Claire.naylies@inra.fr, Justine Bertrand-Michel: justine.bertrand-michel@inserm.fr, Afifa Ait Belgnaoui: afifa.ait.belgnaoui@gmail.com, Vassilia Theodorou: Vassilia.theodorou@inra.fr, Pierre Gourdy: pierre.gourdy@inserm.fr, Laurence Gamet-Payrastre:

laurence.payrastre@inra.fr, Nicolas Loiseau: Nicolas.loiseau@inra.fr, Hervé Guillou: herve.guillou@inra.fr, Laila Mselli-Lakhal: laila.lakhal@inra.fr.

[#] Corresponding author

Contact Information

Laila Mselli-Lakhal, ToxAlim UMR1331 INRA/INPT/UPS, Integrative Toxicology & Metabolism group, 180 chemin de Tournefeuille, BP 93173, 31027 Toulouse Cedex 3, FRANCE. Tel: +33 561285524. Fax: +33 561285310. laila.lakhal@inra.fr.

List of abbreviations

ALT, alanine transaminase; AST, aspartate transaminase; CAR, constitutive androstane receptor; HDL, high-density lipoprotein; LDL, low-density lipoprotein; Sult1a1, sulfotransferase family 1A member 1, Sult2a1, sulfotransferase family 2A member 1; Srd5a1, steroid 5 alpha-reductase 1.

Financial support

This work was supported by grants from the Agence National de la Recherche and from the Midi-Pyrénées region (NEWPOM). Céline Lukowicz is funded by grants from the French National Institute for Agricultural Research, Animal Health, the Région Midi-Pyrénées, and the EI Purpan engineering school.

Abstract

The constitutive androstane receptor (CAR) is a transcription factor involved in detoxification through regulating expression of xenobiotic-metabolizing enzymes. Highly expressed in the liver, it is important in protecting the organism against exogenous and endogenous toxic molecules such as bile acids and bilirubin and in the catabolism of thyroid and steroid hormones. A role has also been assigned to CAR in the regulation of energy metabolism, although related mechanisms have been studied primarily in males and in physiopathological conditions. Here, we compared the impact of CAR deficiency on energy homeostasis regulation between male and female mice in a normal physiological context. Large-scale gene expression analysis in 16-week-old animals revealed significant sexual dimorphism in the hepatic transcriptome of CAR-/- mice. We monitored these mice for different physiological parameters to age 68 weeks. CAR-/- males developed obesity, fasted hyperglycemia, and hyperinsulinemia associated with glucose and insulin intolerance. They also developed dyslipidemia and important steatosis accompanied by increased alanine transaminase and aspartate transaminase, signs of hepatolysis. In contrast, CAR-/- females had a different metabolic profile with overweight, improved glucose tolerance, no dyslipidemia, and no steatosis. Both sexes of CAR-/- mice displayed sex-dependent deregulation of gene expression involved in steroid hormone metabolism, leading to alteration of their corticosterone and sexual hormones levels. Ovariectomized CAR-/- females developed the same metabolic disorders as CAR-/- males, demonstrating that sex-steroid hormones protect female mice against the metabolic disorders observed in CAR-/- males. *Conclusion:* This study reveals a sexually dimorphic role for CAR in the regulation of endocrine and metabolic homeostasis.

Abstract

The pregnane X receptor (PXR, NR1I2) and the constitutive androstane receptor (CAR, NR1I3) are two liver and intestine-enriched nuclear receptors that act as transcriptional regulators of enzymes critical for the detoxification of xenobiotics and endogenous metabolites. Previous works have shown that the expression of CAR and PXR target genes is significantly reduced in the liver of germ-free mice. In this PhD project, we aimed to gain insights into the bidirectional interactions between the gut microbiota and these xenosensors.

We first used a pharmacological approach in WT vs *Pxr*$^{-/-}$ male mice and performed a transcriptomic comparison of the PXR-regulated genes in the liver upon activation via the rodent activator PCN. We confirmed that PXR activation increased liver triglyceride accumulation and significantly regulated the expression of genes, mostly involved in xenobiotic metabolism. We also highlighted a significant overlap between the genes downregulated upon PXR activation and a list of fasting-induced PPARδ target genes. Among these, we identified the well-described PPARδ target fibroblast growth factor 21 (*Fgf21*) as a new PXR-regulated gene. PXR activation abolished plasmatic levels of FGF21. This first set of results provided a comprehensive signature of PXR activation in the liver and identified new PXR target genes that might be involved in the steatogenic and pleiotropic effects of PXR. Next, we compared the hepatic vs. intestinal signature of the pharmacological activation of PXR. This allowed us to unravel the strongest PXR target genes in both organs. Finally, we used *Pxr*$^{+/+}$ and *Pxr*$^{-/-}$ littermate mice and suppressed the gut microbiota using antibiotics (ATB). Using the previously identified PXR targets, we confirmed that ATB significantly decreased *Pxr* activity in the liver and ileum. Liver transcriptomic analyses showed that ATB decreased a much higher number of PXR-dependent genes in the liver of male mice than in females. In males, this gut microbiota-PXR axis controlled xenobiotic metabolism and lipid remodelling. Conversely, 16S sequencing and 1H-NMR-based metabolic profiling of caecal content revealed subtle but significant differences in the gut microbiota composition of male *Pxr*$^{-/-}$ vs. *Pxr*$^{+/+}$ mice, while no difference was observed in females. Our results therefore demonstrate that hepatic PXR is a major sensor of the gut microbiota that controls the host detoxifying capacities and lipid metabolism in a sexually dimorphic way.

In the final chapter, we investigated the microbiota-CAR interactions. In *Car*$^{+/+}$ *and* *Car*$^{-/-}$ littermate mice. Microbiota suppression by antibiotics decreased CAR activity in the liver and ileum of males but only in the liver of females. In caecal content, male-specific and CAR-dependant metabolites were also detected through 1H-NMR-based metabolomics. Furthermore, 16S sequencing confirmed a significant difference in gut microbiota composition of *Car*$^{-/-}$ vs *Car*$^{+/+}$ male mice but not in females. We investigated the potential consequences of this sexually dimorphic CAR-dependent dysbiosis and observed that long-term Car deletion increased adipose tissue accumulation in male mice (at 37 weeks old). Whether the Car-dependent dysbiosis is responsible for this phenotype remains to be determined. In 37-week-old females, *Car* deletion induced a significant increase in spleen weight and a decrease in colon length, therefore suggesting a role for *Car* in systemic and intestinal inflammation. Thus, our result show for the first time that the CAR-gut microbiota interaction is sexually dimorphic and might control adipose deposition in male mice.

Overall, our results shed new light into the crosstalk between the gut microbiota and the host's xenobiotic receptors CAR and PXR, demonstrating that this cross-talk might be involved in the control the host's hepatic lipid and xenobiotic metabolism.

Résumé

Le pregnane X receptor (PXR, NR1I2) et le récepteur constitutif aux androstanes (CAR, NR1I3) sont deux récepteurs nucléaires hépatiques et intestinaux qui régulent la transcription d'enzymes de détoxification des xénobiotiques. Des travaux antérieurs ont montré que l'expression des gènes cibles de CAR et PXR est significativement réduite dans le foie des souris axéniques. Dans ce projet de thèse, nous avions pour objectif de mieux comprendre les interactions bidirectionnelles entre le microbiote intestinal et ces xénosenseurs.

Nous avons d'abord utilisé une approche pharmacologique chez les souris mâles WT vs *Pxr*$^{-/-}$ et comparé la signature transcriptomique des gènes régulés par PXR dans le foie lors de *l'acti*vation via le PCN. L'activation de PXR a augmenté l'accumulation de triglycérides hépatiques. Nous avons observé un chevauchement significatif entre les gènes régulés négativement lors de l'activation de PXR et une liste de gènes cibles de PPARδ induits par le jeûne. Parmi ceux-ci, nous avons identifié le facteur de croissance de fibroblastes 21 (*Fgf21*) comme un nouveau gène régulé par PXR. L'activation de PXR a aboli les taux plasmatiques de FGF21. Ces premiers résultats ont fourni une signature complète de l'activation de PXR dans le foie et ont identifié de nouveaux gènes cibles potentiellement impliqués dans les effets stéatogènes et pléiotropes de PXR.

Ensuite, nous avons comparé la signature hépatique à la signature intestinale de l'activation pharmacologique de PXR, ce qui nous a permis d'identifier les gènes cibles communs de PXR dans ces 2 organes.

Enfin, nous avons utilisé des souris *Pxr*$^{+/+}$ et *Pxr*$^{-/-}$ littermate et supprimé le microbiote intestinal au moyen d'antibiotiques (ATB). En utilisant les gènes cibles de PXR identifiés précédemment, nous avons confirmé que les ATB réduisaient de manière significative l'activité de PXR dans le foie et l'iléon. Des analyses transcriptomiques hépatiques ont montré que les ATB diminuaient un nombre beaucoup plus élevé de gènes PXR-dépendants dans le foie des souris mâles que chez les femelles. Chez les mâles, l'axe microbiote intestinal-PXR contrôlait le métabolisme des xénobiotiques et le remodelage des lipides hépatiques. À l'inverse, le séquençage 16S et la métabolomique par RMN du contenu caecal ont révélé des différences subtiles mais significatives dans la composition du microbiote intestinal des souris *Pxr*$^{-/-}$ par rapport aux souris *Pxr*$^{+/+}$, uniquement chez les mâles. Nos résultats démontrent donc que, dans le foie, PXR est un senseur majeur du microbiote intestinal qui contrôle les capacités de détoxication de l'hôte et le métabolisme des lipides de manière sexuellement dimorphique. Dans le dernier chapitre, nous avons étudié les interactions microbiote-CAR. Chez les souris *Car*$^{+/+}$ et *Car*$^{-/-}$ littermates, la suppression du microbiote par les antibiotiques a diminué l'activité de CAR dans le foie et l'iléon des mâles, mais uniquement dans le foie des femelles. Dans le contenu caecal, le séquençage 16S et la metabolomique ont montré une différence significative dans la composition et l'activité métabolique du microbiote intestinal chez les souris *Car*$^{+/+}$ *vs Car*$^{-/-}$ mâles, mais pas chez les femelles. Nous avons cherché les conséquences potentielles de cette dysbiose CAR dépendante et avons observé que la délétion de CAR augmentait l'accumulation de tissu adipeux chez les souris mâles à 37 semaines. Cependant, l'implication du microbiote CAR-dépendant dans ce phénotype reste à vérifier. Ainsi, nos résultats montrent pour la première fois que l'interaction CAR-microbiote est sexuellement dimorphique et pourrait contrôler le dépôt adipeux chez les souris mâles.

Dans l'ensemble, nos résultats montrent que le dialogue entre le microbiote intestinal et les récepteurs aux xénobiotiques CAR et PXR est impliqué de façon sexuellement dimorphique dans le contrôle des capacités de détoxification de l'hôte, et joue un rôle dans l'homéostasie lipidique.